SPECTROPOLARIMETRIC STUDIES OF THE SUN, THE MOON AND THE DAYTIME SKY.

BY

HASSAN MOHAMMED BASURAH

Thesis
submitted to the
University of Glasgow
for the degree of
Ph.D.

Department of Physics and Astronomy,
The University of Glasgow,
Glasgow G12 8QQ

February 1991

ProQuest LLC.
789 East Eisenhower Parkway
P.O. Box 1346
Ann Arbor, MI 48106 – 1346

To

My Mother

All thanks and respect

CONTENTS

Acknowledgements

It is a pleasure to thank all those who have assisted me with the preparation of this thesis - in particular, Professor R. P. Ferrier and Professor J. C. Brown for the use of departmental facilities.

I am deeply grateful to my adviser Dr. David Clarke for suggesting the research projects, for guidance, and for help in all aspects, giving me the opportunity to have extensive observing experience. I should like to thank him also for his patience and advice, useful discussions, comments on the manuscript and finally for his friendship.

Thanks are also extended to Mrs. M. Morris for her proof reading of the manuscript and improving comments and correcting the thesis. I would also like to thank her for making my stay at the observatory a happy time.

I am very grateful to Prof. P. A. Sweet, Mr. M. Al-Malki, and Mr. J. Naghizadeh and to Mr Y. Al-Mleaky for numerous discussions. I am especially indebted to Mr. S. Al-Amode and Dr. A.A. Abdullah for their advice (programming) and all other people providing me with encouragement, sharing with me their wisdom and knowledge.Thanks are directed to Mr. W. Edgar and Mr. R. Loney for their general friendship.

I give special thanks to my family for their encouragement and their patience.

SUMMARY

Probably the earliest recorded application of polarimetry to astronomy was by Arago in 1809. He found that the light of the daytime sky and also that of the Moon is partially polarized. Since that time, polarimetric studies have grown enormously and now support many areas of astronomical research.

Most of the radiation from the sky can be assigned to single scattering based on Rayleigh theory. In addition, other components are required to describe the situation fully, e.g. secondary scattering, Mie scattering from small particles, etc. As well as these linear mechanisms, Raman scattering is present, altering the spectral distribution of the radiation.

Effects of luminescence/fluorescence may also be important in redistributing the scattered energies to other wavebands. These latter non-linear effects have bearing on the interpretation of the Ring effect - the filling-in of the Fraunhofer spectrum line profiles. The Moon also is thought to display a line filling-in phenomenon which has been modelled in terms of luminescence, Rayleigh-Brillouin scattering etc. These effects have been discovered and explored by spectrophotometry. Polarimetric studies are somewhat sparse but as such measurements give good insight to the understanding of scattering processes in general, they have good potential for investigating any proposed model.

In this thesis, an account is given of the making of some polarimetric observations which hopefully will lead to a better understanding of certain atmospheric and lunar surface phenomena. The experiments have involved the use of instruments capable of performing high precision polarimetry with spectral resolution ≈2Å at the Hα and Hβ Fraunhofer spectral lines.

Photometric and the polarimetric observations are reported for the Ring effect at the zenith (daytime sky) covering many physical conditions which might

be considered as controlling its behaviour. This result enabled the discovery that the polarization within the Fraunhofer lines is enhanced to a degree (when the Sun is high in the sky) which is not explainable by the Raman scattering, one of mechanisms that have been proposed in relation to line filling-in. From the photometric observations with different ground albedos, a strong clue was found that the reflected light from the Earth is not the source of the Ring effect. Also the photometric observational studies reported here suggest that a new phenomenon behaving like airglow has been discovered. It is referred to here as a "daylight flash" and was recorded (for short periods) on three days at both the Hα and Hβ lines with different strengths. The cores of these lines were filled in while the near continua were unaffected.

The lunar spectropolarimetric observations reported here are the first measurements of individual spectral lines with extremely high polarimetric accuracies, even better than any previous broad band measurements. In the literature it had been considered that the lunar luminescence is unpolarized and, if that were the case, its effect would be to reduce the observed degree of polarization at line centres with respect to the continuum. Results presented here show however that there is no such consistent pattern of spectral line polarimetric emerges. So, if lunar luminescence truly exists, the added radiation must be polarized, a result contrary to previous assumptions.

Recently there has been much experimental activity to record the behaviour of the whole disk of the Sun so that direct comparisons can be made with stellar observations. Such studies are sometimes referred to as the "solar-stellar connection". Both photometry and spectrometry of the integrated light have been undertaken by various observers - but very little has been attempted using polarimetry.

In the stellar field, polarimetry has provided details of rotation periods and basic geometries (e.g. inclination of rotation axis) for both early- and late-type stars. With improved instruments, efforts are now being made to explore the polarimetric behaviour of stars closer to the solar spectral type. For reference (and as an experimental challenge) it is of great interest to explore the spectro-polarimetric behaviour of the Sun. Part of this thesis gives an account of some experiments in this direction.

For the whole solar disk measurements, an integrating sphere has been used and successfully tested photometrically using a spectrometer (FMHW≈6Å). With this spectral resolution no detectable polarization for the whole solar disk across the CaII K Fraunhofer line was observed.

Some material from this thesis has already been published. The corresponding thesis sections, the research paper titles and the authors are given below:-

Section 6.3

"Polarization Measurements of The Ring Effect in The Daytime Sky"

D. Clarke, and H. Basurah

Planet. Space Sci. Vol. 37, No.5, pp 627-630, 1989.

Section 5.3.2

"An Investigation of Lunar Luminescence by Spectropolarimetry"

D. Clarke, and H. Basurah

Icarus, Vol.88, pp 396-406, 1990.

PREFACE.

The aims of this thesis were to investigate: I) The ability of the polarimetric technique to detect both the Ring effect at the daytime sky and Lunar luminescence, a technique which removes the requirement of comparative solar measurements; II) The possibility of making polarimetric observations of the whole solar disk to advance the solar-stellar connection, such observations being useful for direct comparison with stars., and III) The disagreements found in the literature concerning the polarization at the line centre of CaI 4227Å and the influence of the Hanle effect on observations.

The first aim has been fulfilled. Daytime sky measurements are presented which display new observational phenomena. Higher levels of polarization were found within Fraunhofer lines than could be expected from either rotational or vibrational Raman scattering. Discussions with Prof. L. D. Barron (Chemistry Department) about the polarimetric observations of the daytime sky confirmed that these enhancements could not be caused by Raman scattering. Lunar spectro-polarimetric observations across spectral lines suggest that if lunar luminescence truly exists, it must be polarized, a result contrary to all previous assumptions.

As for the second aim, although only a few measurements were made of the polarization of the whole solar disk, the major achievement was substantial progress with the establishment of equipment for furthering this investigation.

The third aim was hindered by the optical quality of a key component (half-wave plate) in the polarimetric modulator. The defect in the form of non-parallelism of the wave plate surfaces caused a severe image movement (wobble) as the device was rotated. This prevented performing observations on spatially resolved elements on the solar disk and curtailed the experiments. It is considered

still worthwhile to pursue the observations but a different form of modulator is required, such as a photoelastic waveplate system.

The original work of this thesis constitutes Chapter 2, parts of Chapter 3, and Chapters 4,5 and 6. Chapter 2, presents two models, the first of which has been originally proposed by the author, and which assesses the added light effect (in both the day time sky and the lunar spectrum) on the polarization behaviour across spectral lines. This model helps clarify that the line depth method (which has been used in photometry) can be used and extended to polarimetry. From values of previous photometric measurements made by other workers, this model predicts that polarization variations across spectral lines should be readily measurable. The second model to estimate the polarization of the light from the whole solar disk, was originally made by Stewart (1984), but it has been extended here to include the Hanle effect associated with a weak magnetic field.

The first half of Chapter 3 is a description of the established instrumentation (which has been used for the observations of the daytime sky and the Moon) at the Cochno Observatory. The author assisted in developing the software (namely, the observation programmes). The remaining part of this chapter describes instrumentation which are required for the solar experiments.

Observations of the whole solar disk, (which was the second aim of the thesis) were attempted in three different ways (The first two were not successful and so are not described in the thesis). In the end an integrating sphere (suggested by Dr. D. Clarke) and fibre optic system were developed and used.

For the third aim, a small telescope with different "eyepieces" has been used in order to provide solar images with different diameters, such images being projected onto a special device (solar scanning device, design by the author) allowing measurements to be made along any solar radius. Also the author has estimated overall requirements for this aim.

For the solar experiments a high spectral resolution optical system was required; to achieve this, the combinations of a small grating spectrometer ($\Delta\lambda\approx6$Å) and two Fabry-Perot interferometers ($\Delta\lambda\approx1$Å and ≈0.1Å) were explored. Electric connections of the Fabry-Perot interferometer and the temperature controls of the spectrometric system were undertaken by the author. A system and procedure were developed by the author to calibrate the grating spectrometer and one Fabry-Perot ($\Delta\lambda\approx1$Å) in combination with the grating spectrometer. The grating spectrometer has been used for solar experiments.

It must be pointed out that some of the photometric observations of the whole solar disk (testing the integrating sphere) were supported by Dr. D. Clarke. Since the lunar observations need the presence of two persons at the observatory, they were carried out in co-operation with Dr. D. Clarke. The first stage of the solar experiments, all observations of the blue sky, and the final solar polarimetric observations were achieved independently. All the data reduction and the statistical programmes for the different analyses of the above measurements described throughout the thesis have been performed by the author.

The layout of the thesis follows a natural progression starting with a preliminary introduction describing the phenomena of interest and covers the instrumentation used to make polarimetric measurements of the Sun, the Moon and the daytime sky.

In addition to setting the scene related to polarimetric phenomena that are explored in more detail in the thesis, Chapter 1 contains the basic polarimetric definitions (Stokes parameters), and discussion of the experimental procedures associated with performing polarimetry on three distinct types of source, i.e.the Sun, the Moon, and the daytime sky - each with its own particular problems.

Chapter 2 contains an analytical model for the filling-in effects and associated polarimetry across spectrum lines, based on the line depth method, and defines the requirements of the accuracy necessary to detect the Ring effect in the daytime sky and the lunar luminescence. Another model estimates the whole Sun polarization associated with the resonance scattering and the Hanle effect, as an active region with a small magnetic field moves across the solar disk.

Chapter 3 discusses the instrumental techniques which have been used (for the Moon and the daytime sky), and the optical system specially developed to observe the polarization of the integrated light from the whole solar disk and to investigate solar polarimetry of different parts on its surface.

In Chapter 4, a description is given of the experiment using the novel instrumentation presented in Chapter 3 for observing both the whole disk of the Sun and also specific areas. Although this work did not produce the intended results, substantial progress was made in establishing the equipment and testing its stability.

Chapters 5, and 6 contain the details of the lunar and the daytime sky photometric and polarimetric observations. Measurements which I made of the Moon and the daytime sky are tabulated. The new observational phenomena mentioned above are reported here.

General conclusions from the overall studies are presented in Chapter 7 and suggestions are made for future work.

Chapter 1 Introduction.

1.1 Polarimetric studies.

Intensity and direction of any observed object are the two aspects with which observational astronomy and astrophysics are traditionally concerned. These parameters may be measured as functions of wavelength and time. But the radiation carries a third element of information, viz. its *polarization*. The importance of the polarization in association with astronomical objects is being more and more appreciated in relation to understanding a whole range of celestial phenomena. In the field of astrophysics one of the principal processes leading to the polarization of light is that of scattering. In the case of the Moon and for the daytime sky, the observed polarization is usually fairly strong. The man in the street when wearing polaroid sunglasses may be conscious of the polarization of the daytime sky without fully appreciating the nature of the effect that causes the sky brightness to change according to the movement of his head.

Measurements of the polarized scattered light from the Moon and the daytime sky have demonstrated their importance in giving information about the scattering processes. The strength of polarization is known to change with phase angle (defined as the angle formed by the Sun's centre, observed point and observer) and with wavelength. Spectropolarimetry performed at different phase angles is a powerful diagnostic tool for the investigation of scattering processes. The polarization of scattered light from the Moon depends on the nature of the observed area and on the microstructure of the surface. For the daytime sky, it depends on the meteorological conditions, on the purity of the atmosphere, and on the component back-scattered after reflection from the ground.

The polarizations associated with stars (and the Sun) are usually small effects but nonetheless they provide valuable information on scattering processes, geometries, magnetic fields, etc. The information that polarization carries can be crucial in understanding the nature of a source. Hand in hand with conventional photometry, it maximises our knowledge of any observed system.

The main part of this thesis describes experiments that were undertaken to measure and interpret polarization in light from the Sun, the Moon and the daytime sky.

Each source from the above presents its own peculiar problems in terms of the experimental conditions and requirements. A variety of accuracies of the polarization, of time resolution, and spectral resolution are required. For all measurements the polarimetric standard error depends on the brightness of the object, on the integration time and on the efficiency of the polarimeter. The whole solar disk has almost zero polarization, and high accuracy is required to detect any time-dependent polarimetric variations resulting from solar activity and the movement of active regions across the apparent disk caused by the solar rotation. In particular it is important to keep instrumental polarization to a minimum, hopefully lower than what is generally achieved in stellar work. The problem of designing equipment to measure the integrated light from the whole disk of the Sun is not a trivial one, as has been commented on by Rutten and Cram (1981). The whole disk provides an embarrassment of signal which invariably requires attenuators. The Sun subtends 0.54° and this may pose problems in feeding light from its whole image through the analysing equipment.

Studies of lunar polarization have problems such as tracking a particular site for measurements. The albedo is unequal over the lunar surface with differences which are wavelength dependent; inaccurate tracking introduces noise as well as not knowing what exactly has been measured. Telescope tracking is required for both solar and lunar studies.

Both the solar and lunar studies require spectropolarimetry with high spectral resolution and care must be taken when combining a polarimetric modulator with a spectrometer. For example, mechanical rotation of polarimetric elements can affect the angles of light beams, so causing wavelength displacements of the passbands being monitored. Even if the polarization strength is reasonably high, extremely accurate

measurements are still required to distinguish changes of polarization across the structure of spectral lines.

The experimental problems are different for measurements of the zenith daytime sky; the telescope remains fixed but the intensity and polarization are changing continuously during the course of the observations. Each measurement is smeared and repeated values cannot be obtained for statistical investigation of self-consistency.

Before proceeding further and presenting the background to the observational work on the Sun, the Moon and the daytime sky, it will be useful to define the polarization more specifically.

1.2 Stokes parameters.

The attributes of the "polarization" of a beam of electromagnetic radiation are conventionally described by Stokes parameters (Stokes 1852; and see more modern descriptions, in texts by Shurcliff,1962, and Clarke and Grainger,1971). Very briefly, they may be described as follows.

The electric disturbances associated with a continuous electromagnetic wave can be resolved into two orthogonally polarized components in a fixed plane perpendicular to the direction of travel. The disturbances in this plane may be expressed as

$$E_x = E_{xo}\cos(\omega t + \delta_x) \qquad \text{and} \qquad E_y = E_{yo}\cos(\omega t + \delta_y)$$

where E_{xo}, E_{yo} are the amplitudes in the x and y directions in the plane; δ_x, δ_y are the respective phases, ω is the angular frequency of the wave, and t is time referred to some agreed arbitrary origion.

In this plane, the locus of the tip of the electric vector as a function of time is an ellipse. Two special cases of interest are linear and circular polarization. These occur under the following conditions :-

linear if $\delta = (\delta_y - \delta_x) = m\pi$ where m is an integer.

circular if $E_{xo} = E_{yo}$ and $\delta = (\delta_y - \delta_x) = \pm \frac{\pi}{2}$

In general the electric field behaviour associated with radiation from a source is more complicated, comprising a mixture of classical waves whose amplitudes, directions of vibration and phases are varying in some way. The state of polarization of the total disturbance can be described by the Stokes parameters, viz.:

$$I = <E_{xo}^2 + E_{yo}^2>$$

$$Q = <E_{xo}^2 - E_{yo}^2>$$

$$U = <2E_{xo} E_{yo} \cos(\delta_y - \delta_x)>$$

$$V = <2E_{xo} E_{yo} \sin(\delta_y - \delta_x)>$$

where the expectation values (< >) are determined over the experimental time and over all the wavelengths included in the passband of the equipment. The term I describes the total intensity of the light beam, Q represents the difference of intensity of linear polarization for the components along the x and y axes; U represents the difference of intensity of linear polarization between orthogonal axes at 45° to the x-axis. The Q and U parameters allow the orientation of any linearly polarized light or the major axis of any elliptically polarized light to be described. The fourth parameter V, represents the circular polarization and its sign describes the sense of the handedness of this polarization. The Stokes parameters describing a mixture of incoherent beams of light are the sum of the respective Stokes parameters describing the component beams.

Generally the Stokes parameters are normalised to the total intensity and written as q=Q/I, u=U/I and v=V/I. The V parameter is not used further here since only linear polarization is dealt with. When describing linear polarization only, the Stokes vector

may be reduced to three elements, i.e. {I,Q,U}. The degree of linear polarization "P" and its azimuth "θ" (direction of vibration) are obtained as follows

$$P=\sqrt{q^2 + u^2} \tag{1.1}$$

$$\theta = \frac{1}{2}\tan^{-1}\left(\frac{u}{q}\right) \quad \text{or} \quad \frac{1}{2}\tan^{-1}\left(\frac{U}{Q}\right) \tag{1.2}$$

The value of P represents the fractional amount of polarization in a light beam and is essentially a positive quantity. However, in the literature the term "negative polarization" is sometimes found and P sometimes take "negative" values. In relation to scattering phenomena, the terms "positive" and "negative" are used to describe the orientation of the vibrations in the scattered radiation. Generally the polarization which is produced by scattering of light has vibrations which are perpendicular to the scattering plane. This kind of polarization is called "positive". But if the vibrations lie in the scattering plane, this polarization is referred to as being "negative". Hence the sign of the polarization is used to describe the orientation of the polarization relative to the scattering plane.

1.3 The Sun.

1.3.1 Introduction.

The Sun provides the opportunity to have a close look at the complex detail of magnetic active regions in a stellar atmosphere, something which cannot be done with stars themselves as they appear only as points of light even in the largest telescopes. It therefore serves as a giant nearby "astrophysical laboratory" whereby detailed measurements can be made to understand the physical effects that must also occur in other stars particularly of the same spectral type. Indeed the Sun is the only star whose surface can be studied in detail and it acts as a special observational case of a star. Solar-stellar connections (studying the Sun as a star and vice versa) have been used to provide information related to stars about positions and size of magnetic active regions, the influence of activity cycles, and rotation periods. Most of the work related to solar-stellar connections has been in the area of spectrophotometry. Little or nothing has been attempted using polarization. In this introduction a short review will be given as to some of the simple results that have emerged from spectrophotometry and indications will be presented as to how polarization might play a role in solar-stellar studies.

The first step in making any solar-stellar connection is to identify solar-type behaviour in other stars. Such observations started when Eberhard and Schwarzschild (1913) discovered the CaII H and K emission lines of ionized calcium in stellar spectra. They also noted that some stars have much more calcium emission than the Sun. The CaII H and K lines are formed in the upper photosphere and lower chromosphere, so they have been used to investigate the structure of the chromosphere where most activity is generated within the Sun and stars . As will be described later, studies of the variable emission lines in stars can lead to determinations of rotation periods; for reference purpose, the technique has also been recently applied to the Sun (e.g. see Singh and Livingston, 1987).

1.3.2 The Sun as a star.

Sheeley (1967) has observed the total variations of CaII emission caused by solar activity which in turn depends on the phase of the solar activity cycle. His observations suggest that the intensity of the solar K_2 emission line (bright emission peak within the K line core) varies by up to 40% over the sunspot cycle. Similar results have been noted by Jebsen and Mitchell (1978) and White and Livingston (1981). Bumba and Ruzickova-Topolova (1967), found that there are daily fluctuations of solar activity in the intensities of the core of the CaII K line in integrated sunlight. Figure(1.1) represents variations of the mean of the intensities of K_{2V} and K_{2R} for each day of observation, as compared with Waldmeier's synoptic chart of the solar photosphere for the relevant solar rotation. The K_{2V} and K_{2R} are the violet and red emission peaks on either side of the K line centre, K_3; their positions are illustrated in Figure (1.2).

Bappu and Sivaraman (1971) reported that time variations of the apparent area of a plage on the visible disk of the Sun provided a clear signature of solar rotation. Their observations of the calcium plage areas on the visible disk of the Sun during 1960 to 1962 have been reproduced in Figure (1.3), where the rotation period can be seen within the noisy fluctuations; the rotation period is best seen in the spikes corresponding to minimum area. The change of the amplitudes of variation from sunspot maximum to minimum has also been detected (note the level difference between 1960 and 1962). Detections of solar rotation by observing the whole solar disk and using CaII lines have been described by many authors such as Bappu and Sivaraman (1977), White and Livingston (1978 & 1981), LaBonte (1982), Stimets and Londono (1982), Oranje (1983a), Keil and Worden (1984). Recently Singh and Livingston (1987) have published observations of the K-index (area of the K line profile as bounded by a 1Å band centred on the line centre, i.e. an equivalent width of the line core) for the period from January 1983 to January 1984. Figure (1.4) displays

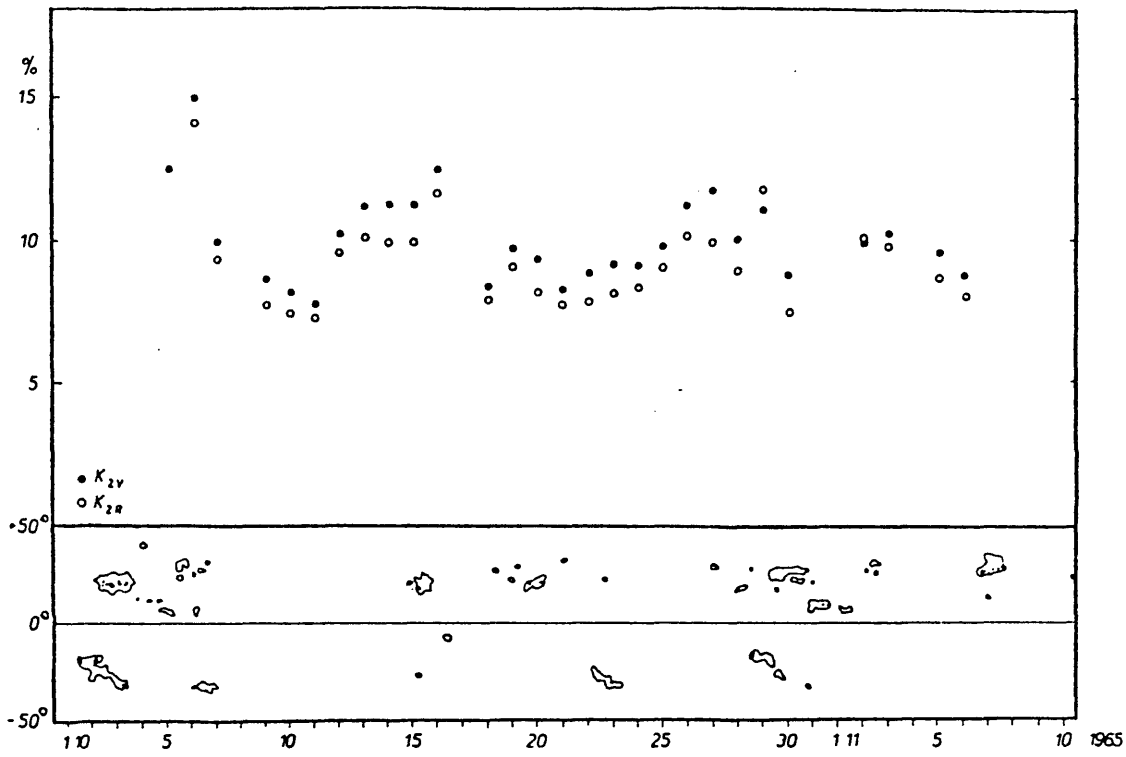

Figure (1.1) The variations of intensity values for K_{2V} (dots) and K_{2R} (open circles) in percent of the continuum, as compared with Waldmeier's synoptic chart of the photosphere for the period of observations (1965 October 5 to November 6). (Taken from Bumba and Ruzickova-Topolova, 1967).

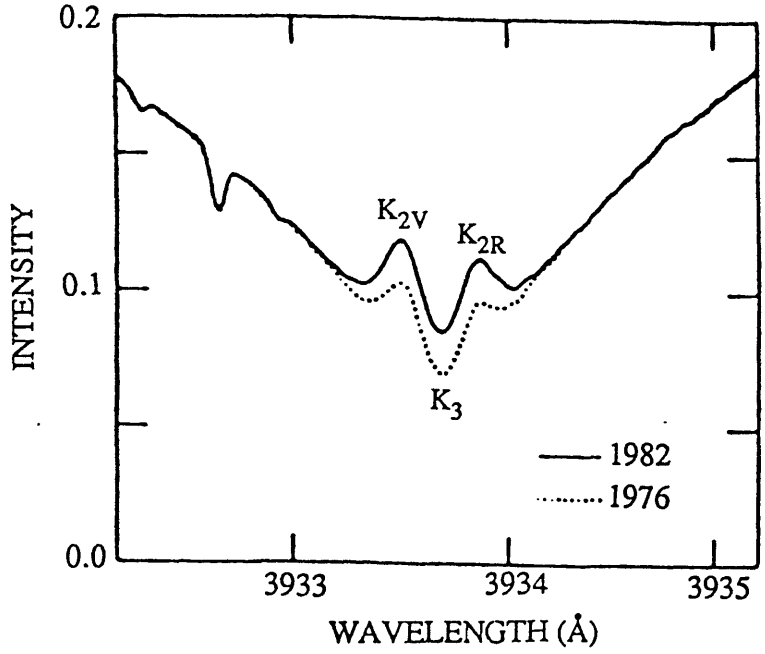

Figure (1.2) The core of the K line as observed in 1976 (near solar minimum) and 1982 (after solar maximum). (Taken from Keil and Worden, 1984).

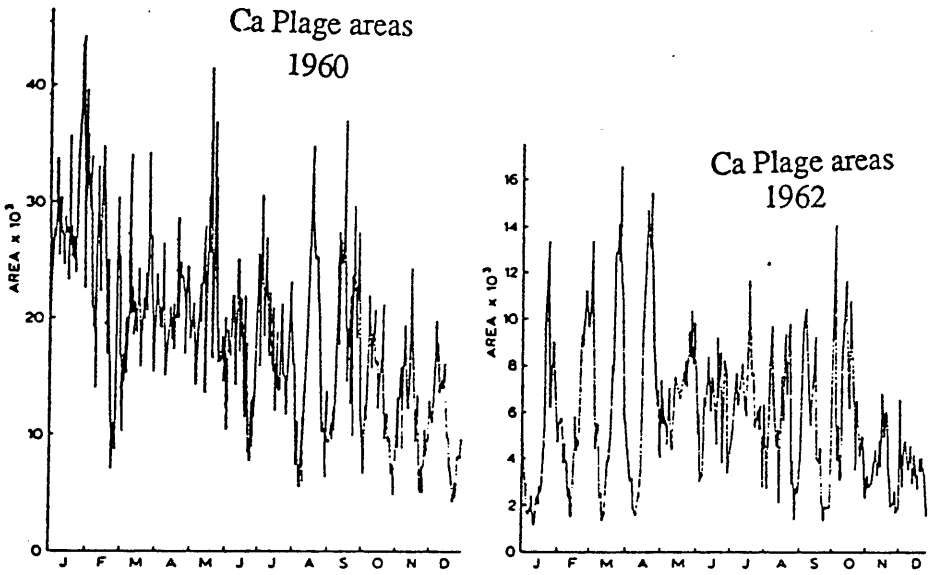

Figure (1.3) Plot of Ca plage areas (mean daily areas) for the years 1960 and 1962. The area is in millionths of visible hemisphere of the sun. (Taken from Bappu and Sivaraman,1971).

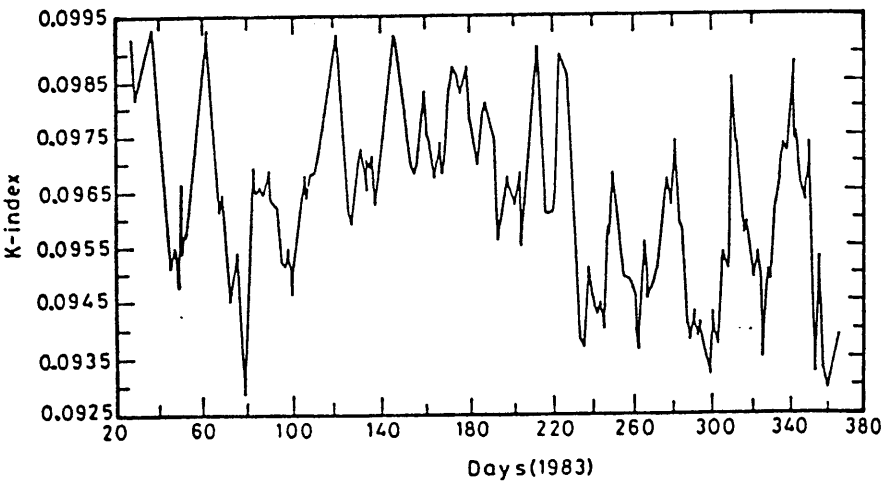

Figure (1.4) Variation of K-index of the Sun as a star for the period from January 1983 to December 1983. (Taken from Singh and Livingston,1987).

their results and clearly indicates the presence of the 27-day rotation period. Observations of chromospheric lines in many stars exhibit similar characteristics to those of the Sun, revealing counterparts of sunspots, flares, coronal holes, etc. Oranje (1983b) found, by comparing solar and stellar CaII K emissions, that the more active stars have plage surface cover of up to 65% of the total disk. Vaughan et al.(1981) observed 46 lower-main-sequence stars and they found 19 of them exhibiting evidence for rotation from their H and K flux variations. Furthermore these results give strong indication that the mean H-K flux output of a star is a function of its rate of rotation. Examples of the data clearly indicating rotation are shown in Figure (1.5). Similar conclusions emerge from the NASA X-Ray satellite observations of lower-main-sequence stars (see Vaughan, 1981). Wilson (1978) concluded that main sequence stars have a cycle of H-K flux variation which increases with later spectral type, see Figure (1.6). The solar activity behaviour fits well with these trends.

The use of polarimetric measurements to diagnose distortions in the homogeneity of the radiation field of a star has been successful both with respect to several classes of early-type stars and late-type supergiants. Both classes show intrinsic polarization of as much as 1% or 2% often with a time dependence. Reviews have been made on polarization results for both spectral types e.g. see Coyne and McLean (1982) for early-type stars and Schwarz (1986) for late-type stars. For this latter category, activity within the photosphere/ chromosphere appears to be the origin of the polarization in connection with subsequent scattering. Intrinsic polarization for solar-type stars is at a much lower level. However, Tinbergen and Zwaan (1981), and Huovelin et al. (1985), have observed linear polarimetric variations in G and K type dwarfs. Spectropolarimetric studies of the whole solar disk are likely to help in developing solar-stellar connections.

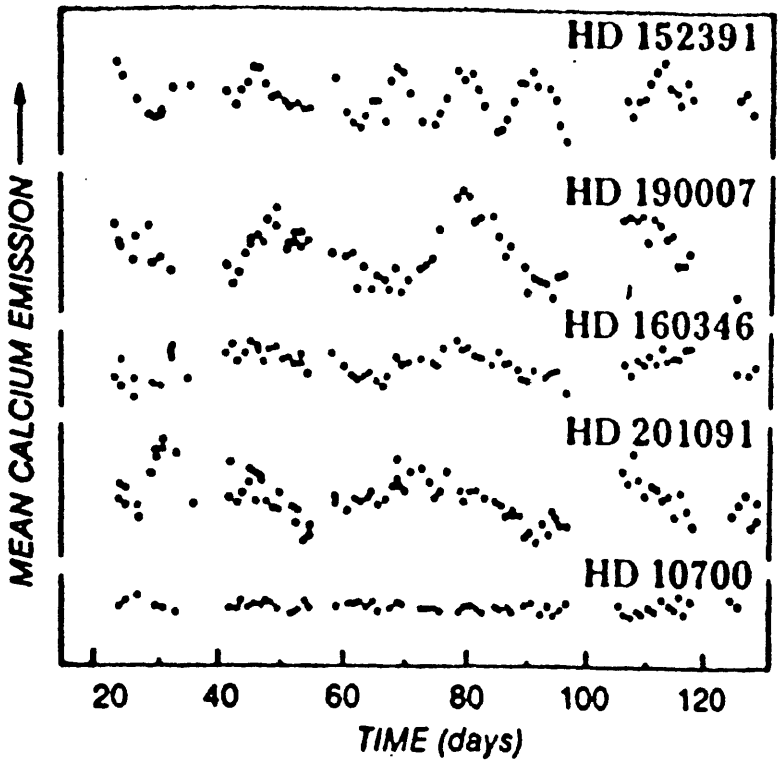

Figure (1.5) Variations of Ca emission from solar type stars, indicating stellar rotation. (Taken from Vaughan et al.,1981).

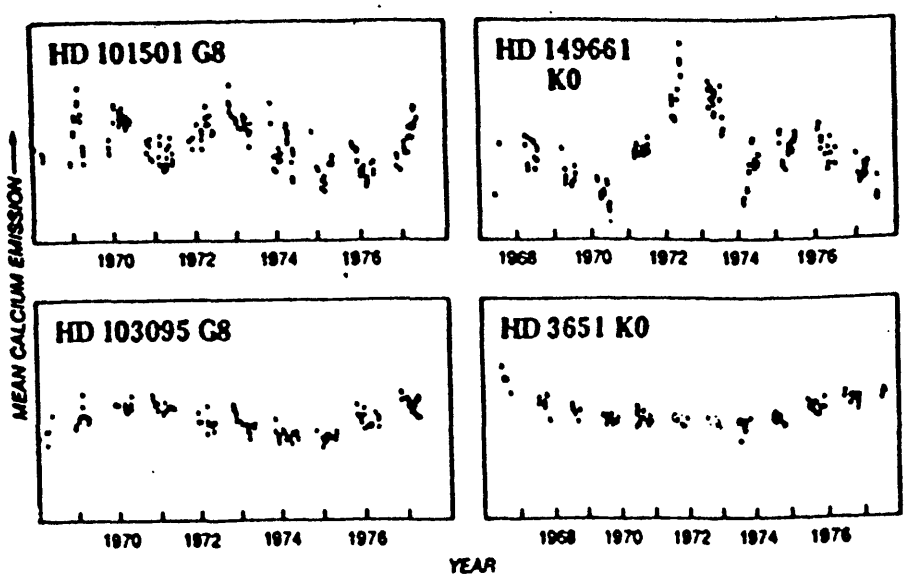

Figure (1.6) Stellar cycles, analogous to the 11-year solar cycle, in the calcium emission from a number of stars like our Sun. (Taken from Wilson,1978).

Full solar disk observations were started at Glasgow Observatory in 1984. The objective of the programme is to measure the net polarization of the whole solar disk both within individual spectral lines and with broad bands to detect any time variations, as the solar rotation moves active regions across the apparent disk. The next sections present the background to the reasons for undertaking such solar polarimetric studies.

1.3.3 Solar polarimetric studies.

From studies of specific regions on the Sun, linear polarization has been observed both in the continuum spectrum and within spectral lines. Continuum polarization may originate from Rayleigh scattering (by atoms), Thomson scattering (by electrons) or by radiative transfer processes. Within solar spectral lines, either the transverse Zeeman effect or coherent scattering can produce polarization.

Measurements of strong solar magnetic fields within spots are generally made from direct observation of polarization in spectral lines. The general solar magnetic field is too small for the transverse Zeeman effect to be recorded outside active regions. Any net polarization from the whole solar disk generated by the Zeeman effect represents the contributions of the active regions substantially diluted by the total light. Over a uniform disk coherent scattering generates polarization increasing in magnitude from the centre towards the solar limb, where the scattering angle is about 90°. The integrated polarization should, however, be zero because of radial symmetry. The situation is different when there are localised active regions and the question is raised as to what overall polarization these might produce.

The first polarimetric measurements of the Sun were by Redman (1941) who used the resonance line CaI 4227Å to measure the polarization near the solar limb. He noticed that the intensities of profiles recorded with direction of vibration selected to be

perpendicular to the limb are not the same as observed with the orthogonal vibration. He concluded that the light was polarized at the limb. The CaI 4227Å line has also been investigated by Brückner (1963) and Wiehr (1975). They found no polarization at the core of the line but only in the line wings, the polarization profile taking on the appearance of an intensity absorption line, (see Figure 1.7a,b). Contrary results have been reported by Stenflo et al. (1980), who observed polarization at the core of the same line from areas of the disk of ≈ 7" (sec of arc) from the limb, (see Figure 1.7c). Stenflo et al. (1983 a,b) have also presented a survey of the linear polarization in the solar spectrum from 3165Å to 9950Å, recorded at 10" inside the solar limb at the heliographic north pole. These last results indicated that the polarization variation through the core of the CaI line was similar to the previous measurements but the strength at the 10" position is lower by a factor of two relative to the 7" position, (see Figure 1.7d). These disparities in the results could possibly ensue from a variation of the Hanle effect (see below).

Polarimetric observations on the solar disk have also been undertaken to investigate the centre-to-limb variations (CLV). These have been performed both in broadband and within Fraunhofer lines. The polarization is measurable at the limb but falls off quickly towards the solar centre. Mickey and Orrall (1974), reported CLV of broadband linear polarization at 5834Å and 6034Å. With high spectral resolution Stenflo et al. (1980) have measured CLV of linear polarization within the CaI 4227Å and CaII H & K Fraunhofer lines, (see Figure 1.8). Sharp increases in the polarization near the limb reflect the rapid increase of coherent scattering as the density (and hence the collision rate) decreases with height in the solar atmosphere. Stenflo (1974), Stenflo et al. (1980) and Wiehr (1975, 1978,1981) have reported the CLV of polarization for many resonance spectral lines. Linear polarization on the quiet solar disk increases from 10^{-5} (0.001%) near the centre to 10^{-3} (0.1%) or higher close to the limb.

Other solar polarimetric observations have been made by Leroy (1972). He found that the polarization along the Sun's equatorial radius is 10% higher than that of the

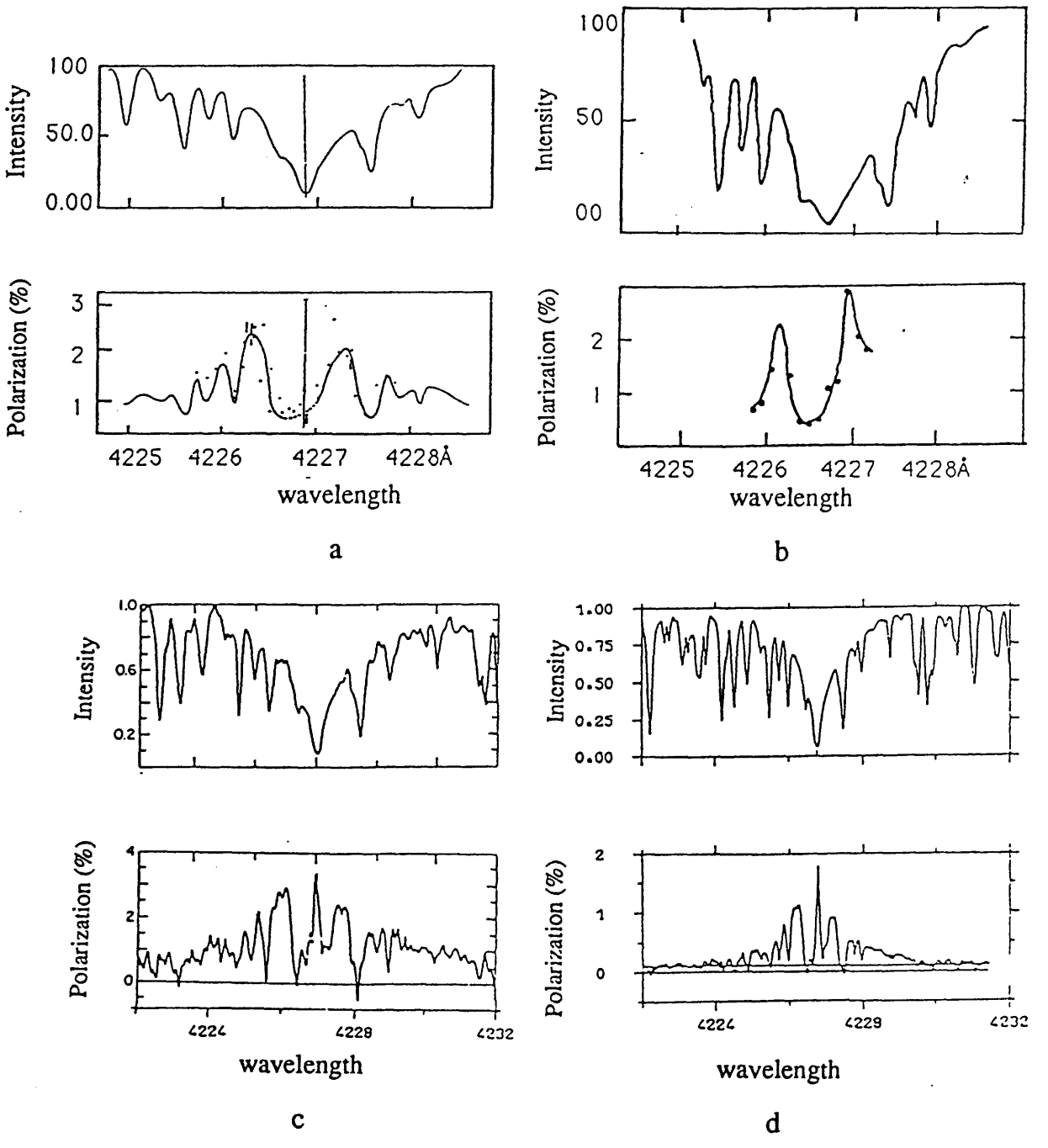

Figure (1.7) Intensity and linear polarization profiles through the CaI line, near the solar limb. Taken from a- Wiehr (1975), b- Brückner (1963), c-Stenflo et al. (1980), and d-Stenflo (1983a).

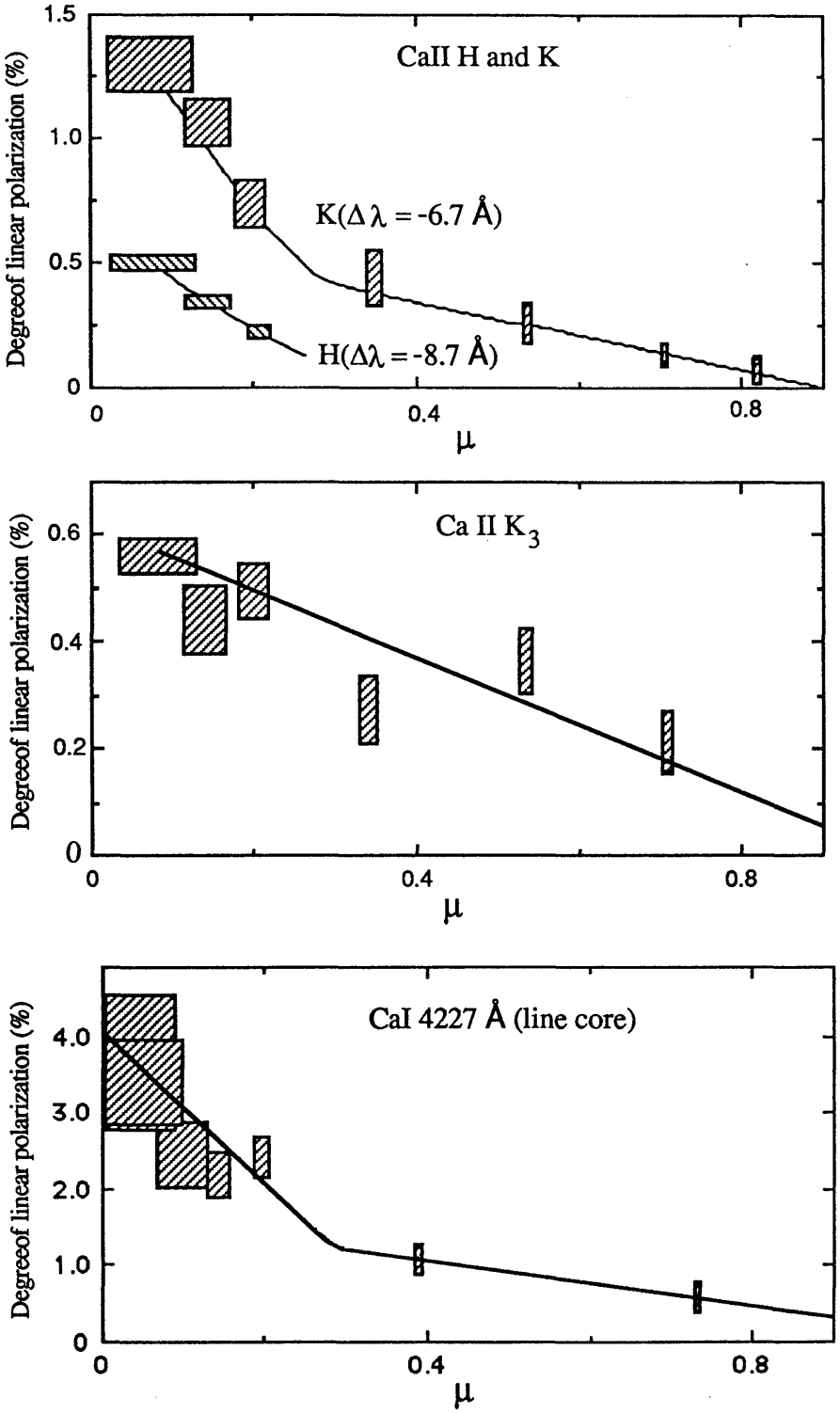

Figure (1.8) Centre-to-limb variations of the polarization in the blue wings of the CaII H and K (top), the CaII K_3 core (mid), and the core of CaI 4227Å (bottom), $\mu = \cos \emptyset$ where $\emptyset$ is the angle between the emergent ray and the normal to the solar surface. (Taken from Stenflo et al.,1980).

polar radius (see the upper part of Figure 1.9); in other observations along the polar radius across a plage, there was a remarkable decrease in the polarization (see the lower part of Figure 1.9).

1.3.4 The Hanle Effect.

If atoms are in a region of a magnetic field, splitting of their energy levels occurs. This is manifested by splitting of the spectral lines in the spectrum of the radiation they emit or absorb. The phenomenon is known as the Zeeman effect. Separation of the Zeeman components can be calculated from the expression, viz.

$$\Delta\lambda = \pm 4.67 \times 10^{-13} g H \lambda^2 (\text{Å}) \qquad (1.3)$$

where $\Delta\lambda$ (Å) is Zeeman displacement, λ is the undisturbed wavelength, H is the magnetic field strength (gauss), and g is the Landé factor. In order to detect the effect, the magnetic field should be strong enough to introduce a measurable displacement greater than the natural line width. If the magnetic field is weak, Zeeman splitting will be too small for detection. However the presence of the weak field might be investigated through the Hanle effect (discovered in 1924 - but see recent translation of this work by Moruzzi and Strumia, 1991) and resonance scattering polarization.

As described in Mitchell and Zemansky (1961), the sensitivity of the resonance polarization to the orientation of a weak magnetic field can be explained in terms of a classical atomic damped oscillator. The effect will be equivalent to a precession of the oscillation axis at the Larmor frequency,ω, around the magnetic field direction. The results are a decrease of the degree of polarization and a rotation of its plane, depending on the strength and the direction of the magnetic field. In terms of the linear polarization, with the dominant vector parallel to the solar limb, the Hanle effect reduces the polarization, and rotates the direction of vibration through an angle $\varnothing$. The polarization

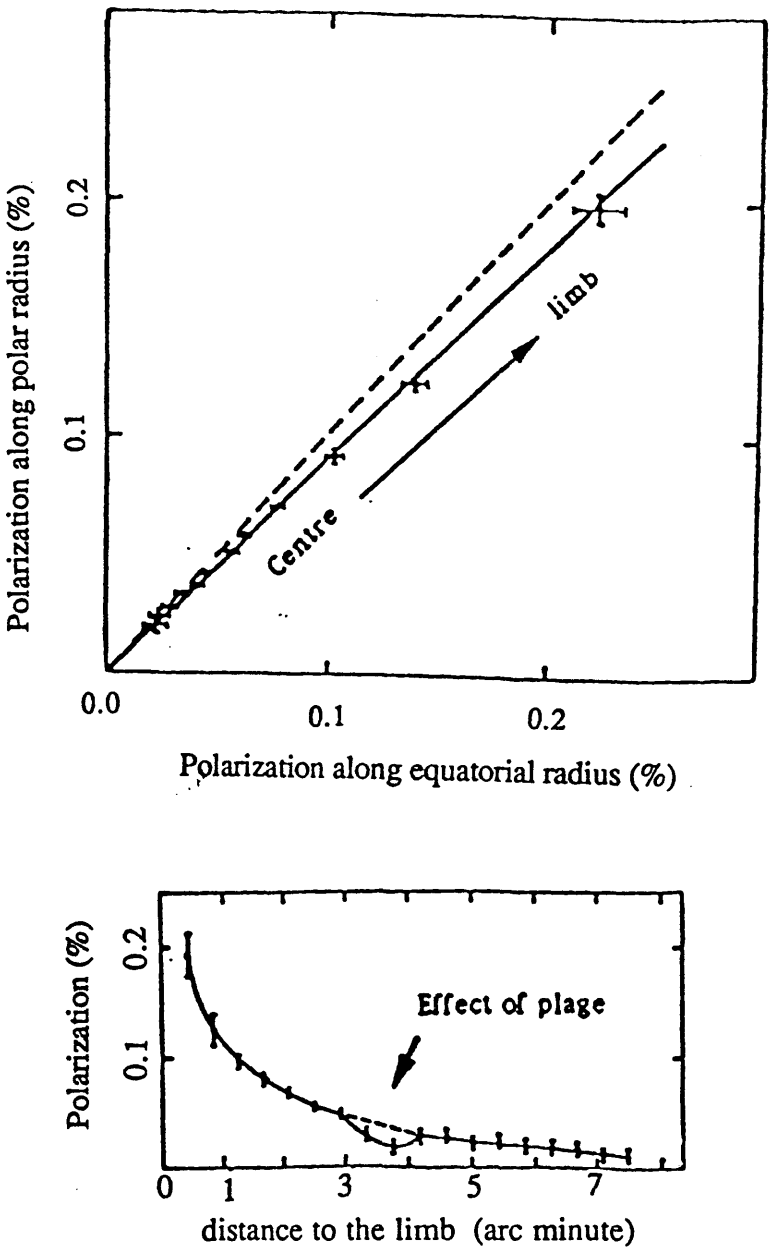

Figure (1.9) Upper- a diagram of polarization measured along an equatorial radius and a polar radius. The dashed line repesents the condition of the polarization being identical along the two radii. Lower- a scan along a solar radius including a plage. (Taken from Leroy, 1972).

reduction (depolarization) Γ, is given by

$$\Gamma = \frac{P_m}{P_*} = \frac{1}{\sqrt{1 + (2\,\omega\,t)^2}} \qquad (1.4)$$

where P_* is the polarization produced by resonance scattering with no magnetic field present, and P_m is the value with a magnetic field, t is the radiative life time = $1/\upsilon_{CL}$, (υ_{CL} is the classical damping constant), $\omega = \frac{e\,H\,g}{2\,m_e c}$, e is the electron charge, c is speed of light, and m_e is the electron mass. The classical expression for the damping constant = $0.22/\lambda^2$ sec^{-1} (where λ is in Å), which is of the order of 10^8 Hz, Minnaert (1953). The rotation $\varnothing$ of the polarization is given by

$$\varnothing = \frac{1}{2} \tan^{-1} (2\omega t) \qquad (1.5)$$

The effect of the magnetic field on the linear polarization can be explained by considering Figure (1.10). As radiation travels from the Sun to the observed point O (lying along the Z axis) one observes scattered light with polarization P_* with plane of polarization parallel to the OX axis. So if there is a weak magnetic field present at the region of scattering, P_* will be modified, this depending on the direction of the magnetic field with respect to the observer. The magnetic field vector is characterized by $\underline{H}$. This latter vector is at angle Ω with respect to the Z axis and its projection onto the XY plaine is at angle Ψ with respect to the line of sight. If the magnetic field direction is normal to the photosphere (along OZ, Ω=0°) it will not affect P_*. On the other hand, a transverse, magnetic field (along OX, Ω=90° and Ψ =90°) will decrease the degree of the polarization without altering its plane of polarization, still being parallel to the OX axis. Further, a longitudinal magnetic field (along OY, Ω=90° and Ψ =0°) will cause both a reduction of the degree of the polarization and a rotation of its direction of vibration by an angle $\varnothing$ (see Equation, 1.5).

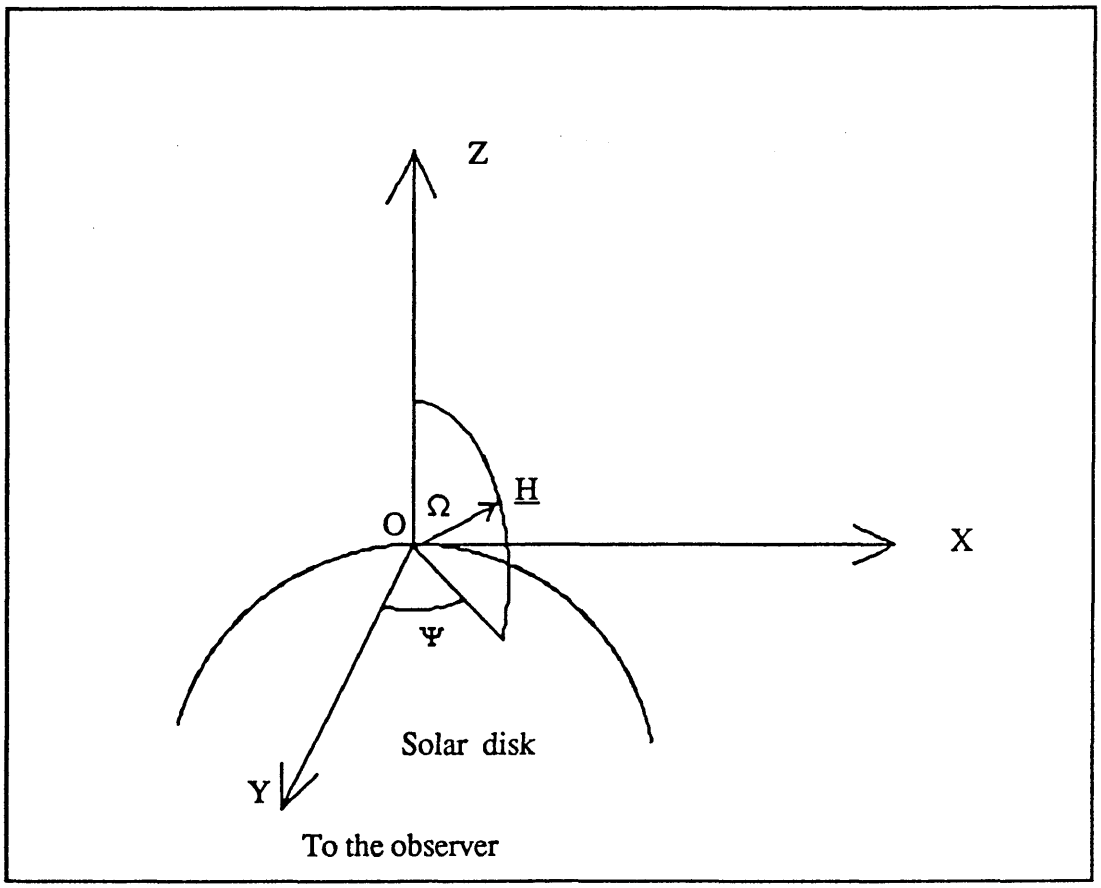

Figure (1.10) Co-ordinate system for describing the Hanle effect on the solar limb.

The first observation of the Hanle effect on the solar disk was made by Stenflo (1981). By using a frame of reference parallel to the limb, the polarization by ordinary resonance scattering would be described by the value of Q only, with U=0. However, Stenflo's observations of the core of the CaI 4227Å line in the spectrum of a plage clearly indicate that U has a non-zero value (see Figure 1.11) which means that the plane of polarization is not parallel to the limb. Calculation from the Stokes parameters, Q and U, shows that the direction of vibration of the linear polarization in the Doppler core has been rotated by 33°. The polarization in the wings is unaffected.

1.3.5 Whole disk polarization.

All the different effects above in association with the existence of active regions may cause some disturbance to the net polarization of the whole solar disk. An estimation for the net polarization of the whole solar disk, in Fraunhofer lines, was made by Stewart (1984). The proposed mechanism for his model was based on the presence of a magnetic spot whose brightness introduces an asymmetry around the annulus in which the spot is contained. So the net polarization from the whole solar disk will be a function of the spot brightness, position (relative to the limb), and size; also limb darkening has been taken into account. In this thesis this model has been modified to include the Hanle effect associated with a weak magnetic field. Predicted values as high as 1.5×10^{-4} indicate the possibility of measuring net polarization from the whole solar disk (see Chapter 2).

It is also worthwhile noting that Leroy and LeBorgne (1989) have considered a mechanism based on a magnetic saturation effect associated with Zeeman splitting. They have estimated that in the U spectral band, the polarization degree which would be measured if one active region only was present on the Sun, would be 0.0021×10^{-4}. This is an extremely low figure and would be virtually impossible to detect. Such a value is about 10^3 times lower than is currently measurable in stars. Their prediction is based

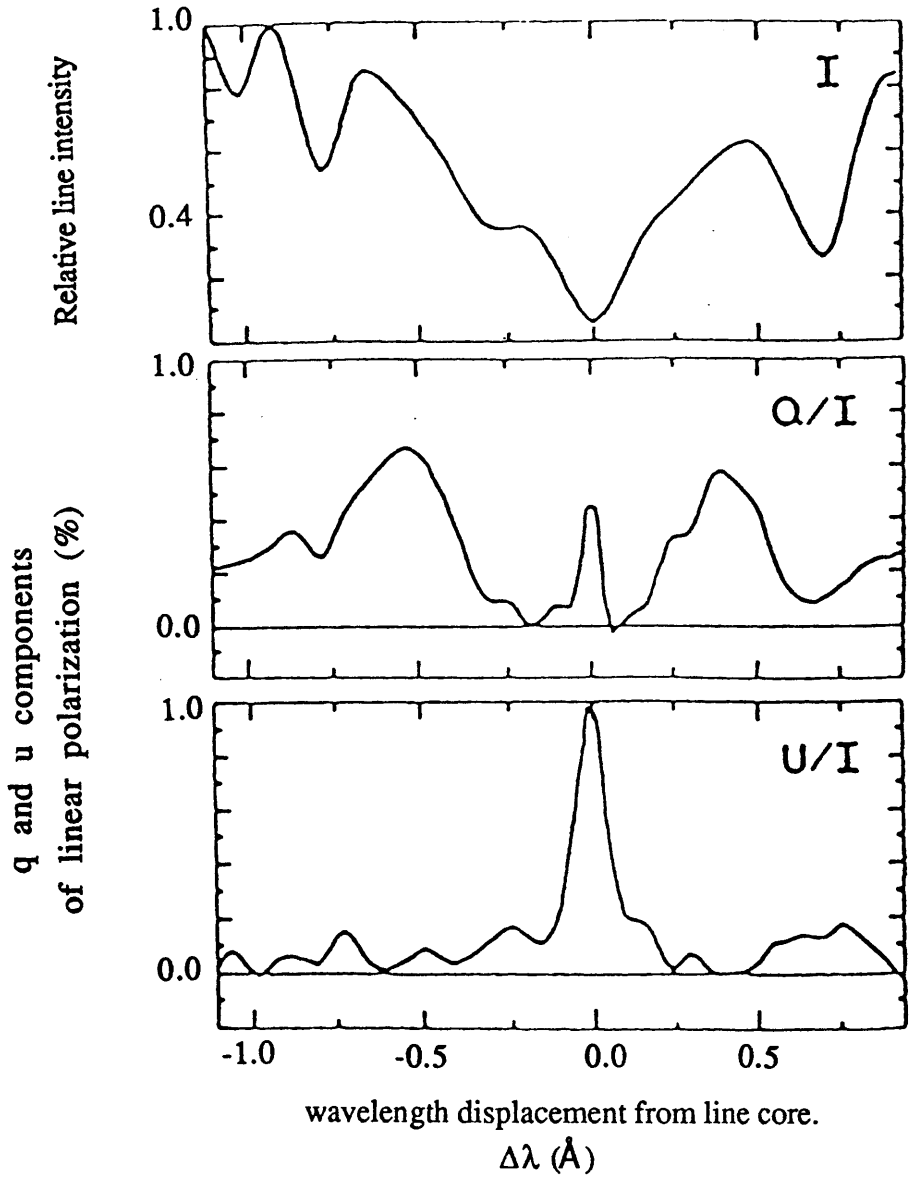

Figure (1.11) Simultaneous recordings of the intensity and the normalized linear Stokes parameters around the centre of the CaI 4227Å line, illustrating the Hanle effect, in a plage area 70 sec of arc inside the east solar limb. (Taken from Stenflo,1981).

on one mechanism only and not on a well defined model involving the position of the spot, the geometry of the magnetic field and limb darkening effect. However, this pessimistic value need not rule out the motivation for experimentation.

1.4 The Moon and The Blue Sky.

1.4.1 Introduction.

The lunar surface, being unprotected either by an atmospheric or a magnetospheric shield, is continuously subjected to the corpuscular and electromagnetic radiations from the Sun. Lunar brightness anomalies are associated with total eclipses; large variations in the brightness level of the eclipsed Moon have been noticed for centuries. The Anglo-Saxon Chronicle, (Ingram 1913), mentions a dark eclipse in 1110. In 1588, Kepler described the disappearance of the Moon during the total eclipse in that year as being affected by the abundance of mists and smoke in the atmosphere, preventing the sunlight penetrating the Earth's atmosphere and refracting to the Moon's surface, (see Keen, 1983). In 1946 Link noted that even at the time of full eclipse, the angular extent of the corona would provide a source of ultraviolet radiation with direct illumination of the lunar surface. He suggested that this energetic radiation might excite minerals on the Moon's surface causing them to fluoresce or luminesce in the optical region of the spectrum. He concluded that the Moon's surface, at least in some locations, luminesces. Link's work summarised in his book - see Link (1969) - represents the commencement of an interest in the brightness behaviour of the Moon in terms of general levels of luminescence and its possible fluctuations.

Sudden anomalous brightness changes at specific regions of the Moon's surface or Transient Lunar Phenomena (TLP), have been reported over the years. Many observers

have reported a glow on the Moon in various spectral regions; the effect has been ascribed to luminescence of minerals comprising the rocks on the lunar surface and to gaseous emission [see, the recent article by Camern, 1991]. However the reporting of such events is very much open to question as many are based simply on visual observations. Here, the discussion will concentrate on the observation of the general levels of luminescence as observed by a particular technique.

A method of investigating luminescence, named by Link as "Central intensity of Fraunhofer lines in the lunar spectrum" involves comparison of the profiles of Fraunhofer lines in lunar light and sunlight. Latterly this method has been referred to by Grainger and Ring (1962c) as the "Line Depth Method" (LDM). If the light from the Moon is pure scattered sunlight, its spectrum, allowing for a wavelength dependent albedo, would be a replica of that of the Sun. The shapes of the absorption line profiles would be identical to the solar Fraunhofer lines. However, if luminescence is present with broad spectral bands, then the lunar line profiles will be shallower, the luminescent intensity affecting the line bottom more than the adjacent continuum.

Absorption Fraunhofer lines of the solar spectrum have a depth which can be defined as the ratio of intensity, I_L, at the centre of absorption line to that, I_C, at the nearby continuum level. An accurate determination of the amount of radiation responsible for any line depth change is possible only if the luminescent radiation has a broad spectral distribution compared with the width of the observed absorption line. If the lunar surface emits radiation of its own (luminescence) in the spectral region occupied by the absorption line, it will be added both at the wavelength of the line centre and to the adjacent continuum. Thus the line ratio measured in lunar light will be altered relative to that of the Sun. (See Section 2.1 and Figure 2.1 for a full algebraic treatment).

Blamont and Donahue (1960) attempted to observe lunar luminescence using the Na D lines but their results were nullified because they compared lunar profiles with sky

profiles and not the solar ones directly, this leading to the discovery of the sodium dayglow. Grainger and Ring (1962a,b), observed the H & K Fraunhofer lines of CaII in daylight spectra and they too were not as deep as in lunar spectra, giving evidence of the existence of light added to the scattered light in the atmosphere. Their measurements also indicated the presence of a lunar luminescence. Also, they concluded that this added light had a broadband spectrum rather than a sharp emission feature central to the line. Thus the LDM has application to both lunar and atmospheric studies and these two topics are now briefly reviewed.

1.4.2 Lunar luminescence.

Many observers have applied the LDM to detect lunar luminescence. Dubois (1959) used photography, and found luminescence of 4% to 25% at wavelengths ranging from 4300Å to 6563Å at more than 40 lunar sites. It was higher on maria than on continents, and it varied appreciably with time. Also using photographic detection, Kozyrev (1961) found that there was luminescence of 16% at Aristarchus, across the CaII H and K Fraunhofer lines. Using a photoelectric scanner with better photometric accuracy than photography, Grainger and Ring (1962c) and Grainger (1963) observed luminescence values ranging from 2% to 10% in the CaII K line. Spinrad (1964) made photographic measurements of the CaII H and K lines of Jupiter and the whole Moon, and noted a substantial filling-in of the lunar lines. Scarfe (1964) with a photoelectric spectrometer used Hα, the sodium D-lines, and a group of FeI lines near 5450Å, to observe luminescence. He found no luminescence at Hα and the D-lines while a variable luminescence reaching as much as 30% was observed near 5450Å. Wildey (1964) used the CaII K line to measure residual intensities of the line centre on different parts of the Moon's surface and for the blue daytime sky. He found that the ratio of the average residual intensity at the centre of the line to the intensity in the adjacent continuum, over all

the features on the Moon, is less than that of the blue sky. Thus as the sky provided shallower profiles than those of the Moon, this confirmed that the filling-in effect is substantially stronger for the daytime sky relative to the Moon.

Righini and Rigutti (1966) obtained a long run of photographs at 6550Å and 5900Å using interference filters, and found no evidence at all for luminescence or time variations. McCord (1967) used photoelectric spectrometry of the CaII H and K Fraunhofer lines to detect the luminescence during six lunations on many different regions; the luminescence was very small and not greater than 5%. Chanin et al. (1982) used the potassium and the sodium lines, 7699Å and 5900Å respectively, to observe the luminescence. They found luminescence as high as 40%, and with wavelength dependence (40% at 7699Å to 15% at 5890Å); the values reduced to a few % after a few days. Figures (1.12) and (1.13) represent their observed dependence of the luminescence on the lunar phase and wavelength. Potter and Mendell (1984), observed the luminescence at Aristarchus using many different lines. The effect was there, but it was found to depend on the equivalent widths of the observed lines rather than having a general wavelength dependence (see Figure 1.14). Returning to the descriptions of the darkness of lunar eclipses, according to Kopal (1965), Danjon in 1920 has reported that the visual brightness of total eclipses depends on the sunspot cycle. Kozyrev (1963) concluded from his observations that the existence of a luminescent glow was not the same for different lunations but there appeared to be no connection with the level of solar activity. Thus there is controversy as to the influence of solar activity.

From all of the above reports, if taken at face value, it can be concluded that line filling-in is always present and that its strength depends on the lunar site, on the lunar phase and on the chosen line used for measurements. The situation is, however, very unsatisfactory as there is no consistency in the reported behaviour other than it being extremely chaotic. Some of the reported strengths of luminescence seem unbelievably

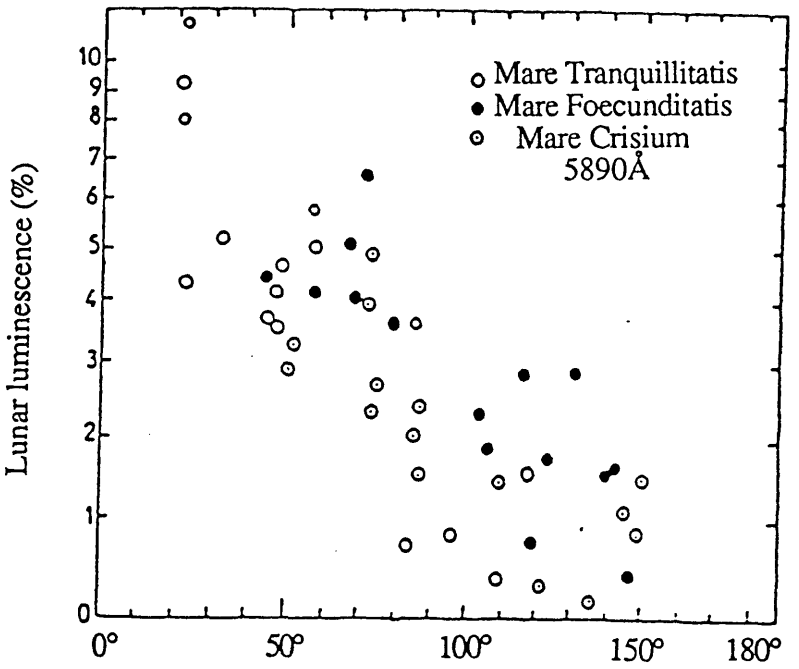

Figure (1.12) The measure of luminescence at 5890Å for Mare Tranquillitatis, Mare Foecunditatis, and Mare Crisium, as a function of the sunrise terminator, 0° corresponding to the sunrise at the given sites. (Taken from Chanin et al., 1982).

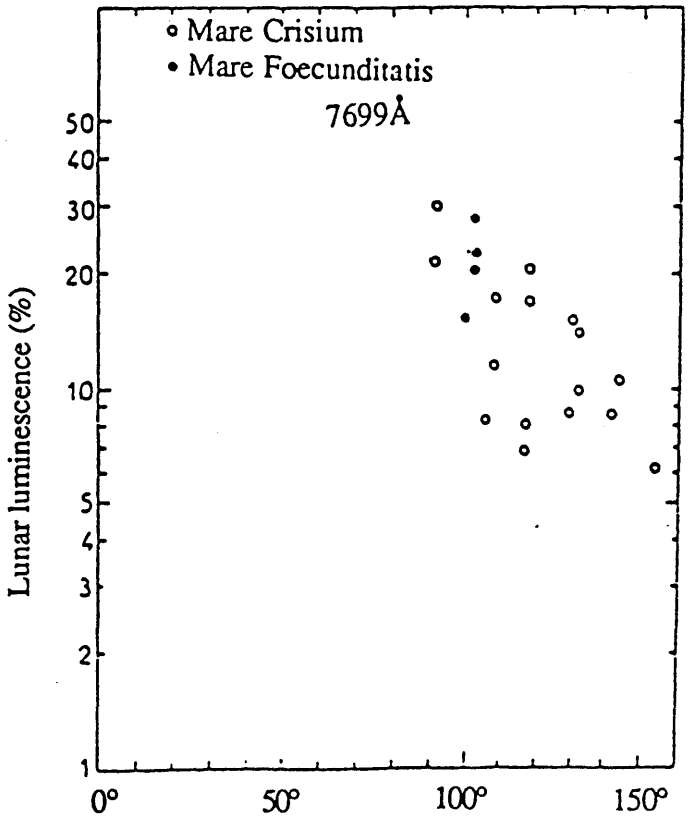

Figure (1.13) The measure of luminescence at 7699Å for Mare Crisium, and Mare Foecunditatis, as a function of the sunrise terminator, 0° corresponding to the sunrise at the given sites. (Taken as above).

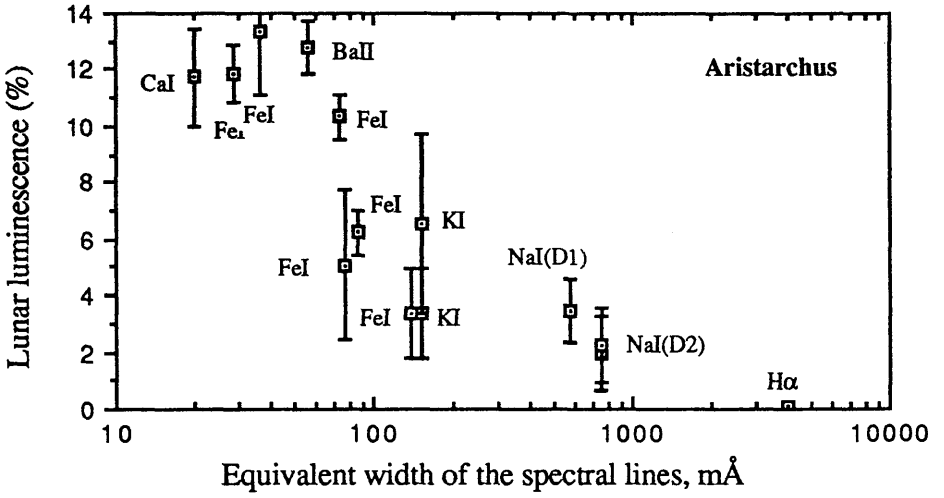

Figure (1.14) Observed variation of apparent lunar luminescence with equivalent width of solar lines. (Taken from Potter and Mendel (1984) and see their Table 1 for details of the wavelength positions of the chosen spectral lines).

high in terms of possible mechanisms for its production.

Various mechanisms for the filling-in of lunar line profiles have been suggested. The original one by Link of a luminescence being energised by short-wave radiation, particularly from the solar corona, has been extended to include the effect of bombardment by the solar wind but Ney et al. (1966) dismissed both these processes as being too inefficient to provide the required fluxes. They suggested an alternative genesis in the form of thermoluminescence. Geake et al. (1970) and Greenman and Gross (1970) found no luminescence in the lunar rocks (Apollo 11) with middle and near ultra-violet excitation.

Rayleigh-Brillouin scattering has also been proposed (Potter and Mendell, 1984) to account for the lunar filling-in but this mechanism cannot be considered as providing a simple additional flux. With this scattering, the change in lunar line depth depends on the original shape of the line profile in the solar spectrum and may depend on the scattering angle.

No matter the source of the excitation, however, all the above effects would act as though an additional light is superimposed in broad spectral bands onto the general scattered light from the regolith.

An alternative method of investigating luminescence is by examining the wavelength dependence of the polarization of the lunar light, as suggested by Teifel (1960). Scattering by a rough surface produces linear polarization with a degree, P, which is approximately inversely proportional to wavelength over the visual spectrum. If the luminescent light has different polarization relative to the scattered light, it will modulate the observed $P(\lambda)$ behaviour over those spectral regions in which it occurs. Previous discussions have considered luminescence as being unpolarized and, if this is the case, its effect will be to reduce the observed degree of polarization produced by the general

scattering from the lunar surface. For a luminescent band covering a Fraunhofer line, the reduction effect will be more pronounced within the depth of the profile relative to its nearby continuum.

In Chapter 5, the first-ever lunar spectropolarimetric observations within line profiles are reported; the polarimetric accuracies of this work are extremely high, even better than any previous broad band measurements. If anything can be deduced from the reported results then, if lunar luminescence truly exists, the added radiation must be *polarized,* a result contrary to all previous assumptions.

1.4.3 The Ring effect in the daytime sky.

The first hint of the filling-in effect in the daytime was by Shefov (1959), who noted that absorption lines in the twilight sky spectrum were shallower than those of direct sunlight. Since this initial discovery, many observers have found the same effect in the absorption lines of the daytime sky spectra. This phenomenon was later to be called the *Ring effect* after one of the discoverers with the name frequently used in the literature. The first report giving quantitative measurements of the effect was that of Grainger and Ring (1962b). They observed a 5% filling-in in the near ultraviolet (3968Å) CaII H line. Noxon and Goody (1965) found that the effect in the blue spectrum (4300Å) and in the yellow (6563Å) was 3% to 1.5%, respectively. Barmore (1975), measured a filling-in of 0.2% to 2% of the continuum at 6300Å.

The magnitude of the added light has been shown to be variable during the daytime; Noxon and Goody (1965) found that the Ring effect decreased as the solar zenith angle increased. In the afternoon it was 3% while two hours before sunset it was 1%, at 4300Å. Similar behaviour has been recorded by Harrison and Kendall (1974). On the other hand, Pavlov et al. (1973), Barmore (1975) and Harrison (1976) found an

opposite trend in that the filling-in increased as the solar zenith angle increased, see Figure (1.15).

There are several suggestions proposed for the mechanism by which the added radiation is produced : (I) Grainger and Ring (1962a) suggested that the daylight airglow causes the filling-in. This was contested by Noxon and Goody (1965), because their high altitude observations revealed that the added light is produced within the lower layers of the Earth's atmosphere and not at high altitude where day airglow originates. (II) Brinkmann (1968) suggested that Raman scattering by nitrogen and oxygen causes the effect by redistribution of the scattered energy to other parts of the spectrum. This idea has been rejected by Noxon and Goody (1965), and Barmore (1975), because the ratio of Raman to Rayleigh scattered light should increase by a factor of about 2 as the solar zenith angle increases from 10° to 90° but this is not observed in the line filling-in changes. (III) Noxon and Goody (1965) and Barmore (1975) suggested that aerosol fluorescence causes the phenomenon. (IV) Hunten (1970) and Harrison and Kendall (1974) have suggested that light reflected by the Earth's surface is altered by Rayleigh-Brillouin effect and is then back-scattered by the air column to contribute to the total observed light, so causing the filling-in effect. This would explain the decrease of filling-in with increasing solar zenith angle. In this case, the amount of line filling-in will depend on the local ground conditions. Related to this proposition, Chanin (1975) reported that the magnitude of the filling-in is greater in winter (when snow covers the ground) than that in summer time (when the ground is grassland or forest), the ground albedos being $\approx$75% and $\approx$20% respectively.

There is a consensus in the literature that the added light causing the Ring effect is unpolarized. Noxon and Goody (1965), found it was very weakly polarized. Barmore (1975) and Kattawar et al. (1981), have also suggested that the added light is unpolarized. Pavlov et al. (1973) have observed the filling-in effect in the H, K, L and N Fraunhofer lines. They reported that the degree of polarization is always 2-6

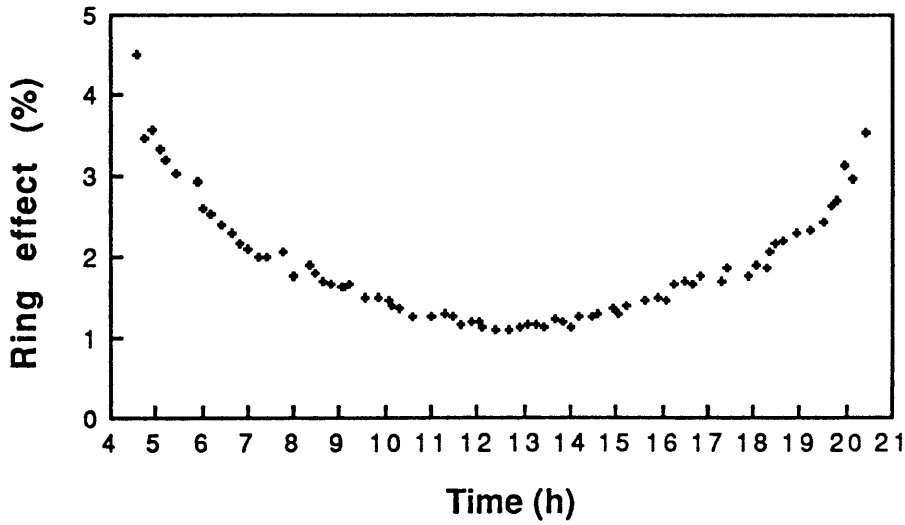

Figure (1.15) Observed variation of Ring effect at 4326Å during the day. (Taken from Harrison, 1976).

per cent lower at the line core of the H and K lines than in the continuum spectra, while in the L and N lines, the depolarization effect is very small or zero. Clarke and McLean (1975c) measured the degree of polarization of the zenith daytime sky at Hβ and found that the reduction in the line centre was commensurate with the added light being unpolarized. All these observations confirm the suggestion that the added light is essentially unpolarized.

Chapter 6 describes the photometric and the polarimetric observations of the filling-in effect at the zenith covering many conditions which might be considered as controlling its behaviour. We will see from the photometric observations with different ground albedos, a strong clue was given that the reflected light from the Earth is not the source of the filling-in.

The chief results are related to the polarization of the light associated with line filling-in. For geometries where the Sun is low in the sky, the Fraunhofer lines exhibit a reduction of the polarization levels - a fact which has helped to contribute to the notion that the "luminescent" light is unpolarized. However, when the Sun is high in the sky, the polarization within Fraunhofer lines has been discovered to be enhanced to a degree which is not explainable by the various mechanisms that are currently being discussed in relation to line filling-in.

The above discussion is related to the general line filling-in phenomenon as though the effect is caused to a large degree by redistribution of the scattered energy with wavelength (i.e. non-linear scattering). It may also be noted that some atmospheric lines are susceptible to airglow effects, whereby particular emission can be seen within the core of the original Fraunhofer lines, sodium airglow being well-known, for example.

The observational studies reported in Chapter 6 also suggest that a new phenomenon behaving like airglow has been discovered. It is referred to here as a "daylight flash" and was recorded on three days at Hα and Hβ with different strengths.

This daylight flash was for short periods (≈20 minutes); the cores of these lines were filled in while the near continua were unaffected.

In this thesis, the principle of the LDM has been extended to cover linear polarization effects. The basic algebra associated with the development is given in the next chapter. One possible advantage of the polarimetric LDM technique is that line filling-in detections can be made without recourse to solar measurements, although absolute determination of the strengths of the added components require assumptions on the nature of its polarization. The principle of the polarimetric LDM has been applied to both lunar and the daytime sky studies.

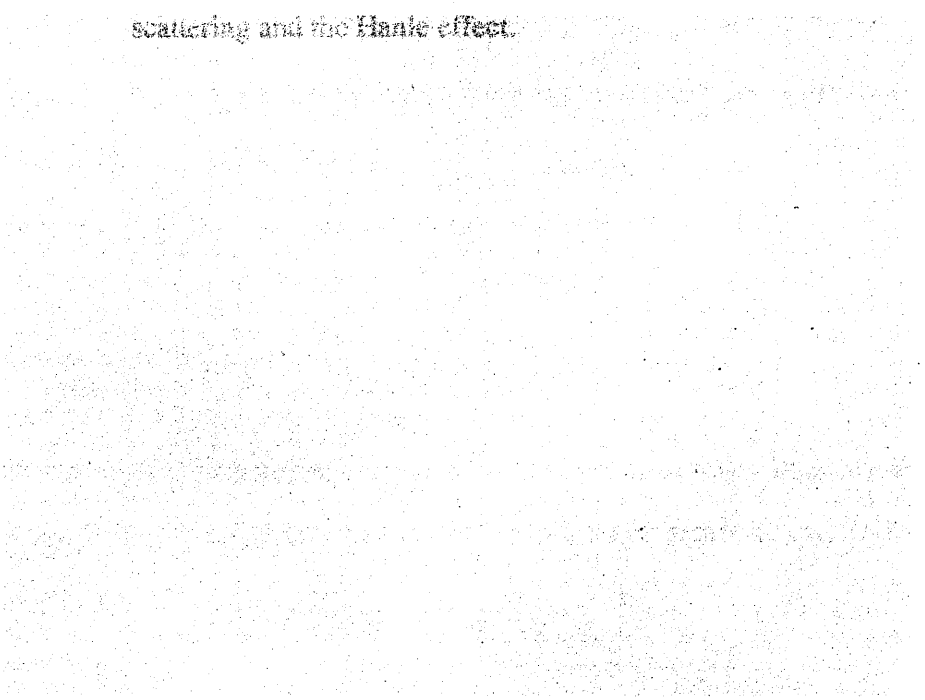

Chapter 2 Estimation of the polarimetric effects associated with the three proposed experiments.

2.1 Lunar and daytime sky studies - Assessment of the added light effect on polarization across spectral lines.

2.2 Estimation for whole solar disk polarization associated with resonance scattering and the Hanle effect.

2.1 Lunar and daytime sky studies - Assessment of the added light effect on polarization across spectral lines.

The light from the Moon and the daytime sky is scattered light and hence will have the same spectrum as the Sun displaying the well-known Fraunhofer lines. The scattering processes introduce linear polarization which is independent of the strength of the original flux. If the mechanism has only a weak wavelength dependence, then the polarization will be the same within a Fraunhofer line relative to the line's nearby continuum. However the situation is changed radically if in addition to the scattered sunlight there is an extra flux with different spectral and polarizational characteristics. A simple model to consider involves a broad luminescent band which straddles a Fraunhofer line within the solar spectrum. In the algebra below, the subscripts C and L refer to values at the continuum and within the line respectively.

By choosing a reference plane which makes $U_C = U_L = 0$, and without the presence of added light, the two Stokes vectors representing the linear polarization at the continuum and the line centre, may be written as:

$$\begin{bmatrix} I_C \\ Q_C \\ 0 \end{bmatrix} \quad \text{and} \quad \begin{bmatrix} I_L \\ Q_L \\ 0 \end{bmatrix} = R \begin{bmatrix} I_C \\ Q_C \\ 0 \end{bmatrix}$$

without the presence of luminescence, where R is the line/continuum intensity ratio. With this condition, P for the continuum and for the line would be identical, i.e.:

$$P_C = Q_C / I_C \quad = Q_L / I_L = P_L$$

Suppose now that added light is present providing a flux, FI_C, constant across the spectral line as indicated by the marked base in Figure (2.1). If the added light has a

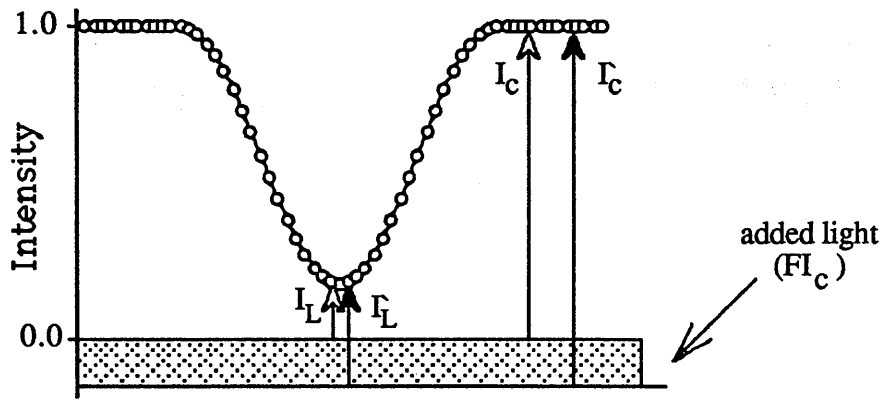

Figure (2.1) A typical Fraunhofer line is represented with a continuum intensity I_C and line core intensity I_L. If an added light flux spans this wavelength region, the intensities may be written as I'_C and I'_L where $(I'_C - I_C) = (I'_L - I_L)$ is the intensity of the added light. It may be noted that $I'_L / I'_C > I_L / I_C$.

different polarization from the scattered light and combines incoherently (subscribt f refer to the added light), the measured Stokes vectors for the continuum and the line core correspond to:

$$\begin{bmatrix} I'_C \\ Q'_C \\ U'_C \end{bmatrix} = \begin{bmatrix} I_C \\ Q_C \\ 0 \end{bmatrix} + \begin{bmatrix} I_f \\ Q_f \\ U_f \end{bmatrix} \quad \text{and} \quad \begin{bmatrix} I'_L \\ Q'_L \\ U'_L \end{bmatrix} = \begin{bmatrix} I_L \\ Q_L \\ 0 \end{bmatrix} + \begin{bmatrix} I_f \\ Q_f \\ U_f \end{bmatrix} \qquad (2.1)$$

with

$$P'_C = \frac{\sqrt{(Q'^2_C + U'^2_C)}}{I'_C} \quad \text{and in general not equal to} \quad \frac{\sqrt{(Q'^2_L + U'^2_L)}}{I'_L} = P'_L$$

The position angles of the polarization are given by:

$$\tan(2\theta'_C) = \frac{U'_C}{Q'_C} \quad \text{not equal to} \quad \tan(2\theta'_L) = \frac{U'_L}{Q'_L}$$

The observed polarimetric behaviour of the light across a spectral line is determined by the Stokes vector additions of the scattered component and the added light. Three situations may be discussed conveniently, viz: (a) unpolarized added light, (b) polarized added light with vibration plane associated with the scattering plane and (c) polarized added light with arbitrary direction of vibration.

Case (a): This condition was assumed by different authors with respect to daytime sky studies (see Chapter 1). Both Q_f and U_f are zero and by using Equation (2.1) the line / continuum ratio of observed degree of polarization may be written as :

$$\frac{P'_L}{P'_C} = \frac{R(1+F)}{(R+F)} \qquad (2.2)$$

Thus the polarization in the line is reduced relative to the continuum. Also, the position angle of the polarization remains constant across the line.

Case (b) : The sign ($\pm$) of the numerical value of Q_f depends on whether the added light is vibrating in the scattering plane or orthogonally to it. The resulting Stokes vectors may be written as:

$$\begin{bmatrix} I_C' \\ Q_C' \\ 0 \end{bmatrix} = \begin{bmatrix} I_C \\ Q_C \\ 0 \end{bmatrix} + \begin{bmatrix} I_f \\ Q_f \\ 0 \end{bmatrix} \quad \text{and} \quad \begin{bmatrix} I_L' \\ Q_L' \\ 0 \end{bmatrix} = \begin{bmatrix} I_L \\ Q_L \\ 0 \end{bmatrix} + \begin{bmatrix} I_f \\ Q_f \\ 0 \end{bmatrix}.$$

With this situation, Equation (2.2) is modified to :

$$\frac{P_L'}{P_C'} = \left(\frac{1+F}{R+F}\right)\left(\frac{R+\psi F}{1+\psi F}\right) \tag{2.3}$$

where ψ is the ratio of the degree of polarization of the added light to that of the directly scattered light, i. e. :

$$\psi = \frac{(Q_f / I_f)}{(Q_C / I_C)} = \frac{(Q_f / I_f)}{(Q_L / I_L)} \tag{2.4}$$

Thus depending on the signs of Q_C, Q_L, and Q_f, and on their numerical values the polarization may increase or decrease. This may be summarized by noting that:

$$\text{If } \psi > 1 \text{ then } P_L' > P_C'$$

$$\text{If } \psi = 1 \text{ then } P_L' = P_C'$$

$$\text{If } \psi < 1 \text{ then } P_L' < P_C'$$

The position angle of the polarization is unaffected by the added light, except for the extreme situation where $Q_f > Q_C$ or Q_L and with the opposite sign, so changing the polarization position angle by 90°. This case agrees fairly well with the real observations but with special conditions, see Chapter 6.

Case (c) : This most arbitrary of cases is described by Equation (2.1) which indicates that both the polarization and the position angle are likely to change across the line profile.

The magnitude of the changes across a spectral profile and the requirements of the accuracy to detect the added light by polarimetric techniques can be estimated by considering appropriate values associated with Case (a). For example, suppose a spectral line gives a value of $R = 0.7$ and that there is luminescent intensity = 0.03 relative to the continuum. According to Equation (2.2), the ratio of observed P values in the line core and continuum = 0.988.

The polarization degree P of the zenith sky changes during the day from minimum at noon to maximum at sunrise and sunset, when the angle of the scattering is 90°. At these times, P is about 75%, dependent on the meteorological conditions of the sky, while at noon it is about 25%, the figure varying according to the scattering angle which in turn depends on the latitude of the observatory and on the season. Based on these figures, the changes of polarization across the line during the course of the day should be of the order of 0.003 to 0.009 (0.3% to 0.9%). Such effects are easily detectable and their variation during the day allows exploration of the constancy (or otherwise) of the luminescence flux. For the Moon the polarization of the scattered light is much less but if observations are at a lunar phase which has a moderately high polarization, say = 0.1, changes of P of the order of 0.0012 (12/100 of 1%) should occur across the line. As reference, many stellar polarimetric measurements are reported with accuracies $\Delta P \approx$

0.0004 and better and hence it should be possible to record the polarizational changes within the lunar spectral lines using existing spectropolarimeters.

From the above outline it can be seen that the line depth method which has been used to investigate the line filling-in effect photometrically, can be extended by polarimetry to give further insight as to the origins of the additional component.

2.2 Estimation of whole solar disk polarization associated with the resonance scattering and the Hanle effect.

In order to consider the experimental requirements necessary to undertake solar polarimetry a simple model needs to be established. The centre to limb variation (CLV) for the polarization of some resonance lines has already been described in Chapter 1. Maximum polarization occurs at the limb when the scattering angle from the source to the observer is about 90°, the vibrations always being parallel to the limb. On a quiet solar disk the net polarization will be zero, because of symmetry. The polarization produced by any annulus can be calculated by dividing it into a number of segments (N). In the case of an undisturbed Sun, for any such small segment producing a polarization, there is a complementary element at an orthogonal position which produces an orthogonal polarization of equal strength. Consideration of elements around the annulus with their complements produces a net polarization of zero.

However, the situation is disturbed if there are active regions, with the overall engendered polarization depending on the size of the region and its position. When the Sun is very active, several regions may need to be considered simultaneously. However, we will consider a simple case of a single active region at the limb, with equator bisecting it. Its dimensions are indicated in Figure (2.2) with angular extension 2ϕ and radial size ΔR. The effect that a single active element might have on overall polarization, can be determined from its contribution in relation to the remainder of the annulus in which it lies. Thus the engendered linear polarization may be represented by :-

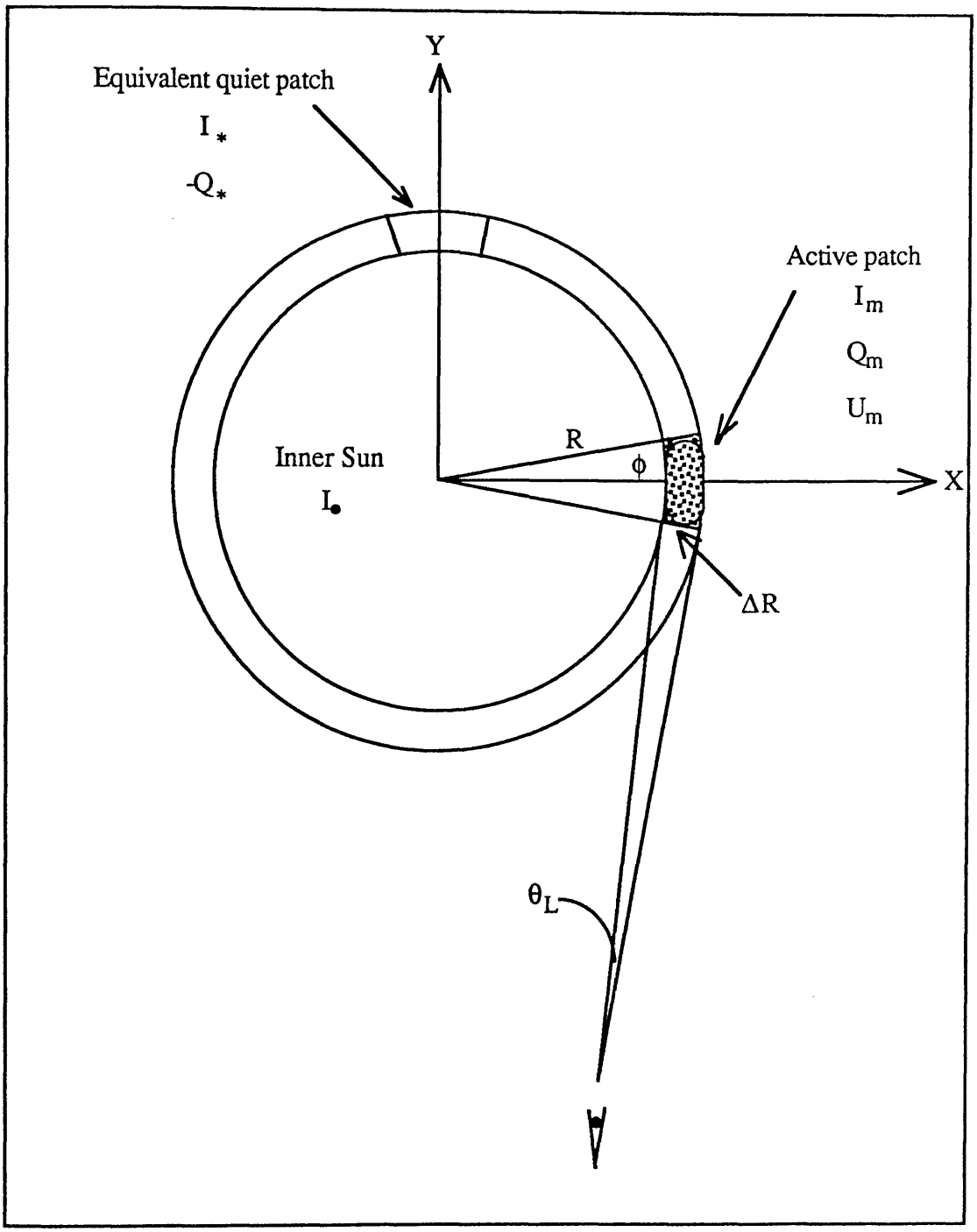

Figure (2.2) A representation of the solar disk with a magnetic bright patch near the solar limb on the equator due to solar activity, and its complementary element in an adjacent quadrant position. θ_L represents the observed angular size of the patch.

$$\begin{bmatrix} I \\ Q \\ U \end{bmatrix} = \begin{bmatrix} I_m \\ Q_m \\ U_m \end{bmatrix} + \begin{bmatrix} I_* \\ -Q_* \\ 0 \end{bmatrix} + (N-2)\begin{bmatrix} I_* \\ 0 \\ 0 \end{bmatrix} + \begin{bmatrix} I_\bullet \\ 0 \\ 0 \end{bmatrix} \qquad (2.5)$$

where on the right hand side, the first vector with subscript m represents the effects of the magnetically disturbed region; the second vector with subscript $*$ represents the complementary undisturbed region at an orthogonal position on the solar disk; the third vector represents the contributions of the (N-2) segments around the limb annulus of the same dimensions as the two patches; and the fourth vector is the intensity of the inner remaining solar disk. The fourth Stokes parameter which represents circular polarization has been assumed zero and omitted.

The degree of polarization that is produced depends on the brightness of the active region. If a weak magnetic field is present, the situation is more complicated in that the Hanle effect will reduce the polarization in the magnetic patch relative to the undisturbed orthogonal patch and rotate the direction of vibration - hence the introduction of the term U_m.

The Hanle effect produces $\left(\dfrac{Q_*}{I_*} > \dfrac{\sqrt{(Q_m^2 + U_m^2)}}{I_m} \right)$.

So the resultant Stokes vector is,

$$\begin{bmatrix} I_m + (N-1)I_* + I_\bullet \\ -Q_* + Q_m \\ U_m \end{bmatrix} \qquad (2.6)$$

and the total degree of polarization would be given by :-

$$P_T^2 = \frac{P_*^2 + P_m^2 Y^2 - \dfrac{2Q_* Q_m}{I_* I_m} Y}{\left(Y + (N-1) + \dfrac{I_\bullet}{I_*} \right)^2} \qquad (2.7)$$

where P_* and P_m are the degrees of polarization of the nonmagnetic patch and the magnetic patch respectively, and $Y = I_m / I_*$ is the intensity ratio of the two patches. Values of P_* and $I_\bullet/I_*$ have been estimated by Stewart (1984) as;

$$P_* = \{ a - \frac{2}{3} b\sqrt{2f - f^2} \} \frac{\sin 2\phi}{2\phi} \qquad (2.8)$$

and

$$I_\bullet / I_* = N (B - 1)$$

where $B = \dfrac{1 - (\frac{u}{3})}{(2f - f^2)\left(1 - u + \frac{2}{3} u\sqrt{(2f - f^2)}\right)}$, u is the limb darkening coefficient obtained from Allen (1973), f is the ratio between the radial size ΔR of the spot to the radius of the solar disk ($f = \Delta R/R$) and values of a=0.040 and b=0.073 are the intercept and the gradient respectively of the linear variation of the polarization (between μ=0 and $\approx$0.4) as taken from Figure (1.8) for the considered wavelength, CaI 4227Å.

Since $\dfrac{Q_m}{I_m} = P_m \cos(2\varnothing)$, then Equation (2.7) may be rewritten as

$$P_T = P_* \frac{\sqrt{1 + \Gamma^2 Y^2 - 2Y\Gamma \cos(2\varnothing)}}{[Y + (N.B) - 1]} \qquad (2.9)$$

where the depolarization factor (Γ) is given by Equation (1.4) and the rotation ($2\varnothing$) of the plane of polarization has been calculated from Equation (1.5), the Landé factor g = 1 for CaI 4227Å (see Nikol'skii and Khetsuriani, 1970).

Expected polarizations from the whole solar disk P_T in hundredths of percent (units of 10^4) are displayed in Table (2.1) for the 4227Å line centre. It can be seen from these values that the polarization detectivity of any instrument needs to be high (better than ΔP=0.001%) and it is also necessary to have high spectral resolution of about 0.1Å, because the predicted values of the polarization have been based on effects within spectral lines, see Chapter 1. Although the predicted polarizations are small, it should be possible

Tables (2.1) Maximum expected polarizations for the whole solar disk in hundredths of a percent (units of 10^4) as a function of Y ($=I_m/I_*$), f ($=\Delta R/R$) and H (gauss) for the CaI 4227Å line centre.

$2\phi = 5^\circ$ $\quad f = 0.01$ ($\equiv \theta_L = 9''.7$)

H\Y	3	4	5	7	10
0	0.062	0.094	0.125	0.188	0.282
2	0.060	0.090	0.120	0.181	0.271
4	0.056	0.083	0.110	0.164	0.245
6	0.051	0.074	0.097	0.144	0.215
8	0.047	0.066	0.086	0.126	0.188
10	0.044	0.060	0.076	0.111	0.164

$2\phi = 5^\circ$ $\quad f = 0.05$ ($\equiv \theta_L = 48''.6$)

H\Y	3	4	5	7	10
0	0.317	0.475	0.634	0.950	1.422
2	0.308	0.460	0.611	0.915	1.369
4	0.287	0.421	0.557	0.830	1.240
6	0.262	0.377	0.494	0.731	1.089
8	0.241	0.336	0.436	0.640	0.949
10	0.224	0.303	0.388	0.563	0.831

$2\phi = 5^\circ$ $\quad f = 0.10$ ($\equiv \theta_L = 97''.2$)

H\Y	3	4	5	7	10
0	0.561	0.840	1.119	1.673	2.499
2	0.545	0.812	1.079	1.612	2.406
4	0.507	0.744	0.983	1.463	2.179
6	0.464	0.666	0.872	1.288	1.914
8	0.427	0.594	0.770	1.127	1.668
10	0.396	0.536	0.687	0.992	1.460

to detect them with current techniques but special instrumentation is required to combine a polarimetric modulator and a high resolution spectrometer.

It is clear that the maximum polarization occurs when the active patch approaches the solar limb, the value depending on the size of the active region. If it has a lifetime considerably larger than the solar rotation period, its appearance on the limb followed by its movement across the projected disk to the opposite limb will produce a polarimetric modulation with double humps, their shape depending on the geometry of the active patch and on the effect of limb darkening. In contrast, the effect of the region on the total intensity will provide a single maximum when the zone lies on the projected meridian, see Figure (2.3).

In this chapter, the polarization effects related to line filling-in phenomena in both the daytime sky and lunar spectra have been explored. Predictions of the polarization variations across spectral lines suggest that they should be readily measurable.

From a simple model of the Sun, spectral line polarization effects that might be seen in the integrated light from the whole solar disk have been considered for resonance scattering in combination with the Hanle effect. The polarizations are predicted to be small and offer an interesting challenge to the observer.

In the following chapter, polarimetric instrumentation will be described related to the undertaking of the line profile spectropolarimetry of the daytime sky, the Moon and the Sun.

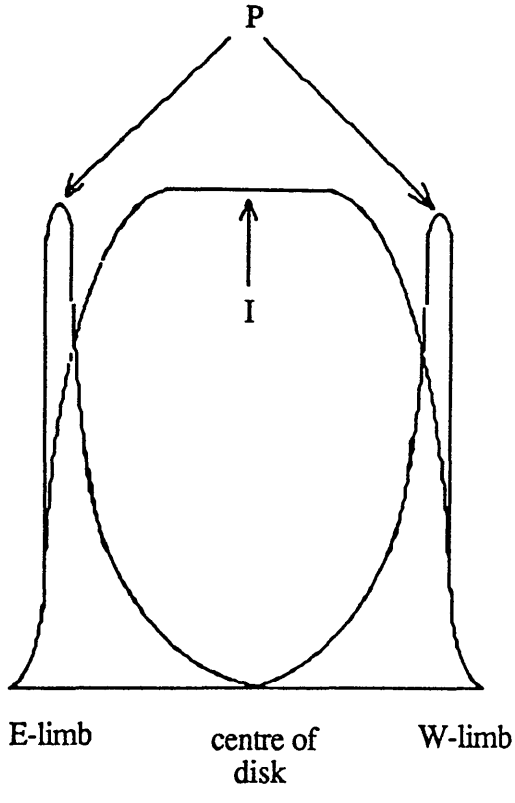

Figure (2.3) Schematic variation of intensity (I) and polarization (P) of one single active region crossing the solar disk.

Chapter 3 Instrumentation

3.1 Introduction.

Spectropolarimetric observations have been considered in relation to three different sources, each with their individual problems in terms of instrument design and methodology of the experiment. For two of the sources (daytime sky and the Moon) the measurements were undertaken with an established polarimeter; for the Sun, special instrumentation was required. The observational polarimetric technique was identical for all measurements, based on rotating a quartz/magnesium fluoride super achromatic half-wave plate in front of a fixed polarizer. The polarimetric signal was recorded by photo-electron counting techniques using scalers to integrate the sine-wave modulation over three sections of its cycle. The electronic circuits, used for the polarimetry, for movement of the filters, and for collecting data were identical for all the experiments.

The observations of the daytime sky and the Moon were carried out using the Glasgow University Photometer Polarimeter (GUPP) on the 0.5m reflector telescope at the Cochno Observatory, north of Glasgow. The GUPP was designed and built in the departmental workshop under the supervision of Dr. Clarke (see, Clarke and Brooks, 1984). It is a two-channel Photometer/Polarimeter which measures linear polarization. The telescope was fixed in a vertical position to observe the zenith sky and tracking was used for the other experiments.

The tilting interference-filter technique to obtain spectral line profiles has been used since 1972 for stellar observations at the Glasgow University Observatory. In an early instrument, the filters were adjusted manually by micrometers and the time intervals between their settings were arbitrary. However, the application of a microcomputer to control stepper motors allows a rapid adjustment of the wavelength settings and in a regular way. Figure (3.1) illustrates the differences with respect to the regularity of data acquisition between the early system and the more automated equipment.

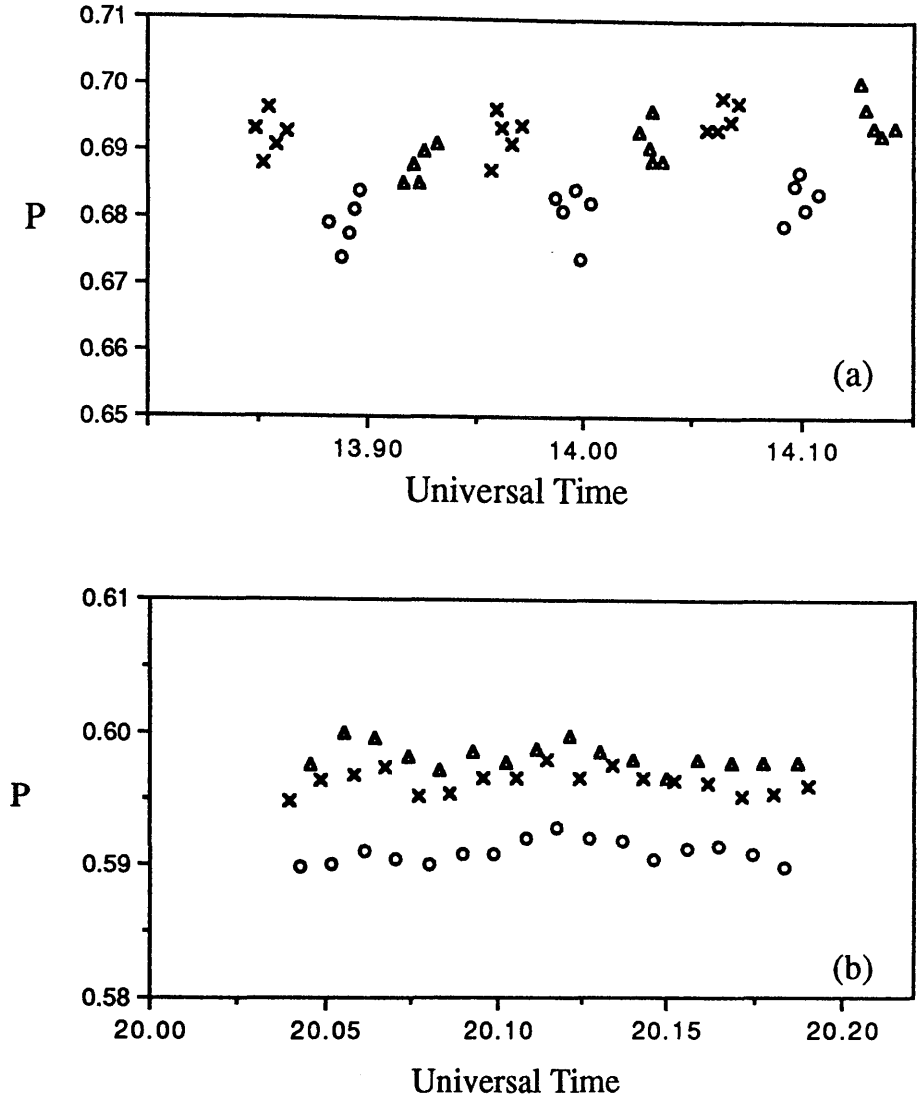

Figure (3.1) (a) The degree of linear polarization P at three wavelength positions (symbols o, x, and Δ represent the line centre and the red and the blue continua respectively) across the Hβ line for daytime sky light plotted against universal time (U.T.). Each position was observed five times before adjustment to the next wavelength value. The movement in wavelength was made by hand so giving unequal mark-to-space ratio between the measurements with the possibility of unequal time intervals (Taken from Clarke and McLean, 1975c)

(b) The data of (1989) illustrate the improvements made by the more automated system for performing polarimetry and adjusting the wavelength positions. Single measurements are made at each wavelength position in a regular cycle with equal time intervals between each data point.

A modified Foster prism (see Foster, 1938, for the original design) splits the light into the two orthogonally polarized beams which emerge with a geometric separation of 90° allowing both to be monitored simultaneously. The beams are collimated and their spectral passbands are selected by narrow band interference filters. The filters of 25mm diameter are mounted in frames and an electronic system controls the tilt (up to about 13°). In these experiments two filters were used providing passbands of 2.8Å for Hα and 1.9Å for Hβ. As the experiment depends on the comparisons between the line cores and their nearby continua, three tilt positions of the filter were chosen, corresponding to the red continuum, the line core and the blue continuum. The photometer head was temperature stabilised to prevent drifts in the wavelength passband of the interference filters. The field of view was limited to 38 arc sec by a circular diaphragm in the focal plane of the telescope. This diaphragm was made of non-conducting material as, according to Serkowski (1974), metallic diaphragms can introduce spurious polarization effects particularly when the star image is not centred. Figure(3.2) shows a cross-sectional view of the two-channel spectropolarimeter.

3.2 The polarimeter.

The two-channel polarimeter was attached to the 50cm, f/8 telescope at the Cochno station. Light from the telescope focal plane is collimated before passing through the half-wave plate, positioned in front of the Foster double beam polarizing prism. The polarizer comprises two prisms of calcite which are fixed with cement; the exit faces are cut to allow the rays to emerge at normal incidence and the angles of the prisms have been chosen to give a geometric separation of 90° between the resolved beams. The half-wave plate was rotated at 20 Hz by a stepper motor so producing a polarimetric modulation of 80Hz. The signals emerging from the system can be evaluated using the Mueller calculus (see Appendix, A), i.e.

$$S(\omega t) = \frac{1}{2}\left[I \pm Q \cos 4\omega t \pm U \sin 4\omega t \right] \qquad (3.1)$$

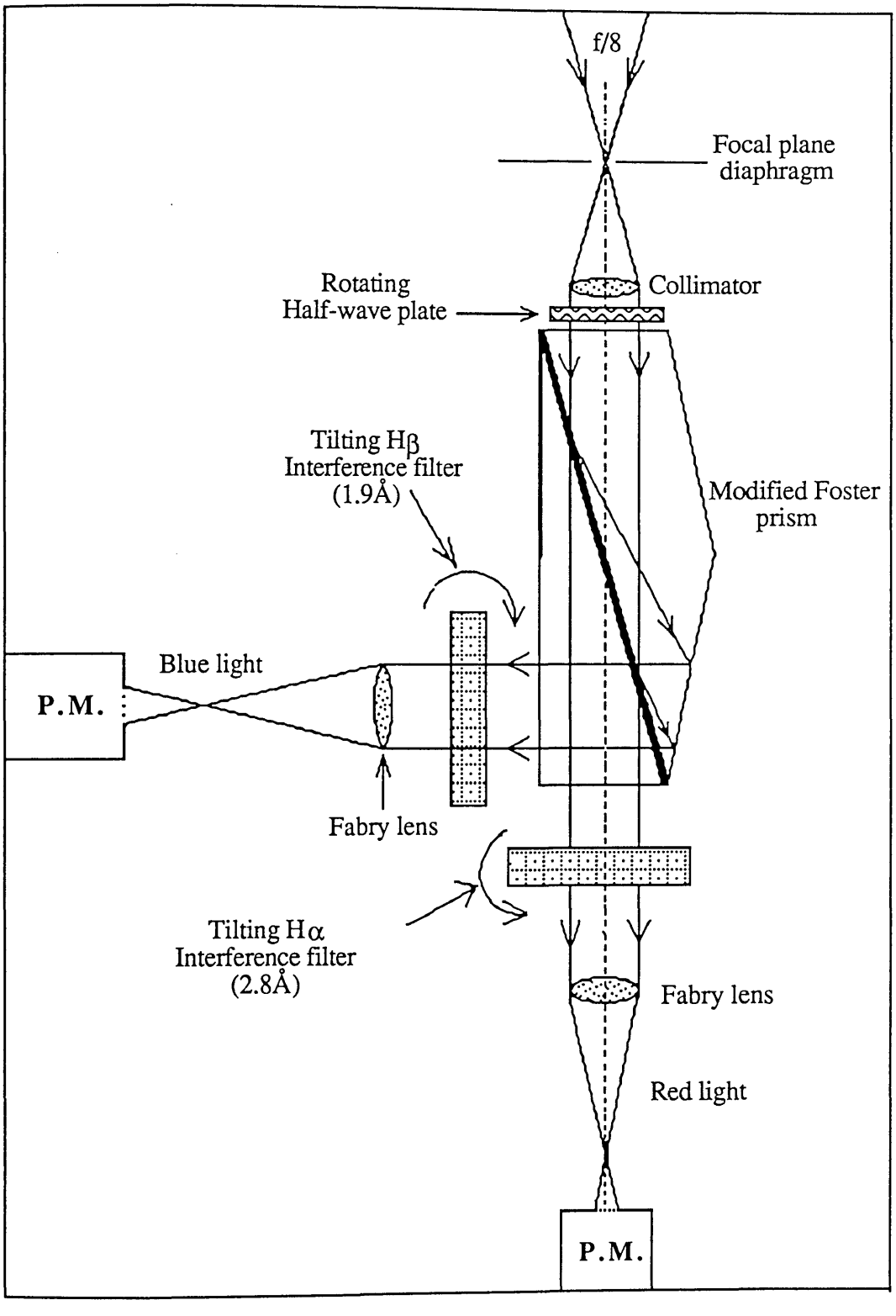

Figure (3.2) Cross-sectional diagram of the two-channel spectropolarimeter.

where I, Q and U are the Stokes parameters as presented in the instrumental frame, this being defined by the axis of the half-wave plate and the orientation of the principal axis of the polarizer, and ω is the angular frequency of the rotating half-wave plate. The positive signs are for the first beam while the negative signs refer to the second beam. The polarimetric resolved beams pass through the interference filters and then to two photomultipliers with Fabry lenses imaging the telescope mirror on to the photo-cathodes.

Following the production of a photo-electron by the cathode, the amplification by the dynode system in the photomultiplier generates an electron pulse at the anode. Each pulse passes through a pre-amplifier, the latter's main purpose being to change the impedance so that transmission of the signal can be achieved along a co-axial cable to digital recording equipment. In this way, the recorded signal is directly related to the number of photons arriving at the detector.

The signals in the form of voltage pulses go to six counters - three for each channel. They record the photo-electron counts over various portions of the polarimetric modulation similar to the method of Klare et al. (1972). The first scaler records the intensity. It opens and accumulates the photon count during the whole time of the rotation of the half-wave plate. The second scaler opens at the same time as the first scaler but closes after a half-period of the polarimetric modulation, opens again after a further half-period and continues this chopping mode until the end of the integration time. The third scaler also operates in a similar chopping mode but is delayed in phase by $\pi/2$ relative to the second counter (see Figure 3.3).

Appendix (B), illustrates an output record of a polarimetric observation, using two channels (six counters), for a file as recorded on a microdrive unit. The three counts for each channel, corrected for background, may be defined as C_1, C_2 and C_3 respectively, and the normalised Stokes' parameters from each integration may be determined from :-

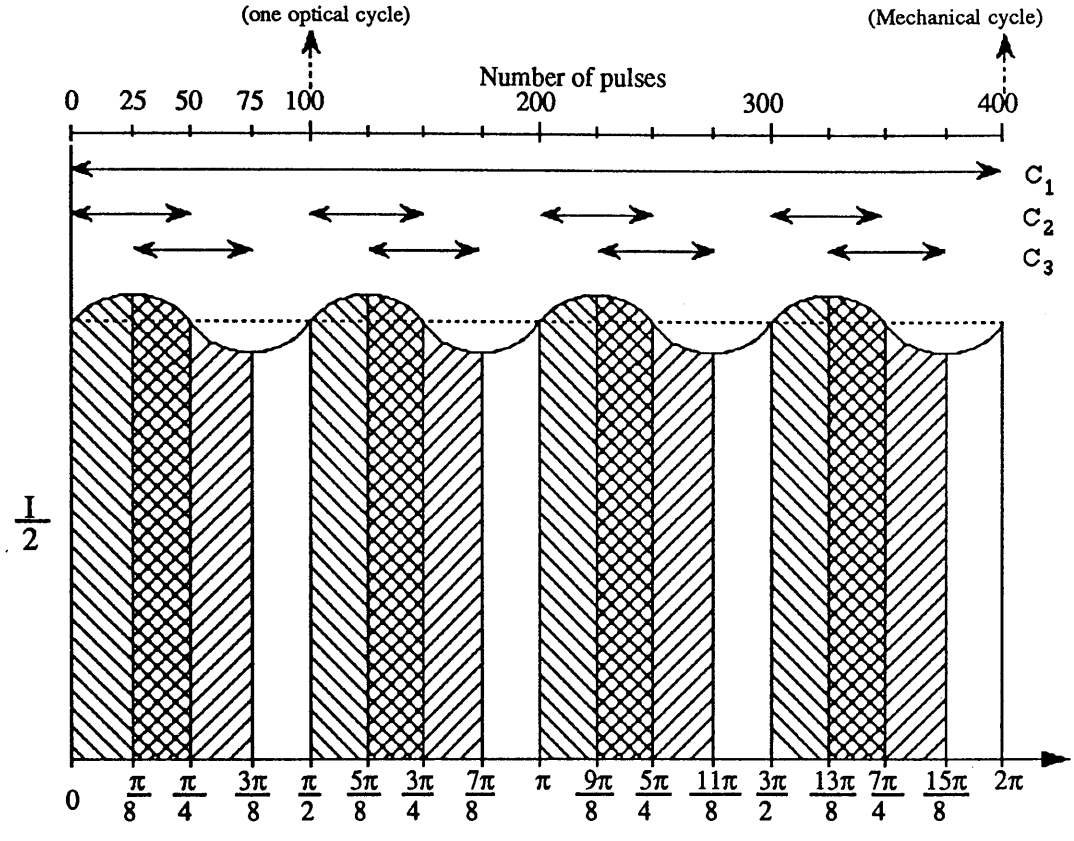

Figure (3.3) Four cycles of intensity modulation correspond to one revolution of the half-wave plate. The integrated parts of the signal required to obtain C_1, C_2 and C_3, from which Stokes parameters I, Q, and U can be calculated are shown. Note also the number of pulses which are required to operate the electronic gates so as to open and close at appropriate times corresponding to the rotation of the half-wave plate.

$$\frac{Q}{I} = q = \pm \frac{\pi}{2}\left(\frac{C_1 - 2C_2}{C_1}\right) \quad \text{and} \quad \frac{U}{I} = u = \pm \frac{\pi}{2}\left(\frac{2C_3 - C_1}{C_1}\right) \qquad (3.2)$$

the plus sign is used for the first channel, while the negative corresponds to the second channel.

The parameters may be affected by a small amount of instrumental polarization q° and u° introduced by the telescope mirrors but likely to be constant across each investigated narrow spectral region. This instrumental polarization (q°,u°) was determined by observations of standard unpolarized stars (α Boö and β Cas). The amounts of the instrumental polarization ($\sqrt{q^{\circ 2} + u^{\circ 2}}$) of the two channels were usually less than the level of 1%. The instrumental polarizations were then applied to all measurements; the revised values of q and u are q* and u*.

$$q^* = q - q^\circ \qquad \text{and} \qquad u^* = u - u^\circ$$

It is important that the values of q°, u° should be known with an uncertainty which is very much smaller than the random errors associated with the measurements of q and u. The degree of polarization and the direction of polarization, in the instrumental system, are respectively

$$P = \sqrt{q^{*2} + u^{*2}} \qquad \text{and} \qquad \theta = \frac{1}{2}\tan^{-1}\left(\frac{u^*}{q^*}\right)$$

The frame of reference for θ is not the same for the Hα and Hβ lines as the super achromatic half-wave plate displays dispersion of its fast axis. The behaviour of this is clearly shown in Figure (3.4). From our blue sky observations as illustrated in Figure (3.5), it can be seen that the difference of the position angle between Hα (6563Å) and Hβ (4861Å) is constant at about 3°.74.

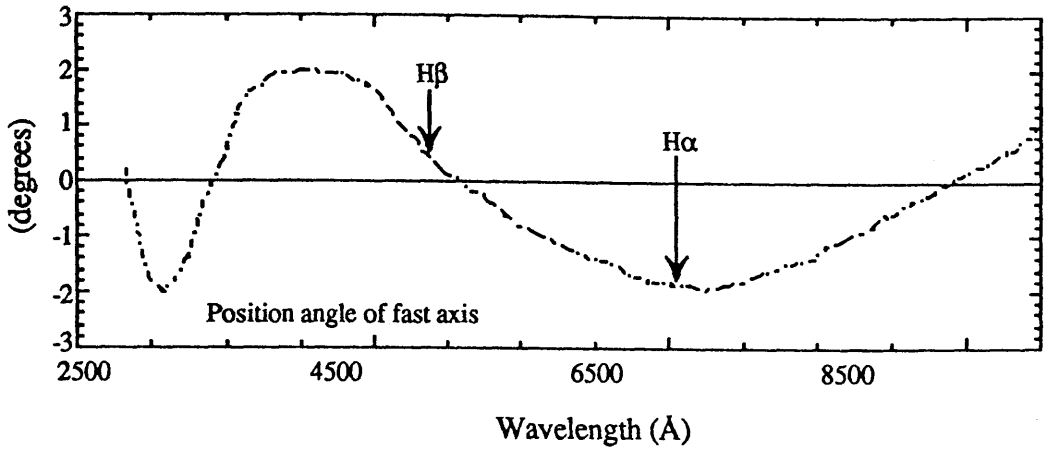

Figure (3.4) The wavelength dependence of the principal axis (fast) of a super achromatic half-wave plate. It is a Pancharatnam combination of three magnesium fluoride and quartz achromatic half-wave plates (Taken from Serkowski, 1974)

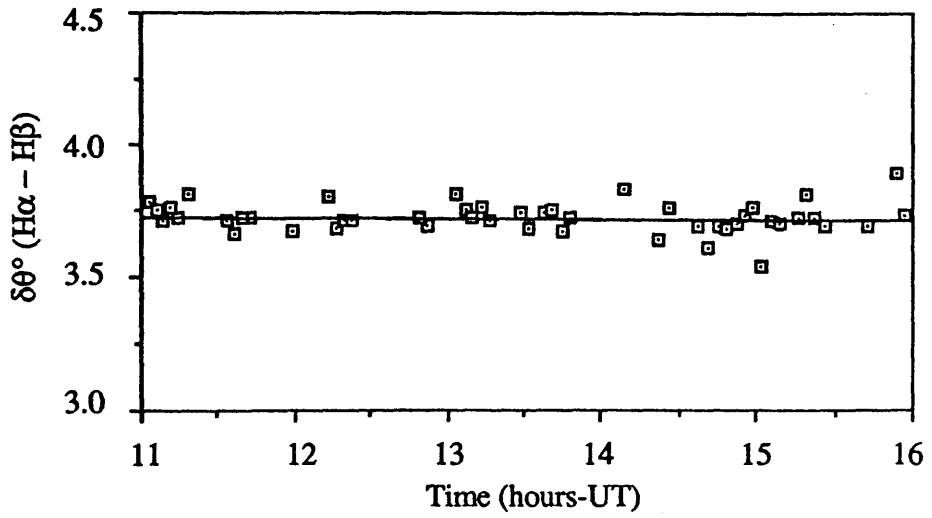

Figure (3.5) A plot of the differences in position angle (θ°) of the polarization between Hα and Hβ throughout the day indicating a constancy corresponding to the wavelength dependence of the principal axis of the super achromatic half-wave plate.

3.3 Electronics

GUPP has recently been upgraded to operate under microcomputer control. The electronic control and data logging system is constructed with modules similar in concept to CAMAC. However the crate and modules are all "home made" and have been designed and built at Glasgow University Observatory by Dr. D. Clarke. For polarimetry, there are eleven modules in the system. The first module is a line receiver to accept photo-electronic pulses from the two channels. The second module is a control board in the form of an interface between the system and the microcomputer. The third module is a pulse generator to control the stepping motors for wavelength scanning. The fourth is designed to control synchronism between the rotating half-wave plate and the gates of the photon counters. The fifth controls the photon counter gates. The next six are denary scalers (three for each channel). Figure (3.6) illustrates the concept and layout of the electronic system.

The interface board has been designed to operate with a serial port of any microcomputer and the Sinclair QL was chosen. Communications are performed using BASIC language with simple programs. Examples of the programs are displayed in the Appendix (D), and they are enumerated in Section (3.4). This board and the concepts of the system have been described by Clarke (1989). The solar experiment uses the same electronic designs but with only three counters (single channel). All the modules are of standard design allowing quick replacement by transferring boards.

The system maximises the use of the experimental time. For example, at the end of each integration, the accumulated photo-electron counts are transferred to buffers which are then interrogated by the computer. While this is being done, counts may be resumed and undertaken with a time loss limited to a single revolution of the half-wave plate. In terms of fractional loss to the experiment, this corresponds to 1/200. The computer provides UT and attaches this to each data line. Basic descriptions of the electronic functions are given under their appropriate sub-heading.

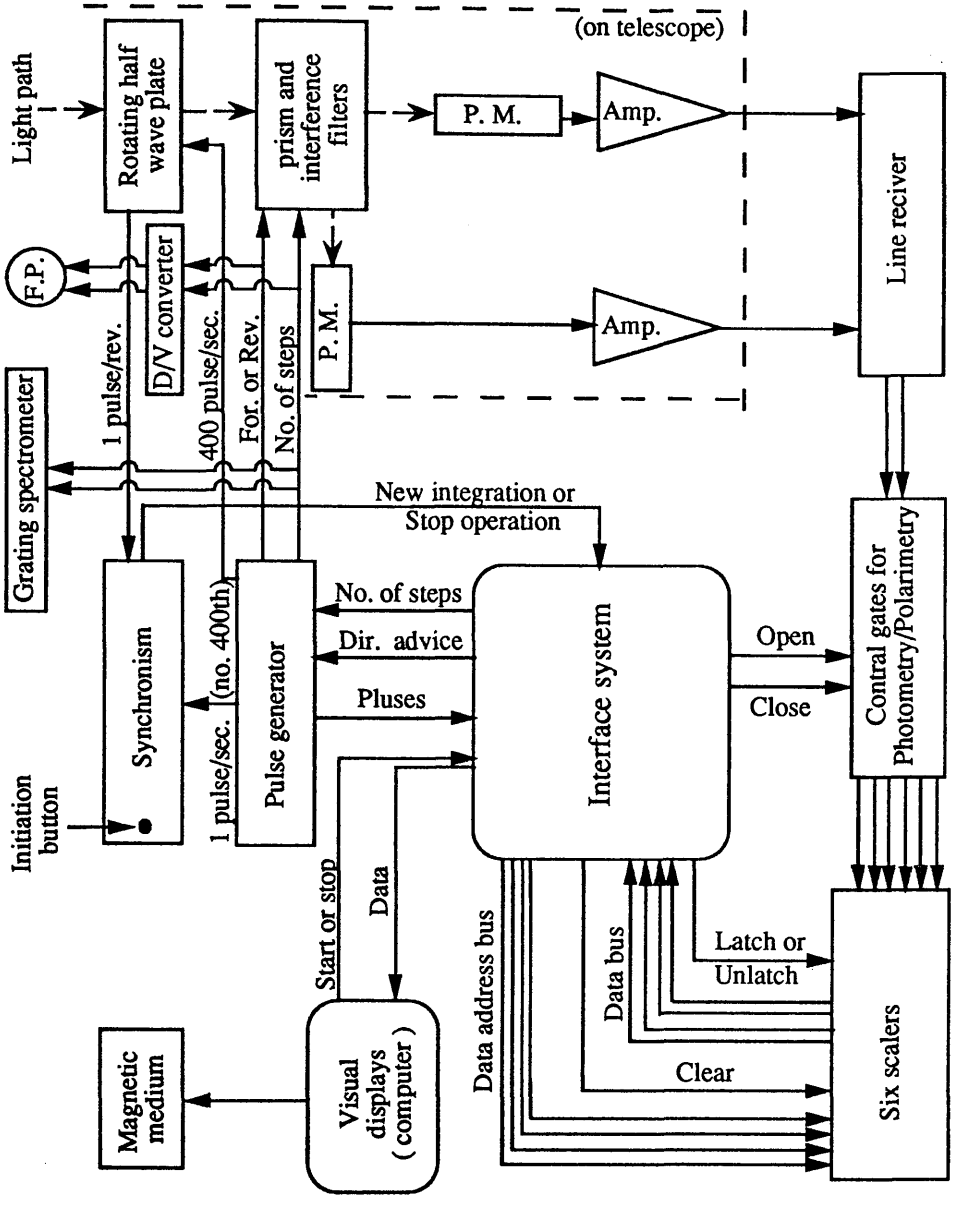

Figure (3.6) Block diagram of the electronics

The Line receiver.

The signal from the photomultiplier tubes is fed to pre-amplifiers and the boosted signal is transmitted on a co-axial line before being fed to the counter via a "line receiver". The line receiver converts the signal into a form suitable for counting by TTL technology.

The interface system.

This can be considered to be the brain of the electronic system, the part which operates the different modules, and collects the data for transmission to the computer. It has to be capable of opening the counters to accept photo-electron pulses, closing them when the integration time has elapsed, latching the counts in temporary stores so that the measurement can still proceed during the data transfer to the computer, clearing the counters, advancing the position of the stepper motors, etc.

The interface is a simple serial-to-parallel converter. Its operation is centred on a standard UART (Universal Asynchronous Receive and Transmit-6402) chip. The system is capable of providing 256 communication lines by decoding the eight bits used to describe any ASCII character dispatched from the microcomputer. For our experiment, only 18 lines were used. Some of these lines are used to control the operations of the observations. Others are used to manipulate a data address bus whereby a counter is chosen for interrogation and a particular digit is despatched from the counter to the computer.

The pulse generator for stepper motors.

Rotation of the half-wave plate was achieved by using a stepper motor. Pulses generated from a 10MHz crystal, and with a number of ÷10 counters to reduce this high frequency to a more manageable one (8000Hz) were applied to the motor control circuitry. At switch-on, this latter frequency was ramped to accelerate the motor to its

working speed. As the stepper motor requires 400 pulses per revolution, the polarimetric sine-wave modulation is 80Hz [i.e. (8000/400)x4]. This board also controls the stepper motors which tilt the interference filters. Direction of movement and number of steps were decided during the operation of the program.

The control gates.

Each channel has three scalers (i.e. C_1, C_2, and C_3) for polarimetric measurements, the first one also being used for photometric studies as its gate is open all the time during each integration. The other two scaler gates are set to open and close at the appropriate positions over the half-wave plate rotation. The 400 pulses which control the rotation of the half-wave plate are also used to operate these gates to open and close at proper times. The second scaler opens with the first pulse and after 25 pulses the third opens; at pulse no. 50, the second scaler closes while the third scaler remains open for another 25 pulses; at pulse no. 75 the third scaler closes. With pulse no. 100 a new optical cycle starts again and the whole sequence is repeated three times to correspond to one mechanical rotation (see Figure. 3.3). The whole process continues for 200 rotations corresponding to one integration.

The synchronism board.

The half-wave plate's stepper motor is free running but, in order for the modulated signal to be phased correctly to the data recording system, the gates of the counters are opened and closed in sequence at the correct time. One of the 400 pulses required to turn the stepper motor through a mechanical cycle is tagged, and may be compared with a reference pulse generated by an optical switch attached to the rotating holder of the waveplate on the telescope. The synchronism is initiated by a push button on the panel and is checked on each rotation of the waveplate. If for some reason the reference pulse does not match the 400th motor pulse, the system aborts and does not record the data line; the synchronism needs to be re-initiated before further measurements can be made.

Counters.

Pulses generated by photons are counted, and displayed in six separate scalers which can be interrogated by the microcomputer. The scalers have been numbered 1, 2, 3 for the first channel and 4, 5, and 6 for the second. Each set of three scalers provides the counts C_1, C_2, and C_3 for the polarimetric method. The scalers have eight digits, seven are used as counters and the eighth digit has been permanently set to identify the scaler number (see, Appendix B). Each scaler uses ÷10 TTL counter chips and by a multiplexing system, the accumulated counts can be transferred to a data bus and then to the microcomputer. Latching and clearing of all counters and scalers can be controlled by the computer program.

3.4 The software.

Software packages have been developed to run all the various observational routines. There are programs written in BASIC to drive the equipment for different purposes such as scanning line profiles, or choosing different parts of the profiles for photometric or polarimetric study, for one or two channels. All programs consist of two parts, viz. :- an introductory part which sets up procedures for controlling the whole electronic system and an operating part which utilizes the procedures. The main programs used in the observations described in this thesis were a scanning program to check the line profile, and a polarimetric program used to control the rotating $\lambda/2$ plate, wavelength positions of the filters, integration time, the collecting and saving of data. Outline structures of the programs are as follows:

Program 1- Scanning program.

The profiles of the Hα and Hβ lines were obtained using this program. This routine has been summarized as a flowchart (see Figure 3.7). When using two

channels the program must be run sequentially to explore the line profiles separately. Usually the motor needs to make about 60 steps to cover the line profile. The intensity values corresponding to the sixty wavelength positions are immediately displayed as a profile on the screen after a normalising process. After that, the data are printed out to allow their inspection so that particular wavelength positions may be selected for specific investigation, e.g. the positions for the line centre and two points in the adjacent continua may be chosen for the subsequent polarimetric program.

Program 2- Polarimetry program.

The summary for this program is again best described by a flowchart (see Figure 3.8). In this program we use the three wavelength positions selected by each filter, these being chosen after running the previous program. Information - i.e. object name; used filter name; filter tilt positions; date; file name; and cartridge name - needs to be typed into the computer. It is echoed on a printer to be saved as an observational log and it is also recorded in the data files which are stored on magnetic medium (see, first two lines of a typical record - Appendix B). After that, the routine commences by taking a record of the background signal. Then the source is measured in a cyclic sequence corresponding to the three selected wavelength positions. Before stopping the program and closing the file there are alternative ways to continue and repeat the measurements for the source or the background.

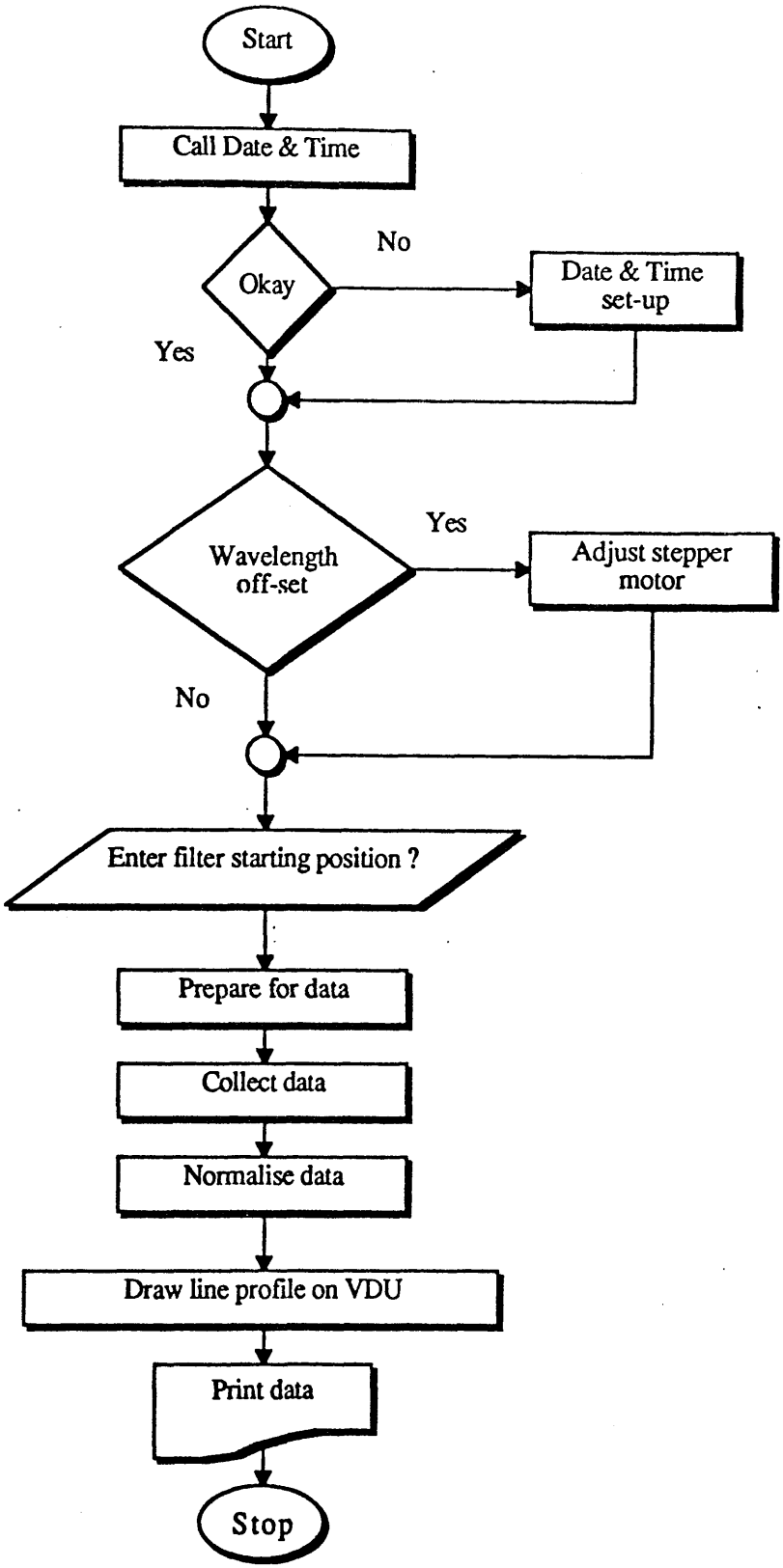

Figure (3.7) Flowchart for the scanning program.

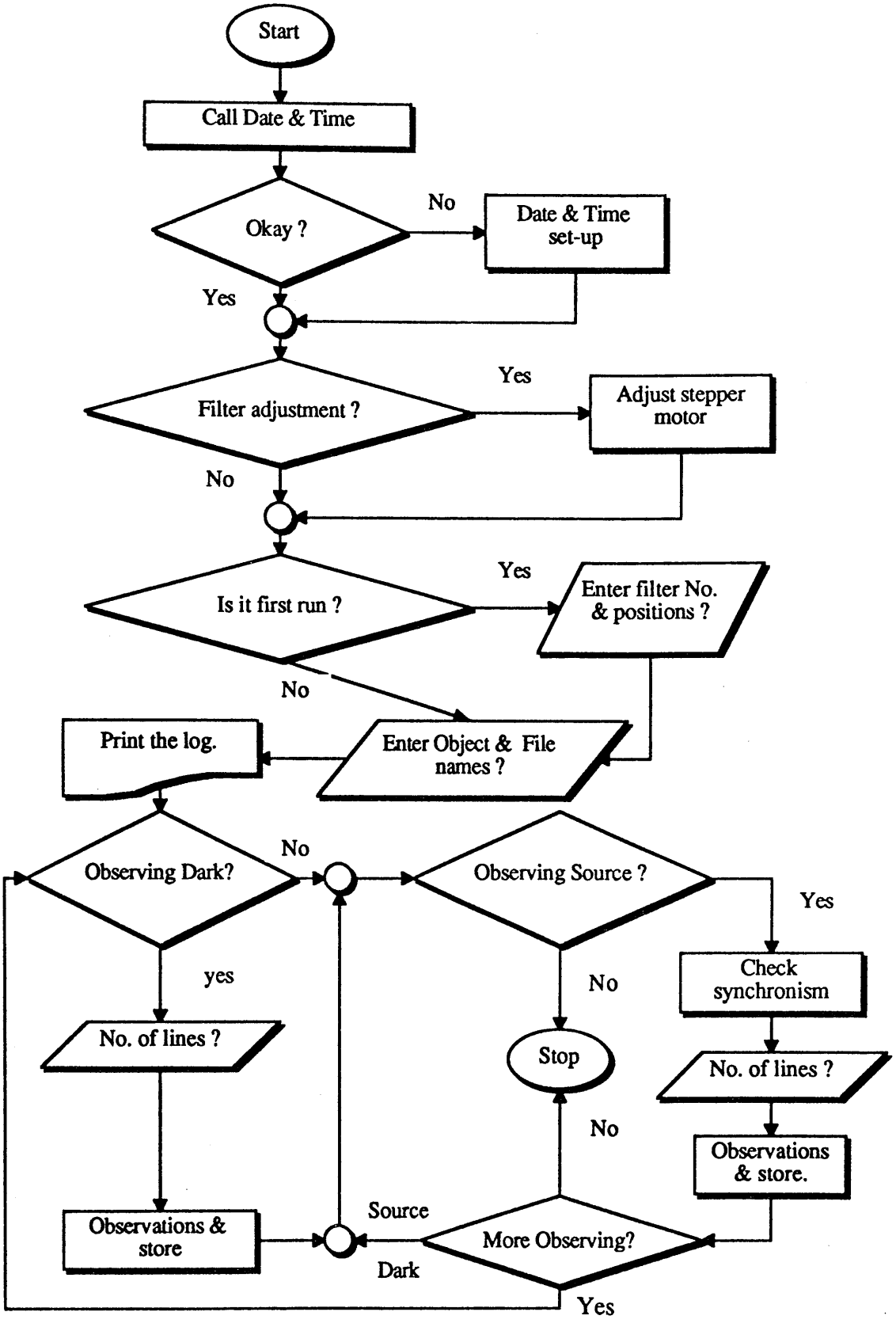

Figure (3.8) Flowchart for the polarimetry program.

3.5 Wavelength resolution.

The selection of the wavelength passbands was by interference filters. They can be considered as equivalent to Fabry-Pérot filters but with a solid gap. The resolution of these filters may be expressed as a bandwidth or full width half maximum (FWHM).

The central wavelength of the transmitted beam depends on the tilt angle, Φ, of the filter in the incident collimated beam. For small angles (< 20°) the wavelength λ_t at the centre of the passband may be expressed as :-

$$\lambda_t = \lambda_0 \left(1 - \left(\frac{\sin^2\Phi}{2\mu^{*2}}\right)\right) \qquad (3.3)$$

where λ_0 is the wavelength which is transmitted at normal incidence (i.e. $\Phi = 0°$), and μ^* is an effective refractive index of the dielectric gap within the filter, resulting from the refractive indices of the cavity and the multilayer reflecting stack. Clearly the shift is towards shorter wavelengths by increasing the incident angle. A typical curve of λ_t/λ_0 against Φ is shown in Figure (3.9). This wavelength scanning technique has been used in several different kinds of astronomical observation. de Vaucouleurs (1967) has applied it for observing late-type stars to measure the CaII H and K line profiles. Eather and Reasoner (1969) have used this technique to investigate emission lines in the aurora. Barbieri et al. (1974) used a tilted interference filter for measuring the line intensities in cometary spectra. At Glasgow University this technique has been used widely - see Clarke and McLean (1974, 1975a&b, 1976), Clarke et al. (1975), Clarke and Brooks (1984 and 1985), and Clarke et al. (1985).

The chosen filter is fitted within a mount which is attached to a rotatable shaft, in the filter plane, located in a ball race. The unit is adjusted in angle using a stepping motor and an anti-backlash gear box.The tilt angles are reproducible to the limit of the

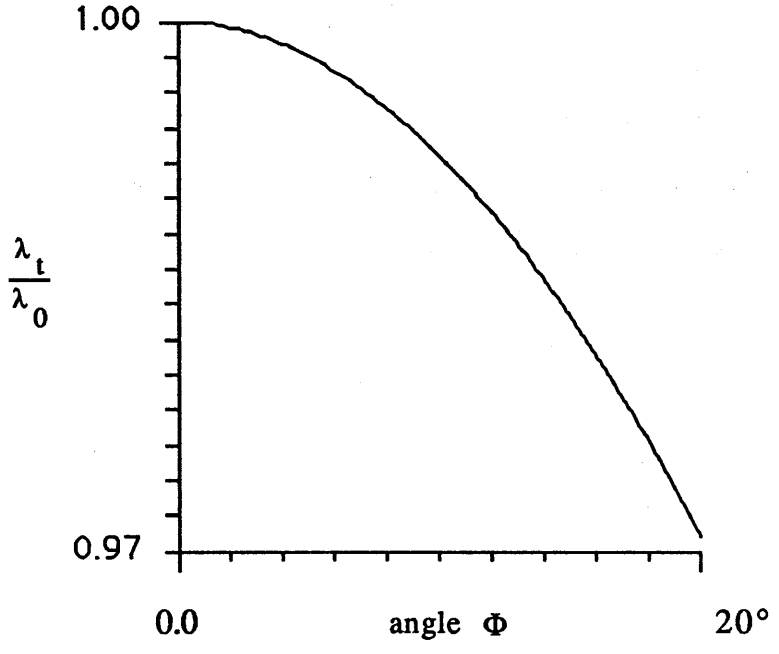

Figure (3.9) The behaviour of λ_t/λ_0 against angle Φ for a high resolution interference filter illuminated with a collimated beam of light.

stationary positions of the stepper motor. The peak wavelength of the passband for the interference filters is temperature dependent. Typical narrow-band filters have a temperature coefficient of 0.25Å/°C (Clarke et al.1975) so, in order to keep any wavelength shifts to much less than the filter FWHM, the environment was temperature stabilised to better than ±0.1°C. Typical scans obtained from the Moon using the Hα and Hβ filters are illustrated in Figure (5.1).

3.6 The photomultipliers.

The detection system consists of two photomultiplier tubes, one for each orthogonal beam as depicted schematically in Figure (3.2). As the observations used the Fraunhofer Hα and Hβ lines, the photomultipliers should have good sensitivity for those observed spectral regions. The photomultipliers presently in use are an EMI 9558Q tube which has an extended red response for the red channel, and an EMI 9789B tube for the blue channel which has its peak quantum efficiency at about 4000Å. The first tube was cooled by means of a thermoelectric cooler which keeps it at −20°C, while the second tube has a low dark count at room temperature, so no cooler has been used for it. The photomultipliers have separate stabilised high voltage supplies, so that their individual optimum working voltages can be accurately set.

In general, the photo-electron count rates are likely to be high and the effect of counting losses needs to be taken into account. Such losses result from the finite bandwidth of the electronic circuits. Because of this, there is a time interval following a pulse, during which the device is not able to respond. This is referred to as the dead time. So any number of photons potentially capable of interacting with the photo-cathode during a time interval equal to the dead time following an actual photo-electron event will not be recorded. The changing of the blue sky (zenith) brightness during a clear day from noon till sunset provides a good example of how corrected and uncorrected signals might behave (see, Figure 3.10). Accurate determination

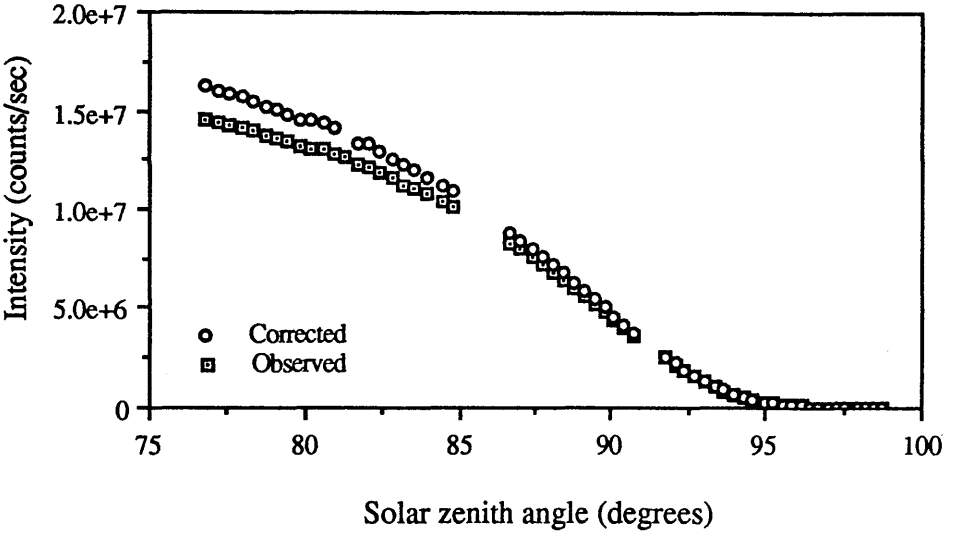

Figure (3.10) The intensity changes of the zenith (blue sky) from after-noon till sunset on 1988 August 7, plotted as raw measurements and with correction for dead time. The difference is very significant in the afternoon while it is virtually unimportant towards sunset, because of the low count rate.

of the dead time is very important to obtain the true values of polarization. The equation describing the effect of dead time on a signal can be written as

$$n = N e^{-\tau N} \qquad (3.4)$$

where n is an observed count rate in counts per second, N is "true" count rate for a perfect system in counts per second, and τ is the dead time coefficient. The dead time of the channels has been measured using a method described in Appendix (C), this assuming that the dead time correction is negligible for low count rates. The dead time was determined as 84.5ns for channel one (Hα) and 279ns for channel two (Hβ).

An approximate correction for polarimetric observations has been given by Hsu and Breger (1982), viz.

$$P_{tru} = P_{obs} (1 + \tau n) \qquad (3.5)$$

where P_{tru} is the true value of polarization, and P_{obs} is the observed value of polarization. Substitution of typical values of τ and n shows the need to apply corrections.

3.7 Instrumental design for solar experiments.

3.7.1 Introduction.

Polarimetric studies of the Sun require a detectability of P of the order of $\Delta P \approx 10^{-5}$ or better (see Kemp et. al. 1987, Leroy, 1989). They require fore-optics which do not themselves introduce polarization. Reflecting telescopes can introduce problems because of non-normal reflections over non-uniformly reflecting mirrors. Refracting telescopes may suffer similar problems by having a transmittance with non-radial symmetry; they may also possess stress birefringence. It is therefore best to place the modulator before any other optical elements.

There are two themes for the intended solar experiments, these being polarimetric observations of the whole solar disk and investigations along various solar disk diameters. A single system for both experiments has been used, see Figure (3.11). The system has a small telescope with aperture of 25mm, and with focal length of 120 mm (F_1). The polarimetric modulator was fixed before the small telescope to eliminate any polarization produced by the remaining optical system. The polarimetric elements were a half-wave plate producing optical modulations of 10Hz (corresponding to mechanical rotation of 2.5Hz), and a fixed Polaroid.

An integrating sphere has been made for the whole solar disk measurements, this being fitted at the focus of the small telescope. The sphere helps to scramble the image structure and remove the effects of solar disk image movement caused by the mechanical rotation of the half-wave plate. For the centre-to-limb observations the same telescope was used with "eyepieces" to give a projected solar image. A special plate was made, called a solar limb scan device, which allowed scanning across any chosen diameter. For both experiments, light was taken to the filters using optical fibres. A high density filter was fitted so that it could be inserted prior to the optical system to allow visual inspection and centering of the solar disk within the diaphragm.

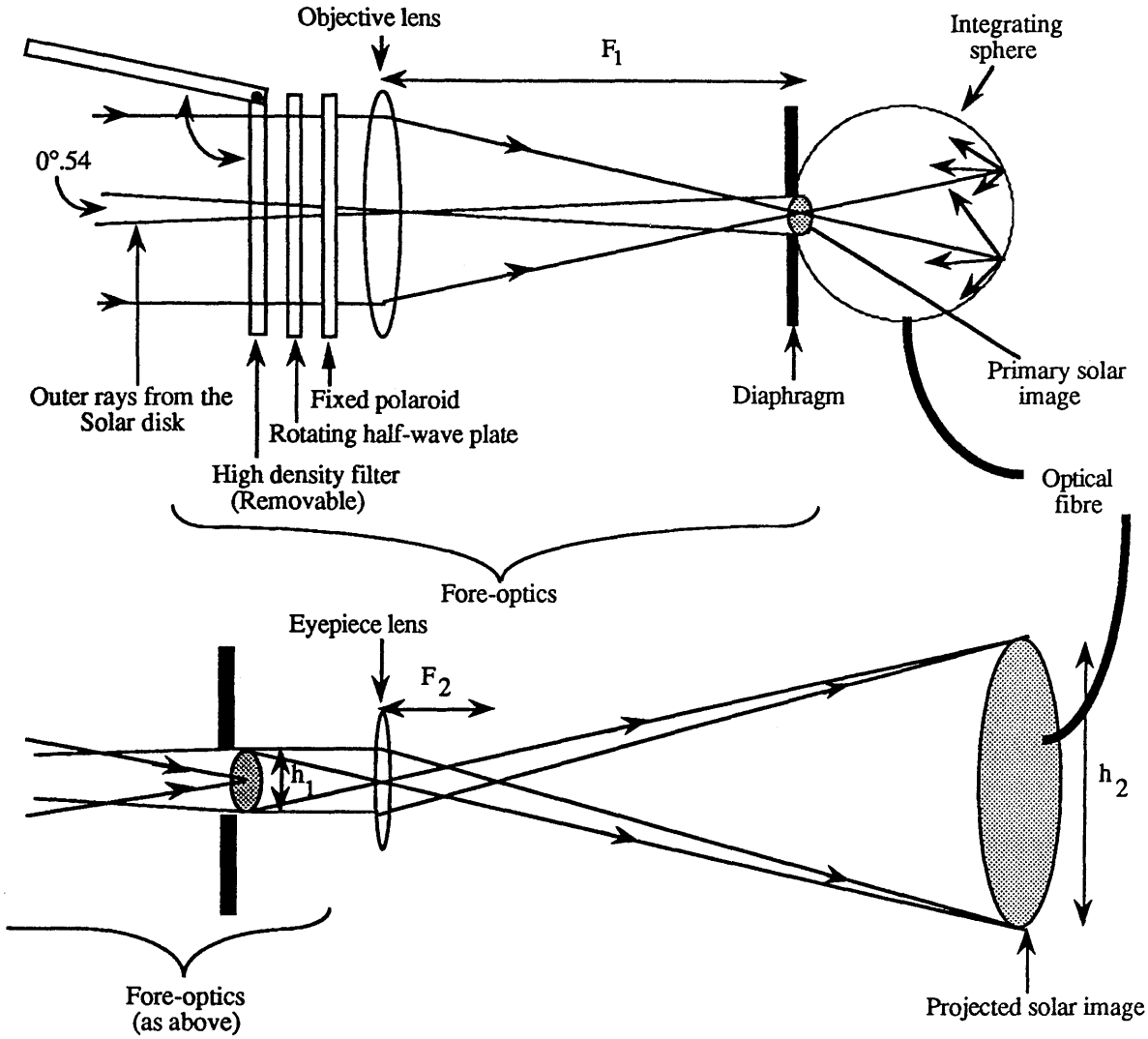

Figure (3.11) A schematic diagram of the solar experimental arrangements. Upper- illustrating the polarimeter, the objective lens of the small telescope and the integrating sphere for the whole solar disk experiment. Lower- illustrating the optical system for measuring the polarization of specific solar areas. An "eyepiece" lens replaces the integrating sphere and produces a projected solar image. The details of the dimensions (F_1 etc.) are given in the text.

The CLV observations were attempted with different sizes of "eyepiece" to produce different sizes of the solar image diameter (h_2). These optical systems were mounted on the upper rim of the 50cm telescope at the Cochno station, the telescope being used only to act as a stable platform with accurate tracking. Another small telescope was used as a guider.

3.7.2 The CLV experiment.

As the Sun is an extended body of about 0.54 degrees then, by using the small telescope described above, the diameter h_1 of the primary image is

$$h_1 = F_1 \times \theta° = 120 \times 0°.54 \times \frac{\pi}{180} = 1.13\text{mm} \qquad (3.6)$$

Three different desired projected solar image diameters (100, 80 and 60mm) have been produced by choosing eyepieces with the appropriate focal length (4, 5, and 6mm) value F_2 and fixing them at their correct positions after the telescope focus. The distance from the primary solar image to its projection was chosen to be 360mm. A black plastic tube covered the gap between the telescope and the solar image to prevent unwanted light entering the system and reduce any scattered light within the system. The magnified solar images were projected on to the limb scan device, rigidly connected by pillars to the end of the plastic tube.

This limb scan device allows observation along any diameter on the solar disk. It comprises a slide, with a hole holding a fibre, and a micrometer is used to move the slide to any position on the solar disk. The solar image could be monitored by two orthogonal windows on the limb scan device. The orthogonal windows were covered with frosted glass marked by three stripes at distances of 30, 40, and 50mm from the centre of the disk (Figure, 3.12). These windows are used for guiding and focussing. Light was carried to the filters and the detector by the fibre. The system gives the opportunity to achieve different spatial resolutions according to the chosen fibre (see Table 3.1).

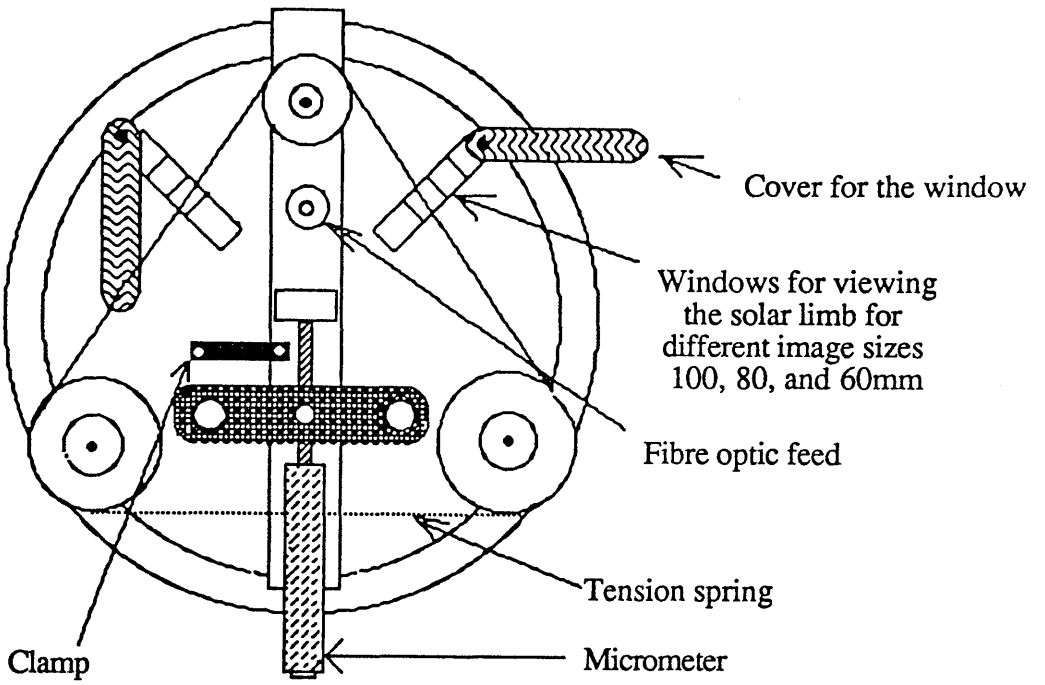

Figure (3.12) Solar disk scanner device.

Fibre size \ h_2	100	80	60mm
200 μm	3.89	4.86	6.48"
150 μm	2.92	3.65	4.86"
100 μm	1.94	2.43	3.24"

Table (3.1) Values of spatial resolution (arc sec) on the solar disk image (h_2), using different size of fibres, 200,150 and 100μm.

Expected photon rates from different parts of the solar disk.

The expected signal in terms of recordable photo-electrons can be estimated by using the absolute flux density F_λ (energy flux per unit wavelength interval) for a given magnitude (zero) star as determined by Johnson (1966). By considering the absorption of the atmosphere of air mass M with extinction coefficient A, allowing for the transmittance T, of the optical system, the passband of the filters $\delta\lambda$, the quantum efficiency of the detector q, the flux received by the telescope of diameter d, converted to photo-electrons per second may be expressed as a count rate given by:

$$n = F_\lambda \, 10^{-0.4\,(m\ +\ AM)} \; T \; \delta\lambda \; q \; \frac{\pi\, d^2}{4} \; \frac{\lambda}{h\,c} \qquad (3.7)$$

where m is the magnitude of the star, h is Planck's constant, c is the velocity of light and λ the wavelength of the centre of the passband.

The transmittances of the various parts of the optical system can be estimated as follows:

Element	Transmittance (%)
Half-wave plate	96
Polarizer	40
Objective lens	95
Eyepiece lens	95
Fibre	40
Blocking filter	75

The efficiency of the instrument is reduced further by the detector quantum efficiency (20%) giving an overall factor for efficiency of 2.1 %.

The expected photo-electron count rate from the Sun (assuming that the Sun is uniformly bright) may be determined according to the values of the various components in Equation (3.7) and by setting m=-26 (the magnitude). The situation will be

modified if only parts of the solar disk are observed. If resolved areas are monitored, limb darkening needs to be taken into account according to the usual expression :-

$$I_{\emptyset} = I_o(1 - u + u \cos \emptyset) \qquad (3.8)$$

where u is the limb darkening coefficient, $\emptyset$ is the angle between the emergent ray and the normal to the solar surface, I_o is the intensity at the centre of the solar disk, and $I_{\emptyset}$ is the intensity at the observed position.

Table (3.2) gives approximate photo-electron count rates which should be collected at different air masses M = 1, 3 and 6, through different fibre sizes = 200, 150 and 100μm under the above considerations and by taking the UV part of the spectrum, i.e. λ =3600Å, F_λ= 4.35×10^{-16} W/cm^2/Å and by choosing values of A=0.2, d=25mm, solar image=100mm, and limb darkening coefficient u= 0.84. If the noise of a polarimetric determination is limited by photo-electron counting statistics, then according to the recording technique used here the uncertainty is given by $\sigma_p = \pi/(2\sqrt{N})$, where N is the accumulated count over the integration time. Hence by using a 100μm fibre at the limb, Table (3.2) indicates that a polarimetric accuracy of 0.14% within times less than 4 minutes could be achieved. This precision should be sufficient to detect the Hanle effect within the CaI 4227Å line, (see Figure 1.11).

3.7.3 The whole disk experiment.

Designing an arrangement for making observations of the integrated light from the Sun is not a trivial task. The chief reasons for this are its extremely high brightness and its angular size. The situation is more complicated if the measurements involve polarimetry. In order to provide attenuation, to scramble the image and to scramble any modulation caused by image wander - this possibly caused by the polarimetric modulator itself - the equipment incorporated an integrating sphere. In addition to its "optical" properties, this device has the advantage that it is easy to fit on the end of the small telescope and collect all the light from the image of the solar disk. There is the

Fibre 200μm

M\cosØ	1	0.8	0.6	0.4	0.2	0.1 .
1	194723	162266	128953	96116	63822	47571
3	134715	112260	89214	66496	44154	32911
6	77520	64599	51337	38264	25407	18939

Fibre 150μm

M\ cosØ	1	0.8	0.6	0.4	0.2	0.1 .
1	109648	91371	72729	53989	36221	26787
3	75858	63213	50316	37352	25098	18532
6	43652	36375	28954	21494	14420	10664

Fibre 100μm

M\ cosØ	1	0.8	0.6	0.4	0.2	0.1 .
1	48762	40634	32292	24423	15982	11913
3	33735	28112	22341	16896	11057	8242
6	19412	16177	12856	9723	6363	4743

Table (3.2) Expected recorded count rates (in counts per second) from different parts of the 100mm solar image, displayed for fibre sizes 200, 150, and 100μm, with values of air mass M=1, 3, and 6.

possibility of inserting several fibres into it for simultaneous measurements at different wavelengths. The fibre may take the light to subsequent optical instruments such as a spectrometer or Fabry-Pérot system. The diameter of the fibre controls the amount of light used for spectropolarimetric analysis; in this sense the integrating sphere and fibre optic combination acts as a variable attenuator.

The interior of the sphere is painted with a KODAK white reflective coating which has an almost perfect Lambertian surface for all wavelengths between 2000 and 25000 Å, this being used successfully by other workers (see Wraight 1989). A diaphragm of 1.25mm was fixed before the focal plane of the small telescope to limit the field of view to be just larger than the solar-image diameter. A special slide holding the integrating sphere and an eyelens was fixed also at the focal plane of the small telescope. The eyelens is used to ensure that the whole solar image is exactly within the diaphragm and at the focus; when viewing the image a high density fiiter is placed over the objective lens of the telescope.

3.7.4 High spectral resolution spectrometry.

It should be noted that the intended solar experiments need high spectral resolution up to 0.1Å. In order to achieve this with the necessary throughput (the ability of a spectrometer to accept light over a rage of cone angles and maintain its resolving power, see Jacquinot 1954), designs were considered involving Fabry-Pérot (F.P.) interferometers. Firstly a grating spectrometer was employed as an order sorter, followed by two tunable Fabry-Pérot interferometers. Each one of the three spectrometric elements can be tuned separately to obtain maximum transmission for a chosen wavelength; when the whole system is combined the selected wavelength is hence isolated by the simultaneous tuning of each of the devices. The pulse generator board is used to control a motor which rotates the predisperser grating. For the F.Ps., their adjustment is achieved by applying voltage to the piezoelectric spacers, this being

generated by a digital to voltage converter under control of a microcomputer, the digital signal again being produced from the pulse generator board.

(i) The predisperser :- A small grating spectrometer with dispersion of 45Å/mm may be used either by itself to provide medium resolution or in combination with the F.Ps, acting as an order sorter. A drive shaft attached to the scanning arm provides a wavelength control of 500 Å/rev. A stepper motor with 48 step/rev. was used to rotate the shaft through a gearbox of ratio 1/10; each motor step corresponds to a wavelength shift of 1.04Å.

(ii) The Fabry-Pérots :- The instruments were commercially produced by Technical Optics. Each one is made from two circular plates of the best optical fused silica, less subject to thermal distortion than glass, coated with uniform reflective layers and of low absorbence. The plates need to be maintained in parallelism better than $\lambda/100$. The parallelism and the tuning of each F.P. is controlled by piezoelectric pads.

The transmission of light through the Fabry-Pérot filter is given approximately by the Airy formula

$$A(\lambda) = \frac{1}{1 + [4R/(1-R)]^2 \sin^2(\delta/2)} \qquad (3.9)$$

where $\delta = 4\pi\mu\sigma d \cos \nu$, R is the reflectance of the plate coatings, d is the space between the plates, ν is the incidence angle within the cavity, μ is the refractive index of the spacer medium, σ is the wave number of the incident light.

The wavelengths λ_m transmitted with maximum intensity are given by

$$\lambda_m = (2 \mu d \cos \nu)/m \qquad (3.10)$$

where m is an integer called the order of interference. Control of the wavelength is available by varying d or μ, or by tilting, which changes the angle ν. Hence, in our

case for a given resolving power (fixed interference order) the F.P. is tuned only by changing d, as $\nu = 0.0°$ and μ are constants. The instrumental profiles for the monochromator and the two F.Ps used in conjunction are illustrated at Figure(3.13).

A metal holder with leaf-spring adjustment systems was built to carry the two F.Ps, allowing the etalons to be set so that they are concentric with each other and kept parallel to each other. A chamber was built to keep the F.Ps in a thermally controlled environment and away from pressure variations. Many problems arose during the experimentation with F.P. systems which prevented their use in the solar measurements. Some were essentially trivial but nevertheless hindered the progress. For example at the time of the trials, an appropriate spectral lamp offering strong lines around CaI 4227Å were not available. At the more fundamental level the small f-ration of the emerging cone from the fibre and the physical size of its aperture made it difficult to collimate the light sufficiently, so as to maintain the hoped for spectral resolution. Three F.P.s were used in the experiment. One was completely adjustable and did provide good circular fringes, the two that were intended to be used in parallel were optically controlled with set gaps but good circular fringes were not achieved after many hours of careful adjustment. It may well be that they suffer from a manufacturing fault. Because of these problems, the whole spectrometer system was not successfully established. However the small grating spectrometer has been used to scan through the Sun's spectrum, for the whole solar disk, and to test the photometric stability of the integrating sphere and the subsequent optics and detector system. A discussion of the results and performance of this solar equipment in respect of spectro-photometry and polarimetry is presented in the following chapter.

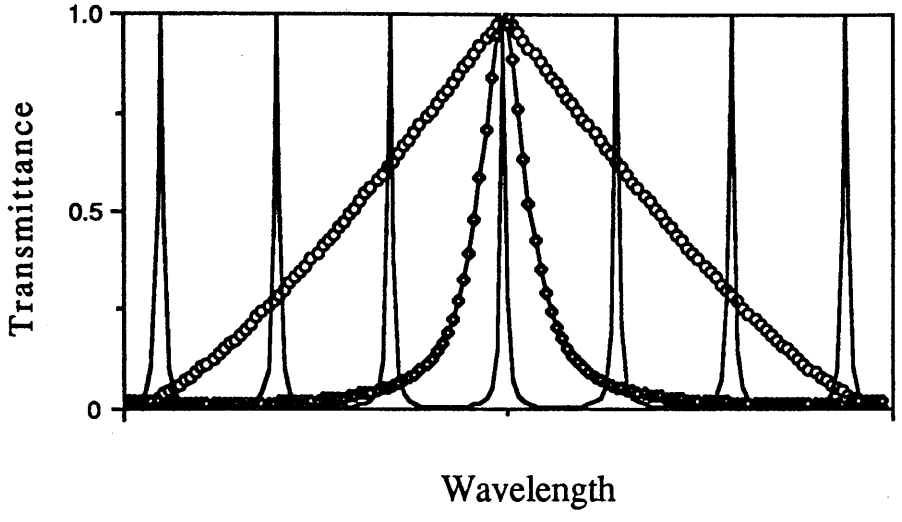

Figure (3.13) Computed instrumental profiles for the three spectrometric elements based on their theoretical capabilities. Symbols (o), (◊) and (—) correspond respectively to the grating spectrometer (FWHM ≈ 6Å), the first Fabry-Pérot with FWHM 1Å, and the second Fabry-Pérot with FWHM 0.1Å. It can be seen that to achieve 1Å resolution, the combination of the grating and first F.P. should be adequate, but to achieve ≈ 0.1Å both F.Ps. need to be used in tandem.

Chapter 4 Measurements across the CaII K line of the Sun.

4.1 Introduction.

The investigations related to solar polarimetry fell into two parts:-

I- It was hoped to investigate the behaviour of the polarization across the solar disk from centre to limb with the aim of resolving the discrepancy between results, by Stenflo et al. (1980) and by Wiehr (1975), of the CaI 4227Å observations at the solar limb [their spectral resolution were of about 30mÅ and 50mÅ respectively]. These discrepancies have been discussed in Chapter 1, and might be interpreted in terms of whether or not the Hanle effect was present at the particular times of the observations.

II- The second experiment comprised polarimetric observations for the whole solar disk to monitor effects associated with solar magnetic activity. Such investigations are useful in allowing direct comparison with stars. Solar activity might be detected through the polarization properties of sensitive resonance lines, such as CaII K and CaI 4227Å, these already having been explored photometrically (see Chapter 1).

After setting up the small telescope with the solar disk scanner device to investigate the polarization from centre to limb of the solar disk, the experiment proved unsuccessful because of the wobbling image of the solar disk caused by the non-parallelism of the layers of the half-wave plate. The effect is explained in more detail in the next section.

The second experiment was an extension of some earlier work by Stewart (1984), but with modified equipment. The new technique used an integrating sphere, the small grating spectrometer (see Chapter 3), a small telescope instead of coelostat mirrors and a microcomputer control system in place of electronic hardware. The computer system gives an improvement of about 20% in using the experimental time for collecting data. The experiments involved observations of the CaII H and K line centres because of their sensitivity to solar activity as described in Chapter 1. Also the wings of the H and K

lines are more suitable for studying fluctuations of the brightness as they are formed over a large range of height within the solar atmosphere. Section 4.3 describes the measurements made during 1989 July and August of the whole solar disk across the CaII K line.

4.2 Solar image wobbling by the polarimetric modulator.

Observations using a rotating half-wave plate modulator will introduce a wobble of the image of any source. This wobbling may be caused by non-parallelism of the half-wave plate layers (prismatic effect) or mis alignment of the optical and mechanical axes. In order to estimate the former mechanism consider the prismatic effect of a single wave plate at a fixed position (see, Figure 4.1). By using the thin prism formula, the angular deviation, α is given by:

$$\alpha = \kappa (\mu - 1) \qquad (4.1)$$

where κ is the small angle associated with the non-parallelism of the plate, and μ is the refractive index. The amount of the physical shift represented by j can be obtained according to

$$j = F_1 \tan(\alpha) \qquad (4.2)$$

where F_1 is the focal length of the objective lens.

From the observations, the final solar image (diameter 100mm) was found to wobble within a circum-circle of diameter 106mm, (the centre of the primary solar image was off from the optical axis by 0.034mm). This is equivalent to a value of α equal to 2.7×10^{-4} rad. By taking a value of $\mu = 1.56$ (quartz- mid visual spectrum), $\kappa = 1.6$ arc min, which is typical of the manufactures specification.

Adjustments were made to alter the tilt of the plate to the mechanical axis but these did not improve the situation. The problem is inherent to the plate and the

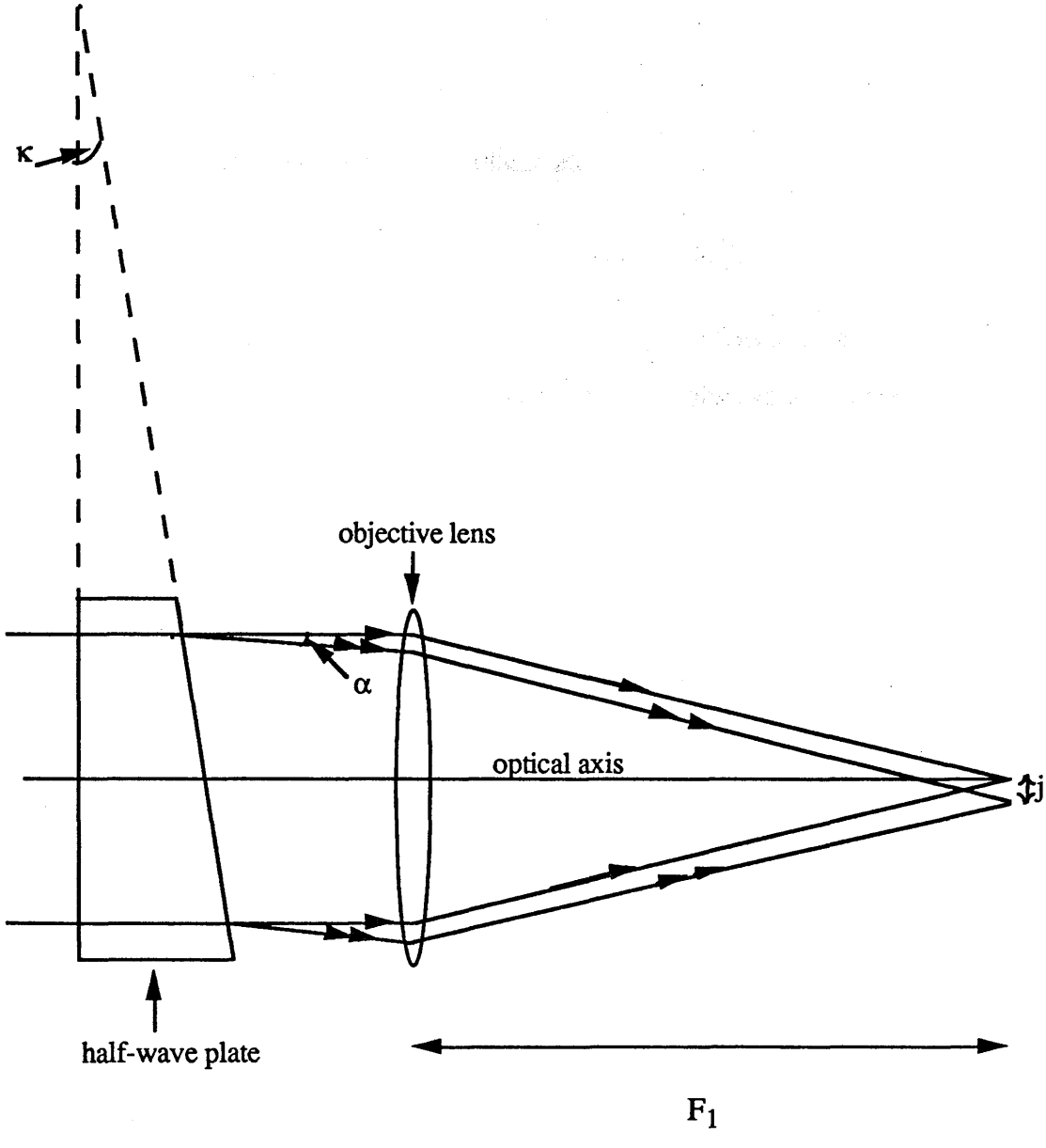

Figure (4.1) Shifting of the primary solar image at the focus of the objective lens, caused by the non-parallelism of the half-wave plate.

manufacture's inability to construct them with high tolerance. In the longer term, the experiment (variation of the polarization from the centre to the limb of the solar disk) requires the use of another kind of modulator without moving parts, such as a photoelastic wave-plate.

4.3 Observations of the whole solar disk.

4.3.1 Photometric measurements of the K line profile.

In order to study the performance of the small telescope and the integrating sphere for polarimetric measurements, some preliminary observations were made to test the stability of the overall system. For these observations the scanning program was used to scan through the K line profile.

The solar spectrum, in spectral region roughly between 4200Å to 3500Å, was first scanned, using the grating spectrometer, to provide wavelength calibration and to identify the positions of the CaII H and K lines (see Figure 4.2) for photometric and polarimetric observations. The region around the CaII K line was selected and repetitive scans were obtained using 50 discrete wavelength positions, measuring the intensities with 1s integration times. Each scan with data logging, etc., took less than one minute. The photo-electron count rate at the line core was about 3.10^5 per second. The photometric accuracy expressed as a percentage is $100/\sqrt{N}$, where N is the number of recorded counts, suggesting that each line profile should be recorded with an accuracy $\approx$0.2%. An example of a scan is in Figure (4.3), which has been normalised to a particular point in the continuum.

For the experiment to investigate the spectrophotometric stability it was decided to make repetitive measurements of the line depth. The value of the recorded line depth is commensurate with the spectrometer having resolution of about 6Å. This was achieved

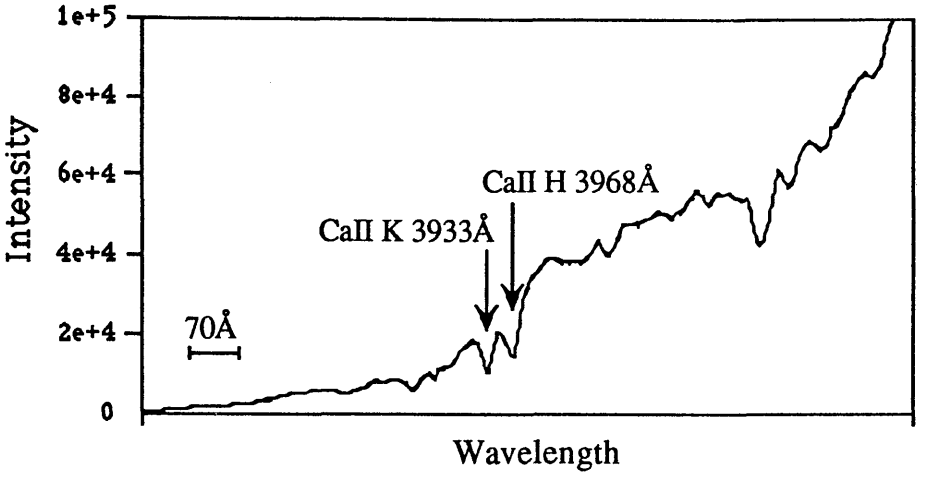

Figure (4.2) Spectrum of the Sun in spectral region between 4200Å to 3500Å obtained by the small spectrometer. The CaII H and K lines are clearly shown. The sloping tail of the spectrum is caused by the atmospheric absorption.

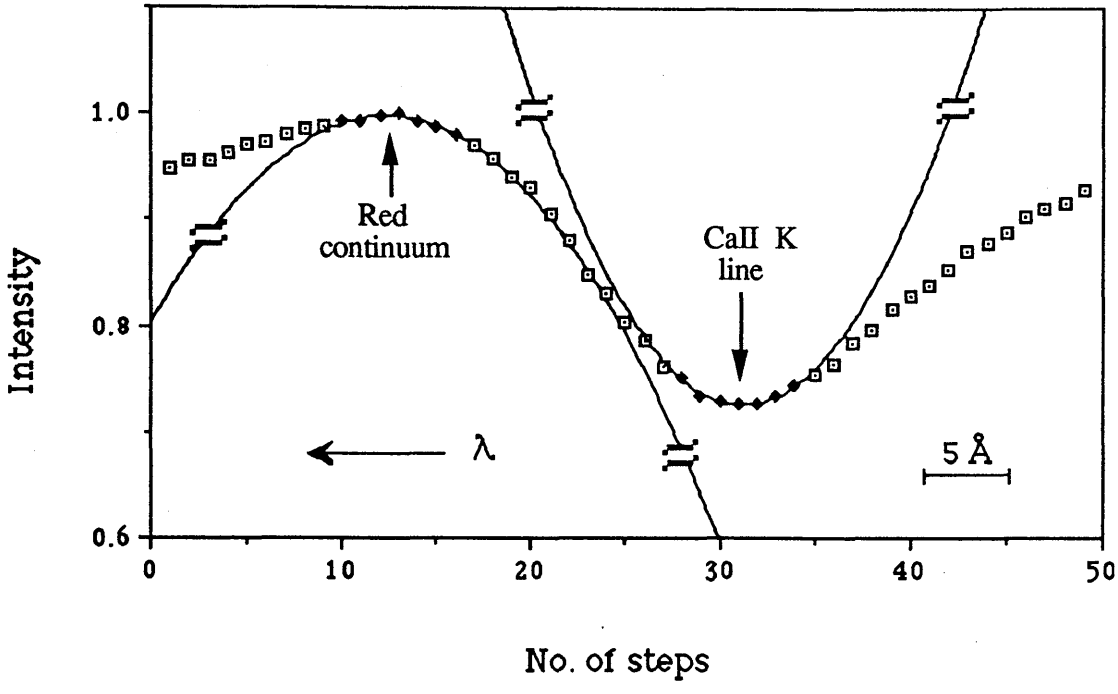

Figure (4.3) A typical record of the CaII K line and the red continuum recorded by the step-scanned spectrometer. The symbols ▫ and ♦ represent the data points. A least squares method has been used to fit a second order polynomial to seven points represented by ♦ on the line core part and to seven other points at the red continuum, to obtain the minimum and maximum intensities. These values then provide a measure of the line intensity ratio R. [The wavelength decreases with step number i.e. with "positive" rotation of the grating, and hence increasing wavelength is towards the left.]

by taken the line profile from Utrecht solar atlas (Minnaert et. al., 1940) and convolute it with triangular instrumental profiles of various bases. The nearby continuum displays a rounded shape at this resolution making it difficult to ascribe a meaningful measure of the line depth. In addition to this problem, the positions of the continuum and the line centre were not stationary during the observing time relative to the wavelength register, due to temperature drifts. In order to monitor the strength of the K line, second degree polynomial equations (see Appendix- E) have been fitted for each scan in the region of the line and at the red continuum (see Figure 4.3). From the determined coefficients, the intensity values of the red continuum and the line core were interpolated, these being used for calculations of R (line intensity ratio). Figures (4.4 to 4.8) display the values of R against the time on different days, each point representing the average of ten values of R with its standard error. The values of the standard errors were found to vary according to the weather conditions. Table (4.1) gives dates, time of the observations and daily mean values of $\bar{R}$ with their standard errors based on the internal distribution of the repeated measurements. Day to day values of $\bar{R}$ were reproducible to better than 1.0%. It may be noted that Barth et. al. (1984) reported fluctuations in the central flux in Hα of about 1% referred to the local continuum. However more observations would be required to confirm whethre the fluctuations which are just above the noise levels of these data are generated by the Sun.

As the CaII K line lies within the U.V. part of the solar spectrum, where the intensity changes are steep due to the slope of the atmospheric extinction, any differential atmospheric absorption across the investigated line will be included in the determined value of R. If this absorption changes with time, say with zenith distance, then R is likely to reflect these changes. However, such effects were not noticeable even through the longest run of observations of about seven hours, on 1989 July 6.

Differences of the noise levels from day to day were caused by marked changes in the haze or turbidity levels. The results which were obtained during 1989 July 11 show

Date	Start (UT)	End	No. scans	Sky condition	$\bar{R}$	$\pm\sigma$
3/7/89	11:28	12:22	44	clear	0.7295	0.0008
5/7/89	9:45	13:52	157	haze	0.7308	0.0007
6/7/89	9:57	16:52	173	milky	0.7361	0.0007
7/7/89	9:45	11:57	78	white	0.7425	0.0014
11/7/89	11:49	13:59	73	very clear	0.7324	0.0003

Table (4.1) Summary of the observation parameters: date, time interval, number of scans obtained of the CaII K spectrum line under the given sky condition. $\bar{R}$ is the average value of R corresponding to the intensity ratio (I_L/I_C), with its standard error, obtained from the distribution of repeated measurements during the day.

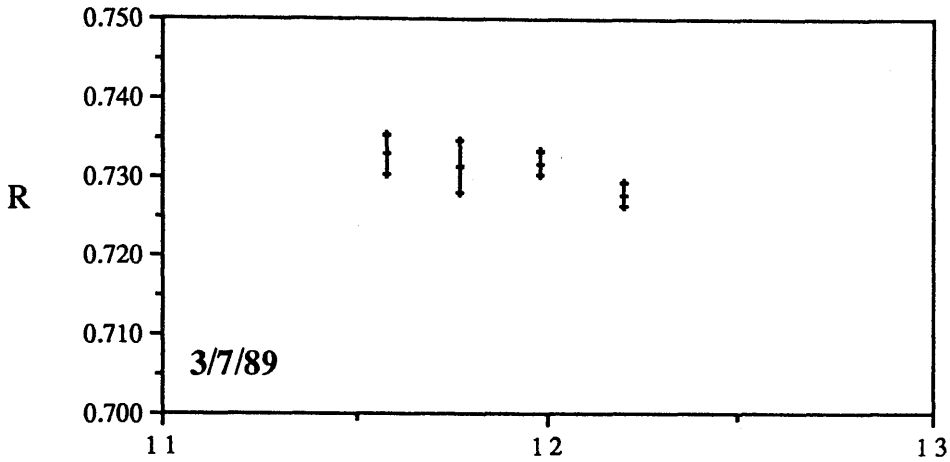

Figure (4.4) Time (U.T.)

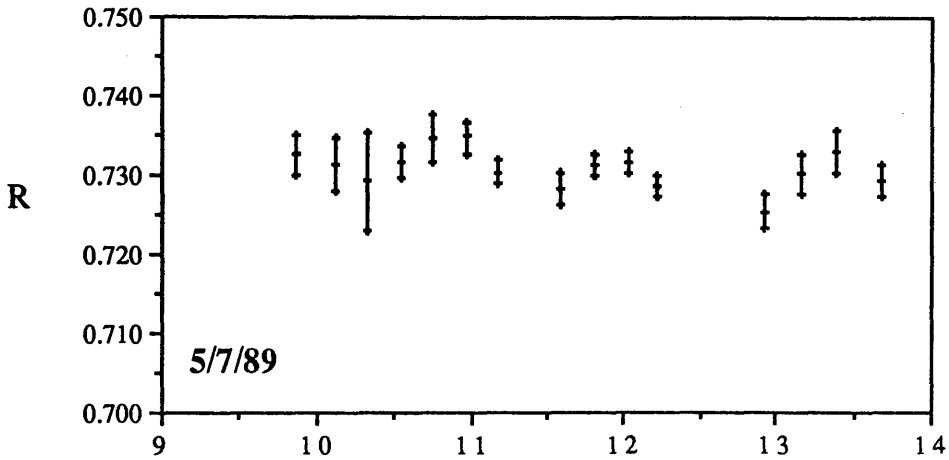

Figure (4.5) Time (U.T.)

Figures (4.4 - 8) Variations of the ratio R (I_L / I_C) of the CaII K line through the day. Each point with its error bar corresponds to the mean from ten values with the calculated uncertainty. The differences of the noise levels from day to day were chiefly caused by marked changes in the haze and turbidity levels.

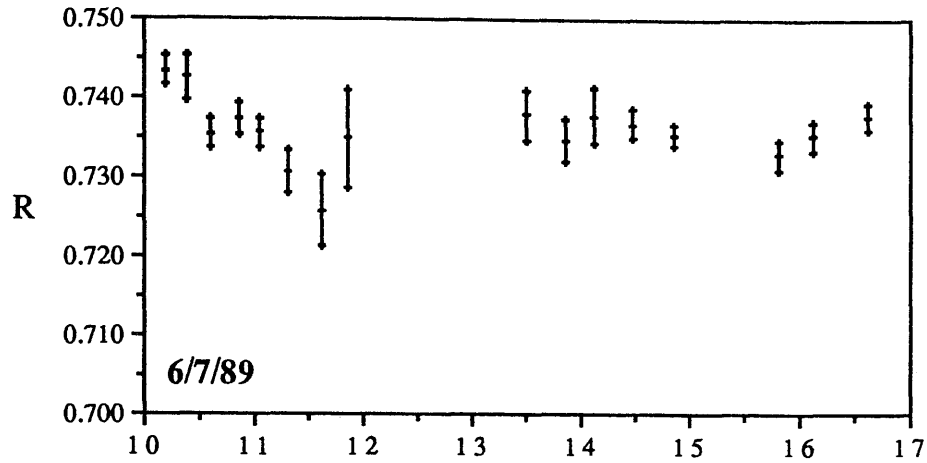

Figure (4.6) Time (U.T.)

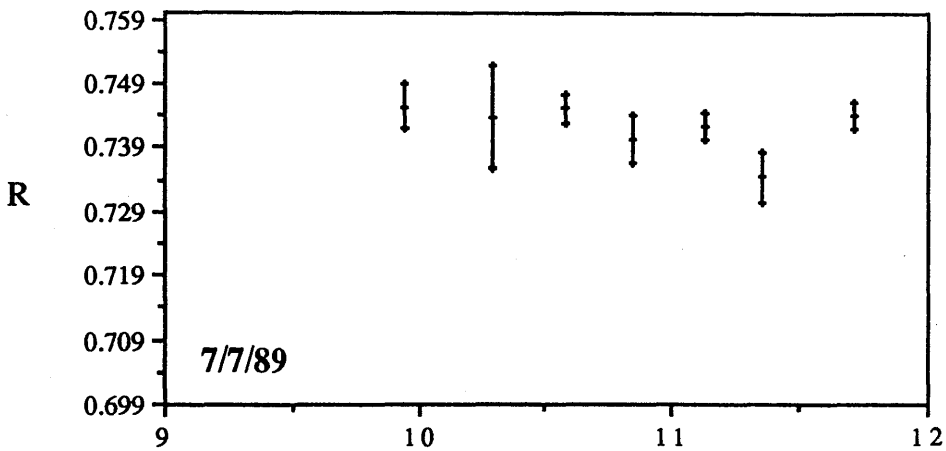

Figure (4.7) Time (U.T.)

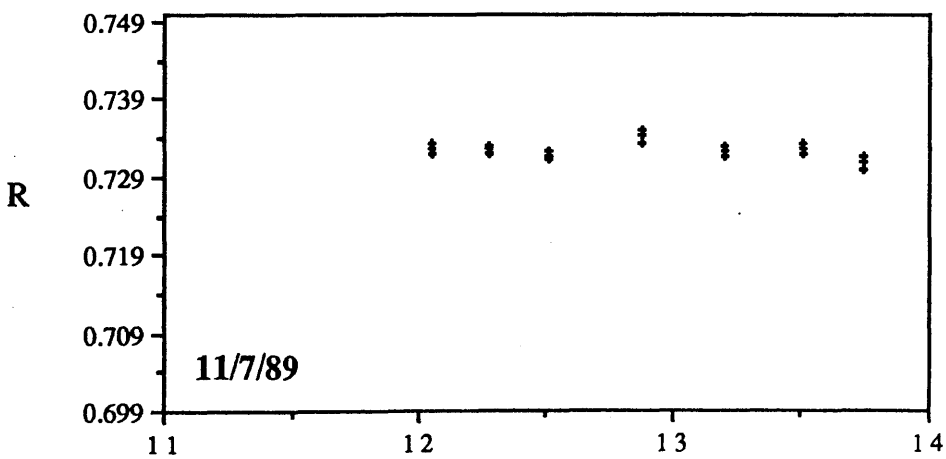

Figure (4.8) Time (U.T.)

the smallest overall error (0.03%) see Table (4.1). This can be clearly seen in Figure (4.8) where the errors on the repeated measurements of blocks of 10 scans show uncertainties which are typically $\approx \pm 0.07\%$; these high quality data were collected when the atmospheric conditions were less disturbed than for the other observations. These results here support the idea that the integrating sphere is an attractive system for monitoring the light from the whole solar disk.

4.3.2 Polarimetric observations.

After the testing of the integrating sphere for photometric stability, the equipment was fitted to the frame of the 50cm telescope at the Cochno site, to provide an accurate tracking platform. The data presented here are from three separate runs which were made during August 1989. Values of the normalised Stokes parameters q and u with a pooled standard error for the whole solar disk have been calculated for three wavelength positions across the CaII K line, and are plotted in Figure (4.9); the observed degrees of polarization with their uncertainties have been tabulated in Table (4.2).

Welch tests (Brown and Forsythe,1974) allow comparisons to be made between sets of observations with differing numbers of measurements and with differing variances, and they provide an estimation as to whether the sets can be considered as originating from an identical underlying value. As a requirement for the Welch test, the measurements for each wavelength position were first confirmed as being representative of normal distributions using Skewness and Kurtosis tests (see Appendix F). The Welch test has been applied previously to polarimetric measurements (Clarke et al., 1985 and Clarke and Stewart, 1986). The Welch tests for the data sets revealed no significant differences and it can be concluded that at these detection levels no spectral variation of polarization has been found. As can be seen in Figure (4.9) the observed Stokes parameters with their associated uncertainties overlap the origin, i.e. with reference to the origin, no polarization has been detected. Without any other experimental noises,

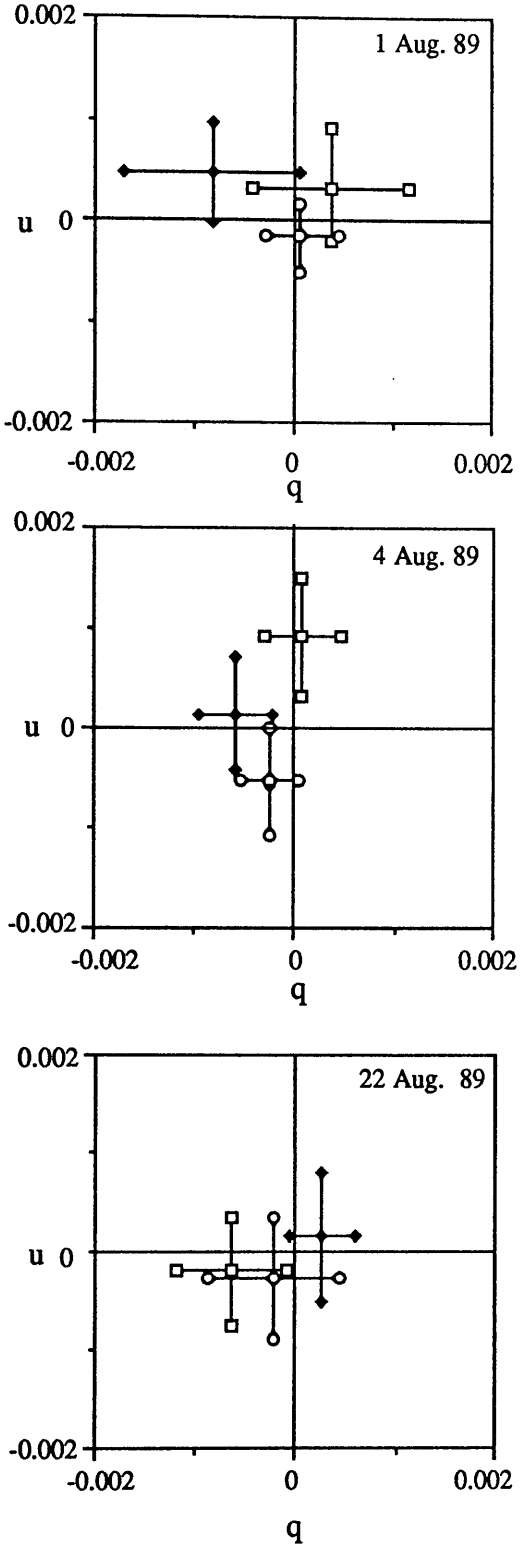

Figure (4.9) Normalised Stokes parameters with their standard errors for the continuum and the CaII K line. The symbols □ and ♦ represent the continua (Blue & Red) and o the line centre.

Data	Position	N	P	σ
1 August 89	R	5	0.0009	±0.0004
=	L	5	0.0002	±0.0001
=	B	5	0.0005	±0.0002
4 August 89	R	8	0.0006	±0.0004
=	L	8	0.0006	±0.0003
=	B	8	0.0009	±0.0004
22 August 89	R	15	0.0003	±0.0003
=	L	15	0.0003	±0.0004
=	B	15	0.0007	±0.0004

Table (4.2) The mean values of measured polarization (P) with their uncertainties (σ) are given for the CaII K line, for the whole solar disk. (R and B represent the red and the blue continua, L is the line centre), and N refers to the number of integrations performed to obtain the tabulated measurements.

polarimetric accuracy is ultimately limited by the total photo-electron count. From the typical count rate of this experiment (3.10^5 per second), an accuracy in P of 0.0019% could be achieved by a 6 hour integration time but this is somewhat impractical. Improved accuracy can only be achieved by increasing the count rates say, by using a wider fibre optic from the integrating sphere. Although this solar polarimetric experiment provided a null result, there is no reason why it should not be pursued using equipment operates with higher photo-electron counts and ultimately higher polarimetric accuracy.

4.4 Conclusion.

The CLV experiment to detect the Hanle effect, by measuring the polarization at the solar limb, has failed because of the prismatic effect of the half-wave plate. Future experiment require the use of a different type of modulator. For measurements of the whole solar disk, an integrating sphere has been investigated. The stability of this system has been successfully tested photometrically using a spectrometer (FMHW≈6Å). With this spectral resolution no detectable polarization for the whole solar disk across the CaII K Fraunhofer line was observed at a level of $\Delta p \pm 0.0002$.

Chapter 5 Lunar observations.

5.1 Introduction.

In Chapter 1, it was pointed out that Teifel (1960) suggested that lunar luminescence might be detected by spectropolarimetry. If the luminescent light has different polarization relative to the general scattered light, it will modify the observed $P(\lambda)$ behaviour over those spectral regions in which it occurs. Teifel assumed that the luminescent radiation was unpolarized, so combining with the purely scattered component to reduce the overall observed polarization according to Equation (2.2). The main purpose of this chapter is to report on the experiments undertaken to investigate the possible polarization changes at the Hα and Hβ lines based on the estimates of the polarimetric effects as described in Chapter 2. Twenty-six sets of data have been obtained from selected regions of the lunar surface, these areas being chosen because of uniformity of albedo, with measurements being less susceptible to tracking errors. The main measurements presented here were achieved on 1988 May 22, November 20 and 1989 March 16 when the lunar phases were about 106°, 62°, and 80° respectively and when the polarization was moderately high. The lunar positions are identified in Table (5.1) with their approximate selenographic co-ordinates.

5.2 The observations.

The observations were made with the Glasgow University Photometer/ Polarimeter. In these experiments two interference filters were used providing passbands ≈2.0Å for wavelengths just redwards of Hα and Hβ, the central wavelength being controllable through the cores of these chosen Fraunhofer lines by adjusting the tilt of the filters in the collimated beams. The field of view was limited to 38 arcsec by a diaphragm in the focal plane of the telescope. Tracking of a chosen lunar feature was achieved by an offset guiding telescope. Before each observation, spectral records of the Hα and Hβ lines were obtained by taking photo-electron counts with 1s integration time at 60 equally spaced angles of tilt of the filters using the scanning program (see

Site	Name	λ°	β°
A	Mare Crisium	60.0E	16.1N
B	Palus Somnii	43.0E	13.0N
C	Rømer	34.3E	24.6N
D	M. Tranquillitatis	23.1E	2.5N
E	M. Serenitatis	19.4E	21.1N
F	M. Serenitatis (West)	15.8E	22.2N
G	O . Procellarum	61.5W	1.0S

Table (5.1) The lunar areas monitored in the polarimetric observations, named to help identify the region, are listed with their approximate selenographic co-ordinates.

Section 3.4). The records were used to allow the selection of three positions of the filters corresponding to

Red continuum	(R)
Line centre	(L)
Blue continuum	(B)

Examples of such spectral line records indicating the positions at which the photometry/ polarimetry were performed are depicted in Figure (5.1). The Moon has marked spatial variations of polarization, so that comparison of sequential measurements at the positions R/ L/ B are subject to systematic error as a result of tracking inaccuracies or guidance drifts between the data sets for each of the wavelength positions. In order to minimise such effects, the observations were performed with a series of integrations of 10s with adjustment between the chosen wavelength positions conducted in a cyclic manner.

In the first observations, (1988 May 22) measurements were made using a technique of observing two wavelength positions corresponding to the red continuum and the line centre, and another run for the line centre and the blue continuum. However two wavelength position comparisons do not immediately allow distinction of the effects of the general $P(\lambda)$ behaviour of lunar scattering. Later observations employed three-position polarimetry (R/ L/ B), a cycle of measurements being achieved every 33s. These extra 3 seconds above the basic integration times are lost in terms of data collecting and correspond to intervals in which the filters move from one wavelength position to another. For the measurements reported here, some 100 complete cycles of 3-spectral-point polarimetry were performed for each selected area. Observations on 1988 May 22 have been made by using one channel only ($H\beta$), while for the other two nights, the two channels ($H\alpha$ & $H\beta$) have been used. All of the accumulated counts were corrected for detector background and also for losses caused by the deadtime of the photon counting electronics. The determined Stokes

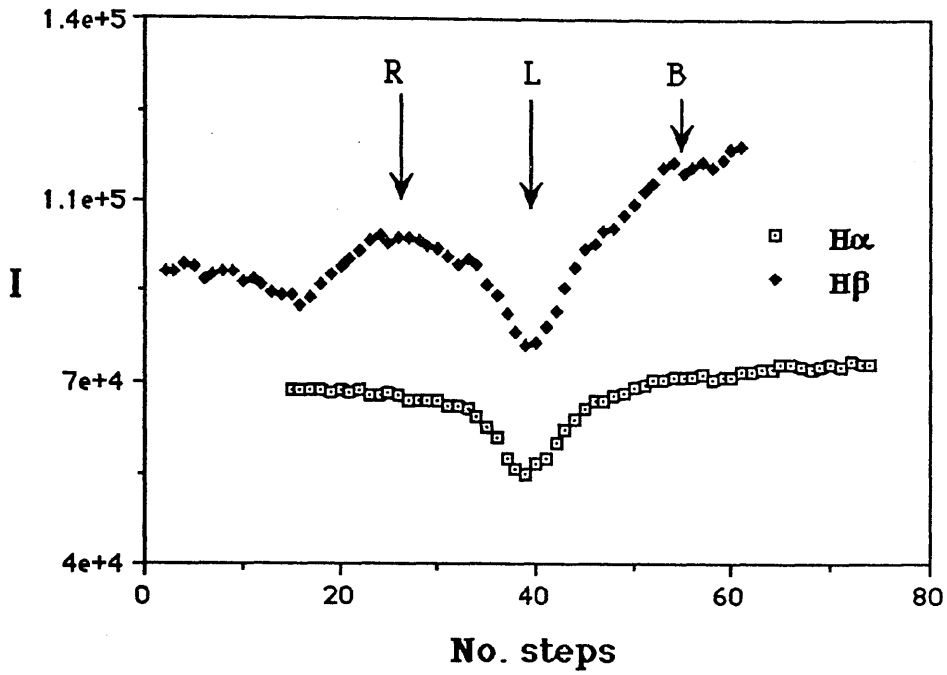

Figure (5.1) Typical 60 point Hα and Hβ scans (counts s^{-1}) of a lunar region. Spectral positions where subsequent polarimetry was performed have been marked according to the red and blue continua (R and B) and the line core (L). The wavelength scale is in uncalibrated units of the stepper motor and differents for Hα and Hβ. Step 0 represents a position close to normal incidence of the light beam on the interference filter and clearly the shift is towards shorter wavelengths by increasing the incident angle. Note also the dip in the upper record towards the red of Hβ; it corresponds to a blend of iron, titanium and nickel lines. This part of the spectrum has been used for the measurements which are illustrated at Figures (5.13b&d).

parameters were calculated in the instrumental frame.

The unpolarized standard stars α Boo and β Cas were chosen to determine the instrumental polarization. The recorded polarization values for these stars indicated that the instrumental polarization was less than 1% and with a suggestion of a weak wavelength dependence between Hα and Hβ - but essentially constant across each of the investigated spectral regions. This was subtracted from the lunar measurements, although it is strictly not really necessary for the differential comparisons of the three colour polarimetry reported in Section 5.3.2, the important thing being its constancy across the investigated spectral interval.

5.3 Measurements.

5.3.1 Photometry. To investigate possible time dependent fluctuations or site-to-site differences of the behaviour of the spectral lines, the ratio R of the residual intensity at the core relative to the intensity of the adjacent continuum have been obtained, using the first counter (first scaler) of each channel, as explained in Section 3.2.

However, before any site intercomparisons can be contemplated, the possibility of there being differences in R caused by the variation of the wavelength dependence of the albedo from site to site must be considered. This has been done using an indirect method as follows. The relation between degree of polarization and the albedo is an inverse correlation – the so-called Umov effect. The effect has been explored by Bowell (1971), his results providing the following relationship:

$$\log A = -0.724 \log P_m - 1.808 \qquad (5.1)$$

where A is the albedo and P_m is the maximum polarization value at some particular

phase angle.

Using this equation the lunar albedo has been calculated for different regions on the lunar surface. Values of P_m were obtained from Dollfus and Bowell (1971) at different wavelengths for those regions. Hence values of A according to wavelength can be predicted and these have been plotted in Figure (5.2). Since the wavelength dependence of lunar albedo $A(\lambda)$ has very small slope, then the albedo within the 30Å intervals between the two continua, covering the $H\alpha$ and $H\beta$ lines, can be considered as constant. Even if there is a slight change of the albedo between the two continua, its effect on the R values is removed by taking the average of the intensities of the two continua. This average intensity has been used with the intensity of the line core to obtain the ratio. The ratio values have been listed in Table (5.2) for the two nights when the two wavelength channels have been used; their errors are based on the repeated measures of each observation. The standard errors of the first night (1989 November 20) are typically just less than ±0.05% for both spectrum lines on the different sites, but for the second night (1989 March 16) they were large at $H\alpha$ (<0.5%), while for $H\beta$ they were quite small (<0.2%). Comparison between the line ratios recorded on the two nights is not fruitful, because the observing conditions were not the same and also the solar activity was not at the same level. The observations of 1989 March 16 were made during very strong solar activity, which had started two weeks before the observations and with its maximum on 1989 March 14 (see Verschuur, 1989).

Site E (Serenitatis) was observed several times during the night of 1989 March 16/17. Values of R for $H\alpha$ and $H\beta$ were the same within the limit of the errors except for the last measurements (between 00:42 and 01:24). For, these the values of R increased by just more than 2% and 6% for $H\alpha$ and $H\beta$ respectively. Unfortunately these changes occurred at the end of an observational run and could not be compared with later records.

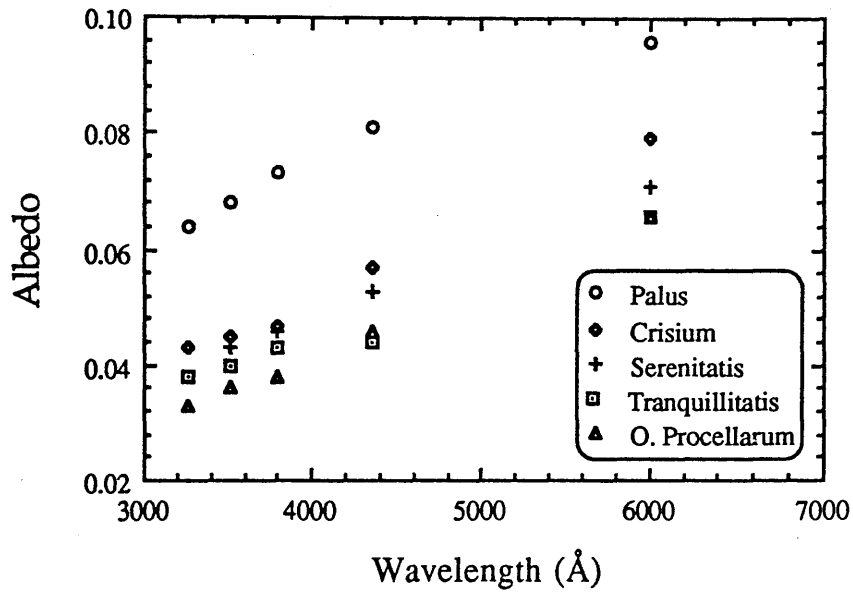

Figure (5.2) Variation of the albedo of the lunar features with wavelength λ, calculated from polarimetric measurements by Dollfus and Bowell (1971).

		Hα		Hβ	
Site	Date	R	σ	R	σ
M. Tranquillitatis	20/11/88	0.7149	0.0004	0.7566	0.0003
M. Serenitatis	=	0.7129	0.0003	0.7481	0.0005
O. Procellarum	=	0.7105	0.0004	0.7504	0.0004
M. Crisium	16/3/89	0.7005	0.0011	0.7423	0.0006
M. Serenitatis	=	0.7020	0.0025	0.7369	0.0008
M. Tranquillitatis	=	0.7148	0.0043	0.7355	0.0006
M. Serenitatis (W)	=	0.7007	0.0014	0.7354	0.0005
Palus Somnii	=	0.7067	0.0016	0.7404	0.0020
M. Serenitatis	=	0.7004	0.0017	.....	.....
M. Serenitatis	=	0.7176	0.0014	0.8024	0.0005

Table (5.2) The lunar areas, listed with their date of observation and the mean values of measured line ratio with their uncertainties for the Hα and Hβ Fraunhofer lines. Note the increase of the last value of R for the M.Serenitatis in comparison with the other values taken at different times for the same region.

From Table (5.2) it is clear that the ratio is not equal for the different regions for each night. These variations in R are larger than the internal errors. However, it is difficult to interpret the cause of this. There is always a problem that the same exact site is not being monitored on each occasion and there may also be short time-scale changes in the levels of luminescence that are not coherent over the whole of the lunar surface. Apparent variation in R from site to site may also be influenced by scattered light entering the instrument from nearby lunar areas. There is no explanation available for the anomalous change in the values of R at Site E (Serenitatis). In the next section the results illustrate that there were no anomalous changes of polarization across the Hα and the Hβ lines that can be correlated with R.

5.3.2 Polarimetry.

The observed degree of polarization (P) is dependent on the scattering angle and hence on the lunar phase. It is approximately inversely proportional to wavelength when P is positive and virtually independent of wavelength when P is negative, see Figure (5.3). Over the small spectral interval covered by the investigated Fraunhofer lines, it can be assumed to be constant for the purposes of preliminary assessments. It can be seen in Table (5.12) that the polarization was ≈ 0.07 at Hα and ≈ 0.10 at Hβ and that the uncertainties are of the order of $\approx \pm 0.0005$ to as low as $\approx \pm 0.0002$. It will be noted immediately that such signal-to-noise levels are in excess of those predicted earlier as being necessary to detect the effect of luminescence.

The normalised Stokes parameters (q and u), as measured in the instrumental frame, for each integration have been determined by the method described in Chapter 3. It is possible to investigate the data in two ways so that the polarization values in the line and continua can be compared and these procedures are outlined below.

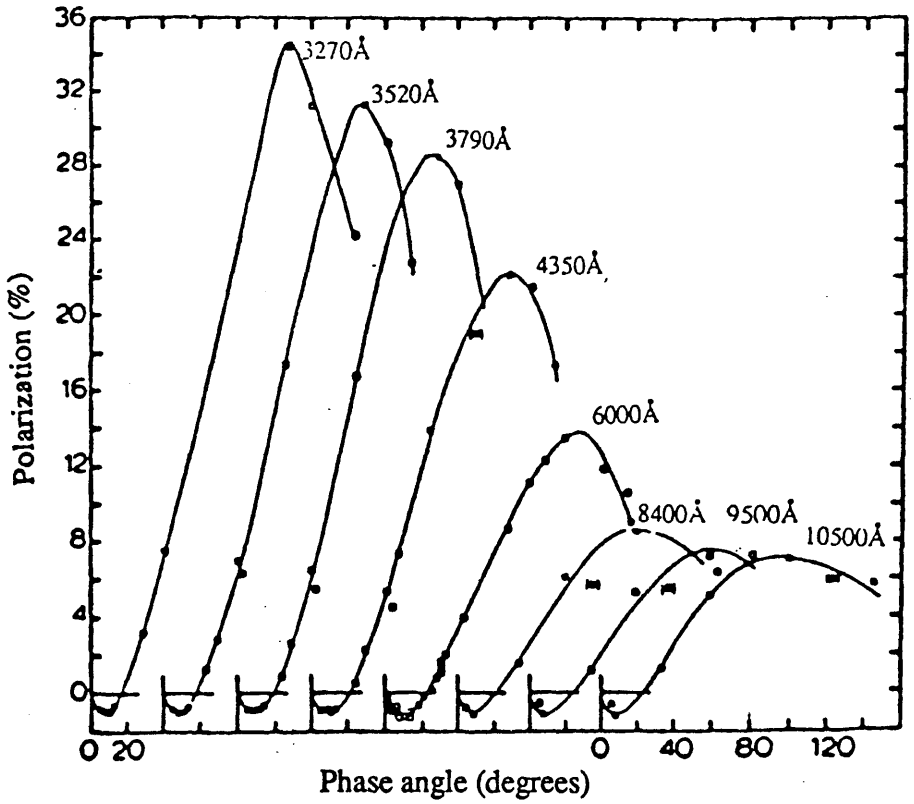

Figure (5.3) Polarization curves as a function of phase angle for eight different spectral regions in Oceanus Procellarum. (Taken from Bowell, 1971).

Method (1): Comparison of Means.

For a given lunar site the observations provide cyclic polarimetric measurements for R/ L/ B. Mean values of the Stokes parameters may be obtained for each of the selected wavelength positions. Variances based on the internal distributions of the repeated records may also be calculated. However, means formed in this way carry noise introduced by tracking errors, especially when the chosen area and surrounding region have irregularities of albedo and polarization. Averaging of this noise should be approximately the same for each of the wavelength positions but its effect will tend to smear out the possible polarization differences between wavelengths.

Method (2): Comparison of the means of Cycle by Cycle differences.

The effects of imprecise telescope tracking are minimised by determining any spectral polarimetric differences cycle by cycle, with the statistical behaviour of the repeated comparisons being assessed. By this method there is less chance of the tracking defects affecting the wavelength comparisons. This has been done using the B position values as reference. For each spectral cycle (i.e. every 33s), differences of the Stokes parameters corresponding to L-B and R-B were obtained. From these values mean differences were calculated together with an internal estimate of the errors.

Observations on the first night, 1988 May 22, used only two wavelength positions in the cycle (the line centre and one of the continua) and Method (1) has been applied to these data. Stokes parameters have been plotted in Figures (5.4I to 5.4VI), each figure containing the polarization properties of the line centre and one of the continua [see Table (5.3) for more details of these observations]. From the diagrams it is easy to assess the polarimetric behaviour semi - quantitatively. For example in Figure(5.4II) there is a hint for M.Tranquillitatis that the polarization is reduced in the line relative to the blue continuum. In Figures (5.4V) and (5.4VI), there is a hint for

Rømer that the position angle for the line core is rotated with respect to the continuum.

Both Methods (1) and (2) have been applied to the data collected on the other two nights. In all cases it was noticeable that the polarizational differences between spectral positions individually exhibited the same patterns for the two analytical procedures. However, for the second method, the overlap of some of the error bars was more noticeable because the data points are generally closer together. The polarization parameters with their uncertainties, observed area, times of observation, and number of repeated measurements are given in Tables (5.4 to 5.13). Figures (5.5 to 5.14) depict the data reduced by the two methods. Figures (5.13b&d) are for measurements made at a dip in the spectrum redwards of Hβ corresponding to a group of the iron/titanium and nickel lines (see Figure 5.1).

The Welch test is again applicable here to allow intercomparison of the measured normalised Stokes parameters for the three selected wavelength positions. As anomalies occur, then pair comparisons R,L − L,B − R,B were conducted to see which wavelength positions provided disparate data or whether all three sets could be considered as having differing polarization values. From these statistical analyses, several data sets suggest that there are significant polarimetric variations across either the Hα or Hβ lines at about the 95% confidence level, with some at the 99% level. However the results show that there were no general patterns of behaviour, but the number of "detections" of polarimetric differences across the lines is significantly in excess (20% of the assessments) of what might be explainable in terms of the statistical behaviour of repeated tests operating on noisy data. This suggests that at least some of the " detections " must be real. The positive results from the Welch tests have been listed in Table (5.14), giving an indication of the differences in the mean values of q and u from one wavelength to another, with the confidence level of the detection of those differences.

An attempt to determine the required rotation for the conversion from the instrumental frame to the scattering plane was made by considering the measurements from the various sites and plotting them as in Figures (5.15a&b), where it can be seen that the data are approximately co-linear. The vector from the origin running through the measurements represents the positive Q direction of the scattering plane and is designated $q_{\mathfrak{D}}$. It will be noted that the position angle of the instrumental frame for Hα is different from Hβ because of the dispersion of the reference axis in the achromatic half-wave plate (see Chapter 3). Figures (5.15a&b) also suggest that the data are noisy in position angle about the estimated $q_{\mathfrak{D}}$ direction. This may partly result from variations of the projection of the local scattering plane from region to region over the Moon but the more likely cause is the secular change in the lunar declination during the observing run. The results of this effect can clearly be seen in Figures (5.16a&b) where the values of the position angle of the polarization with their standard errors based on the distribution of repeated measurements are plotted as they occurred during the course of the night of 1989 March 16. Examination of the direction of vibration, θ, of the polarization again shows that it remained constant to within ≈ 0°.1 across the Hβ line and Hα on 1988 November 20 (see Tables 5.3 to 5.13), but for the observations of 1989 March 16, the situation at Hα appears to be different. Firstly, one region (Site B-Palus Somnii, see Figure 5.16) displayed anomalous values of θ with all three measurements (R, L and B) being rotated by the order of 3° with respect to the other lunar areas, the line centre being significantly less rotated than the nearby continua. The reason for this is obscure but it may be related to the strong solar activity just prior to the observations (see Verschuur, 1989) and the high albedo of this site (see Figure 5.2), it being the only selected region with a rough terrain and not a mare floor. Although none of the mare sites individually displays a statistically significantly different value of θ across Hα, the collection of measurements suggests that a rotation effect is present, the value of θ in the line core being displaced ≈ 0°.25 relative to the

continua. For the night of 1988 November 20, the measurements for two (Sites D and E, Tranquillitatis and Serenitatis) out of the three regions observed, demonstrate the same effect but again without individual statistical significance.

Headings for Tables (5.3 to 5.13)

The Stokes parameters, degree of polarization and azimuth with their uncertainties for the measurements Hα and Hβ, name of the area, date, and times of observation (the tabulated data correspond to Figures 5.4 to 5.14). The abbreviations are as follows:

W.P.	Wavelength Position.
R	Red continuum
L	Line centre
B	Blue continuum
No.	Number of cycles.
Q/I, U/I	Normalized Stokes parameters.
P	Degree of polarization.
θ	Azimuth vibration angle.
L-B	Average value of the differences between the line and the blue continuum. [Method 2]
R-B	Average value of the differences between the red continuum and the blue continuum.[Method 2]

Information related to Figures (5.4 to 5.14)

In the plots of lunar spectropolarimtric observations, the following symbols represent the Red continuum, Line centre and Blue continuum measurements.

o ——— R

□ ——— L

Δ ——— B

In Figure (5.4), labels I, II, III, IV, V, and VI - indicate plots of the normalised Stokes parameters with their 1σ errors for L and one of the continua B or R of the Hβ Fraunhofer line.

In Figures (5.5) to (5.14), labels a & b - indicate plots of the normalised Stokes parameters with their 1σ errors for R, L and B across the Hα and Hβ Fraunhofer lines.

Similarly, labels c & d - indicate plots of the mean difference of the R and L values with respect to B; the error bars correspond to the standard error of the means.

Hβ

Mean time of measurements 22/5/88 (UT)	W. P.	NO.	Q/I	U/I	P	θ .
				Mare Tranquilltatis		
21: 43: 48	R	20	0.151	-0.0810	0.171	165.89
TO			±.001	±0.0005	±.001	±00.07
21:52:04	L	20	0.150	-0.0809	0.171	165.85
			±.001	±0.0005	±.001	±00.06
21:57:44	L	20	0.142	-0.076	0.161	165.88
TO			±.002	±0.001	±.002	±00.09
22:05:54	B	20	0.142	-0.078	0.162	165.54
			±.002	±0.001	±.002	±00.08
				Mare Crisium		
22: 11: 53	R	20	0.080	-0.048	0.093	164.53
TO			±.002	±0.001	±.002	±00.10
22:19:55	L	20	0.078	-0.047	0.091	164.43
			±.002	±0.001	±.002	±00.09
22:24:06	L	20	0.077	-0.046	0.090	164.47
TO			±.002	±0.001	±.003	±00.08
22:32:08	B	20	0.079	-0.049	0.093	164.23
			±.002	±0.001	±.002	±00.11
				Rømer		
22: 36: 57	R	20	0.0489	-0.0336	0.0594	162.77
TO			±.0003	±0.0002	±.0003	±00.08
22:45:04	L	20	0.0497	-0.0330	0.0597	163.23
			±.0004	±0.0003	±.0004	±00.12
22:49:13	L	20	0.0499	-0.0328	0.0597	163.34
TO			±.0003	±0.0002	±.0003	±00.13
22:57:25	B	20	0.0492	-0.0335	0.0595	162.89
			±.0003	±0.0003	±.0004	±00.10

Table (5.3) [See page 111 for details]

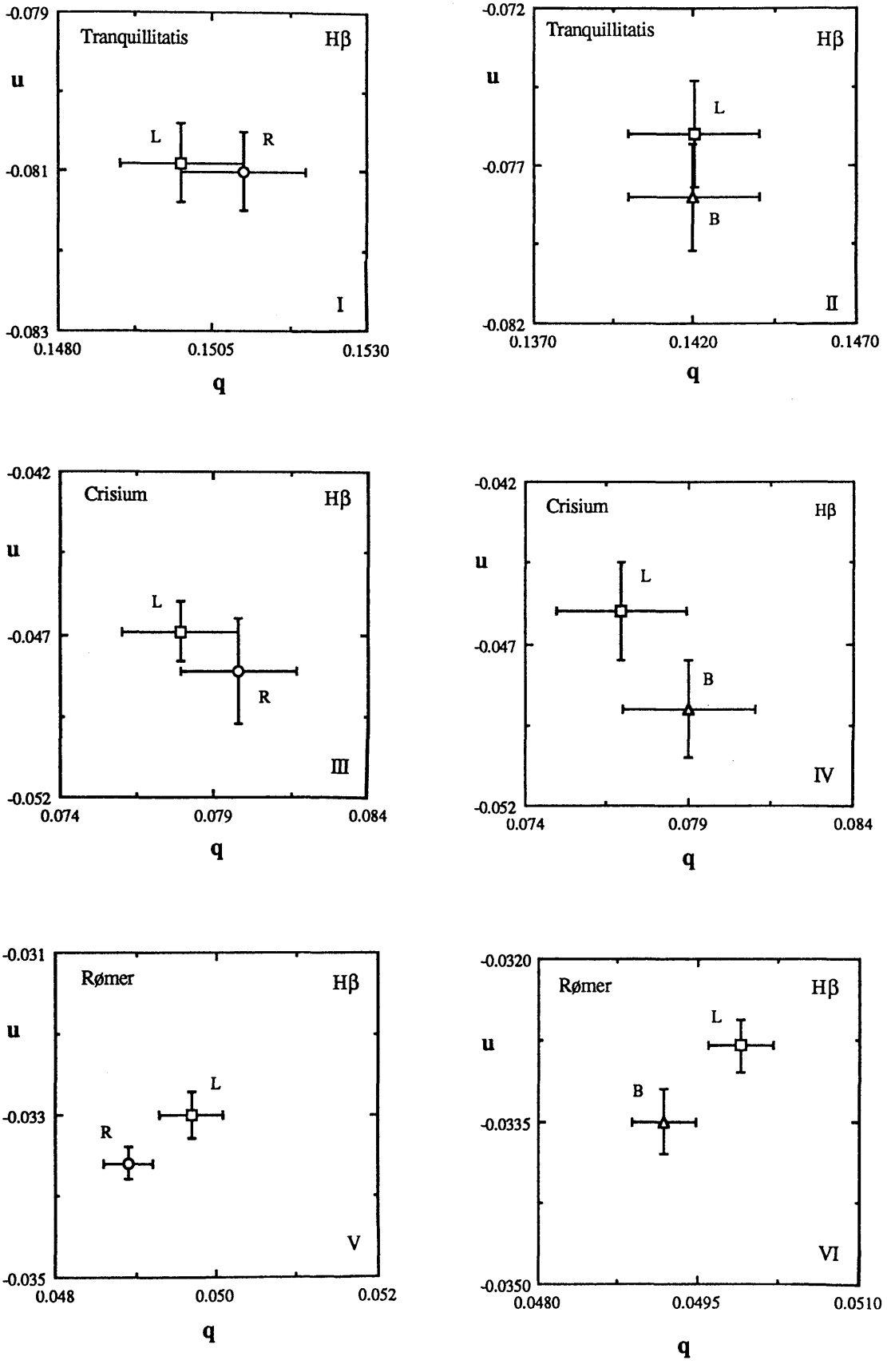

Figure (5.4) Material from the opposite table [see page 112 for details]

Mare Tranquilltatis E23.1° & N2.5°

Mean time of measurements 1988 Nov. 20 (UT)	W. P.	NO.	Hα Q/I	Hα U/I	Hα P	Hα θ	Hβ Q/I	Hβ U/I	Hβ P	Hβ θ
	R	95	0.0186 ±0.0002	−0.0204 ±0.0002	0.0277 ±0.0002	156.8 ±0.2	0.0175 ±0.0002	−0.0327 ±0.0002	0.0371 ±0.0002	149.1 ±0.1
19: 12: 57 TO	L	95	0.0189 ±0.0002	−0.0205 ±0.0002	0.0279 ±0.0002	156.3 ±0.2	0.0179 ±0.0002	−0.0332 ±0.0002	0.0378 ±0.0002	149.2 ±0.1
20: 45: 03	B	95	0.0187 ±0.0002	−0.0212 ±0.0002	0.0284 ±0.0002	155.7 ±0.2	0.0170 ±0.0002	−0.0328 ±0.0002	0.0369 ±0.0002	148.7 ±0.1
	L-B		0.0001 ±0.0003	0.0008 ±0.0003	-------- --------	------ ------	0.0010 ±0.0002	−0.0005 ±0.0003	-------- --------	------ ------
	R-B		-0.0001 ±0.0003	0.0008 ±0.0003	-------- --------	------ ------	0.0005 ±0.0002	0.0001 ±0.0003	-------- --------	------ ------

Table 5.4 [See page 111 for details]

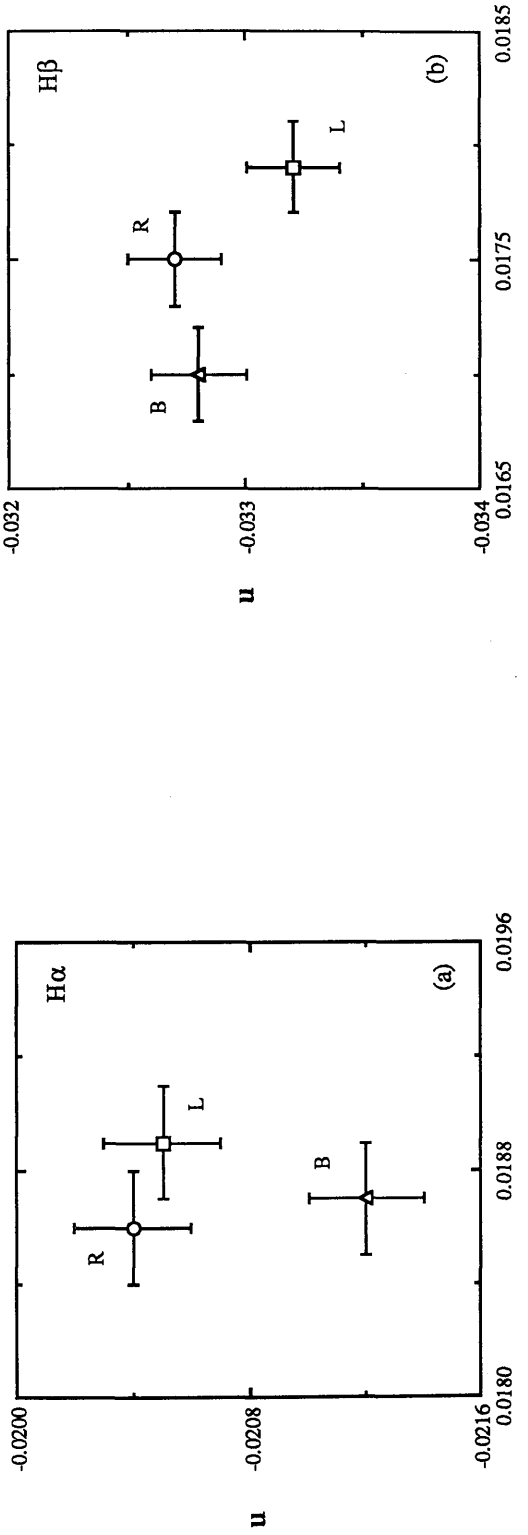

Figure (5.5) Material from the opposite table [see page 112 for details]

Mare Serenitatis E19.4° & N21.1°

Mean time of measurements	W. P.	NO.	Hα Q/I	Hα U/I	Hα P	Hα θ	Hβ Q/I	Hβ U/I	Hβ P	Hβ θ
1988 Nov. 20 (UT)	R	100	0.0160 ±0.0002	−0.0168 ±0.0002	0.0233 ±0.0002	156.8 ±0.3	0.0163 ±0.0002	−0.0288 ±0.0002	0.0331 ±0.0002	149.8 ±0.1
21: 21: 06 TO	L	100	0.0159 ±0.0002	−0.0165 ±0.0002	0.0231 ±0.0002	157.0 ±0.2	0.0163 ±0.0002	−0.0287 ±0.0002	0.0331 ±0.0002	149.8 ±0.1
23: 13: 54	B	100	0.0159 ±0.0002	−0.0172 ±0.0002	0.0235 ±0.0002	156.4 ±0.2	0.0158 ±0.0002	−0.0282 ±0.0002	0.0324 ±0.0002	149.6 ±0.1
	L-B		0.0001 ±0.0003	0.0006 ±0.0002	-------- --------	------ ------	0.0005 ±0.0002	−0.0005 ±0.0003	-------- --------	------ ------
	R-B		0.0001 ±0.0003	0.0004 ±0.0003	-------- --------	------ ------	0.0005 ±0.0002	−0.0006 ±0.0002	-------- --------	------ ------

Table 5.5 [See page 111 for details]

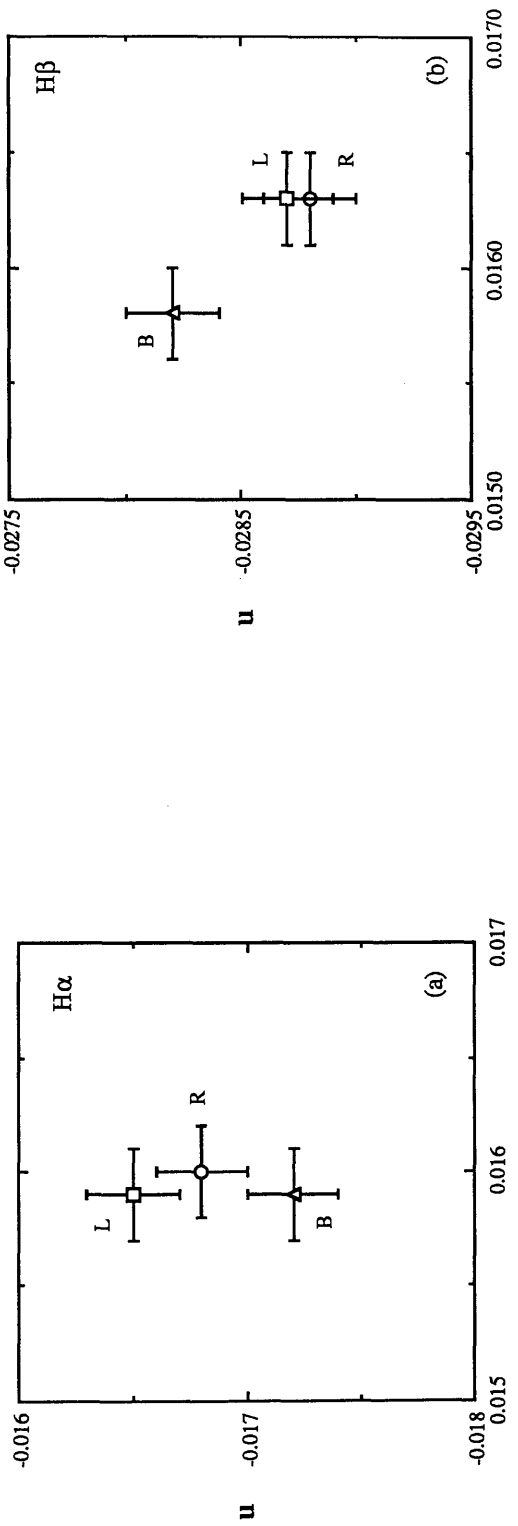

Figure (5.6) Material from the opposite table [see page 112 for details]

O. Procellarum W61.5° & S1°

Mean time of measurements 1988 Nov. 20 (UT)	W. P.	NO.	Hα Q/I	Hα U/I	Hα P	Hα θ	Hβ Q/I	Hβ U/I	Hβ P	Hβ θ
	R	95	0.0158 ±0.0003	−0.0140 ±0.0003	0.0213 ±0.0003	159.2 ±0.3	0.0174 ±0.0002	−0.0220 ±0.0002	0.0281 ±0.0002	154.2 ±0.2
23: 29: 18	L	95	0.0157 ±0.0003	−0.0141 ±0.0003	0.0213 ±0.0003	159.0 ±0.4	0.0166 ±0.0003	−0.0218 ±0.0002	0.0275 ±0.0002	153.6 ±0.3
TO										
00: 50: 11	B	95	0.0157 ±0.0002	−0.0141 ±0.0002	0.0212 ±0.0002	159.0 ±0.3	0.0165 ±0.0002	−0.0214 ±0.0002	0.0271 ±0.0002	153.8 ±0.2
	L-B		0.0000 ±0.0004	0.0000 ±0.0004	-------- --------	------ ------	0.0001 ±0.0003	−0.0004 ±0.0004	-------- --------	------ ------
	R-B		0.0001 ±0.0003	0.0001 ±0.0003	-------- --------	------ ------	0.0009 ±0.0003	−0.0007 ±0.0003	-------- --------	------ ------

Table 5.6 [See page 111 for details]

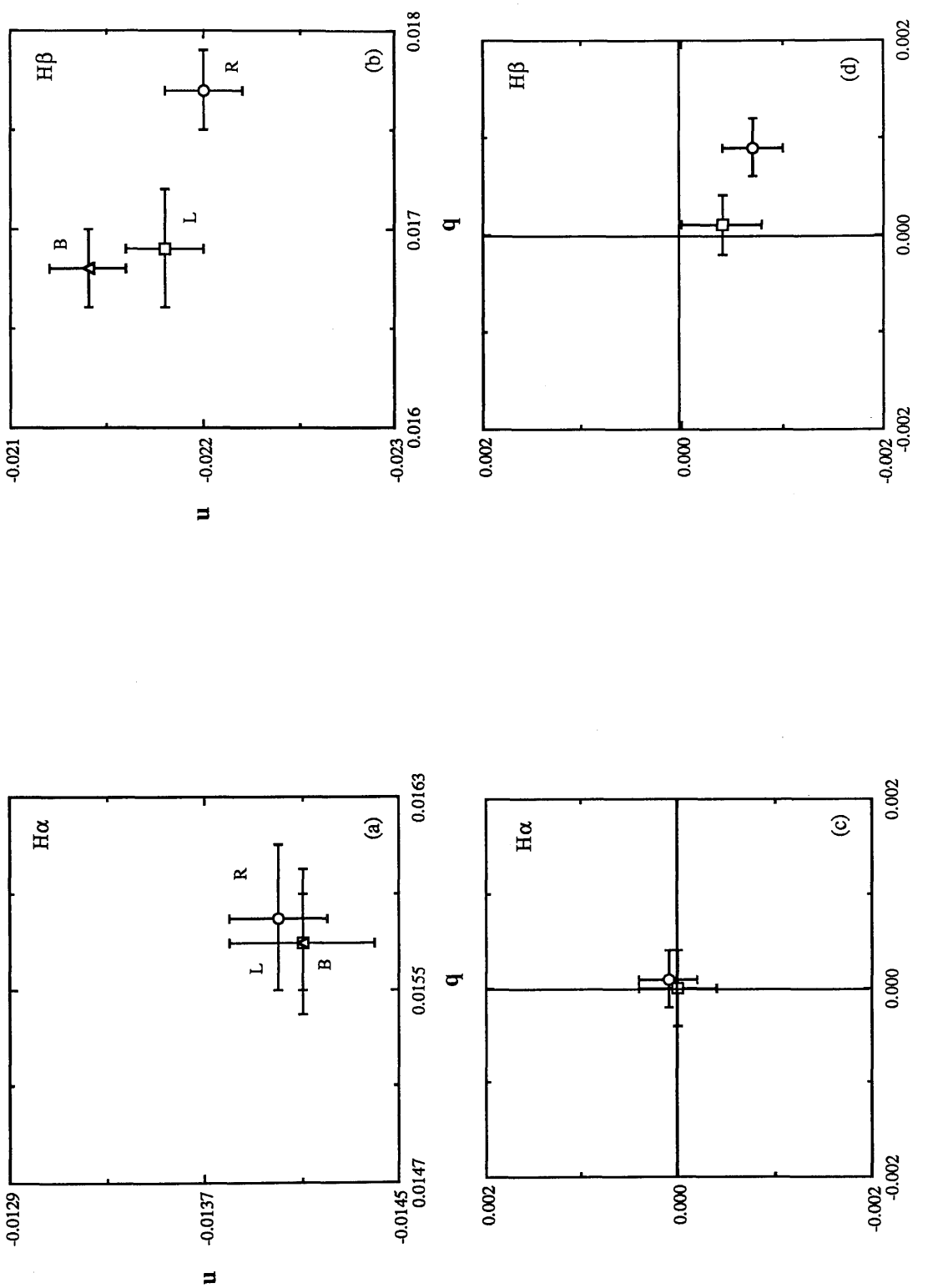

Figure (5.7) Material from the opposite table [see page 112 for details]

Mare Crisium E60° & N16.1°

Mean time of measurements	W. P.	NO.	Hα Q/I	Hα U/I	Hα P	Hα θ	Hβ Q/I	Hβ U/I	Hβ P	Hβ θ
1989 March 16 (UT)	R	25	-0.0240 ±0.0005	0.0614 ±0.0004	0.0660 ±0.0004	55.7 ±0.2	-0.0208 ±0.0004	0.0841 ±0.0005	0.0867 ±0.0005	51.9 ±0.1
20: 44: 13 TO	L	25	-0.0254 ±0.0006	0.0628 ±0.0005	0.0679 ±0.0005	56.0 ±0.3	-0.0197 ±0.0004	0.0847 ±0.0006	0.0870 ±0.0006	51.5 ±0.1
21: 06: 09	B	25	-0.0243 ±0.0005	0.0625 ±0.0004	0.0671 ±0.0004	55.6 ±0.2	-0.0205 ±0.0004	0.0841 ±0.0005	0.0865 ±0.0005	51.8 ±0.1
	L-B		-0.0011 ±0.0008	0.0003 ±0.0006	-------- --------	------ ------	0.0008 ±0.0004	0.0007 ±0.0006	-------- --------	------ ------
	R-B		0.0003 ±0.0007	-0.0011 ±0.0005	-------- --------	------ ------	-0.0003 ±0.0005	0.0000 ±0.0005	-------- --------	------ ------

Table 5.7 [See page 111 for details]

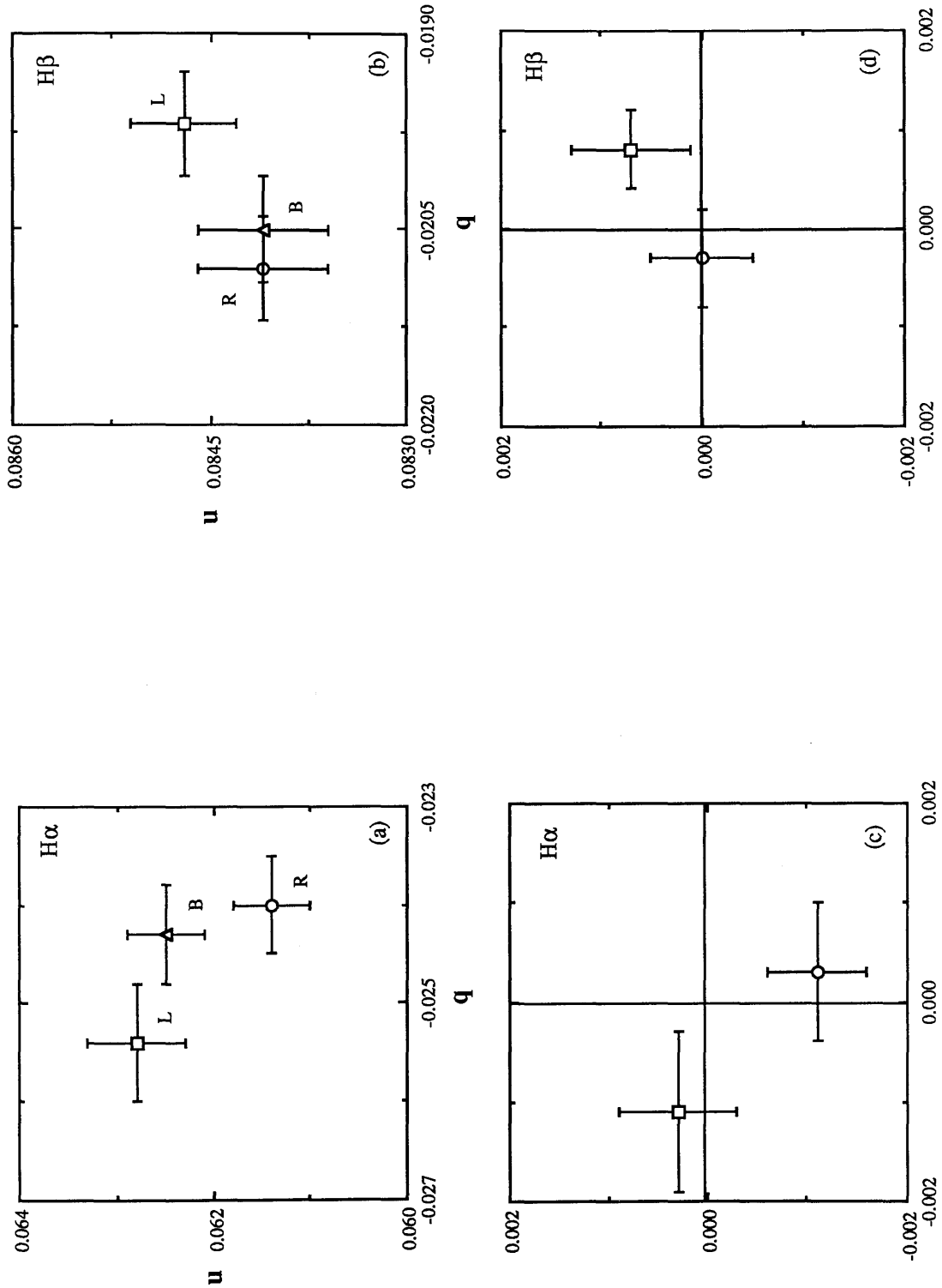

Figure (5.8) Material from the opposite table [see page 112 for details]

Mare Serenitatis E19.4° & N21.1°

Mean time of measurements 1989 March 16 (UT)	W. P.	NO.	Hα Q/I	Hα U/I	Hα P	Hα θ	Hβ Q/I	Hβ U/I	Hβ P	Hβ θ
	R	30	−0.0328 ±0.0005	0.0748 ±0.0007	0.0817 ±0.0007	56.8 ±0.2	−0.0254 ±0.0004	0.1021 ±0.0004	0.1052 ±0.0004	52.0 ±0.1
21: 09: 43 TO	L	30	−0.0347 ±0.0006	0.0760 ±0.0008	0.0836 ±0.0009	57.3 ±0.2	−0.0248 ±0.0005	0.1025 ±0.0004	0.1055 ±0.0004	51.8 ±0.1
21: 35: 55	B	30	−0.0330 ±0.0006	0.0751 ±0.0007	0.0821 ±0.0007	56.9 ±0.2	−0.0244 ±0.0004	0.1024 ±0.0004	0.1053 ±0.0004	51.7 ±0.1
	L-B		−0.0017 ±0.0008	0.0009 ±0.0008	-------- --------	------ ------	−0.0004 ±0.0006	0.0001 ±0.0006	-------- --------	------ ------
	R-B		0.0002 ±0.0006	−0.0003 ±0.0009	-------- --------	------ ------	−0.0010 ±0.0006	-0.0003 ±0.0005	-------- --------	------ ------

Table 5.8 [See page 111 for details]

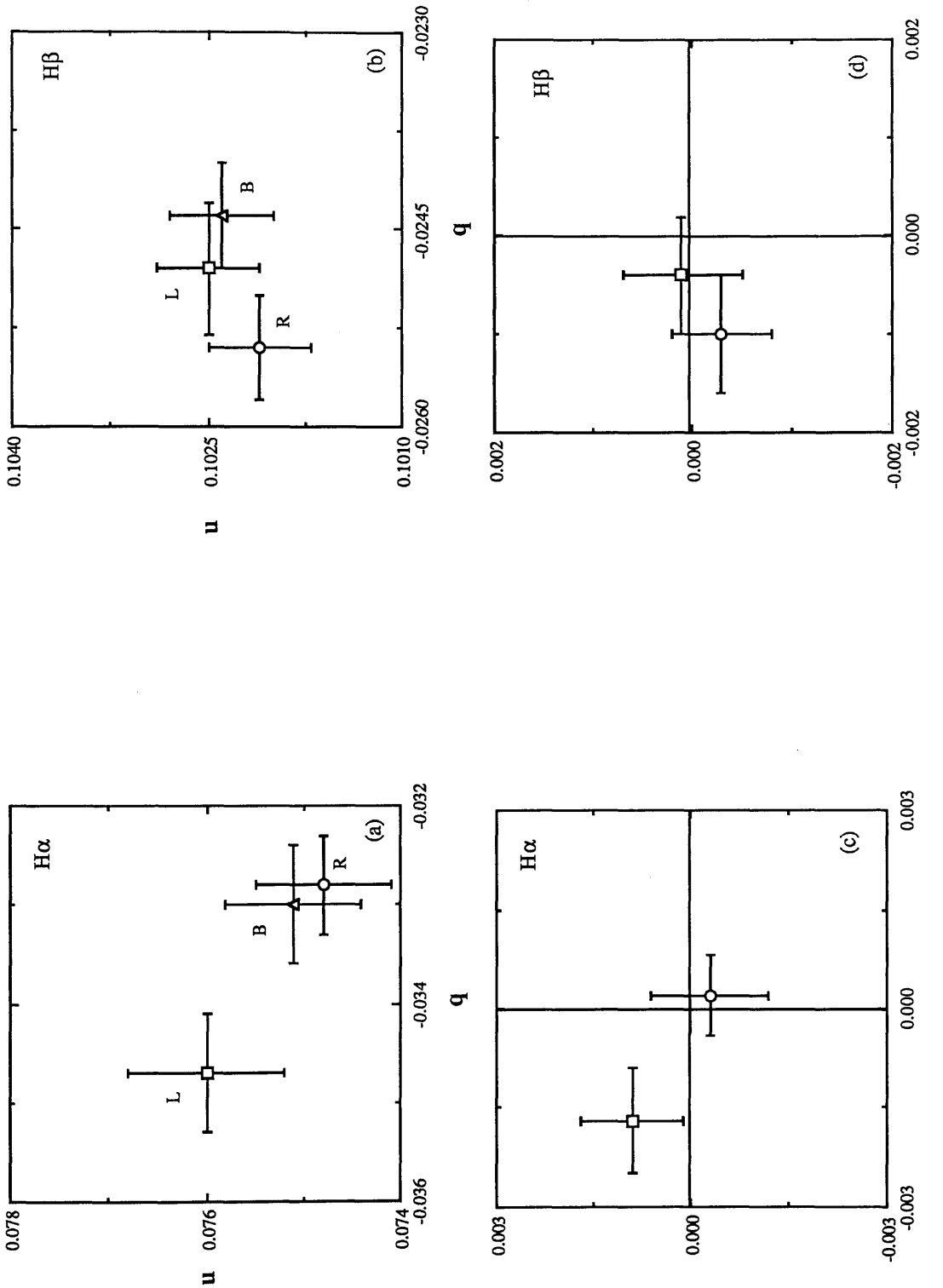

Figure (5.9) Material from the opposite table [see page 112 for details]

Mare Tranquilltatis E23.1° & N2.5°

Mean time of measurements 1989 March 16 (UT)	W. P.	NO.	Hα Q/I	Hα U/I	Hα P	Hα θ	Hβ Q/I	Hβ U/I	Hβ P	Hβ θ
	R	25	−0.0257	0.0606	0.0658	56.5	−0.0232	0.0921	0.0950	52.1
			±0.0004	±0.0008	±0.0008	±0.2	±0.0004	±0.0005	±0.0004	±0.1
21: 38: 23 TO	L	25	−0.0262	0.0588	0.0644	57.0	−0.0235	0.0919	0.0949	52.2
			±0.0008	±0.0009	±0.0009	±0.3	±0.0005	±0.0005	±0.0005	±0.1
21: 59: 48	B	25	−0.0251	0.0597	0.0648	56.4	−0.0235	0.0918	0.0948	52.2
			±0.0005	±0.0008	±0.0008	±0.2	±0.0003	±0.0004	±0.0004	±0.1
	L-B		−0.0011	−0.0009	--------	------	0.0000	0.0001	--------	------
			±0.0009	±0.0009	--------	------	±0.0005	±0.0006	--------	------
	R-B		−0.0006	0.0009	--------	------	0.0003	0.0003	--------	------
			±0.0004	±0.0008	--------	------	±0.0005	±0.0006	--------	------

Table 5.9 [See page 111 for details]

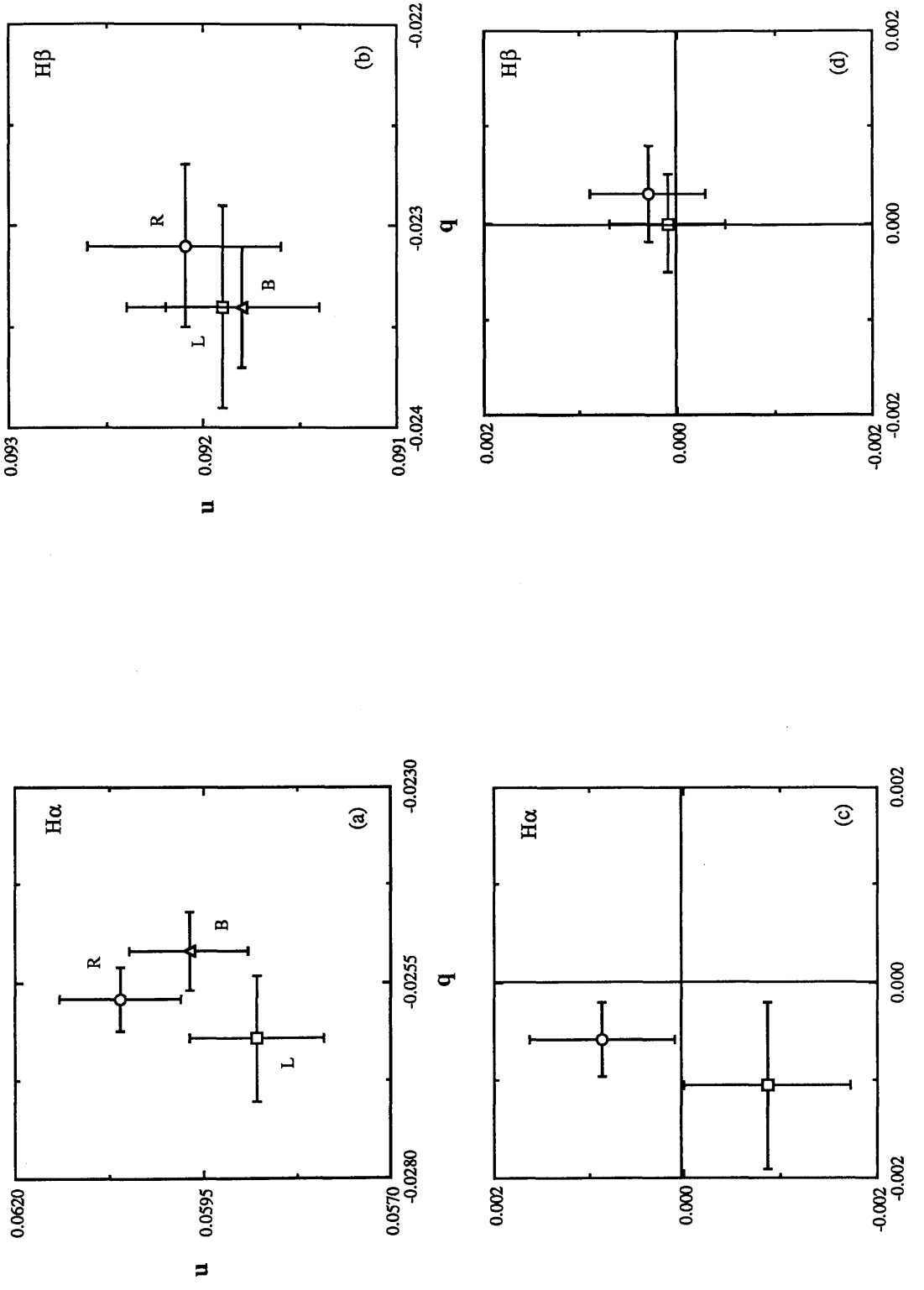

Figure (5.10) Material from the opposite table [see page 112 for details]

W- Mare Serenitatis E15.8° & N22.2°

Mean time of measurements	W. P.	NO.	Hα Q/I	Hα U/I	Hα P	Hα θ	Hβ Q/I	Hβ U/I	Hβ P	Hβ θ
1989 March 16 (UT)	R	55	−0.0260 ±0.0004	0.0619 ±0.0004	0.0672 ±0.0004	56.4 ±0.2	−0.0232 ±0.0003	0.0894 ±0.0004	0.0924 ±0.0004	52.3 ±0.1
22: 05: 48 TO	L	55	−0.0267 ±0.0004	0.0612 ±0.0005	0.0668 ±0.0005	56.8 ±0.2	−0.0235 ±0.0004	0.0901 ±0.0004	0.0931 ±0.0004	52.3 ±0.1
22: 43: 19	B	55	−0.0266 ±0.0004	0.0622 ±0.0004	0.0677 ±0.0004	56.8 ±0.2	−0.0234 ±0.0003	0.0894 ±0.0004	0.0925 ±0.0004	52.3 ±0.1
	L-B		−0.0001 ±0.0006	−0.0010 ±0.0007	-------- --------	------ ------	−0.0001 ±0.0004	0.0006 ±0.0004	------- -------	------ ------
	R-B		0.0006 ±0.0005	−0.0003 ±0.0005	-------- --------	------ ------	0.0002 ±0.0004	0.0000 ±0.0005	------- -------	------ ------

Table 5.10 [See page 111 for details]

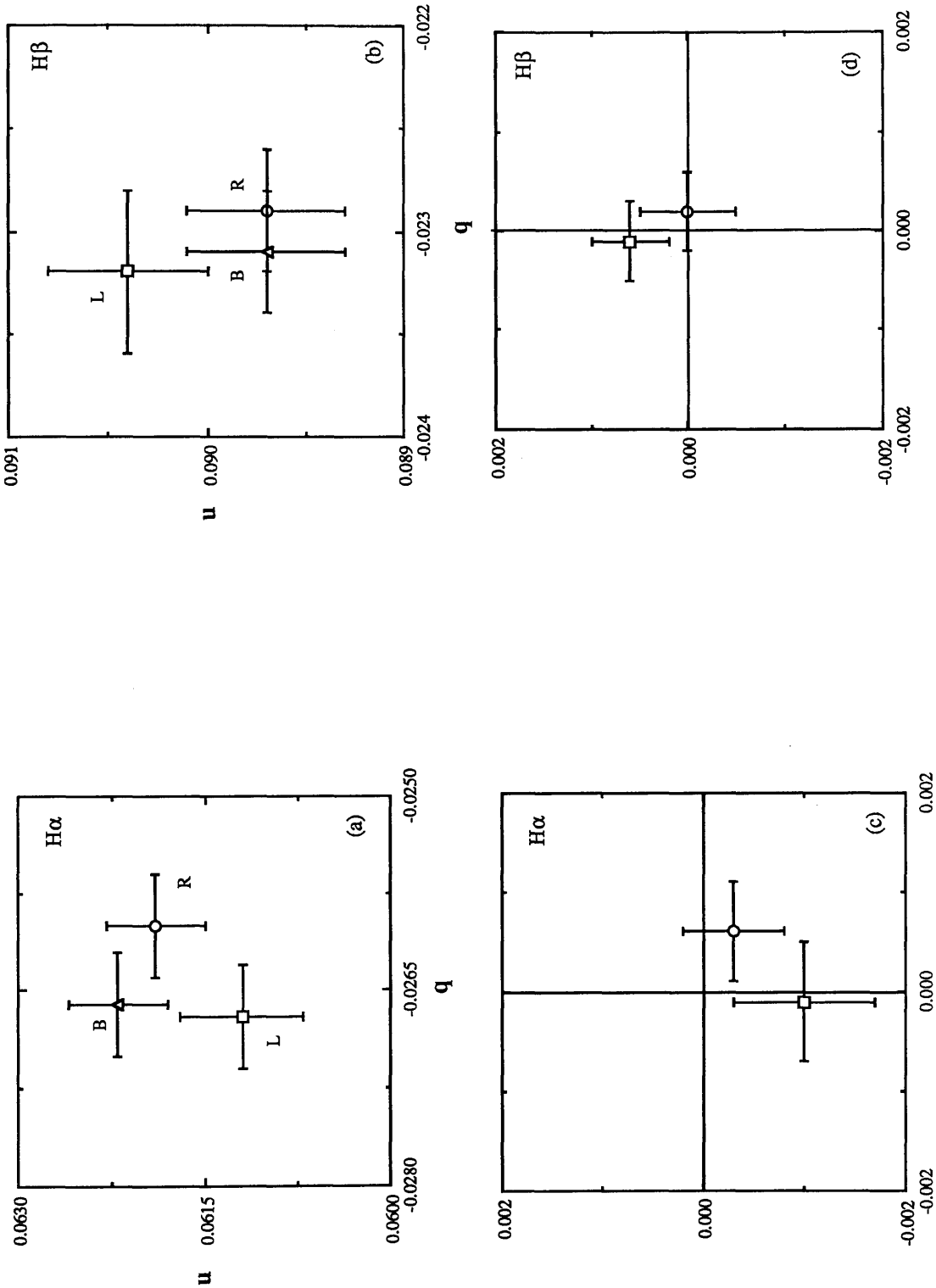

Figure (5.11) Material from the opposite table [see page 112 for details]

Palus Somnii E43° & N13°

Mean time of measurements 1989 March 16 (UT)	W. P.	NO.	Hα Q/I	Hα U/I	Hα P	Hα θ	Hβ Q/I	Hβ U/I	Hβ P	Hβ θ
	R	50	−0.0094	0.0324	0.0337	53.1	−0.0112	0.0416	0.0431	52.5
			±0.0002	±0.0002	±0.0002	±0.2	±0.0002	±0.0002	±0.0002	±0.1
22: 50: 41 TO	L	50	−0.0105	0.0319	0.0336	54.1	−0.0113	0.0415	0.0431	52.6
			±0.0003	±0.0003	±0.0003	±0.2	±0.0002	±0.0003	±0.0003	±0.1
23: 24: 08	B	50	−0.0095	0.0324	0.0338	53.2	−0.0108	0.0410	0.0424	52.4
			±0.0002	±0.0002	±0.0002	±0.2	±0.0002	±0.0003	±0.0003	±0.1
	L-B		−0.0010	−0.0005	--------	------	−0.0004	0.0006	--------	------
			±0.0003	±0.0003	--------	------	±0.0002	±0.0003	--------	------
	R-B		0.0001	0.0000	--------	------	−0.0003	0.0006	--------	------
			±0.0002	±0.0003	--------	------	±0.0003	±0.0003	--------	------

Table 5.11 [See page 111 for details]

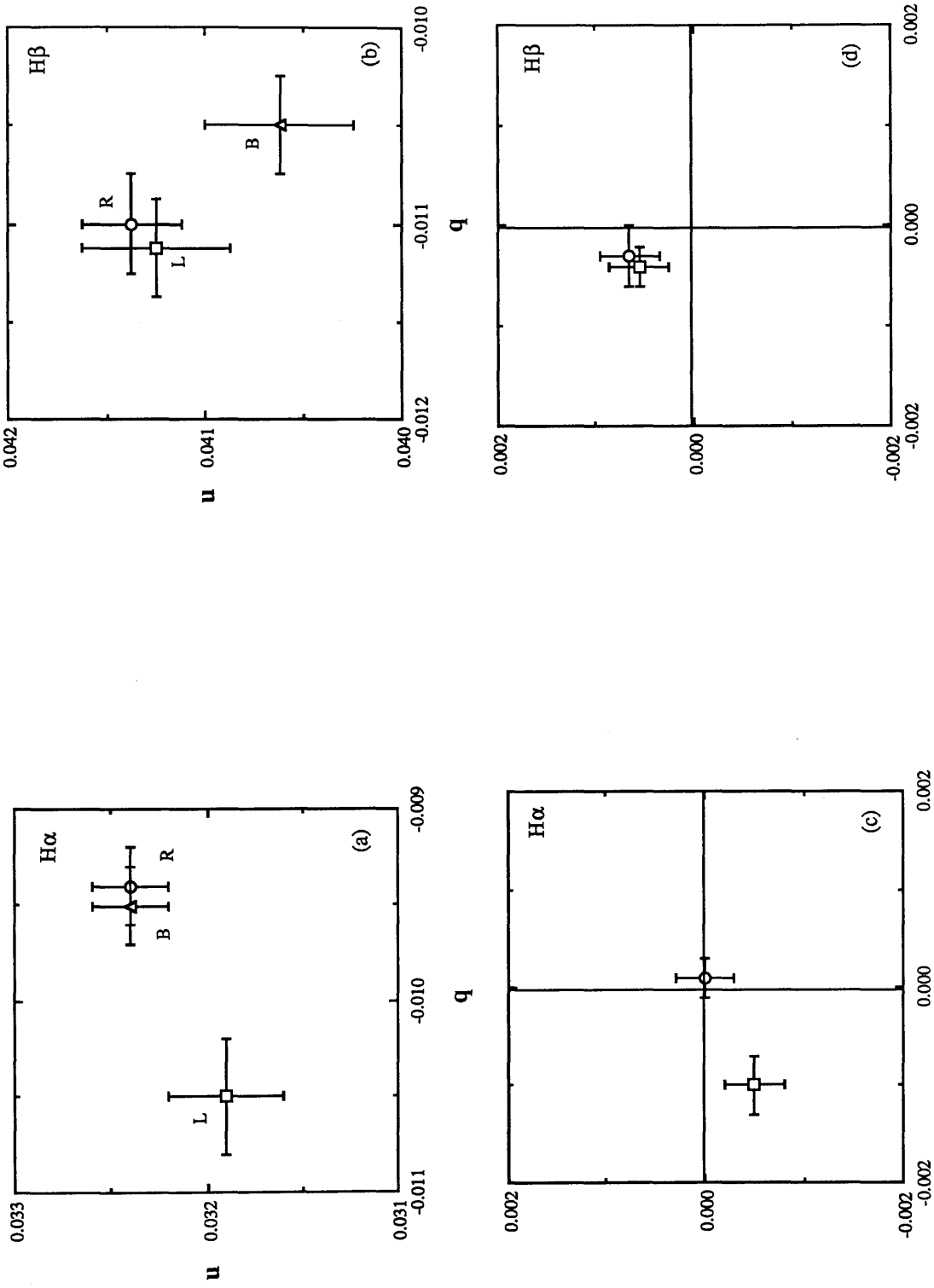

Figure (5.12) Material from the opposite table [see page 112 for details]

Mare Serenitatis E19.4° & N21.1°

Mean time of measurements	W. P.	NO.	Hα Q/I	Hα U/I	Hα P	Hα θ	>Hβ Q/I	>Hβ U/I	>Hβ P	>Hβ θ
1989 March 16 (UT)	R	44	−0.0323 ±0.0004	0.0710 ±0.0004	0.0781 ±0.0004	57.2 ±0.1	−0.0268 ±0.0004	0.0999 ±0.0003	0.1035 ±0.0004	52.5 ±0.1
23: 39: 28 TO	L	44	−0.0327 ±0.0005	0.0717 ±0.0005	0.0789 ±0.0006	57.3 ±0.2	−0.0264 ±0.0003	0.0997 ±0.0004	0.1032 ±0.0004	52.4 ±0.1
00: 30: 49	B	44	−0.0319 ±0.0003	0.0715 ±0.0005	0.0783 ±0.0005	57.0 ±0.1	−0.0267 ±0.0003	0.0999 ±0.0004	0.1035 ±0.0004	52.5 ±0.1
	L-B		−0.0009 ±0.0006	0.0002 ±0.0005	-------- --------	------ ------	0.0003 ±0.0005	−0.0002 ±0.0005	-------- --------	------ ------
	R-B		−0.0004 ±0.0005	−0.0006 ±0.0006	-------- --------	------ ------	−0.0001 ±0.0005	0.0000 ±0.0005	-------- --------	------ ------

Table 5.12 [See page 111 for details]

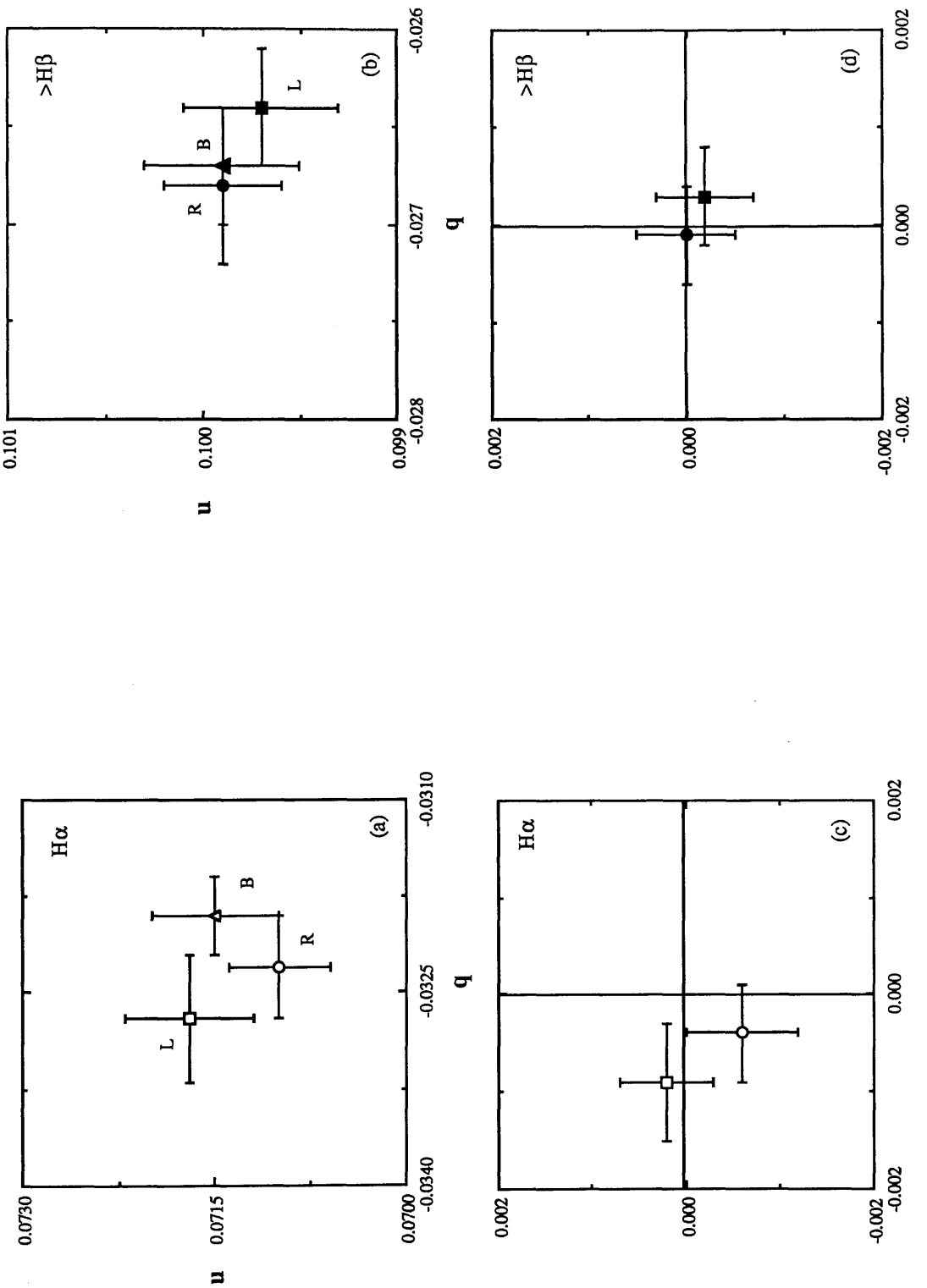

Figure (5.13) Material from the opposite table [see page 112 for details]

Mare Serenitatis E19.4° & N21.1°

Mean time of measurements	W. P.	NO.	Hα Q/I	Hα U/I	Hα P	Hα θ	Hβ Q/I	Hβ U/I	Hβ P	Hβ θ
1989 March 17 (UT)	R	60	−0.0302 ±0.0004	0.0653 ±0.0004	0.0720 ±0.0004	57.4 ±0.1	−0.0266 ±0.0003	0.0992 ±0.0004	0.1027 ±0.0004	52.5 ±0.1
00: 41: 56 TO	L	60	−0.0304 ±0.0004	0.0643 ±0.0005	0.0712 ±0.0005	57.7 ±0.2	−0.0268 ±0.0003	0.0988 ±0.0003	0.1024 ±0.0003	52.6 ±0.1
01: 24: 38	B	60	−0.0296 ±0.0004	0.0663 ±0.0004	0.0727 ±0.0004	57.1 ±0.1	−0.0264 ±0.0003	0.0983 ±0.0003	0.1018 ±0.0003	52.5 ±0.1
	L-B		−0.0008 ±0.0005	−0.0020 ±0.0005	-------- --------	------ ------	−0.0004 ±0.0004	0.0005 ±0.0004	-------- --------	------ ------
	R-B		−0.0006 ±0.0005	−0.0010 ±0.0005	-------- --------	------ ------	−0.0003 ±0.0004	0.0008 ±0.0004	-------- --------	------ ------

Table 5.13 [See page 111 for details]

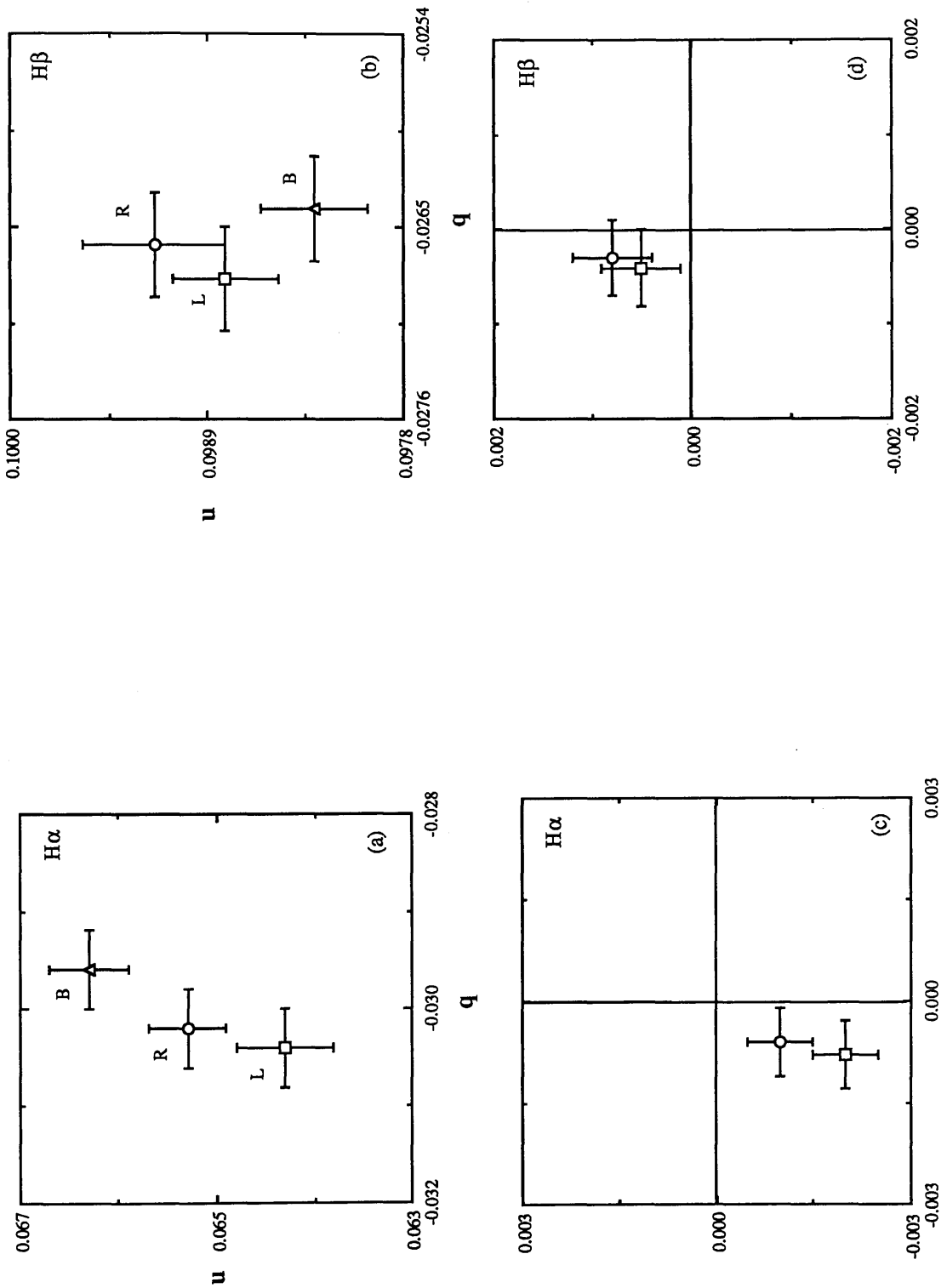

Figure (5.14) Material from the opposite table [see page 112 for details]

Fig.No.	site	Filter	S.P	All	L&B	L&R	R&B
5.4v	C	Hβ	q			2	
=	=	=	u			3	
5.4vi	=	=	q		3		
=	=	=	u		3		
5.5a	D	Hα	q	3	3	3	3
=	=	=	u	2	1	3	1
5.5b	=	Hβ	q	1	1	2	1
=	=	=	u	1	1	1	3
5.6a	E	Hα	q	3	3	3	3
=	=	=	u	3	2	3	3
5.6b	=	Hβ	q	1	1	3	1
=	=	=	u	2	2	3	2
5.7b	G	Hβ	q	1	3	2	1
=	=	=	u	3	3	3	2
5.8a	A	Hα	q	3	3	2	3
=	=	=	u	3	3	2	3
5.8b	=	Hβ	q	3	3	2	3
=	=	=	u	3	3	3	3
5.12a	B	Hα	q	1	1	1	3
=	=	=	u	3	3	3	3
5.12b	=	Hβ	q	3	3	3	3
=	=	=	u	2	3	3	2
5.14a	E	Hα	q	3	3	3	3
=	=	=	u	1	1	3	3
5.14b	=	Hβ	q	3	3	3	3
=	=	=	u	3	3	3	2

Table (5.14) Results of the statistical Welch test, for the data within the figures showing disparity of means with categories of difference, 1, 2, and 3 being confidence levels of >99%, >95% <99%, and <95% respectively that the data sets do not originate from the same parent distribution of q and u. Column 5: All data (R, L, B); column 6: for data of (L and B); column 7: for (L and R), and column 8: for (R and B).

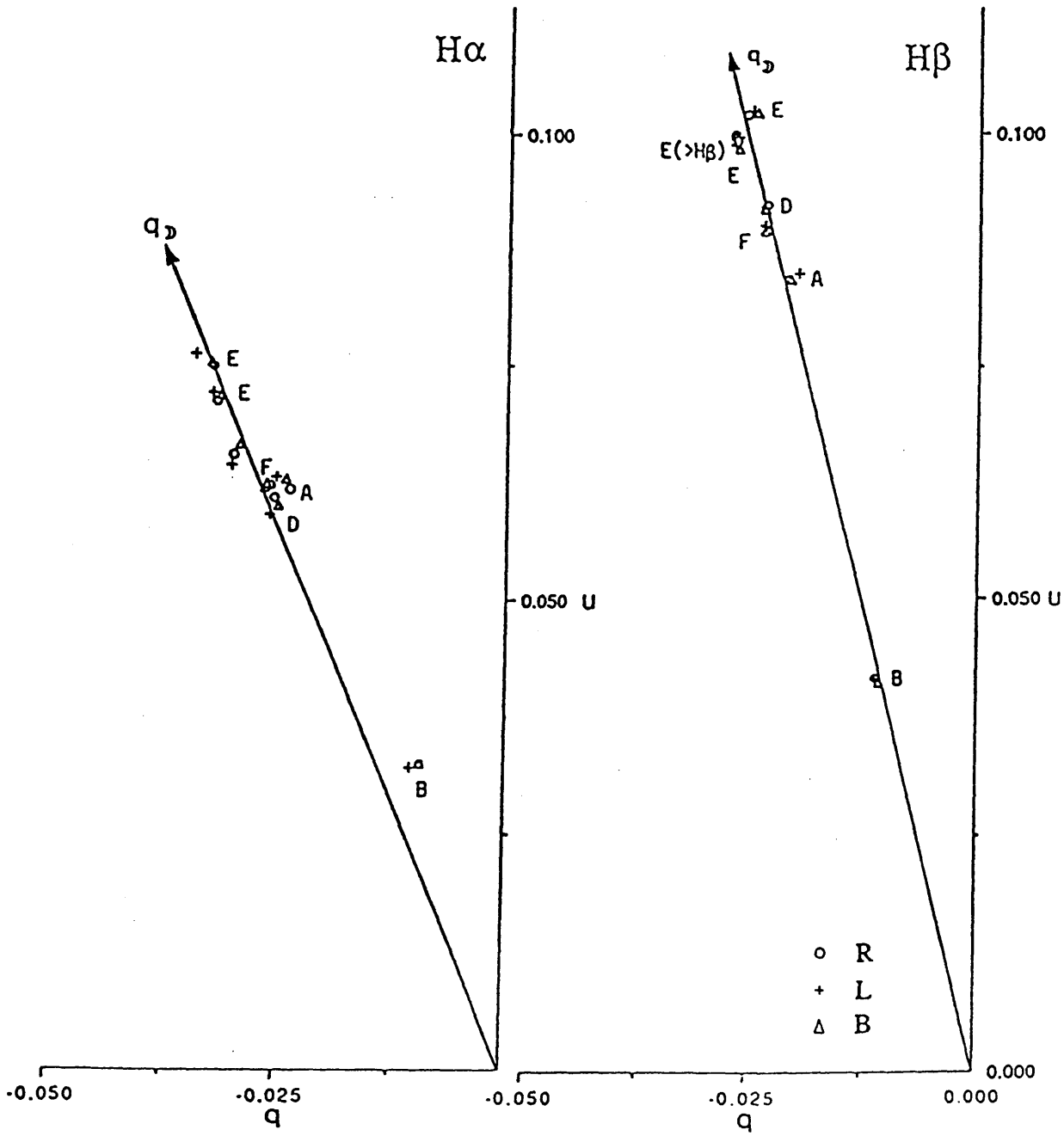

Figure (5.15a&b) The polarimetric data at Hα and Hβ respectively are displayed in the instrumental frame. The direction from the origin to $q_{\mathfrak{D}}$ defines the reference frame associated with the scattering plane. The data show that for Hα the displacements from $q_{\mathfrak{D}}$ are larger than for Hβ. Site B at Hα displays an anomalous departure.

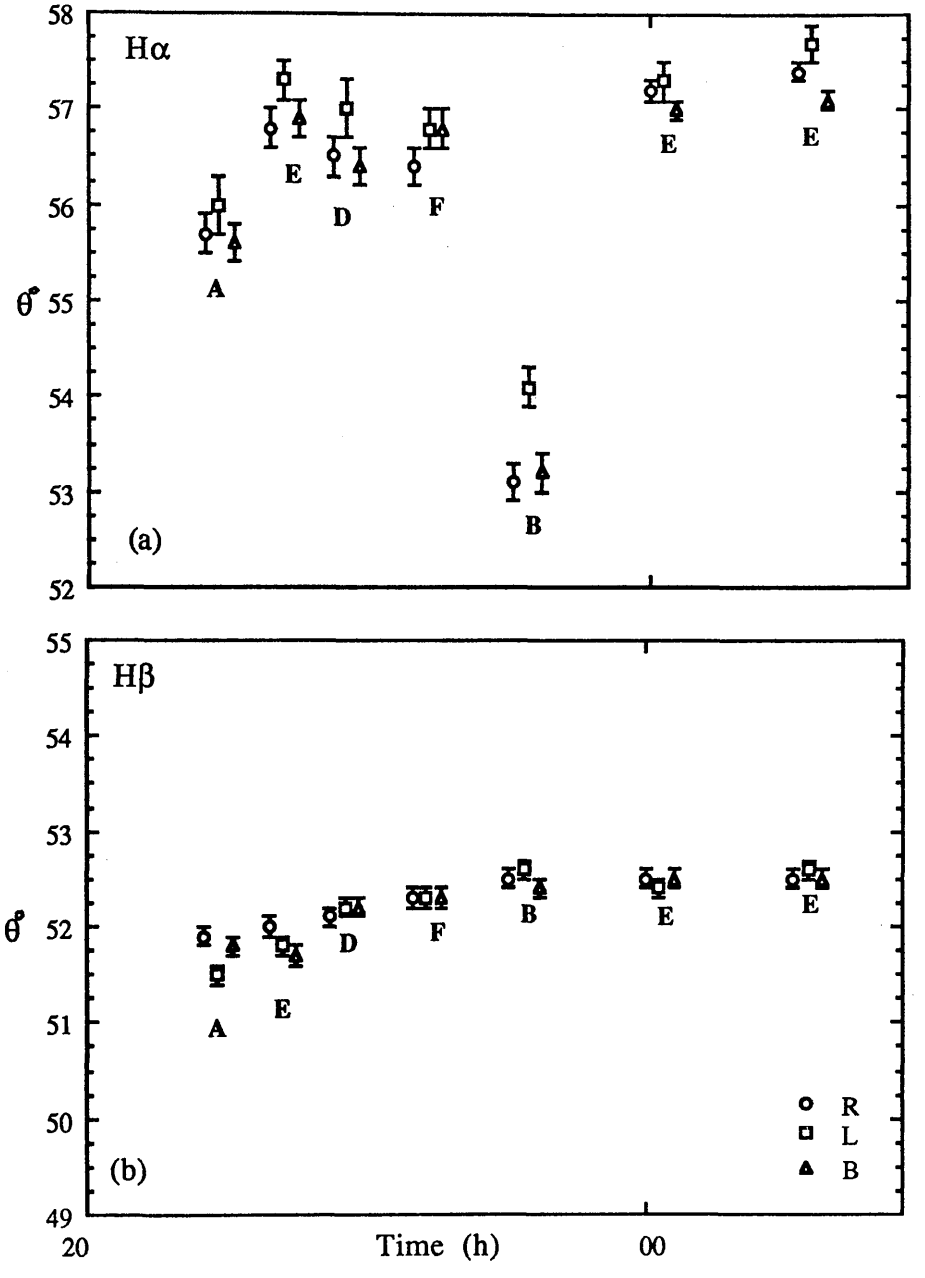

Figure (5.16a&b) Measures of the position angle of the polarization referred to the instrumental frame for the wavelength positions R, L, and B are displayed for the various investigated sites (A-E) according to the time of observation for the night of 1989 March 16. It can be seen for the Hα data that the measurements for the core of the line are consistently displaced with respect to the continuum. Note also the disparate value at Hα associated with Site B (Palus Somnii). The data for Hβ reveal no differences between line core and continua but display the systematic drift of the scattering plane relative to the instrumental frame due to the Moon's orbital motion with respect to the equatorial frame.

5.4 Conclusion.

It has been demonstrated that if the filling-in effect as observed photometrically by others in lunar spectra is ascribed to luminescence, then this contribution to the total lunar light will also produce polarizational changes across Fraunhofer lines. It has been considered that the luminescence is unpolarized and, if this is the case, its effect will be to reduce the observed degree of polarization produced by the general scattering from the lunar surface according to the model described in Chapter 2. For a luminescent band covering a Fraunhofer line, the reduction effect will be more pronounced within the depth of the profile relative to its nearby continuum. Based on the luminescent light being unpolarized and according to its intensity as measured by spectrophotometry, it was expected that polarization reduction at the centre of the line profile should be detectable. However the predicted effects were not observed despite the measurements being made with a sufficient signal - to - noise ratio.

For those data sets which suggest that marginal differences have been recorded, no consistent pattern of behaviour has emerged; sometimes it is the measurement at the line core which appears to be disparate, sometimes it is one of the continuum measurements which is possibly different. For example, the data in Figures (5.12a) and (5.14a) suggest that the line has disparate values relative to the red and blue continua; Figures (5.5a) and (5.6b) show that the polarization for the blue continuum is disparate relative to the line and the red continuum; Figure (5.7b) shows a possible progressive change in P over R/ L/ B from 0.0281±0.0002 to 0.0271±0.0002 (see Table 5.6, Hβ).

In some cases, the records may only be reflecting the small polarizational variation which is expected to occur across the spectral extent of an absorption line as a result of the general $P(\lambda)$ of lunar scattering. For phase angles providing $P \approx 10\%$, typical gradients ($\delta P/\delta\lambda$) are $\approx -10^{-5}$ Å^{-1} (see Figure 5.3). As the difference between

R and B is of the order of 30Å, it is to be expected that the P values at B would be higher than those at R by ≈0.0003, this figure being of the order of the noise of the measurements.

The Palus Somnii area exhibits a rotation of the plane of polarization by ≈ 4° at the red and the blue continua of the Hα, and by 3° at the Hα line centre with respect to the other sites (see Figure 5.16). There is also weak statistical evidence that the Hα core for all lunar regions displays a rotation of position angle relative to that of the local continuum. On this evidence it is tempting to suggest that there is perhaps a luminescent band at Hα but not one at Hβ, and that its flux certainly cannot be simply unpolarized. However, in order to mimic the results, the luminescence would require to be polarized with a position angle closer to the U direction rather than Q, i.e. at ≈ 45° to the scattering plane, so imposing a constraint on our model described in Chapter 2 which would be difficult to explain.

Chapter 6 Measurements across Hα and Hβ in the daytime sky.

6.1 Introduction.

When spectra of the daytime sky are compared with those directly from the Sun, it is found that the depths of the Fraunhofer lines are reduced. The first full report of the measurements of the effect in the daytime sky was by Grainger and Ring (1962b) who found that the filling-in amounted to an additional light component of about 3% in the H and K lines of Calcium. The phenomenon is now referred to as the Ring effect. A variety of Fraunhofer lines has been used to explore the effect, all lines displaying filling-in to some degree with indications of variability during the day, although these diurnal changes appear not to be systematic (see Chapter 1). Most previous work on the line filling-in effect has been performed spectroscopically, with the notion that the added component is at all times unpolarized, as suggested by Pavlov et al. (1973) and Harrison (1976). Measurement of the degree of polarization across the line and its variation through the day provides an alternative tool to direct spectrophotometry for investigating any changes in the line filling-in strength, the principle also removing the requirement of comparative solar measurements directly or indirectly using an attenuator.

The maximum value of the zenith blue sky polarization occurs at a scattering angle of 90° - sunrise and sunset - and the minimum value at noon when the scattering angle is smallest. According to Rayleigh scattering, if the scattering angle is ϑ then the polarization P is given by:-

$$P = \frac{1 - \cos^2(\vartheta)}{1 + \cos^2(\vartheta)} \qquad (6.1)$$

this suggesting that P should be 100% at sunrise and sunset.

The observations reported here started in 1988 June, with the best measurements using one channel (Hβ) on 1988 June 24 and August 7. The maximum polarization was ≈0.70 (i.e. 70 per cent). Figure (6.1) displays the changes of the polarization during the

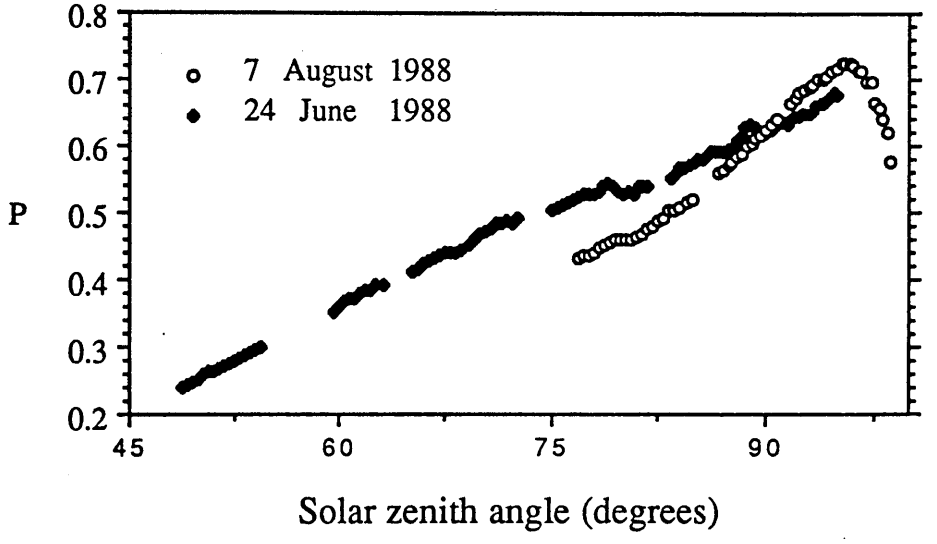

Figure (6.1) Typical variation of the degree of polarization at the zenith as a function of solar zenith angle.

runs. The departure from the polarization being 100% (at sunrise and sunset) is caused by several effects; multiple scattering accounts for ≈6%, reflection by the ground ≈5%, and the effect of molecular anisotropy ≈6%, while the residual dilution is due to aerosols suspended in the atmosphere even when the sky looks a very strong clear blue (Gehrels, 1962). Molecular anisotropy occurs by the effect of the incident radiation introducing a stress within the molecule structure; this gives rise to anisotropic scattering and an effective depolarization relative to pure Rayleigh scattering.

The general scattered light of the blue sky is polarized and as the additional component may or may not also be polarized, then according to the model in Chapter 2, the line filling-in effect should be detectable by performing spectropolarimetry and indeed this has been achieved. As the filling-in effect needs measurements at the line centre and the continuum, three wavelength positions on the spectrum line profile have been chosen for monitoring, in just the same way as for the lunar experiment. The observational technique allows both photometery and polarimetry to be performed simultaneously.

Without the filling-in effect, the observed polarization degree at the three wavelengths should be equal at any time (at a particular scattering angle), because the polarization is essentially independent of wavelength. However, filling-in alters this situation. Clarke and McLean (1975c) measured the degree of polarization of the zenith daytime sky at Hβ and found a reduction in the line centre which was commensurate with the added light being unpolarized. But if the added light is polarized the situation will be more complicated as will be seen below. The azimuth of vibration (equatorial position angle) of the zenith polarized light is normal to the scattering plane (a plane through the centres of the Sun and the Earth and through the direction of observation - the Zenith - see Figure 6.2). The scattering plane also defined by an angle φ_r, which its values can be predicted if φ_s (Sun's azimuth) is known. For observations of the zenith, φ_s can be predicted from Figure (6.2) as:-

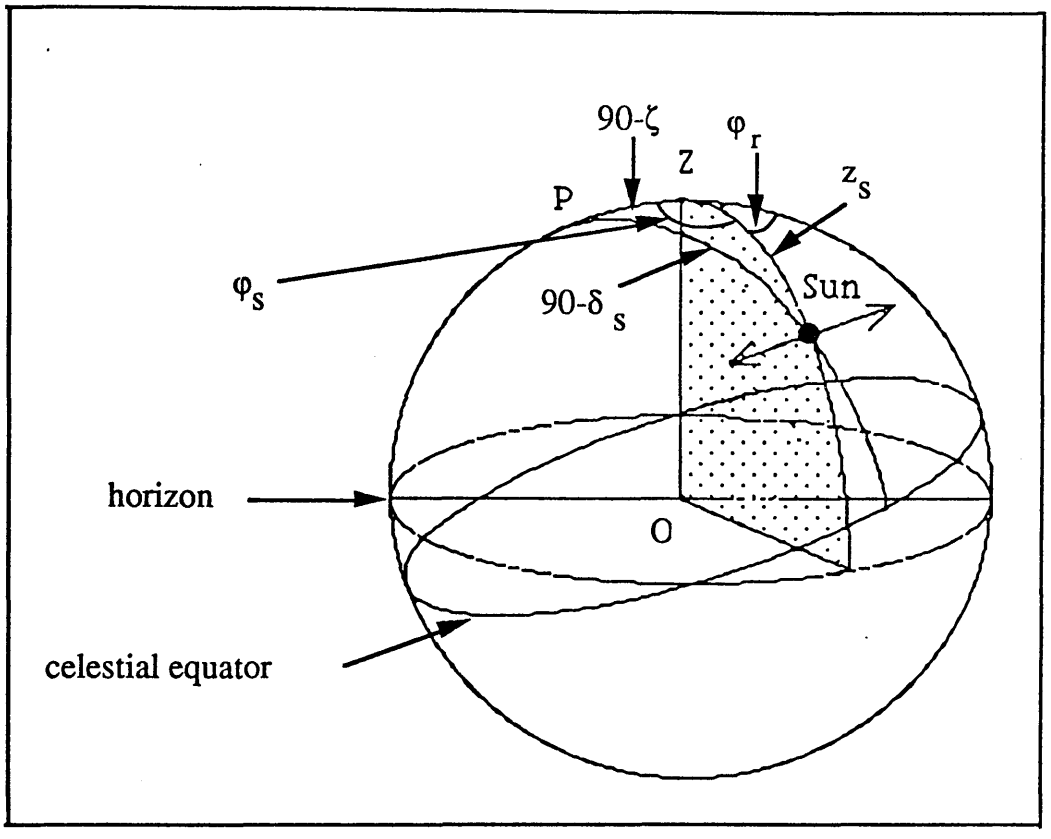

Figure (6.2) Celestial sphere for an observer at latitude, ζ , illustrating the scattering plane, which contains the observer O, zenith Z and the Sun. The azimuth of vibration is perpendicular to that plane.

$$\cos \varphi_s = \frac{\sin \delta_s - \sin \zeta \cos z_s}{\cos \zeta \sin z_s} \qquad (6.2)$$

where δ_s and z_s are the declination and zenith angle of the Sun respectively, and ζ is the latitude of the observatory. The Sun's zenith angle z_s as a function of the hour angle H_s of the Sun is given by:

$$\cos z_s = \sin \delta_s \sin \zeta + \cos \delta_s \cos \zeta \cos H_s \qquad (6.3)$$

From Equations (6.2) and (6.3), φ_r can be evaluated. If there is no difference between the observed vibration at the line centre relative to the continuum, then any added light is either unpolarized, or its polarization is in, or orthogonal to, the scattering plane [see Cases (a) and (b) of the model in Chapter 2].

6.2 The observations.

The zenith blue sky has been observed on the clearest days during 1988 and 1989 using the same equipment as for the lunar observations. The early observations used Hβ only; later a second channel became available to allow measurements at Hα. The data collection techniques were similar to those used for the lunar experiment, see Section 5.2.

The observations were made in different seasons, with different ground cover around the observatory affecting the local albedo. One of the immediate problems of the experiment is the apparent movement of the Sun around the sky causing large but smooth changes of both the light brightness and polarization. These strong diurnal effects need to be removed from the data before any small fluctuation can be investigated. The instrumental polarization was always sufficiently low to be ignored for the daytime sky experiment.

6.3 Data reductions.

6.3.1 The filling-in measurements.

Simple Rayleigh scattering theory suggests that there should be a λ^{-4} dependence for the brightness of the sky. It is by such scattering that the sky appears blue. Because of this strong wavelength dependence, the continuum levels are unlikely to be the same on either side of a Fraunhofer line. As a result of changes during the day of aerosol content, humidity levels, absorption along the observed column etc, the continuum levels are likely to change with respect to each other. Care must be taken in determining the interpolated intensity value of the continuum level above the line centre in order that the line depth can be calculated. So, to minimize the effects of the secular changes in brightness occurring between the measurements at the three wavelength positions, the records have been divided into blocks each one containing five measurement cycles, the integration time for the block being about 165 seconds. For each block, the time variation of the intensities of the two continua (I_R , I_B) and the line core I_L were fitted by lines with characteristics determined by least squares. From the relationship, the intensity values can be unified to a particular time and then the average of the continuum measurements value can be obtained for comparison with the line core intensity.

The spectral line profiles of the integrated solar disk are virtually constant with time and any fluctuations of line depths in the spectra of the terrestrial atmosphere mirror the changes of the added light during the day. Since comparisons were not made directly with solar spectra, our photometric measurements for detecting the filling-in cannot give quantitative values for the added light intensity, but may still display its variations during the day. The differences between the line centre and the continuum in terms of intensities or polarizations (degree and angle of vibration) have been obtained by subtracting the values of the line from the average value of the two continua and normalising to the continuum according to the following equations :-

$$\rho_I = \frac{I_C - I_L}{I_C} \qquad (6.4)$$

$$\rho_P = \frac{P_C - P_L}{P_C} \qquad (6.5)$$

$$\delta\theta = \theta_C - \theta_L \qquad (6.6)$$

where $I_C = (I_R + I_B)/2$, $P_C = (P_R + P_B)/2$, and $\theta_C = (\theta_R + \theta_B)/2$,

I is the intensity, P is the polarization degree , θ is the angle of polarization, and L, R and B are the positions on the line profile corresponding to the line centre, red, and blue continuum. Values of I have been corrected for the dead time of the counter circuits.

The first attempts to measure quantitatively changes in ρ_I , ρ_P and $\delta\theta$ were undertaken on 1988 June 14. Excellent observations taken on 1988 June 24, yielded new facts on the variation of the added light and its polarization during the day according to the scattering angle, or zenith angle of the Sun. The results are displayed in Figure (6.3). When the solar zenith angle is large, so providing a similarly large scattering angle, the reduced polarization, at the line centre, is readily seen (see Figure 6.3c). These results are similar to those obtained previously by Pavlov et al. (1973), and Clarke and McLean (1975c), see Figure (3.1a). However, as the solar zenith angle reduces, the polarization in the line becomes closer to that of the nearby continuum (see Figure 6.3b) and eventually at the smallest scattering angles, the line polarization is higher than the nearby continuum (see Figure 6.3a). This obviously violates the condition that P_L should be less than P_C according to the previous studies. If the added light of the Ring effect is influencing the polarization across the spectral line then, at least for some scattering angles, it must be polarized to some degree. For the conditions where the line enhancement of polarization is observed, the constancy of polarization direction across the line requires a filling-in component with a value of P higher than that of the general scattered light and with an aligned vibration. At solar zenith angles for which a polarization reduction is observed at the line centre, the added light could be unpolarized,

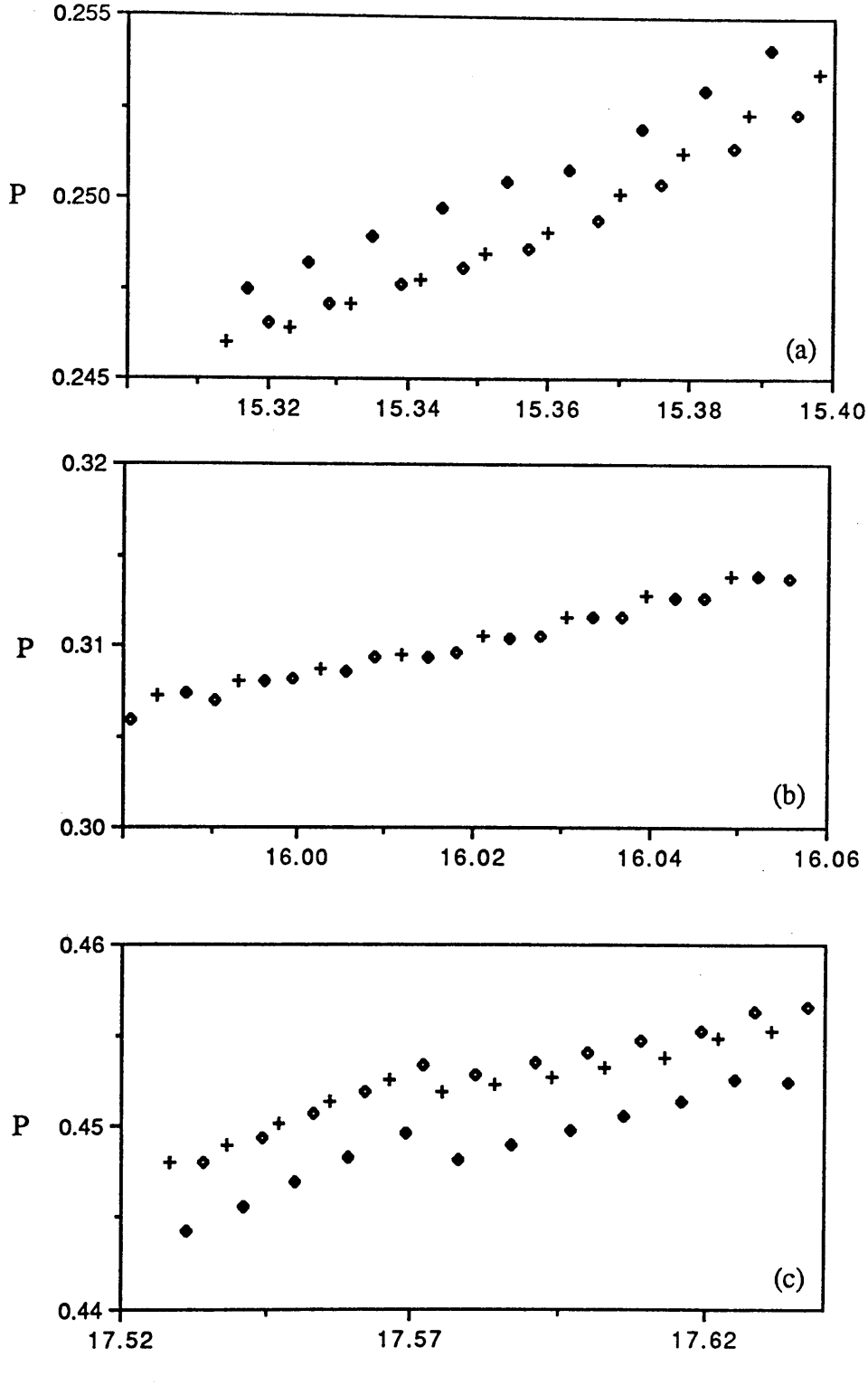

Figure (6.3) The variation of the degree of polarization, P, at the Hβ line of the zenith sky as a function of UT during three portions of the day 1988 Jun 24. Points marked ◆ refer to measurements in the core of the line, those marked +, ◇ refer to measurements in the red and blue continua respectively.

or have a polarization with the same plane but with a strength less than that of the general scattered component, or a polarization orthogonal to the Rayleigh component,these three possibilities being distinguishable only by reference to the intensity of the filling-in component. Thus the observed polarimetric behaviour of the zenith light across a spectral line depends on the relative contribution of the scattered component and the added light and their behaviour through the day.

The observed values of ρ_I, ρ_P and $\delta\theta$, are plotted against the zenith angle, for the data of 1988 June 14, 24, July 4 and August 7, in Figures (6.4 to 6.7). From these figures, it is clear that the filling-in effect has controlled the behaviour of the variation of ρ_I and ρ_P during the day. The values of ρ_I of the longest data run (June 24) display a general change throughout the after noon decreasing from 0.215 to 0.200; a similar decrease was observed on June14.

The level of these changes in no way can be explained in terms of instrumental effects. The filter chamber was temperature controlled so that the wavelength registration did not drift by more than the equivalent of ±1 motor step. Even if a drift of this magnitude occurred, so that the setting for the line core was slightly in error, the apparent change in the value of ρ_I would be less than 2%.

The observations of August 7 show a large decrease of 7% in the values of ρ_I with respect to the other days. This again cannot be an instrumental effect caused by imprecise wavelength setting. The values of ρ_I show a progressive drift as the solar zenith angle increases.

The plotted values of ρ_I on 1988 June 24 give a hint of fluctuation possibly with a periodicity, (Figure 6.5a) through the day. However when the data were investigated for periodicity by the method of cosine and sine summations (akin to performing a Fourier transform), the power spectrum strongly resembled the sinc^2 function associated with the window (time interval) of the data. The power associated with this dominates

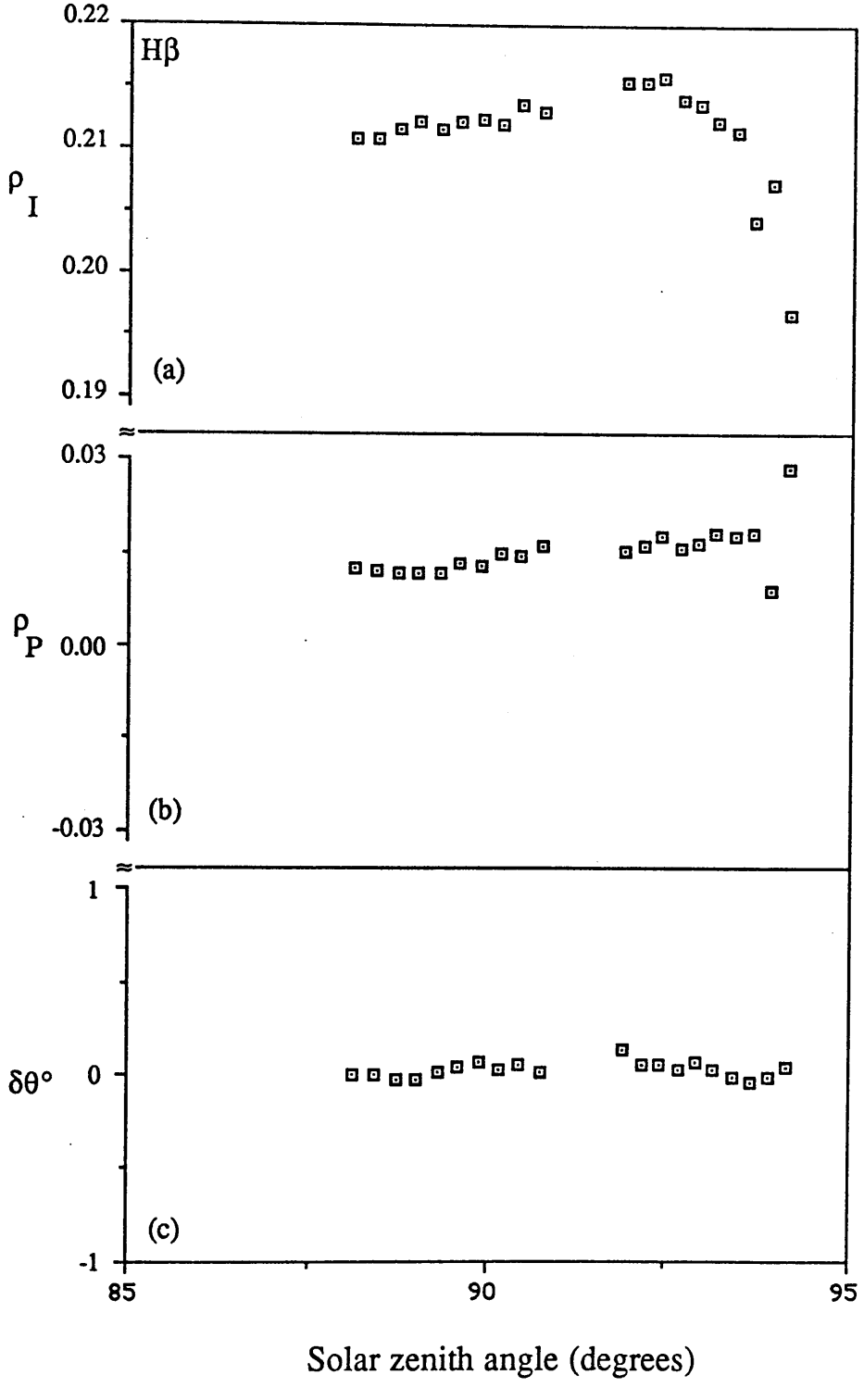

Figure (6.4) (a) The variation with time of the line filling-in parameter, ρ_I, on 1988 June 14. (b) The similar variation of ρ_P. (c) The behaviour of the difference of the direction of vibration of the polarization across the line $\delta\theta=\theta_C-\theta_L$, measured in degrees.

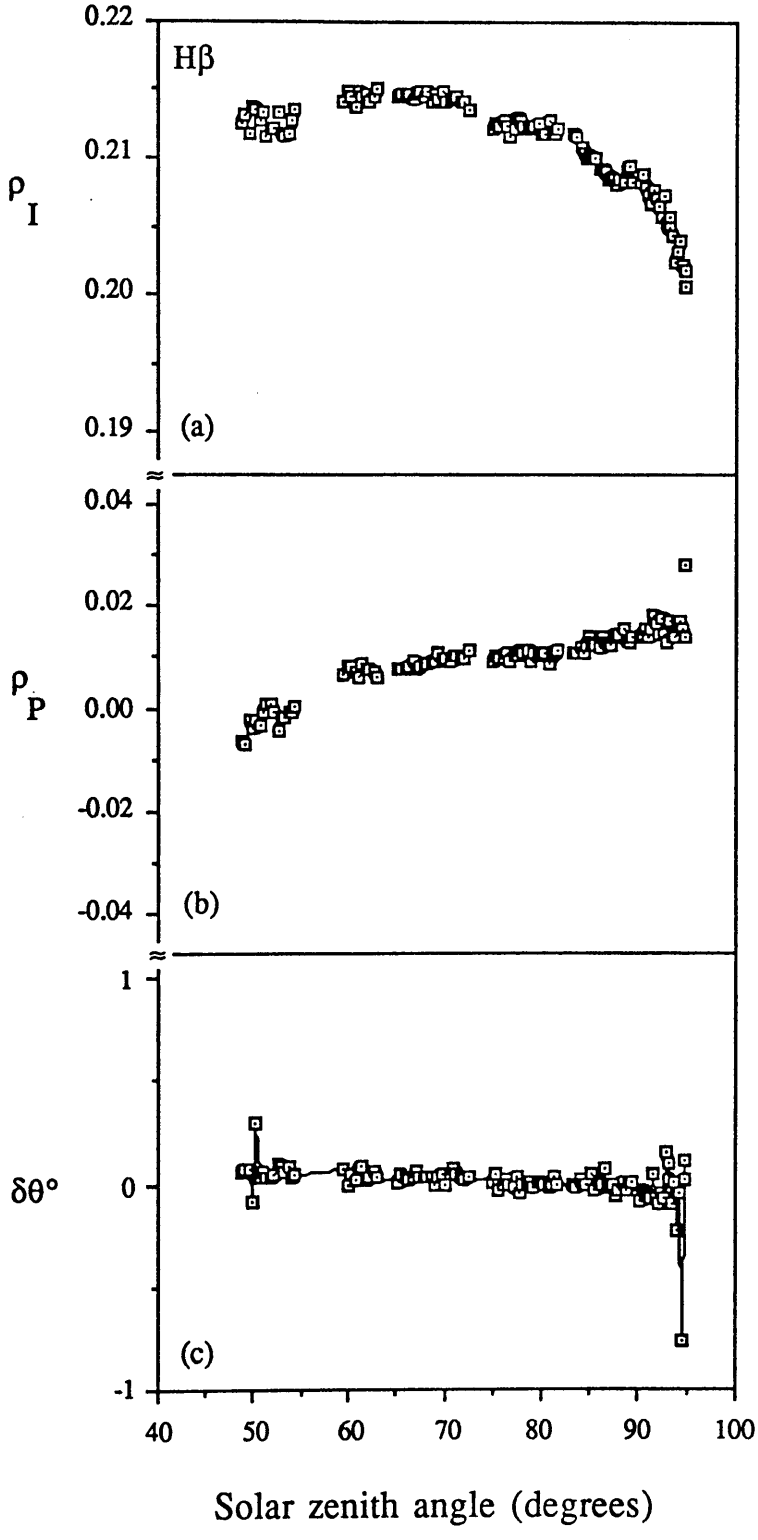

Figure (6.5) Similar to Figure (6.4) but for 1988 June 24.

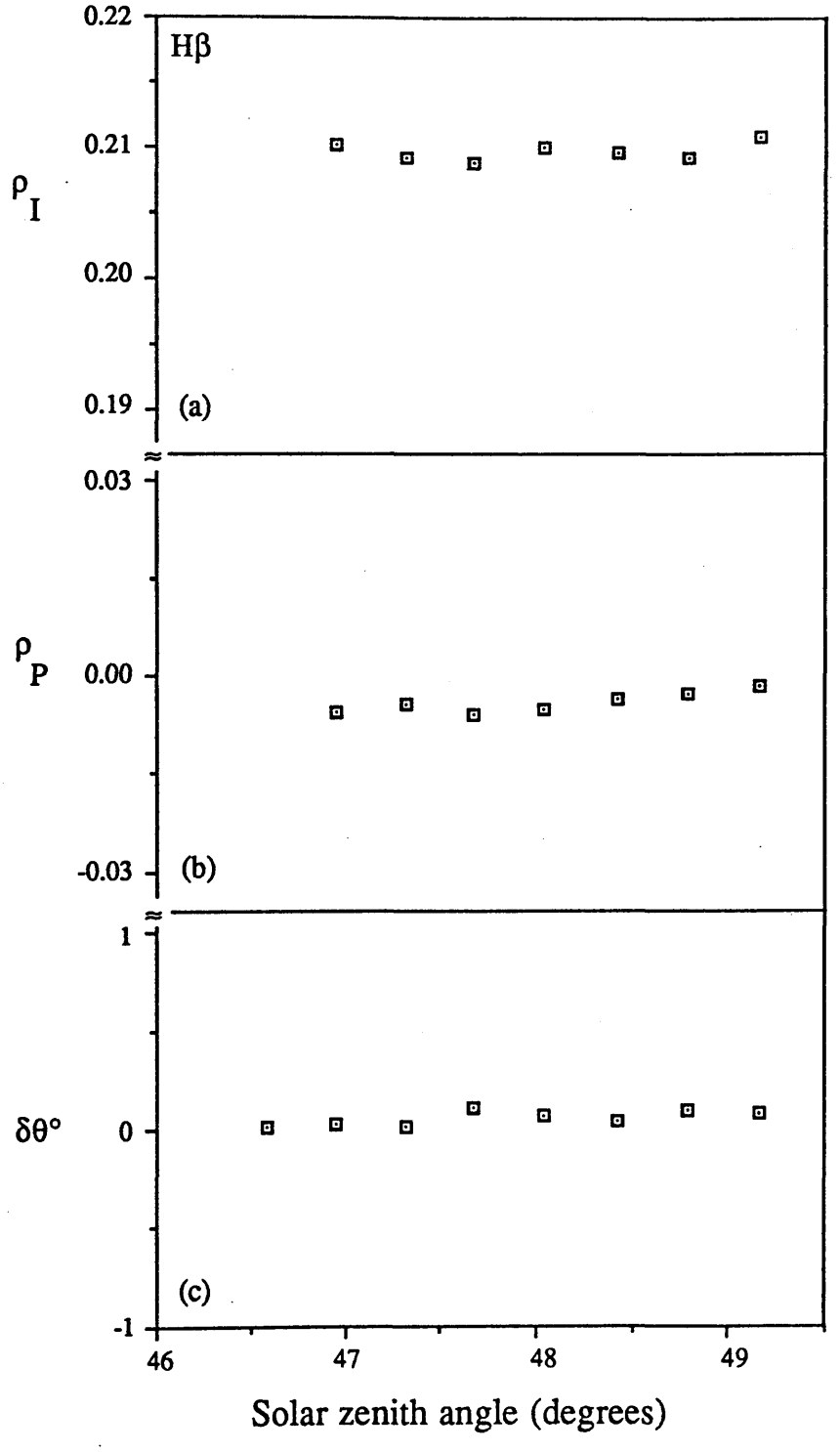

Figure (6. 6) Similar to Figure (6.4) but for 1988 July 4.

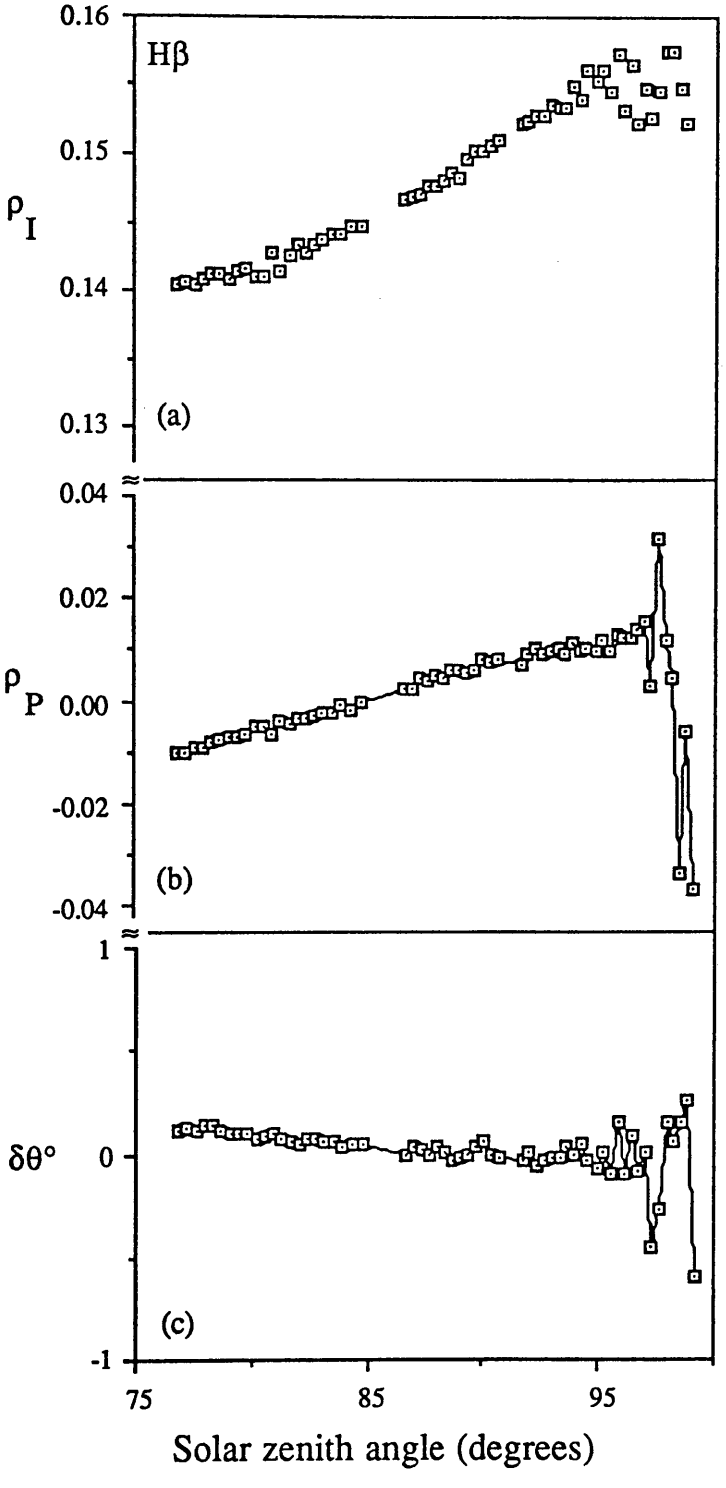

Figure (6.7) Similar to Figure (6.4) but for 1988 August 7.

anything which might have originated by "real" oscillations within the data and the subject was not pursued further.

The values of ρ_P always increase from negative to positive as the scattering angle increases. From the observations of June 24 (Figure 6.5b), the negative values when the polarization at the line is greater than that at the continuum, occur at small scattering angles. When the ρ_P value is equal to zero this situation represents the condition for which the polarization degree of the added light is equal to that of the general scattering; positive values correspond to the polarization at the line being less than that at the continuum. The observations on August 7 show the same behaviour for ρ_P but the crossing from negative to positive has occurred at a larger scattering angle (see, Figure 6.7b). This means that the added light was more polarized on the second occasion, possibly due to the large decrease of the values of ρ_I on this day, or possibly due to a genuine increase in the intensity of the added light or both. The behaviour of ρ_P and $\delta\theta°$ (see, Figure 6.7b&c) following sunset indicates sudden changes but such interpretation must be treated with caution because at these times the sky brightness is decreasing very quickly and the noise levels associated with the determination of ρ_P and $\delta\theta°$ are increasing rapidly.

At all times no difference in the polarization angle, θ, was detected across the line, the differences between consecutive measurements of line centre and continuum exhibiting a noise of $\delta\theta = \pm 0.°1$. Figure (6.8) shows the variation of θ_L compared with predicted values, the displacement between the two curves resulting from the difference of the co-ordinate frames plus a constant to include, say, the Earth magnetic field which affect the plane of polarization, the Faraday effect. The parallelism between the two curves suggests that the azimuth variation at the line centre was not affected during the progressive change of ρ_P.

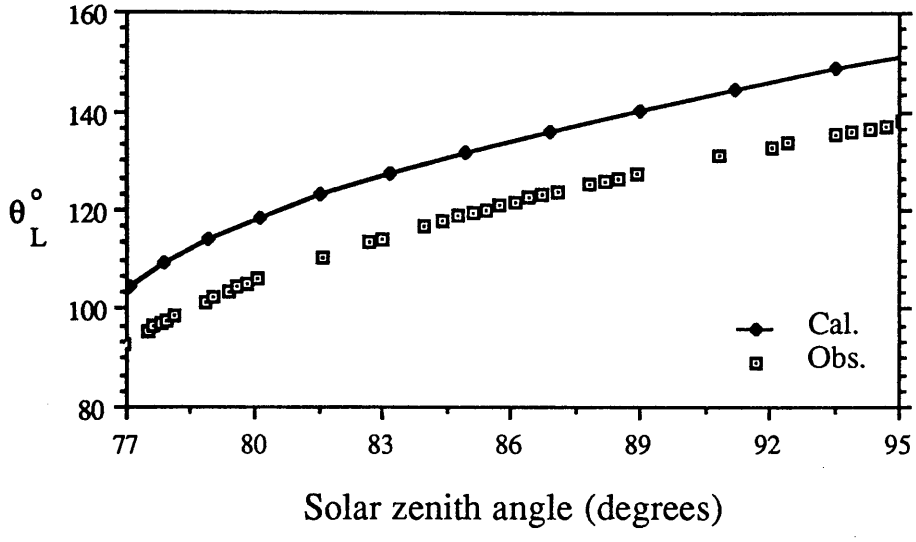

Figure (6.8) Typical variation of the calculated and observed azimuth of the polarization of the zenith sky with the solar zenith angle. The difference between the observed and the calculated values is the off set of the half-wave plate axis relative to the frame used for the calculations.

The above observed behaviour of ρ_P could be explained by using Case (b) of the model which has been evaluated for the filling-in effect in Section 2.1, by considering a situation in which the added light has a fractional intensity F and a polarization P_a remaining constant through the day. For a spectral line having a given value of R, the $\rho_P \left(= 1 - \frac{P_L}{P_C}\right)$ values depend only on the behaviour of the general scattering polarization at the zenith, according to, Equation (2.3). For example, the predicted behaviour of ρ_P is given in Figure (6.9) for values of F and P_a of 6%, 30% and 5%, 45% respectively and R=0.7. The chosen values of F are typical of the photometric behaviour of the line filling-in effect and those of P_a are required to match the general polarization of the zenith sky at the time where the cross-over from negative to positive values of ρ_P occur. The variations of the value of ρ_P in this figure with the polarization degree of the general scattered light can be seen to agree fairly well with the real observations reported here and support the idea that the added light is polarized. This model can be taken as a first step to explain our results of the zenith sky but is perhaps a little artificial because of the restriction on the constancy of F and P_a.

The next section will provide a discussion of the wavelength behaviour of this phenomenon (polarization enhancement /reduction effect at the line centre).

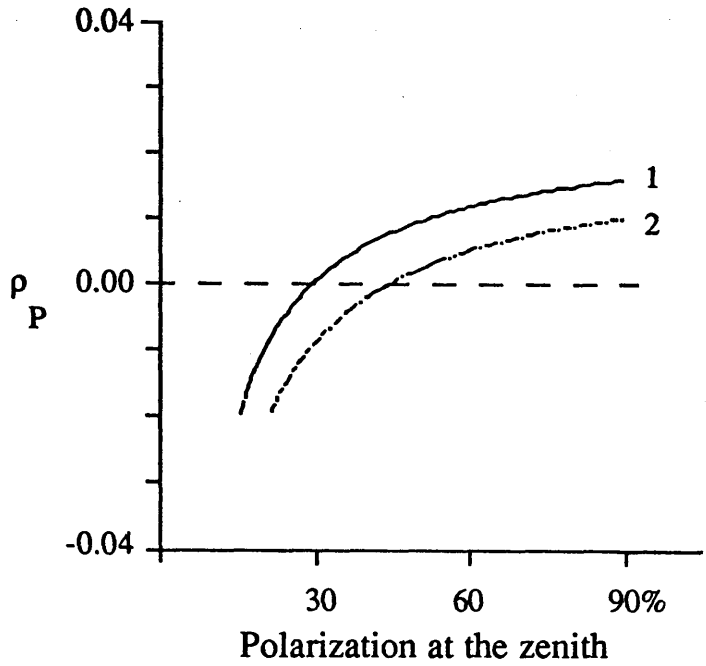

Figure (6.9) Computed variations of ρ_p for two strengths (F) of added light with polarization (P_a), as a function of the zenith polarization. (F and P_a are assumed to be constant but superimposed on the variable zenith sky scattering). Curve (1) is for F = 6% and P_a = 30% while curve (2) is for F = 5% and P_a = 45%. The behaviour matches the observed values of ρ_p, being negative at small zenith angles but being positive at large zenith angles

6.3.2 The wavelength dependence of the filling-in effect.

The discovery that the added light is polarized was first made using the Hβ line only. The effect was later explored in the Hα line after attaching the second channel to the instrument, at the end of 1988 August. This system gave the chance to observe the wavelength dependence of the polarization of the filling-in effect and to explore the time dependence of ρ_P at these two spectral regions. During 1988-1989 many observational sets of data were collected using the Hα and Hβ lines, for days exhibiting a variety of meteorological conditions. The values of ρ_I, ρ_P and, $\delta\theta$ were calculated as for the previous analyses. The results show no uniformity for the added light intensity, its value certainly depending on the solar zenith angle and on the kind of day (clear or turbid). The behaviour of ρ_P was the more consistent, having the same character for both wavelength regions, i.e. always increasing with the solar zenith angle. For all observations the ρ_P values for Hα tend to have the same time-dependent behaviour as for Hβ. The observations on 1989 July 16 during morning time showed for both wavelengths the same decrease as the solar zenith angle decreased (see Figure 6.15b)

Previous works on the intensity filling-in effect indicated that the added light is stronger at short wavelengths i.e. the effect at Hβ is stronger than at Hα. This was impossible to check out with our technique, but the relative variations during the day could be compared. Without considering times around twilight and the "daylight flash" (see next section), the average values of ρ_I have been tabulated in Table (6.1). Some of these measurements have been plotted against the zenith angle in Figures (6.10a to 6.15a). Any variation of the values of ρ_I may be assumed to correspond to the changes of the strength of the added light during the observation time. From these figures the values of ρ_I for Hα and Hβ seem to be constant during the observation time except for the time around sunset when twilight is observed. At this time the geometry of the situation is different as for example, there is no component from ground backscattered into the column. The observations for Hα and Hβ on 1988 October 15 exhibit opposite

behaviour of ρ_I (see Figure 6.11a); the values of Hα decreased by 3% during twilight from their daytime value, while the values of Hβ increased by 1%.

In Figure (6.14a) corresponding to 1988 November 20 the values of the ρ_I for both wavelengths were constant during the time of observations (about five hours), except for the first six points whose behaviour will be described in the next section. These observations were made while the area surrounding the observatory was covered by snow, and the Sun's zenith angle having moved from 76° to 99°. As the Sun approaches the horizon, the ground illumination decreases and hence its contribution to the brightness of the zenith air column falls. If the ground albedo is the source of the added light, then its effect should be pronounced on the values of ρ_I for this day, but there is no hint of any such effect.

From the above discussion the pattern of the behaviour of the filling-in is dominantly governed by meteorological processes. This could well explain the discrepancies in the previous reported observations by various workers which described the strength of the filling-in intensity as decreasing in some cases or increasing in others according to increasing solar zenith angle.

Date		ρ_I (Hβ)	±σ	ρ_I (Hα)	±σ
1988	14 June	0.2126	0.0004	------	------
1988	24 Jun	0.2211	0.0003	------	------
1988	4 July	0.2111	0.0003	------	------
1988	7 August	0.1455	0.0012	------	------
1988	15 September	0.2341	0.0006	0.2817	0.0189
1988	15 October	0.2409	0.0005	0.2834	0.0009
1988	28 October	0.2050	0.0015	0.2535	0.0013
1988	29 October	0.2543	0.0093	0.2563	0.0093
1988	2 November	-------	-------	0.2748	0.0003
1988	20 November	0.2372	0.0008	0.2752	0.0005
1989	3 July	0.2440	0.0026	0.2113	0.0067
1989	15 July	0.2320	0.0007	0.2680	0.0011
1989	16 July	0.2485	0.0007	0.2573	0.0008
1989	18 July	0.2314	0.0017	0.2852	0.0008

Table (6.1) The average values of ρ_I for the Hα and Hβ lines, where there are no twilight or daylight flash effects.

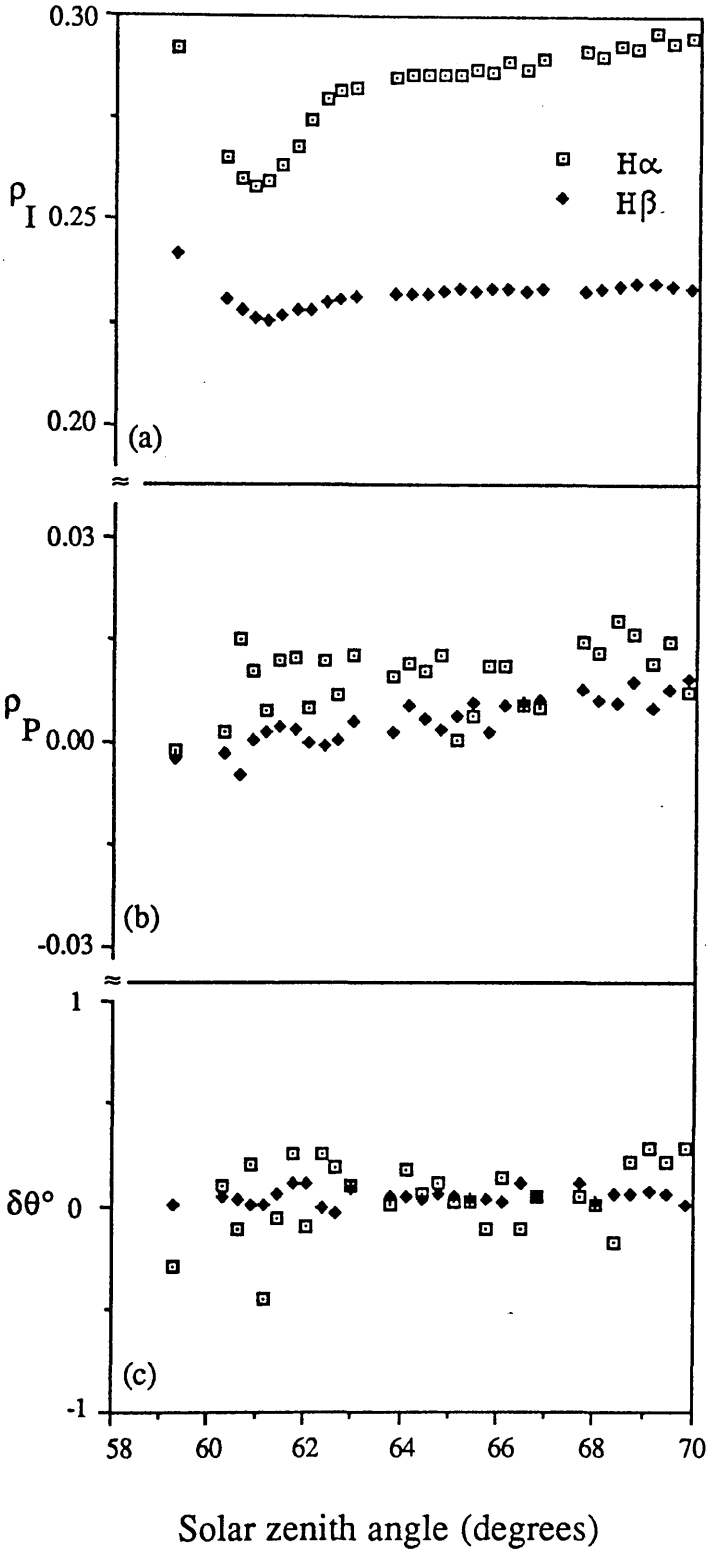

Figure (6.10) (a) The variation with zenith angle of the line filling-in parameter, ρ_I, on 1988 September 15, for the Hα and Hβ Fraunhofer lines. (b) The similar variation of ρ_P. (c) The behaviour of the difference of the direction of vibration of the polarization across the line, $\delta\theta=\theta_C-\theta_L$, measured in degrees.

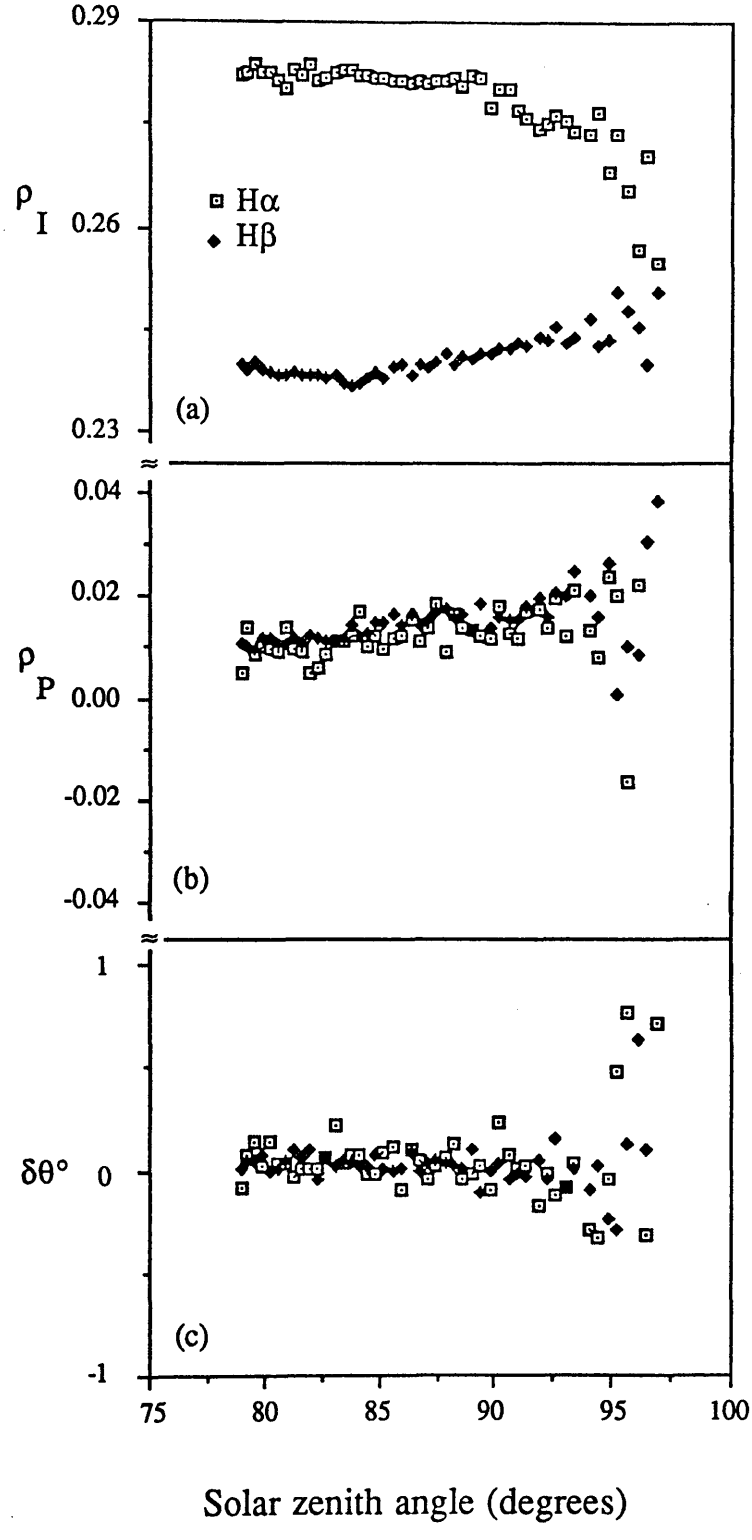

Figure (6.11) Similar to Figure (6.10) but for 1988 October 15.

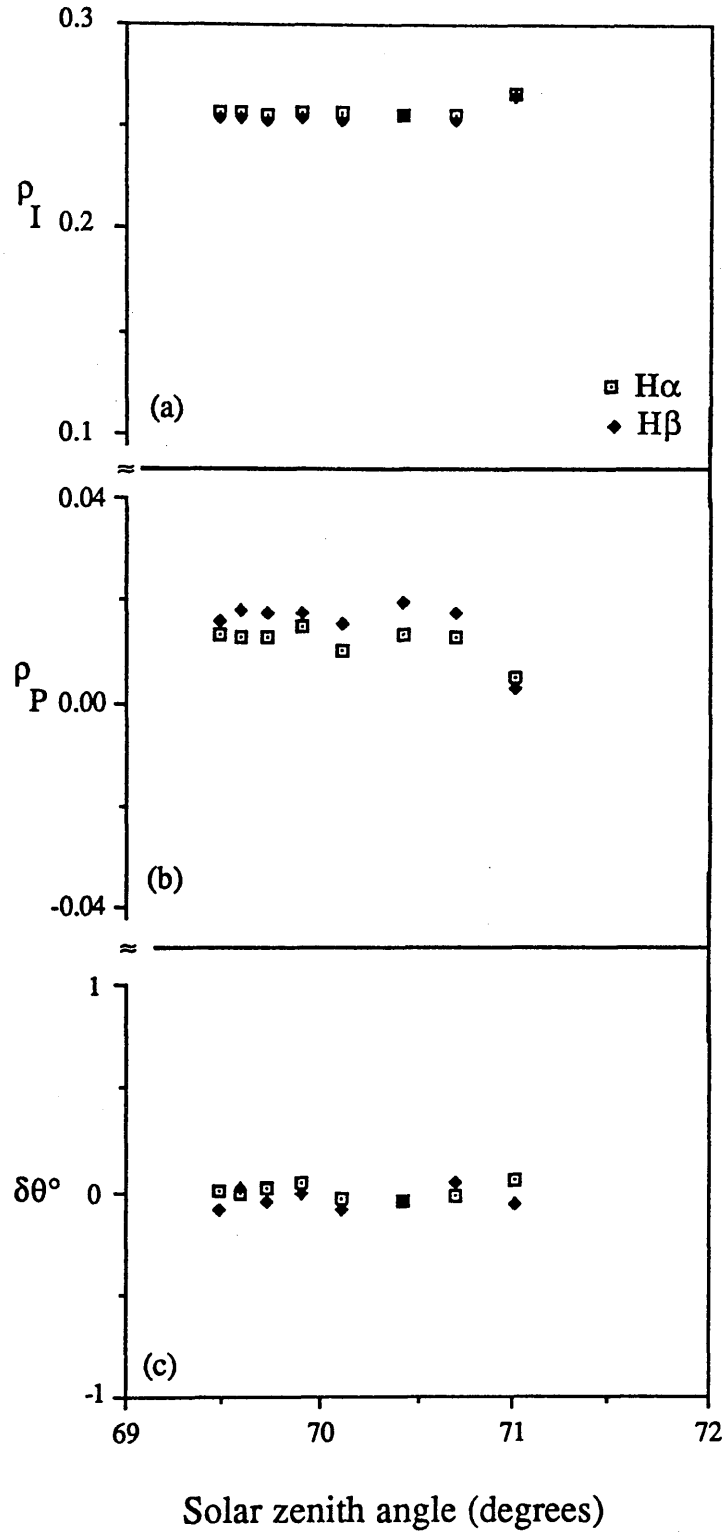

Figure (6.12) Similar to Figure (6.10) but for 1988 October 29.

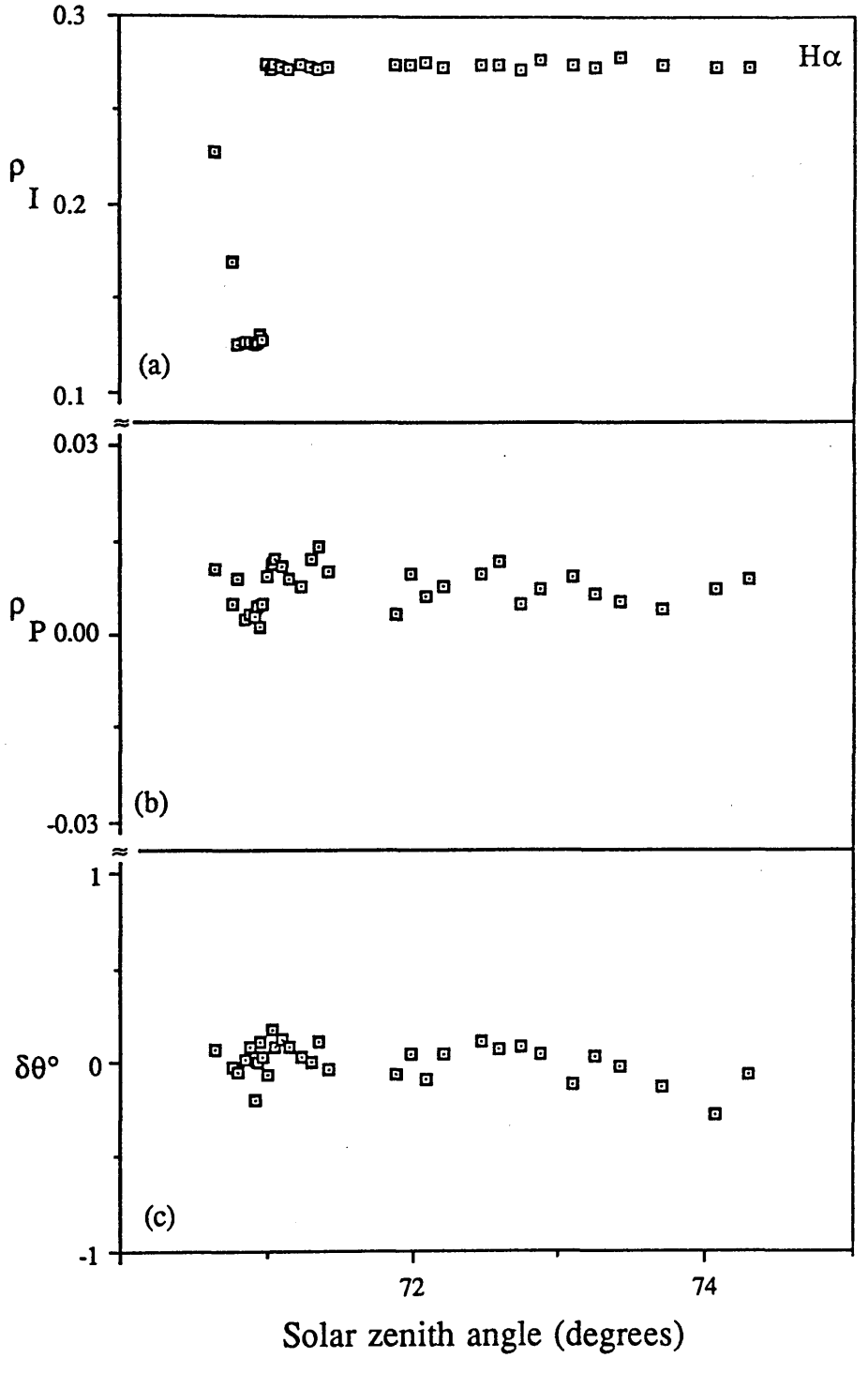

Figure (6. 13) Similar to Figure (6.10) but for 1988 November 2.

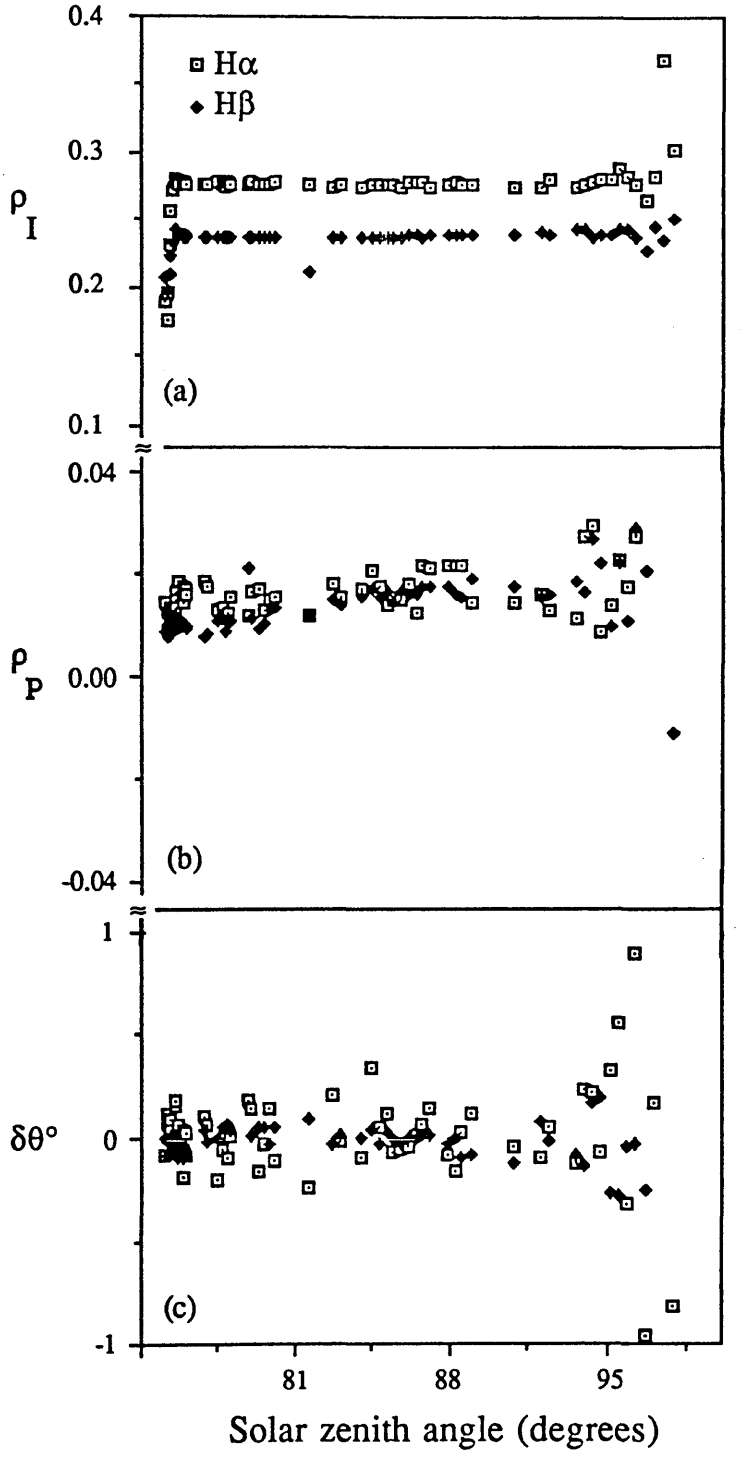

Figure (6.14) Similar to Figure (6.10) but for 1988 November 20.

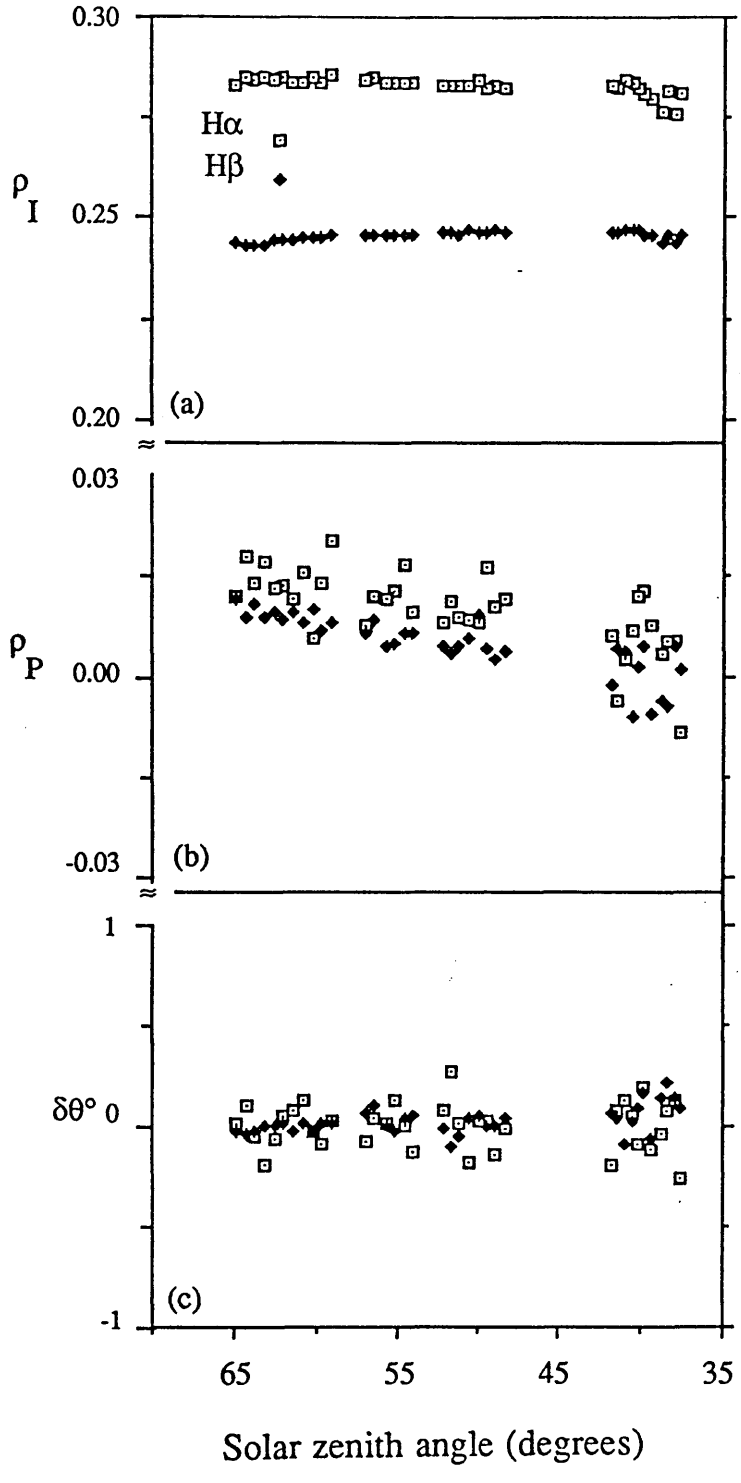

Figure (6.15) Similar to Figure (6.10) but for 1989 July 16.

6.3.3 Detections of a daylight flash.

In addition to the Ring effect, it is well known that airglow can affect specific lines, the sodium airglow being a good example, (see Chapter 1). Effects of airglow are difficult to observe during the day, but are more readily detected at twilight and in the night sky. deVaucouleurs (1967) has observed (using a similar observational technique as here, i.e. by tilting an interference filter) an enhancement in the K line core of about 3% relative to the H line, this being explained in terms of an airglow emission.

Events similar to a bright glow have been detected during the course of our daytime sky observations, producing short-lived dips in ρ_I. Such deviations have been observed clearly on 1988 September 15, November 2 and 20 (see Figure 6.16). For the observations on 1988 November 20 the ground was covered by snow, while on the other two days the surrounding land was green. The dips were observed in the Hα and Hβ lines at the same time, which strongly supports the idea that the deviations were not technical faults, but real atmospheric events. The effects were much stronger in Hα than in Hβ. Two of these events were detected right at the beginning of the observational run making it difficult to estimate their starting time. Values of ρ_I can be estimated by calculation from the scans of the profiles made before commencing the three wavelength point monitoring program. These values give good matches with the values at the end of the daylight flash effect, (see Figures 6.16b&c). Unfortunately the observations of November 2 were made at the Hα line only, because the Hβ channel had a technical fault. The observed daylight flash on November 20 was about five times stronger than that of September 15 for both lines, a result which may be related to the high albedo (snow) around the observatory on the former date. The changes in Hα is about twice as strong as for Hβ. On November 20, the values of ρ_I changed from $\approx$0.28 to $\approx$0.18 and from $\approx$0.24 to $\approx$0.19 for the Hα and Hβ lines respectively. By examining the time-dependence of the three photometric records corresponding to the continua and line

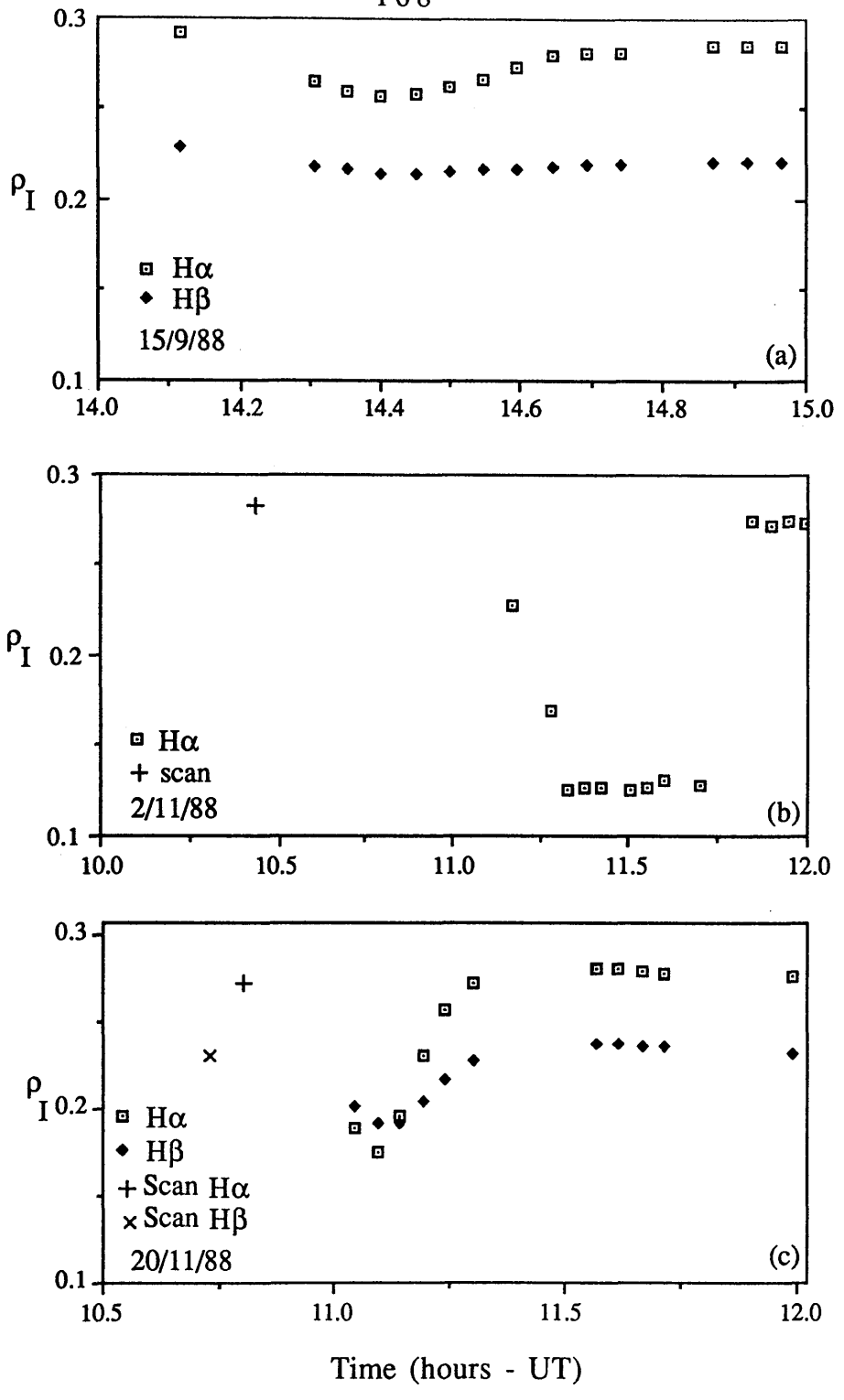

Figure (6.16) Selected sections of the daylight flash, which caused remarkable changes in the values of ρ_I, as function of time, on the different days. Symbols ▫ and ♦ represent values of ρ_I for Hα and Hβ respectively. Symbols + and × represent values of ρ_I for Hα and Hβ respectively, obtained from the line scans prior to the running of the main observational program. The uncertainties associated with each point are small, the associated error bars being smaller than the symbols used to depict the data.

centre, the daylight flash appears to be the result of light being emitted in the core of the line.

From our observations, we have noted that if there is any thin cloud crossing the field of the observed column, it will affect the intensities of the three wavelength positions simultaneously by the same magnitude. However in these records of daylight flash, the deviations of the values of ρ_I are caused by the intensity at the line core increasing while the continua are not affected. Figures (6.17a,b) show the change of the intensities at the three wavelength positions during the observation time for measurements on 1988 November 20, for Hα and Hβ respectively. The maximum intensities were around local noon time and by extrapolating the general behaviour of the curves prior to this time, the "daylight flash" appears as an enhancement to the line core. However there were no apparent changes in polarization in the line centre or in the continua during the event. Without more observations with good skies, the origin of these dayflashes remains obscure.

6.4 Conclusion.

Data on the line filling-in effect have been taken by both photometry and polarimetry at different times of the year with the Sun culminating over a range of zenith angle, and also with a variety of albedo surrounding the observatory site. However, the largest factor controlling the brightness variations and the degree of polarization is the meteorological condition. The experiment described here proves that the filling-in results from there being polarized added light. It affects the degree of polarization across both the Hα and Hβ Fraunhofer lines, depending in detail on the solar zenith angles. The increase of ρ_P with increasing zenith angle immediately negates the possibility of using polarimetry as a direct means of monitoring the diurnal variations of the line filling-in effect in terms of quantitative photometric effects without reference to a direct solar spectrum, but is of interest in its own right.

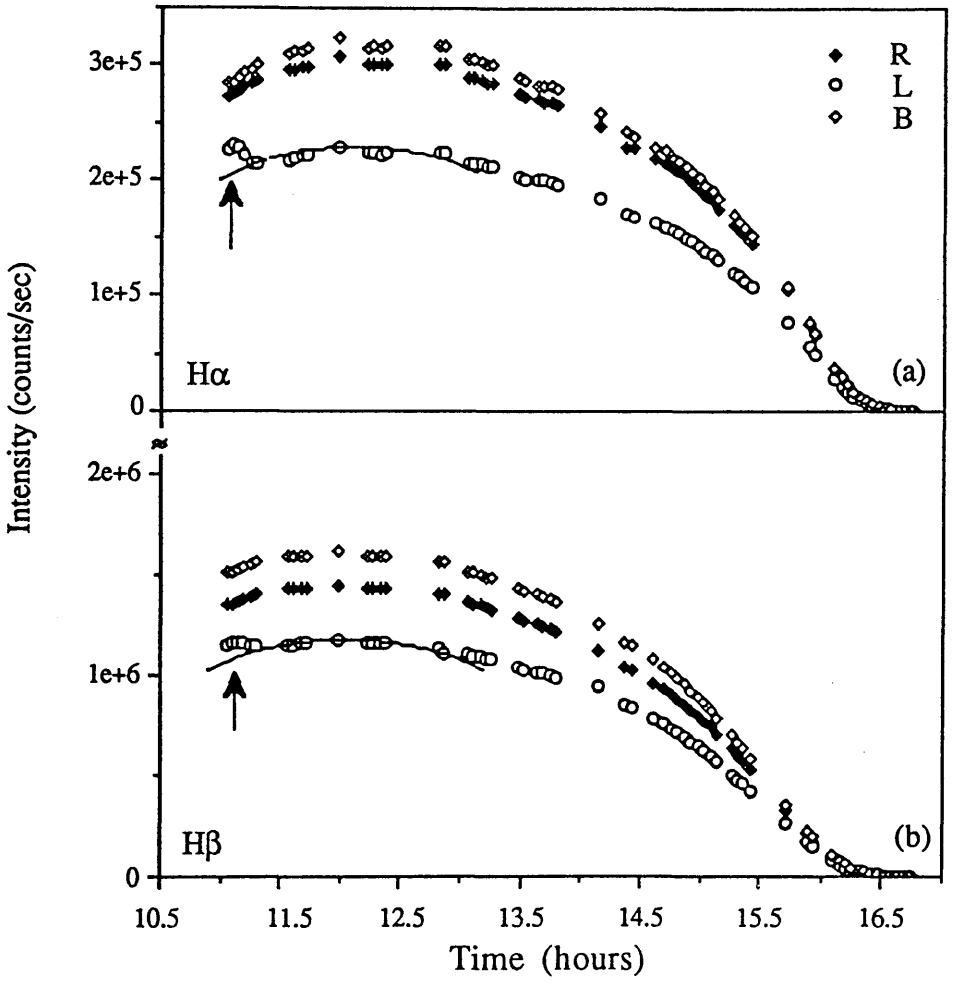

Figure (6.17) Typical variations of the zenith intensity with time on 1988 November 20 for the blue continuum (◊), line centre (o) and the red continuum (♦), for the Hα and Hβ line profiles. A curve has been drawn through the data corresponding to the line centre and indicates the symmetry around local noon. The daylight flash is marked by the arrow; no corresponding enhancement of brightness is seen in the data for the two continua.

For the geometry associated with Figure (6.3a), where the polarization at the line core has been enhanced, the polarization of the added component must be greater than 20-25%, thus ruling out rotational Raman scattering as being its chief source. Rotational Raman scattering exhibits a polarization whose strength depends on the scattering angle, but only achieves a maximum of 8% when the angle is 90°. Vibrational Raman scattering can generate higher polarization than the rotational Raman mechanism but the intensity is too low to account for the strength of the filling-in component, according to Brinkmann (1968). It therefore appears that Raman scattering cannot explain completely the line filling-in effect. The idea that the reflected light from the ground could be the source of this added light has been rejected as well. These results suggest that some alternative or additional mechanism, which at present cannot be identified, is required to explain the filling-in effect. Many more observations are needed to resolve the complicated issues and at a site that is more reliable in terms of the stability of the weather. Further, measurements of CaII H and K Fraunhofer lines could be useful since the filling-in is greater towards shorter wavelength.

Chapter 7 Overall conclusions.

7.1 The Sun.

7.2 The Moon.

7.3 The daytime sky.

The work presented in this thesis covers three main spectropolarimetric experiments involving observations of : (1) the whole solar disk; (2) the Moon; and (3) the daytime sky. A short resume of this work contained within each section is given below with suggestions for future studies.

7.1 The Sun.

Polarimetry was attempted with special instrumentation. The system allowed measurement of the Stokes parameters (linear polarization). By putting the modulator prior to the overall optical system, lenses, fibres, etc., instrumental polarization effects were minimised.

The main solar experiment was aimed to measure any linear intrinsic polarization of the whole disk of the Sun within spectral lines, associated with solar magnetic activity. As well as being of interest in its own right, the study was made with a view to making connections with intrinsic line effects by the same polarizational mechanisms in other middle-to-late type stars. Such effects may be detected through the polarization properties of resonance lines such as CaII K and CaI 4227Å which are photometrically enhanced in local active regions.

For the experiments, the final solar image size was about 1mm in diameter and to carry light to the spectrometer a wide diameter fibre optic would be needed, or a fibre bundle. This latter would present problems in that there are gaps between the fibres and any movement of the image over the structure is likely to induce noise. Because the solar image size and concentration of heat, it is also impractical to focus the solar image directly on the fibre aperture. To overcome the problem, an integrating sphere was used to accept the light from the whole solar disk. This device had many technical advantages and also allows the possibility of several measurement channels being available

simultaneously by inserting more than one fibre into it. Spectrophotometric measurements have revealed the stability of the system. Preliminary polarimetric measurements have demonstrated the usefulness of the integrating sphere and the observed level of polarization gives a hint that there is no general broadband effect present from the whole solar disk.

Another experiment was attempted to detect the Hanle effect on the solar limb, using a solar disk scanner device. Unfortunately this failed because of the prismatic effect of the (non-parallel) rotating half-wave plate. To make progress here, the modulator needs to be changed perhaps by using a time-dependent wave-plate such as a photoelastic device to avoid problems with mechanical movement.

Future work:- In order to pursue spectro-polarimetric studies, a spectral resolution of 1Å or better is desirable. This might be achieved by using a cascade of filters (Fabry-Perot and narrowband interference filters); these have now been purchased. The stability and the efficiency of the integrating sphere appears to be ideal for directing the radiation from the whole solar disk to the monochromator components. Regular spectro-polarimetric measurements of the whole solar disk could lead to determinations of the solar rotation period by detecting the polarization variation with time, as active regions move across the solar disk. Experience in this area is important in deciding how to make comparative measurements of stars of similar spectral type.

The polarization of the whole solar disk is very small while its flux is very high, making photon counting photometry subject to dead-time losses. In order to take advantage of the potential accuracy carried by the photon flux, a solid state device such as a good quality photo-diode, is required. This kind of detector has a high quantum efficiency, and provides a voltage output. In order to digitise this, a voltage-to-frequency (V-F) converter is needed. As the degree of polarization is small, the output of the detector will provide a large DC component with a small AC signal superimposed. The

latter component might be detected better by using a differential subtraction technique whereby the immediate DC level of the detector output is subtracted and recorded and further amplification is given to the AC portion before recording it. The fraction that is subtracted and the amplification factors of the component records would need to be calibrated.

7.2 The Moon.

The existence of a luminescent effect on the Moon's surface has been observed previously by spectrophotometry (see Chapter 1). The first discussion about the effect of luminescence with regard to polarimetric studies was given by Teifel (1960). He performed photographic broadband polarimetry on some regions of the lunar surface and concluded that an unpolarized luminescence intensity had affected his measurements. Our experiment is the first photoelectric spectropolarimetric observation of individual spectral lines with the aim of detecting lunar luminescence. From our measurements a number of interesting points arise:-

(1) If it truly exists, lunar luminescence must essentially be polarized to the same degree as the general scattered light, since there is no detectable decrease in polarization at the line centres.

(2) No consistent pattern of spectral line polarimetric behaviour has emerged from site to site; sometimes it is the measurement at the line centre which appears to be disparate and sometimes it is one of the continua measurements which is possibly different.

(3) There is no noticeable difference between spectral line polarimetric measurements which were made after solar activity and those which were made at quiet Sun.

(4) The position angles of the polarization from the Palus Somnii area at Hα were rotated by the order of 3° with respect to the other lunar areas on the same night of observation. It is worth noting that in this area Kolovos et al. (1988) observed a remarkable flash on 1985 May 23.

(5) If the lunar luminescence were caused by a thermal effect, then its level would not be the same at all points on the lunar surface. As the flux of luminescence is likely to be controlled by temperature, its apparent strength would depend on the solar elevation and hence on the longitude of the observed site. No such variation has been observed.

Future work:- It would be useful to obtain more results over a larger range of lunar phase angles. Higher spectral resolution would be an advantage with sampling at more wavelength positions through the line profile; the three wavelength positions on the profile are insufficient to investigate the fundamental cause of any filling-in effect. If the observed region is surrounded by mountains then secondary scattering will take place and will contribute to the total observed light. The amount of the secondary light will depend on the terrain of the observed area and on the phase angle, so maria are more reliable for investigating the filling-in measurements. Potter et al. (1984) reported that the strength of lunar luminescence is correlated with the equivalent widths of the monitored spectrum lines, increasing as the equivalent width decreases. Polarimetric observations need to be undertaken to cover a range of lines with different equivalent widths to explore further the reasons for this.

7.3 The daytime Sky.

The depolarization of the Fraunhofer spectrum line centres in the light from the sky has been reported by Pavlov et al. (1973). Other observations by Clarke and McLean (1975c) indicated that the polarization at the core of the Hβ line is less than the polarization of the continuum and they concluded that the depolarization is attributable to

the addition of an unpolarized component. However our survey of spectropolarimetric observations, for the zenith daytime sky during different seasons, using the Hα and Hβ Fraunhofer lines has discovered that the filling-in effect exhibits various strengths of polarization dependent on the time of day (scattering angle) and on the meteorological conditions. The observations revealed both polarization enhancements and reductions within the Fraunhofer lines, according to the solar zenith angle. The observed polarization enhancement at the line centre revealed that the added light is substantially polarized (greater than 20 to 25%) particularly at some times of the day. This degree of polarization at these times, at small solar zenith angles, is substantially higher than is predicted by rotational Raman scattering from air molecules. For example, rotational Raman scattering exhibits a polarization whose strength depends on the scattering angle, but only achieving a maximum of 8% (Brinkmann, 1968) when the angle is 90°. So this rules out rotational Raman scattering as being the chief source of the filling-in effect. In fact, all the possible mechanisms that have been proposed at various times in the past are inadequate to explain the degree of the enhanced polarization. More detailed observations of the polarizational behaviour across the whole of the profile rather than just at the line core could be important in any future investigations. The model in Chapter 2, without knowledge of the filling-in mechanism, has yielded a good qualitative agreement with the observational behaviour of ρ_p. This model considers that the added light is polarized and that its polarization and intensity remain constant through the day; it assumes that its vibration is aligned to the same plane associated with the general Rayleigh scattering.

Interesting and important points have also been raised from the photometric analyses. The variation of the intensity ratio ρ_I gives some indication about the behaviour of the strength of the added light intensity during the observation time. These variations do not have a regular behaviour, but depend strongly on the meteorogical conditions. Its constancy from after noon till sunset, while the ground around the observatory was covered by snow, gives a clue that the added light does not arise from

ground reflection, otherwise the values of ρ_I would be minimum at noon and maximum at sunset.

Another new phenomenon requiring further investigation is the anomalous change of the ρ_I values for Hα and Hβ over a period of a few minutes - referred to as a "daylight flash". No polarimetric variations are associated with these events.

Future work:- A high resolution spectrometer needs to be used to explore in more detail the polarization variations at the cores of different spectral lines. It is clear that more observations need to be taken at a more reasonable site, *away* from Glasgow for the following reasons.

1- It would be useful to have long observational runs through the day without the disturbances of the changes of atmospheric conditions.

2- Observations at a low latitude site are required to observe the negative values of ρ_p (where the enhancement of the polarization at the spectrum line cores are maximum) at solar zenith angles smaller than those available in Glasgow. This will help in improving the understanding of the situation.

Appendices

(A) Mueller calculus.

(B) Data formatting.

(C) Dead time determination of the photon counters.

(D) Observing programs.

(E) Polynomial fitting of the spectral profile.

(F) Skewness and Kurtosis tests.

(G) Welch test.

Appendix (A) Mueller calculus.

In 1943, by grouping the Stokes parameters into a column vector, Hans Mueller devised a matrix method for describing the effects of optical devices. The column vector describes the polarizational properties of a beam of light referred to a stationary x, y, and z right-handed cartesian co-ordinate system. If the light passes through an optical element, its Stokes parameters will be affected. The resultant beam's vector can be evaluated by Mueller calculus. In the first place a matrix [R] should be used to change the Stokes parameters from the x, y, and z co-ordinates to new co-ordinates corresponding to the descriptive axes of the optical element, (see Figure A.1)

$$\begin{bmatrix} I_e \\ Q_e \\ U_e \\ V_e \end{bmatrix} = [R] \cdot \begin{bmatrix} I_i \\ Q_i \\ Ui \\ V_i \end{bmatrix} \qquad (A.1)$$

where $$[R] = \begin{bmatrix} 1 & 0 & 0 & 0 \\ 0 & \cos 2\theta & \sin 2\theta & 0 \\ 0 & -\sin 2\theta & \cos 2\theta & 0 \\ 0 & 0 & 0 & 1 \end{bmatrix}$$ is the

rotation matrix and, θ is the angle between the principal axis of the optical device and the x-axis, and is measured from x through y.

Each optical element has its own Mueller matrix. The Mueller matrix which represents a polarizer is:

$$[P] = \frac{1}{2}\begin{bmatrix} 1 & 1 & 0 & 0 \\ 1 & 1 & 0 & 0 \\ 0 & 0 & 0 & 0 \\ 0 & 0 & 0 & 0 \end{bmatrix} \qquad (A.2)$$

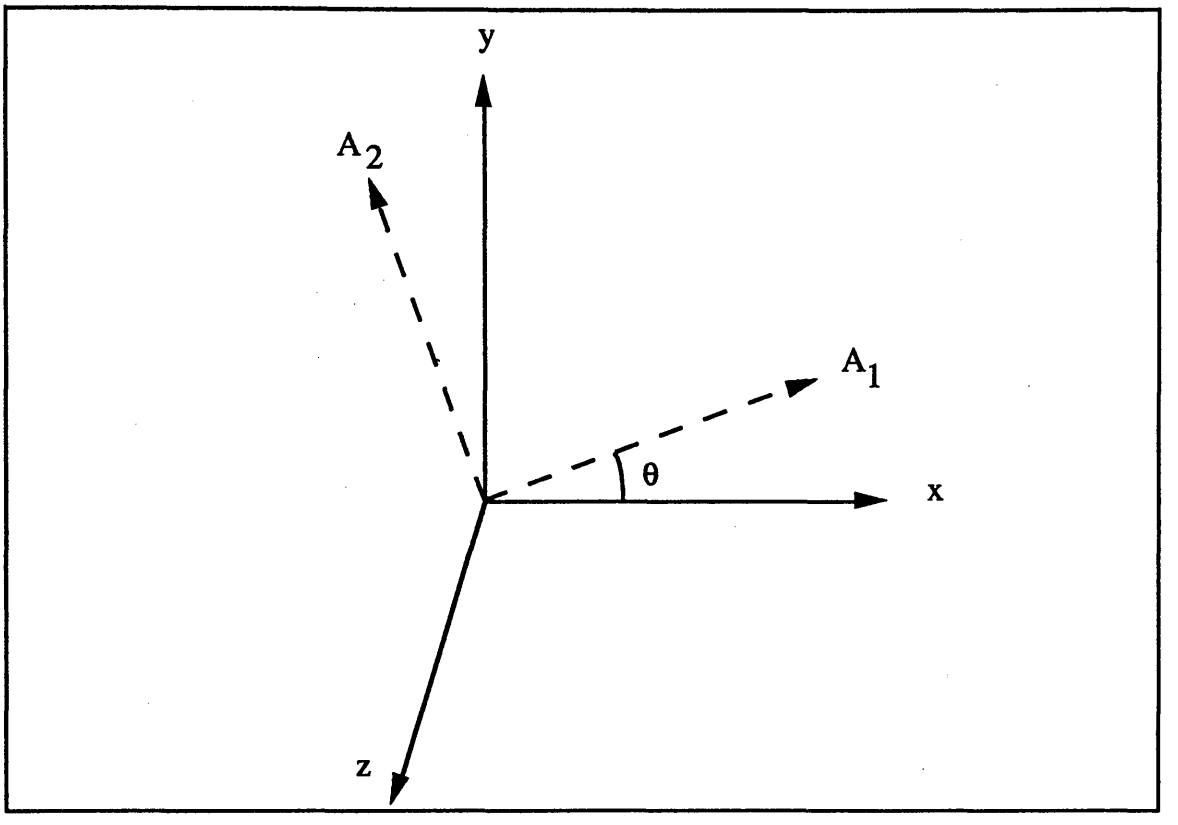

Figure (A.1) For a general representation of the behaviour of light travelling along the z-axis, its polarization properties may be described by considering the electric field disturbances in the x, y plane. If an optical device is inserted in that plane, its effect is calculated by first rewriting the electric field disturbances in the co-ordinate frame A_1, A_2 and z, which is rotated by θ from the original frame, where A_1 and A_2 represent the principal axes of the optical device, e.g. A_1 is the principal transmittance axis of a polarizer or the fast axis of a retarder.

The Mueller matrix describing a partial polarizer is

$$[P(k_1, k_2)] = \frac{1}{2}\begin{bmatrix} k_1 + k_2 & k_1 - k_2 & 0 & 0 \\ k_1 - k_2 & k_1 + k_2 & 0 & 0 \\ 0 & 0 & 2(k_1 k_2)^{\frac{1}{2}} & 0 \\ 0 & 0 & 0 & 2(k_1 k_2)^{\frac{1}{2}} \end{bmatrix} \qquad (A.3)$$

where k_1 and k_2 are the intensity transmission coefficients of the polarizer for light perfectly linearly polarized in the orthogonal directions 1 and 2 respectively.

A retarder or waveplate of differential retardation Δ is represented by

$$[\Lambda] = \begin{bmatrix} 1 & 0 & 0 & 0 \\ 0 & 1 & 0 & 0 \\ 0 & 0 & \cos\Delta & \sin\Delta \\ 0 & 0 & -\sin\Delta & \cos\Delta \end{bmatrix} \qquad (A.4)$$

The two familiar retardations are with $\Delta = \pi$ or $\pi/2$ corresponding to a half and a quarter-wave plate respectively.

The GUPP polarimeter has a modulator comprising a rotating retarder before a fixed polarizer. Hence, its overall description may be expressed as:

$$\begin{bmatrix} I_e \\ Q_e \\ U_e \\ V_e \end{bmatrix} = [P] \,.\, [-R] \,.\, [\Lambda] \,.\, [R] \,.\, \begin{bmatrix} I_i \\ Q_i \\ U_i \\ V_i \end{bmatrix} \qquad (A.5)$$

where [−R] represents a matrix which returns the vibration direction to its original frame after emerging from the retarder. From (A.5) the intensity transmitted through the half wave plate with optical axis at position angle θ followed by an analyser with principal plane at position angle zero (upper signs) or 90° (lower signs) corresponding to the two resolved beams from a polarizing prism is given by :

$$s(\theta) = \frac{1}{2}(I \pm Q\cos 4\theta \pm U\sin 4\theta) \qquad (A.6)$$

The Stokes parameters I, Q, and U could be obtained by integrating (A.6) using the appropriate limits. Such integrations are controlled in GUPP by the electronics with the opening and closing of photon counters (scalers) at the desired times according to the angular positions of the half-wave plate (see Section 3.3)

As the first scaler is open for the full cycle or N cycles, its measured signal is C_1, given by

$$C_1 = 4N \int_0^{2\pi} s(\theta)\, d\theta = N\pi I \qquad (A.7)$$

The second and third scalers are integrated for the same N cycles to provide records C_2 and C_3 over portions of the modulation as follows:

$$C_2 = 4N \int_{j\pi/4}^{(j+1)\pi/4} s(\theta)\, d\theta = N(\frac{\pi}{2} I + U) \qquad (A.8)$$

$$C_3 = 4N \int_{i\pi/8}^{(i+2)\pi/8} s(\theta)\, d\theta = N(\frac{\pi}{2} I - Q) \qquad (A.9)$$

where j=0,2,4,6 and i =1,5,9,13.

From the values of C_1, C_2 and C_3, the normalised Stokes parameters q and u are given by :

$$q = \frac{Q}{I} = \pi \left(\frac{1}{2} - \frac{C_3}{C_1} \right) \quad \text{and}$$

$$u = \frac{U}{I} = \pi \left(\frac{C_2}{C_1} - \frac{1}{2} \right)$$

from which the polarization degree P and the azimuth θ can be calculated (see Chapter 1).

Appendix (B) Data formatting.

Examples for the polarimetric and photometric data output, as transmitted from the hard-wired electronic equipment instruments to the microcomputer, are displayed on the next page. The data are in eight columns with codes (first digit) to identify the measurements. An explanation is as follows:

Column No. 1 - code for computer interpretation of the line [provided by the microcomputer at the time of measurement]

2/3/4 - Normally contain records of photo-electron counts for first beam, the first digit identifies the scaler number.

5/6/7 - As above but for the second beam.

8 - Normally contains UT.

Interpretation of codes

0 - Data line holds basic information for identifying the data, the object, choice of filters, etc.

1 - Dark current measurements.

2/3/4 - Identifies the three wavelength positions selected for polarimetry.

9 - End of file.

Polarimetric and photometric output from the two channels.

1	2	3	4	5	6	7	8
0	32	marsA1	1988	Dec 06	00000000	00000000	00000000
0	00000021	00360051	00660000	00000012	00530068	00830000	00000000
1	10000462	20000237	30000228	40000019	50000008	60000009	23:16:42
1	10000477	20000228	30000246	40000008	50000006	60000001	23:16:52
1	10000545	20000285	30000271	40000016	50000010	60000006	23:17:02
1	10000613	20000303	30000295	40000009	50000006	60000008	23:17:12
1	10000537	20000265	30000271	40000011	50000004	60000007	23:17:23
1	10000520	20000224	30000273	40000012	50000007	60000004	23:17:33
1	10000552	20000254	30000272	40000004	50000001	60000001	23:17:43
1	10000557	20000280	30000289	40000009	50000006	60000004	23:17:53
1	10000503	20000255	30000243	40000010	50000006	60000008	23:18:03
1	10000626	20000332	30000317	40000014	50000009	60000008	23:18:14
2	10046219	20023404	30022803	40022239	50010890	60011325	23:20:29
3	10034573	20017478	30017208	40021752	50010720	60011180	23:20:40
4	10048671	20024660	30024088	40021539	50010551	60011111	23:20:52
2	10046884	20023733	30023086	40022709	50011184	60011471	23:21:04
3	10034891	20017557	30017174	40021831	50010700	60011061	23:21:15
4	10048366	20024734	30024054	40021865	50010580	60011146	23:21:27
2	10046898	20023752	30023154	40022642	50011052	60011429	23:21:39
3	10034945	20017511	30017312	40022187	50010929	60011331	23:21:50
4	10047330	20023828	30023306	40021483	50010546	60010831	23:22:03
2	10045825	20023010	30022886	40022007	50010974	60011239	23:22:14
3	10033056	20016710	30016415	40021264	50010396	60010803	23:22:25
4	10045296	20022912	30022330	40020323	50009970	60010262	23:22:38
2	10043487	20022082	30021606	40021134	50010512	60010723	23:22:49
3	10031939	20016292	30015858	40020950	50010304	60010789	23:23:00
4	10045017	20022806	30022236	40020043	50009997	60010280	23:23:13
2	10026806	20013446	30013209	40011992	50005996	60006088	23:23:45
3	10030703	20015404	30015457	40019662	50009756	60010000	23:23:56
4	10042841	20021733	30021115	40018409	50009159	60009361	23:24:09
2	10040822	20020637	30020283	40019019	50009401	60009709	23:24:20
3	10028993	20014876	30014398	40017380	50008591	60008768	23:24:31
4	10041692	20020993	30020684	40016881	50008374	60008609	23:24:44
2	10040953	20020742	30020310	40017597	50008513	60008987	23:24:55
3	10030073	20015261	30014919	40018582	50009214	60009433	23:25:06
4	10042289	20021434	30020889	40017840	50008776	60009124	23:25:19
2	10040840	20020827	30020054	40018486	50009202	60009537	23:25:30
3	10030188	20015156	30014944	40018652	50009229	60009442	23:25:42
4	10043573	20021937	30021430	40018605	50009228	60009491	23:25:54
2	10042492	20021522	30021032	40019397	50009608	60009838	23:26:05
3	10030085	20015273	30014748	40018533	50009192	60009468	23:26:17
4	10044277	20022442	30021836	40018761	50009270	60009502	23:26:29
9	10000000	20000000	30000000	40000000	50000000	60000000	23:52:02

Appendix (C) Dead time determination of the photon counters.

The signals in the photometric/polarimetric experiments were recorded by photo-electron pulse counting techniques. For the most accurate measurements it is important to correct the accumulated counts for the "dead time". Each pulse has a finite time width and at high count rates there will be occasional overlap of pulses such that adjacent pulses will be counted as one rather than two. For bright sources the relationship between intensity and recorded count rate is nonlinear and is represented by the following equation:

$$\frac{n}{N} = e^{-\tau N} \qquad (C.1)$$

or by taking the natural logarithm of each side, by the equation:

$$\ln\left(\frac{N}{n}\right) = \tau N \qquad (C.2)$$

where N is the true number of photo-electrons (per second), n is the observed number of pulses (per second), and τ is the dead time (seconds).

The dead time can be determined by recording bright and faint sources and considering that for the low count rate, the dead time correction is negligible. If light of a bright source is measured directly and then through an attenuator of known factor $1/\eta$, the ratio of the true intensities will be

$$\frac{N_H}{N_L} = \eta$$

(H and L represent measurements for the high and low count rates)

$$N_H = \eta N_L \approx \eta n_L \qquad (C.3)$$

Equation (C.2) can be rewritten as:

$$A = \ln\left(\frac{\eta n_L}{n_H}\right) = \tau \eta n_L \qquad (C.4)$$

By taking sets of measurements for various values of N_H and its associated values of ηN_L, the dead time can be obtained by plotting A against ηn_L; the slope of the best fitted line represents the dead time coefficient. With the value of τ it is still not easy to use Equation (C.1) directly to determine the underlying values of N from the measurements; an iterative technique is required to solve this equation. The routine is started by substituting the observed count rate n for the true rate N allowing a corrected count rate n_L to be obtained. This is in turn substituted for N and the process repeated until the value of n does not change.

Large differences corresponding to the high and low count rates were obtained using two stops within an illuminated field. Diaphragms of 0.007" and 0.032" diameter were used, the attenuating factor depending on the ratio of their areas. The telescope's aperture was covered by a uniformly white transparent card, the light source being a tungsten lamp. The various intensity levels were achieved by moving the lamp by different angles to the polar axis of the telescope. The following Figures (C.1) demonstrate how the dead time for the two channels, which have been used for the observations of the Moon and the blue sky, were calculated.

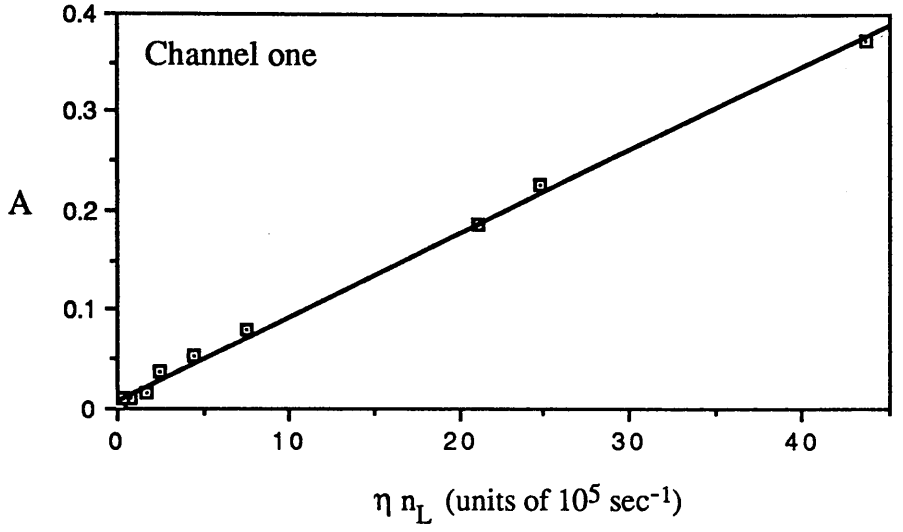

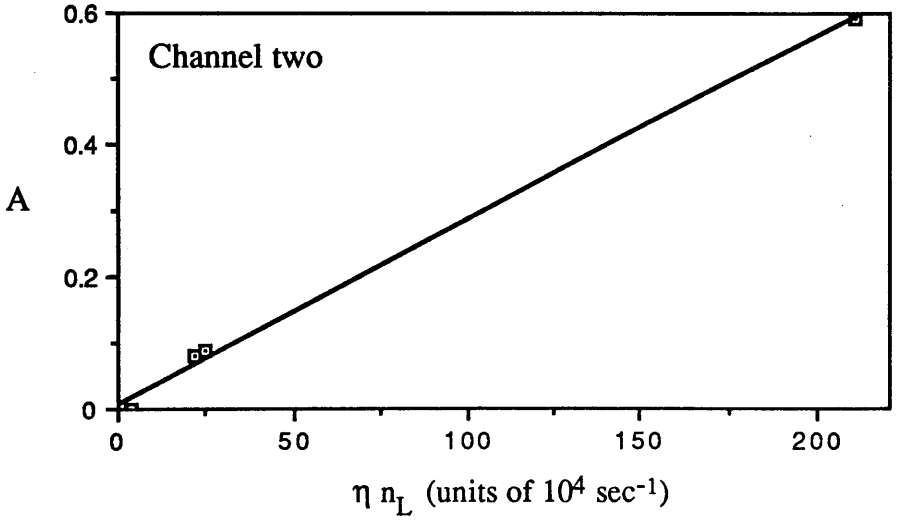

Figure (C.1) The dead time of the two photomultipliers is the gradient of the graphs ($\tau = \partial A/\partial \eta n_L$). Note the higher signals of channel one (blue) with respect to channel two (red) as reflected in the values of ηn_L; this difference is mainly caused by the choice of filters in the light beams.

Appendix (D) Observing programs.

D.1- Scanning program. This is used to tilt the filters in the light beam to record the profiles of the spectrum lines, so allowing choice of desirable wavelength positions for other studies.

D.2- Polarimetric program. This is used for the photopolarimetric measurements at the chosen wavelength points according to the scanning program.

D.1- The Scanning program.

```
100 REMark  * Programme Name: Qscan1 *
110 REMark  * Allows Line Profile to be Recorded From Beam 1 *
120 REMark  * Output on Screen as Graph *
130 REMark  * Data Points Printed Out *
140 REMark ** Subroutines Required: Control, Channel, Clean **
150 REMark ** Timeset, Waveset, Type, Wavetype1 **
160 REMark ** Subroutine Name: Control **
170 REMark ** Defines Characters for Decoding **
180 REMark ** By the Interface Board **
190 DEFine PROCedure z
200 PRINT £5,CHR$(0);
210 END DEFine
220 DEFine PROCedure r1
230 PRINT £5,CHR$(1);CHR$(0);
240 END DEFine
250 DEFine PROCedure sr1
260 PRINT £5,CHR$(2);CHR$(0);
270 END DEFine
280 DEFine PROCedure rd
290 PRINT £5,CHR$(3);CHR$(0);
300 END DEFine
310 DEFine PROCedure ad
320 PRINT £5,CHR$(4);CHR$(0);
330 END DEFine
340 DEFine PROCedure rs
350 PRINT £5,CHR$(5);CHR$(0);
360 END DEFine
370 DEFine PROCedure as
380 PRINT £5,CHR$(6);CHR$(0);
390 END DEFine
400 DEFine PROCedure l
410 PRINT £5,CHR$(7);CHR$(0);
420 END DEFine
430 DEFine PROCedure ul
440 PRINT £5,CHR$(8);CHR$(0);
450 END DEFine
460 DEFine PROCedure s
470 PRINT £5,CHR$(9);CHR$(0);
480 END DEFine
490 DEFine PROCedure wipe
500 PRINT £5,CHR$(16);CHR$(0);
510 END DEFine
520 DEFine PROCedure b
530 PRINT £5,CHR$(32);CHR$(0);
540 END DEFine
550 DEFine PROCedure i
560 PRINT £5,CHR$(48);CHR$(0);
570 END DEFine
580 DEFine PROCedure au
590 PRINT £5,CHR$(64);CHR$(0);
600 END DEFine
610 DEFine PROCedure aw
620 PRINT £5,CHR$(80);CHR$(0);
630 END DEFine
640 DEFine PROCedure w
650 PRINT £5,CHR$(96);CHR$(0);
660 END DEFine
670 DEFine PROCedure f
680 PRINT £5,CHR$(112);CHR$(0);
690 END DEFine
700 DEFine PROCedure r
710 PRINT £5,CHR$(128);CHR$(0);
720 END DEFine
730 DEFine PROCedure master
740 PRINT £5.CHR$(144);
```

```
750 END DEFine
760 REMark ** Subroutine Name: Channel **
770 REMark ** Opens Ser2 as £5 - Sets Baud Rate **
780 DEFine PROCedure channel
790  OPEN £5,ser2
800  BAUD 9600
810  i
820 END DEFine
830 REMark ** Subroutine Name: Clean **
840 REMark ** Clears Buffer of £5 **
850 DEFine PROCedure clean
860  REPeat cl
870  IF INKEY$(£5,0)="" THEN EXIT cl
880  END REPeat cl
890 END DEFine
900 REMark ** Subroutine Name: Timeset **
910 REMark ** Allows Time to be Set **
920 DEFine PROCedure timeset
930  REPeat ts
940   CLS:MODE 4
950   PRINT DATE$: INPUT "O.K.?:  (Y)es ";T$
960    IF T$="Y" OR T$="y" THEN :EXIT ts:ELSE
970     INPUT "Set Universal Time: Year: ",Ye
980     INPUT "Month: ",Mo
990     INPUT "Day: ",da
1000     INPUT "Hour: ",Ho
1010     INPUT "Mins: ",Mi
1020     INPUT "Secs: ",se
1030     SDATE Ye,Mo,da,Ho,Mi,se
1040    END IF
1050  END REPeat ts
1060 END DEFine
1070 REMark ** Subroutine Name: Waveset **
1080 REMark ** Allows Wavelength Stepper Motors to be Set **
1090 DEFine PROCedure waveset
1100  REPeat ws
1110  CLS:aw:INPUT "Adjustment F or R or N? ";adj$
1120   IF adj$="n" OR adj$="N" THEN :EXIT ws
1130   END IF
1140    IF adj$="f" OR adj$="F" THEN :f:ELSE :r
1150    END IF
1160  INPUT "No: of Steps? ",wj
1170   FOR wk=1 TO wj
1180    w:PAUSE 2
1190   END FOR wk
1200  END REPeat ws
1210  r:w:PAUSE 2:f:w:i
1220 END DEFine
1230 REMark ** Subroutine Name: Type **
1240 REMark ** Collects 8 Digits from a Scaler **
1250 DEFine PROCedure type
1260  sri:rd
1270  FOR d=1 TO 8
1280  s:dq$=INKEY$(£5,-1)
1290  a$=a$&dq$
1300  ad
1310  END FOR d
1320 END DEFine
1330 REMark ** Subroutine Name: Wavetype1 **
1340 REMark ** Collects Data from a Scaler **
1350 REMark ** Number of Lines to be Defined Beforehand **
1360 REMark ** Adds Line Numbers **
1370 REMark ** Returns Wavelength Position to Beginning **
1380 DEFine PROCedure wavetype1
1390  DIM lx$(11,11)
1400  FOR n=0 TO 11-1
```

```
1410  a$="":b$=n
1420  ls=LEN(b$)
1430  IF ls<2 THEN :b$="0"&b$:END IF
1440  b$=b$&" "
1450  dql$=INKEY$(£5,-1)
1460  type
1470  ul:ri
1480  lx$(n)=b$&a$
1490  PRINT lx$(n)
1500  END FOR n
1510  i:r:aw
1520  FOR n=0 TO ll
1530  w:PAUSE 2
1540  END FOR n
1550  f:w
1560 END DEFine
1570 REMark ** Subroutine Name: Qfotl **
1580 REMark ** Provides Normalised Scan on Screen **
1590 REMark ** And Print Out of Data for Beam 1 **
1600 channel
1610 CLS:INPUT "Do you wish to give Off-set", q$
1620 IF q$="y" THEN waveset:END IF
1630 CLS:INPUT "Filter Off-Set: ",of%:CLS
1640 INPUT "How Many Wavelength Steps?",ll
1650 INPUT "Check on Phot/Wavelength Switches:",dumb$
1660 i:clean:f:wipe:ul:ri:au:rs:as
1670 dql$=INKEY$(£5,-1):aw:ul:PRINT "Scanning Started":wavetypel
1680 REMark *Normalisation*
1690 DIM ii(ll)
1700 FOR n = 0 TO ll-1
1710 ii(n)=lx$(n)(5 TO 11)
1720 END FOR n
1730 mib=(ii(0)+ii(1)+ii(2))/3
1740 mie=(ii(ll-3)+ii(ll-2)+ii(ll-1))/3
1750 gra=(mie-mib)/(ll-2-1)
1760 cep=mib-gra
1770 FOR n = 0 TO ll-1
1780 ii(n)=ii(n)*50/(gra*n+cep)
1790 END FOR n
1800 REMark *Graph*
1810 CLS
1820 LINE 10,10 TO 10,60
1830 LINE 10,10 TO ll-1+10,10
1840 FOR n= 0 TO ll-1
1850 POINT n+10,10+ii(n)
1860 END FOR n
1870 OPEN £6,serl
1880 PRINT £6, DATE$, "Beam 1"
1890 PRINT £6, "Filter:              Position Off-Set: ",of%:PRINT £6
1900 FOR n=0 TO ll-1
1910 PRINT £6,lx$(n)(1 TO 3),lx$(n)(5 TO 11)
1920 END FOR n
1930 PRINT £6:PRINT £6
1940 CLOSE £6
```

D.2- The polarimetric program.

```
100 REMark ** Programme Name: Linepol2 **
110 REMark ** Performs Polarimetry for Both Beams at 3 Wavelengths **
120 REMark ** Subroutines Required: Control, Channel, Clean **
130 REMark ** Timeset, Storeset, Waveset, Type, Poltype2, Pol2, W3P2 **
140 REMark ** Subroutine Name: Control **
150 REMark ** Defines Characters for Decoding **
160 REMark ** By the Interface Board **
170 DEFine PROCedure z
180 PRINT £5,CHR$(0);
190 END DEFine
200 DEFine PROCedure ri
210 PRINT £5,CHR$(1);CHR$(0);
220 END DEFine
230 DEFine PROCedure sri
240 PRINT £5,CHR$(2);CHR$(0);
250 END DEFine
260 DEFine PROCedure rd
270 PRINT £5,CHR$(3);CHR$(0);
280 END DEFine
290 DEFine PROCedure ad
300 PRINT £5,CHR$(4);CHR$(0);
310 END DEFine
320 DEFine PROCedure rs
330 PRINT £5,CHR$(5);CHR$(0);
340 END DEFine
350 DEFine PROCedure as
360 PRINT £5,CHR$(6);CHR$(0);
370 END DEFine
380 DEFine PROCedure l
390 PRINT £5,CHR$(7);CHR$(0);
400 END DEFine
410 DEFine PROCedure ul
420 PRINT £5,CHR$(8);CHR$(0);
430 END DEFine
440 DEFine PROCedure s
450 PRINT £5,CHR$(9);CHR$(0);
460 END DEFine
470 DEFine PROCedure wipe
480 PRINT £5,CHR$(16);CHR$(0);
490 END DEFine
500 DEFine PROCedure b
510 PRINT £5,CHR$(32);CHR$(0);
520 END DEFine
530 DEFine PROCedure i
540 PRINT £5,CHR$(48);CHR$(0);
550 END DEFine
560 DEFine PROCedure au
570 PRINT £5,CHR$(64);CHR$(0);
580 END DEFine
590 DEFine PROCedure aw
600 PRINT £5,CHR$(80);CHR$(0);
610 END DEFine
620 DEFine PROCedure w
630 PRINT £5,CHR$(96);CHR$(0);
640 END DEFine
650 DEFine PROCedure f
660 PRINT £5,CHR$(112);CHR$(0);
670 END DEFine
680 DEFine PROCedure r
690 PRINT £5,CHR$(128);CHR$(0);
700 END DEFine
710 DEFine PROCedure master
720 PRINT £5,CHR$(144);
730 END DEFine
740 REMark ** Subroutine Name: Channel **
750 REMark ** Opens Ser2 as £5 - Sets Baud Rate **
760 DEFine PROCedure channel
770  OPEN £5,ser2
780  BAUD 9600
790  i
800 END DEFine
```

```
810 REMark ** Subroutine Name: Clean **
820 REMark ** Clears Buffer of £5 **
830 DEFine PROCedure clean
840  REPeat cl
850  IF INKEY$(£5,0)="" THEN EXIT cl
860  END REPeat cl
870 END DEFine
880 REMark ** Subroutine Name: Timeset **
890 REMark ** Allows Time to be Set **
900 DEFine PROCedure timeset
910  REPeat ts
920   CLS:MODE 4
930   PRINT DATE$: INPUT "O.K.?:  (Y)es ";T$
940    IF T$="Y" OR T$="y" THEN :EXIT ts:ELSE
950     INPUT "Set Universal Time: Year: ",Ye
960     INPUT "Month: ",Mo
970     INPUT "Day: ",da
980     INPUT "Hour: ",Ho
990     INPUT "Mins: ",Mi
1000     INPUT "Secs: ",se
1010     SDATE Ye,Mo,da,Ho,Mi,se
1020    END IF
1030  END REPeat ts
1040 END DEFine
1050 REMark ** Subroutine Name: Waveset **
1060 REMark ** Allows Wavelength Stepper Motors to be Set **
1070 DEFine PROCedure waveset
1080  REPeat ws
1090  CLS:aw:INPUT "Adjustment F or R or N? ";adj$
1100   IF adj$="n" OR adj$="N" THEN :EXIT ws
1110   END IF
1120    IF adj$="f" OR adj$="F" THEN :f:ELSE :r
1130    END IF
1140  INPUT "No: of Steps? ",wj
1150   FOR wk=1 TO wj
1160    w:PAUSE 2
1170   END FOR wk
1180  END REPeat ws
1190  r:w:PAUSE 2:f:w:i
1200 END DEFine
1210 REMark ** Subroutine Name: Storeset **
1220 REMark ** Creates Data Store on Mdv2_ using £7 **
1230 DEFine PROCedure storeset
1240  CLS:MODE 4
1250  INPUT "Name of Cartridge: ";cart$
1260  INPUT "Load Cartridge in Mdv2_ !";dumb$
1270  INPUT "Name of Storage File: ";name$
1280  MODE 8:FLASH 1:PRINT "Loading"
1290  OPEN_NEW £7,"mdv2_"&name$&"_dat"
1300  PAUSE 700:FLASH 0:MODE 4
1310 END DEFine
1320 REMark ** Subroutine Name: Type **
1330 REMark ** Collects 8 Digits from a Scaler **
1340 DEFine PROCedure type
1350  sri:rd
1360  FOR d=1 TO 8
1370  s:dq$=INKEY$(£5,-1)
1380  a$=a$&dq$
1390  ad
1400  END FOR d
1410 END DEFine
1420 REMark ** Subroutine Name: Poltype2 **
1430 REMark ** Reads in Polarimetric Data for Both Beams **
1440 DEFine PROCedure poltype2
1450  rs
1460  FOR scal=1 TO 6
1470  a$=a$&" ":as:type
1480  END FOR scal
1490  ri:ul
1500 END DEFine
```

```
1510 REMark ** Subroutine Name: Pol2 **
1520 REMark ** Performs Polarimetry and Collects Data for k Lines **
1530 DEFine PROCedure pol2
1540  wipe:ul:ri:clean
1550  FOR m=1 TO k
1560   b:e$=INKEY$(£5,-1)
1570   l:wipe
1580   IF m<k THEN b:END IF
1590   sri:a$=code$:poltype2
1600   dt$=DATE$
1610   b$(m)=a$&dt$(12 TO 20)
1620   PRINT b$(m)
1630  END FOR m
1640 END DEFine
1650 REMark ** Subroutine Name: W3P2 **
1660 REMark ** Performs Polarimetry at 3 Wavelengths for k lines **
1670 REMark ** For Both Beams **
1680 DEFine PROCedure w3p2
1690  wipe:ul:ri:f:aw:clean:b
1700   FOR m=1 TO k
1710    e$=INKEY$(£5,-1)
1720    l:wipe
1730    FOR n=1 TO scan1
1740     w:PAUSE 2
1750    END FOR n
1760    PAUSE 10:b:sri
1770    a$="2":poltype2
1780    dt$=DATE$
1790    b$(m)=a$&dt$(12 TO 20)
1800    PRINT b$(m)
1810    e$=INKEY$(£5,-1)
1820    l:wipe
1830    FOR n=1 TO scan2
1840     w:PAUSE 2
1850    END FOR n
1860    PAUSE 10:b:sri
1870    a$="3":poltype2
1880    dt$=DATE$
1890    b2$(m)=a$&dt$(12 TO 20)
1900    PRINT b2$(m)
1910    e$=INKEY$(£5,-1)
1920    l:wipe:r
1930    FOR n=1 TO (scan1+scan2+1)
1940     w:PAUSE 2
1950    END FOR n
1960    f:w:PAUSE 2:PAUSE 10
1970    IF m<k THEN b:END IF
1980    sri:a$="4":poltype2
1990    dt$=DATE$
2000    b3$(m)=a$&dt$(12 TO 20)
2010    PRINT b3$(m)
2020   END FOR m
2030  i
2040 END DEFine
2050 REMark ** Subroutine Name: W3Polar2 **
2060 REMark ** Performs Polarimetry for Both Beams at 3 Wavelengths **
2070 REMark ** Set Up The Log **
2080 channel
2090 DIM b$(100,64),b2$(100,64),b3$(100,64)
2100 CLS:MODE 4:INPUT "Wavelength Adjustment? ",e$
2110 IF e$="y" THEN waveset:END IF
2120 INPUT "Is it first observing run ? ";or$
2130 IF or$="Y" OR or$="y" : GO TO 2170 : END IF
2140 INPUT " Do you still using the same wavelength positions ";Dp$
2150 IF Dp$="Y" OR Dp$="y" : GO TO 2280
2160 CLS: PRINT "New setting "
2170 INPUT "Filter Number in Beam 1?  ",f1$
2180 INPUT "Filter Number in Beam 2?  ",f2$
2190 INPUT "Beam 1 Filter Starting Position?  ",s1$:PRINT
2200 INPUT "Beam 1 Filter Second   Position?  ",s2$:PRINT
```

```
2210 INPUT "Beam 1 Filter Third    Position?  ",s3$:PRINT:PRINT
2220 INPUT "Beam 2 Filter Starting Position?  ",ss1$
2230 scan1=s2$-s1$:scan2=s3$-s2$
2240 ss2$=ss1$+scan1:ss3$=ss2$+scan2
2250 PRINT "First  Wavelength Interval = ",scan1
2260 PRINT "Second Wavelength Interval = ",scan2
2270 REPeat adf
2280 IF or$="y" OR or$="Y" :  GO TO 2310 : END IF
2290 INPUT " Do you wish to change the observed area or the file ?";fp$
2300 IF fp$="N" OR fp$="n" : GO TO 3100
2310  ls=LEN(f1$)
2320  IF ls=4 THEN :EXIT adf:ELSE
2330  f1$="0"&f1$
2340  END IF
2350 END REPeat adf
2360 REPeat adf
2370  ls=LEN(f2$)
2380  IF ls=4 THEN :EXIT adf:ELSE
2390  f2$="0"&f2$
2400  END IF
2410 END REPeat adf
2420 REPeat ads
2430  ls=LEN(s1$)
2440  IF ls=4 THEN :EXIT ads:ELSE
2450  s1$="0"&s1$
2460  END IF
2470 END REPeat ads
2480 REPeat ads
2490  ls=LEN(s2$)
2500  IF ls=4 THEN :EXIT ads:ELSE
2510  s2$="0"&s2$
2520  END IF
2530 END REPeat ads
2540 REPeat ads
2550  ls=LEN(s3$)
2560  IF ls=4 THEN :EXIT ads:ELSE
2570  s3$="0"&s3$
2580  END IF
2590 END REPeat ads
2600 REPeat ads
2610  ls=LEN(ss1$)
2620  IF ls=4 THEN :EXIT ads:ELSE
2630  ss1$="0"&ss1$
2640  END IF
2650 END REPeat ads
2660 REPeat ads
2670  ls=LEN(ss2$)
2680  IF ls=4 THEN :EXIT ads:ELSE
2690  ss2$="0"&ss2$
2700  END IF
2710 END REPeat ads
2720 REPeat ads
2730  ls=LEN(ss3$)
2740  IF ls=4 THEN :EXIT ads:ELSE
2750  ss3$="0"&ss3$
2760  END IF
2770 END REPeat ads
2780 INPUT "Name of Object? ",obj$
2790 REPeat aob
2800  ls=LEN(obj$)
2810  IF ls=9 THEN :EXIT aob:ELSE
2820  obj$=obj$&" "
2830  END IF
2840 END REPeat aob
2850 storeset
2860 REPeat adc
2870  ls=LEN(cart$)
2880  IF ls=9 THEN :EXIT adc:ELSE
```

```
2890  cart$=cart$&" "
2900  END IF
2910 END REPeat adc
2920 REPeat adn
2930  ls=LEN(name$)
2940  IF ls=9 THEN : EXIT adn:ELSE
2950  name$=name$&" "
2960  END IF
2970 END REPeat adn
2980 dt$=DATE$
2990 a$="0 "&cart$&name$&dt$(1 TO 4)&"      "&dt$(6 TO 11)&"  "&" 00000000"&" 000
00000"&" 00000000"
3000 PRINT a$:PRINT £7,a$
3010 a$="0 "&"0000"&f1$&" "&s1$&s2$&" "&s3$&"0000 0000"&f2$&" "&ss1$&ss2$&" "&ss
3$&"0000 00000000"
3020 PRINT a$:PRINT £7,a$
3030 OPEN £6, ser1
3040 PRINT £6,"Both Beams 3 Lambda Pol of ",obj$,DATE$
3050 PRINT £6,"Data recorded on Cartridge: ",cart$,"and under File: ",name$
3060 PRINT £6,"Filter: ",f1$," With Off-set at: ",s1$:PRINT £6
3070 PRINT £6,"Moving to Postions: ",s2$," and: ",s3$
3080 PRINT £6,"Filter: ",f2$," With Off-set at: ",ss1$:PRINT £6
3090 PRINT £6,"Moving to Postions: ",ss2$," and: ",ss3$
3100 REMark **                          **
3110 REMark ** Prepare to Record Dark **
3120 REMark **                          **
3130 PRINT:INPUT "Do You Wish to Observe Dark?",e$
3140 IF e$="n" THEN GO TO 3350
3150 INPUT "Check Pol Switch and Synch!  -  Press Enter when Checked",dumb$
3160 INPUT "How Many Lines for Dark? ",k
3170 INPUT "Prepare to Record Dark - Press Enter",dumb$
3180 CLS:code$="1":PRINT "Running"
3190 pol2
3200 FOR n=1 TO k
3210 PRINT £7,b$(n)
3220 END FOR n
3230 REMark **                          **
3240 REMark ** Prepare to Record Source **
3250 REMark **                          **
3260 PRINT:INPUT "Do you wish to observe the Source?",e$
3270 IF e$="n" THEN GO TO 3350
3280 INPUT "How Many Triple Data Lines? ",k
3290 INPUT "Prepare For Source - Press Enter When Synch Checked!",dumb$
3300 CLS:PRINT "Running"
3310 w3p2
3320 FOR n=1 TO k
3330 PRINT £7,b$(n):PRINT £7,b2$(n):PRINT £7,b3$(n)
3340 END FOR n
3350 INPUT "More Data? - Source = s; Dark = d",e$
3360 IF e$="s" THEN GO TO 3230:END IF
3370 IF e$="d" THEN GO TO 3100:END IF
3380 dt$=DATE$
3390 term$="9 10000000 20000000 30000000 40000000 50000000 60000000"&dt$(12 TO 2
0)
3400 PRINT term$:PRINT £7,term$
3410 CLOSE £6:CLOSE £7
```

Appendix (E) Polynomial fitting of the spectral profile.

The ratio of line centre to continuum intensities for the CaII K Fraunhofer line of the whole solar disk was calculated for each scan. As the line core and the continuum peaks did not correspond to exact registration points on the wavelength scale, the ratio was obtained from interpolated values. The maxima and minima values corresponding to the continua and core points, were chosen from curves fitted though the continuum peak and the line core.

The curves were obtained as follows: for the continuum, the highest intensity was chosen with the three values on each side, and for the core, the lowest value was chosen with three points on each side. In both cases the seven intensity values were fitted to a second-degree of polynomial with the form:-

$$Y_i = \beta_\circ + \beta_1 X_i + \beta_2 X_i^2 \qquad \text{(E.1)}$$

The values of the constants $\beta_\circ$, β_1 , and β_2 may be chosen such that the sum of the squares of the residuals given by

$$\sum_{i=1}^{7} (Y_i - \beta_\circ - \beta_1 X_i - \beta_2 X_i^2)^2 \qquad \text{(E.2)}$$

is least. This is done in the standard way, as follows.

Differentiate (E.1) partially with respect to β_o to obtain

$$\sum_{i=1}^{7} (Y_i - \beta_\circ - \beta_1 X_i - \beta_2 X_i^2) = 0 \qquad \text{(E.3)}$$

Similarly differentiate (E.1) with respect to β_1 , and β_2 respectively to obtain

$$\sum_{i=1}^{7} X_i (Y_i - \beta_\circ - \beta_1 X_i - \beta_2 X_i^2) = 0 \qquad \text{(E.4)}$$

$$\sum_{i=1}^{7} X_i^2 \, (Y_i - \beta_\circ - \beta_1 X_i - \beta_2 X_i^2) = 0 \qquad \text{(E.5)}$$

By expanding (E.3 - E.5), it is easy to show that

$$\begin{aligned} S_\circ\beta_\circ + S_1\beta_1 + S_2\beta_2 &= t_\circ \\ S_1\beta_\circ + S_2\beta_1 + S_3\beta_2 &= t_1 \\ S_2\beta_\circ + S_3\beta_1 + S_4\beta_2 &= t_2 \end{aligned} \qquad \text{(E.6)}$$

where $S_k = \sum_{i=1}^{7} X_r^k$ and $t_k = \sum_{i=1}^{7} X_r^k \, Y_r$

This is a system of three equations in three unknowns. In matrix form, Equations (E.6) become

$$A\,X = b$$

where $A = \begin{bmatrix} S_\circ & S_1 & S_2 \\ S_1 & S_2 & S_3 \\ S_2 & S_3 & S_4 \end{bmatrix}$, $X = \begin{bmatrix} \beta_\circ \\ \beta_1 \\ \beta_2 \end{bmatrix}$ and $b = \begin{bmatrix} t_\circ \\ t_1 \\ t_2 \end{bmatrix}$

To solve this system we use a method called the Gaussian-elimination method which produces the required values of $\beta_\circ$, β_1, and β_2. By applying these constants to (E.1) we can obtain interpolated values at any position and hence at the maximum (continuum) and minimum (line core) intensity values.

Appendix (F) Skewness and kurtosis tests.

Before the Welch tests can be applied to groups of data to see if they can be considered to have originated from the same parent value, the normality of the groups needs to be assessed. This was done by applying Skewness and Kurtosis tests to measure the asymmetry and peakedness respectively. For a sample of n repeated measurements of x, the Skewness and Kurtosis values are calculated from :-

$$\text{Skewness} = \frac{\dfrac{\sum_{i=1}^{n} (x_i - \bar{x})^3}{n}}{\left(\dfrac{\sum_{i=1}^{n} (x_i - \bar{x})^2}{n}\right)^{\frac{3}{2}}} = S$$

$$\text{Kurtosis} = \frac{\dfrac{\sum_{i=1}^{n} (x_i - \bar{x})^4}{n}}{\left(\dfrac{\sum_{i=1}^{n} (x_i - \bar{x})^2}{n}\right)^{2}} = K$$

where $\bar{x} = \dfrac{\sum_{i=1}^{n} x_i}{n}$.

Estimates of the values S and K are spread around their true values for a normal distribution i.e. 0 and 3 respectively. The sign of any significant departure of S from 0 indicates the sense of the Skewness. The departures of K from the value 3 indicates whether the distribution is more or less peaking than a normal distribution; a value of $k>3$, is called a "leptokurtic" distribution, i.e. it has broad tails, and values of $K<3$ is called a "platykurtic" distribution i.e. with sharp central peak. Any drived values of S and K are compared with the 95% and 99% confidence tables derived in Brooks (1984) to see if they are depart significantly so as to indicate a non-normal distribution.

Appendix (G) Welch test.

The Welch test (see Brown & Forsythe 1974) is a useful technique to compare sets of observations with different numbers of measurements, $n_1 \neq n_2 \neq n_3 \neq \text{-----} \neq n_k$, and with different standard mean errors $\sigma_1^2 \neq \sigma_2^2 \neq \sigma_3^2 \text{-----} \neq \sigma_K^2$. This test will estimate whether the sets can be considered as originating from an identical underlying value. As a requirement for the Welch test, the measurements of each group were first confirmed as having normal distribution by investigating the Skewness and Kurtosis values. The Welch statistic W is calculated as follows:

$$W = \frac{\sum_{i=1}^{k} w_i \left(q_i - \hat{q}\right)^2 / (k-1)}{\left[1 + \left(\frac{2(k-2)}{k^2-1}\right) \sum_{i=1}^{k} \left(1 - \frac{w_i}{X}\right)^2 / (n_i - 1)\right]}$$

where $w_i = \frac{1}{\hat{\sigma}_i^2}$, $\quad X = \sum_{i=1}^{k} w_i \quad$ and, $\quad \hat{q} = \sum_{i=1}^{k} (w_i \; q_i) / X$

W is distributed approximately as an F statistic with k-1 and f degrees of freedom, where f is defined by

$$\frac{1}{f} = \left[3/(k^2-1)\right] \sum_{i=1}^{k} \left(1 - \frac{w_i}{X}\right)^2 / (n_i - 1)$$

The hypothesis of equality of population means is rejected at the usual 95% or 99% confidence level.

References.

Allen, C. W.: (1973), "*Astrophysical Quantities*", Athlone Press, 3rd Edition, P.171

Bappu, M. K. V., and Sivaraman, K.R.: (1971) , *Solar Phys.*, **17**, 316

Bappu, M. K. V., and Sivaraman, K.R.: (1977), *Mon. Not. R. astr. Soc.*, **78**, 279

Barbieri, C., Comovici, C. B., Michel, K. W., Nishimura, T., and Roche, A. E.: (1974), *ICARUS*, **23** , 568

Barmore, F. E.: (1975), *J. Atmos. Sci.*, **32**, 1489

Barth, S. B., Brynildsen, N., and Engvold, O.: (1984), *Oslo Observatory Report*, **59**, 27

Blamont, J. E., and Donahue, T.: (1960), *Compt. Roy. Acad. Sci.*, **251**, 2750

Bowell, E. L. G.: (1971), "*Geology and Physics of the Moon*" Edit. by Fielder, G., 127 (Elsevier Publishing Company)

Brinkmann, R. T.: (1968), *Ap. J.*, **154**, 1087

Brooks, A.: (1984), Internal report - Dept. of Physics and Astronomy, Glasgow Univ.

Brown, M. B. and Forsythe, A. B.: (1974), *Technometrics*, **16**, 129

Brückner , G.: (1963), *Z. Astrophys.*, **58**, 73

Bumba, V., and Ruzickova-Topolova, B.: (1967), *Solar Phys.*, **1**, 216

Cameron, W. S.: (1991), *Sky and Telescope*, **81**, 265

Chanin, M. L., Lepine, V., and Blamont, J. E.: (1982), *The Moon and the Planets*, **27**, 143

Chanin, M. L.: (1975), *J. Geophys. Res.*, **18**, 2859

Clarke, D., and Brooks, A.: (1984), *Mon. Not. R. astr. Soc.*, **211**, 737

Clarke, D., and Brooks, A.: (1985), *Mon. Not. R. astr. Soc.*, **212**, 211

Clarke, D., and Grainger, J.: (1971), "*Polarized Light and Optical Measurement*" (Pergamon Press.)

Clarke, D., and McLean, I. S.: (1974), *Mon. Not. R. astr. Soc.*, **167**, 27P

Clarke, D., and McLean, I. S.: (1975a), *Mon. Not. R. astr. Soc.*,**172**, 545

Clarke, D., and McLean, I. S.: (1975b), *Mon. Not. R. astr. Soc.*, **173**, 21P

Clarke, D., and McLean, I. S.: (1975c), *Planet. and Space Sci.*, **23**, 557

Clarke, D., and McLean, I. S.: (1976), *Mon. Not. R. astr. Soc.*, **174**, 335

Clarke, D., and Stewart, B. G.: (1986), *Vistas in Astronomy*, **29**, 27

Clarke, D., McLean, I. S., and Wyllie, T. H. A., (1975), *Astron. Astrophys.*, **43**, 215

Clarke, D., Schwarz H. E., and Stewart, B. G.: (1985), *Astron. Astrophys.*, **145**, 232

Clarke, D.: (1989), "*Practical Electronics*", **October**, 12

Coyne, G. V., and McLean, I. S.: (1982), *I.A.U. Symposium*, **98**, 77

Dollfus, A., and Bowell, E. L. G.: (1971), *Astron. Astrophys.*, **10**, 29

Dubois, J.: (1959), *Rozpr. Cesk. Akad. Ved.*, **69**, 1

Eather, R. H., and Reasoner, D. L.: (1969), *Appl. Optics*, **8**, 227

Eberhard, G., and Schwarzschild, K.: (1913), *Ap. J.*, **38**, 292

Foster, L. V.: (1938), *J. of the Optical Society of America*, **28**, 124

Geake, J. E., Dollfus, A., Garlick, G. F. J., Lamb, W., Walker, G., Steigmann, G. A., and Titulaer, C.: (1970), *Science*, **167**, 717

Gehrels, T.: (1962), *J. of the Optical Society of America*, **52**, 1164

Grainger, J. F., and Ring, J.: (1962 a), *Nature*, **193**, 762

Grainger, J. F., and Ring, J.: (1962 b), *Space Research*, **3**, North-Holland Publ. Co. and Inter-science, 989

Grainger, J. F., and Ring, J.: (1962 c), *I.A.U.Symposium*, **14**, 445

Grainger, J. F.: (1963), *Astron. Contrib., University of Manchester Series III*, **104**, 1

Greenman, N. N., and Gross, G.: (1970), *Proceedings of the Apollo 11 Lunar Science Conference.*, **3**, 2155

Harrison, A. W., and Kendall, D. J. W.: (1974), *Can. J. Phys.*, **52**, 940

Harrison, A. W.: (1976), *Can. J. Phys.*, **54**, 1000

Hsu, J. and Breger, M.: (1982), *Ap. J.*, **262**, 732

Hunten, D. M.: (1970), *Ap. J.*, **159**, 1107

Huovelin, J., Linnaluoto, S., Piirola, V., Tuominen, I., and Virtanen, H.: (1985), *Astron. Astrophys.*, **152**, 357

Ingram, J.: (1913), "*The Anglo-Saxon Chronicle*". (Dutton, New York)

Jacquinot , P.: (1954), *J. of the Optical Society of America*, **44**, 761

Jebsen, D. E., and Mitchell, W. E. Jr.: (1978), *Solar Phys.*, **57**, 309

Johnson, H. L.: (1966), *Ann. Ref. Astron. Astrophys.*, **4**, 193

Kattawar, G. W., Young, A. T., and Humphreys, T. J.: (1981), *Ap. J.*, **243**, 1049

Keen, R. A.: (1983), *Science*, **222**, 1011

Keil, S. L., and Worden, S. P.: (1984), *Ap. J.*, **276**, 766

Kemp, J. C., Henson, G. D., Steiner, C. T., and Powell, E. R.: (1987), *Nature*, **326**, 270

Klare, G., Neckel, Th., and Schnur, G., (1972), *Astron. Astrophys. Suppl.*, **5**, 239

Kolovos, G., Seiradakis, J. H., Varvoglis, H. and Avgoloupis, S.: (1988), *ICARUS*, **76**, 525

Kopal, Z.: (1965), "*The Nature of the Lunar Surface*", Edit. by Hess, W. N., Menzel, D. H., and O'Keefe, J. A. (The Johns Hopkins Press)

Kozyrev, N. A.: (1961), *Jet Propulsion Laboratory Astronautics Transl.*, **18.**

Kozyrev, N. A.: (1963), *Nature*, **198**, 979

LaBonte, B. J.: (1982), *Ap. J.*, **260**, 647

Leroy, J. L and LeBorgne, J. F.: (1989), *Astron. Astrophys.*, **223**, 336

Leroy, J. L.: (1972), *Astron. Astrophys.*, **19**, 287

Link, F.: (1969),"*Eclipse Phenomena in Astronomy* ", (Springer-Verlag, New York)

McCord, T. B.: (1967), *J. Geophys. Res.*, **72**, 2087

Mickey, D. L., and Orrall, F. Q.: (1974), *Astron. Astrophys.*, **31**, 179

Minnaert, M.: (1953), "*The Sun* "; Edit. by Kuiper, G. P. (The University of Chicago Press)

Minnaert, M., Mulders, G. F. W., and Houtgast, J.: (1940), "Potometric atlas of the solar spectrum", (Utrecht Observatory)

Mitchell, A. C. G., and Zemansky, M. W.: (1961), "*Resonance Radiation and Excited Atoms*", (Cambridge University Press.)

Moruzzi, G., Strumia, F.: (1991), "*The Hanle effect and level crossing spectroscopy* ", (Pleanm Press.)

Ney, E. P., Woolf, N. J., and Collins, R. J.: (1966), *J. Geophys. Res.* **71**, 1787

Nikol'skii, G. M. and Khetsuriani, S. Ts., (1970), *Soviet Astron.*, **13**, 815

Noxon, J. F., and Goody, R. M.: (1965), *Atm. Oceanic Phys.*, **1**, 275

Oranje, B. J.: (1983a), *Astron. Astrophys.*, **122**, 88

Oranje, B. J.: (1983b), *Astron. Astrophys.*, **124**, 43

Pavlov, V. E., Teifel, Ya. A., and Golovachev, V. P.: (1973), *Soviet Physics* , **17**, 1038

Potter, A. E., and Mendell, W.: (1984), *J. Geophysical Research Supplement*, **89**, C240

Redman, R. O.: (1941), *Mon. Not. R. astr. Soc.*, **101**, 266

Righini, JR., and Rigutti, M.: (1966), *ICARUS*, **5**, 258

Rutten, R. J., and Cram, L. E.: (1981), "*The Sun as a Star*" NASA AP-**450**, 473

Scarfe, C. D.: (1964), *Mon. Not. R. astr. Soc.*, **130**, 19

Schwarz, H. E.: (1986), *Vistas in Astronomy*, **29**, 253

Serkowski, K.: (1974), "*Planets, stars, and nebulae studied with photopolarimetry*", Edit. by Gehrels, T. (The University of Arizona Press)

Sheeley, N. R.: (1967), *Ap. J.*, **147**, 1106

Shefov, N. N.: (1959), *Izd. Akad. Nauk*, **1**, 25

Shurcliff, W. A.: (1962), "*Polarized Light*", (Harvard Univ. Press, Boston)

Singh, J., and Livingston, W. C.: (1987), *Solar Phys.*, **109**, 387

Spinrad, H.: (1964), *ICARUS* , **3**, 500

Stenflo, J. O., Baur, T. G., and Elmore D. F.: (1980), *Astron. Astrophys.*, **84**, 60

Stenflo, J. O., Twerenbold, D., and Harvey, J. W.: (1983a), *Astron. Astrophys. Suppl.*, **52**, 161

Stenflo, J. O., Twerenbold, D., Harvey, J. W., and Brault J. W.: (1983b), *Astron. Astrophys. Suppl.*, **54**, 505

Stenflo, J. O.: (1974), *Solar Phys.*, **37**, 31

Stenflo, J. O.: (1981), "*Solar Instrumentation. What's Next?* " Ed.by Dunn R.

Stewart, B. G.: (1984), *PhD. Thesis, University of Glasgow.*

Stimets, R. W., and Londono, C.: (1982), *Solar Phys.*, **76**, 167

Stokes, G. G.: (1852), *Trans. Cambridge Phil. Soc.*, **9**, 399

Teifel, V. G.: (1960), *Soviet Astron.*, **4**, 669

Tinbergen, J., and Zwaan, C.: (1981), *Astron. Astrophys.*, **101**, 223

Vaucouleurs, G. de.: (1967), *I.A.U. Symposium*, **30**, 91

Vaughan, A. H., Baliunas, S. L., Middelkoop, F., Hartmann, L. W., Mihalas, D., Noyes, R. W., and Preston, G. W.: (1981), *Ap. J.*, **250**, 276

Vaughan, A. H.: (1981), *Anuual Report of the Mount Wilson Observatories* , 599

Verschuur, G.: (1989), *Astronomy*, **17**, 48

White, O. R., and Livingston, W. C., (1978), *Ap. J.* , **226**, 679

White, O. R., and Livingston, W. C., (1981), *Ap. J.*, **249**, 798

Wiehr, E.: (1975), *Astron. Astrophys.*, **38**, 303

Wiehr, E.: (1978), *Astron. Astrophys.*, **67**, 257

Wiehr, E.: (1981), *Astron. Astrophys.*, **95**, 54

Wildey, R. L.: (1964), *Publ. Astr. Soc. Pacif.*, **76**, 112

Wilson, O. C.: (1978), *Ap. J.*, **226**, 379

Wraight, P. C.: (1989), *J. Phys. E. Sci. Instrum.*, **22**, 962